Multivariate bias corrections of climate simulations seen through impact model

Denis Allard, Bastien François, I. García de Cortázar-Atauri, Mathieu Vrac

Multivariate bias corrections of climate simulations seen through impact model

Results of the COMPROMISE project

Denis Allard[1]
Bastien François[2]
Iñaki Garcia de Cortazar[3]
Mathieu Vrac[4]

[1] INRAE, BioSP, 84914 Avignon, France
[2] Royal Netherlands Meteorological Institute (KNMI), Research and Development Weather and Climate (RDWK), De Bilt, The Netherlands
[3] INRAE, Agroclim, 84914 Avignon, France
[4] Laboratoire des Sciences du Climat et de l'Environnement (LSCE-IPSL), CEA/CNRS/UVSQ, Université Paris-Saclay, Centre d'Etudes de Saclay, Orme des Merisiers, 91191 Gif-sur-Yvette, France

Abstract

Atmospheric variables simulated from climate models often present biases relative to the same variables calculated by reanalysis in the past (SAFRAN reanalysis for example). In order to use these models to assess the impact of climate change on processes of interest, it is necessary to correct these biases. Currently, the bias correction methods used operationally correct one-dimensional time series and are therefore applied separately, physical variable by physical variable and site by site. Multivariate bias correction methods have been developed to better take into account dependencies between variables and in space. In this work, we propose a comparison between two multivariate bias correction methods (R2D2 and dOTC) and a univariate correction (CDF-t) through several highly multivariate impact models (phenological stage, reference evapo-transpiration, soil water content, forest weather index) integrating the climatic signal throughout a season. The data, the impact models and the statistical methods are first presented. The experimental design is then described. Extensive results are illustrated but not commented.

Keywords. Climate change, quantile correction, multivariate bias correction, agroclimatic indicators, Forest Weather Index

Acknowledgement

This technical report is part of the COMPROMISE project funded by the metaprogram Adaptation of Agriculture and Forest to Climate Change (AAFCC) of the French National Research Institute for Agriculture, Food & Environment (INRAE).

Contents

Chapter 1

Introduction, material and methods

1.1 Introduction

Simulations from global and regional climate models are used to assess future climate change. Their output variables then serve as input variables for agronomic impact models, enabling us to understand and adapt to the consequences of future climate conditions. Climate change impacts agroforestry systems through rising temperatures, changing precipitation patterns and increasing CO_2 concentration in the atmosphere, see for example the Green Paper from the CLIMATOR project (Brisson and Levrault, 2010).

A recurring problem with this approach is that the "raw" outputs of climate models often present biases relative to variables calculated by reanalysis in the past, such as SAFRAN data (Vidal et al., 2010). Climate model outputs must therefore be "adjusted" or "corrected" before being used in impact models (François et al., 2020). Various bias correction methods have been developed over the last few decades.

The benchmark bias correction (BC) method in operational use today is the "quantile correction" correction, and its many variations (Michelangeli et al., 2009). It is applied separately, physical variable by physical variable, site by site and date by date. The corrected simulations may then be physically unrealistic or may not reproduce the spatial consistency observed on the historical data. This mismatch is propagated in the impact models, affects the outputs of these models, and ultimately hampers the decision-making processes that may result from them. Realistic consideration of dependencies in bias correction methods is therefore necessary.

François et al. (2020) intercompared four existing MBCs to correct simulation bivariate series of temperature and precipitation outputs. It was found that most of the methods reasonably correct inter-variable and spatial correlations. Major differences were found concerning the applicability and stability of the methods in high-dimensional contexts and in their capability to reproduce the multidimensional changes in the model. In the conclusion, it was mentioned that "bias-adjusted simulations are particularly valuable for impact studies. [...] Evaluating how the quality of multivariate biascorrected data influences the results of complex impact models is an important perspective. Providing such an analysis will be useful for the scientific community working on climate change impacts, e.g., in hydrology, agronomy or ecology."

One of the objective of the COMPROMISE project, supported by the ACCAF Metaprogram at INRAE, was to compare several multivariate bias correction methods applied to climatic series that will be used as input variables for several impact models. This working document, which can be seen as a follow-up of François et al. (2020) presents some of the outputs that were obtained in this project. We focus on indicators computed on impact models during the Summer season (the 92 days in June, July and August). All indicators (which will be detailed below) are computed using 5 physical variables (tas, pr, scfWind, rsds and hurs) simulated by the climate model IPSL-CM6A-LR (Boucher et al., 2020). These data were regridded to the SAFRAN 8 km $\times$ 8 km mesh (hence, with no correction) and corrected on the same grid using one of the bias correction methods presented in Section 1.3. We will consider a past period (1985-2014) during which the historical reference data SAFRAN is available and a projection period (2036-2065).

The structure of the document is the following. In this introduction (Chapter 1), we first present the data, the impact models and the indicators that are considered for the analysis, along with the multivariate bias correction that will be tested. We then present the statistical methods used for assessing the obtained output series. We will not only evaluate the correction on average, but we will also assess whether the variability iw correctly reproduced, as measured through the variance and the spatial covariance function. Then in the following chapters, we will show the results of our analysis. They will be illustrated with boxplots, plots of covariance function, p-value tables and maps of bias and variance ratios.

1.2 Data and models

1.2.1 Model simulations and reference data

The climate model used in this study is the IPSL-CM6A-LR coupled model developped at the Institut Pierre-Simon Laplace (IPSL) (Boucher et al., 2020), part of the 6th Coupled Models Intercomparison Project (CMIP6, Eyring et al., 2016). Daily values of 5 phyisical variables that are used as input variables for impact models have been extracted over a historical period (1985-2014), which will be used for comparison and calibration, and a future period (2036-2065): daily mean temperature (tas), total precipitation (pr), near-surface wind speed (scfWind), short-wave downwelling radiation (rsds) and near-surface relative humidity (hurs). We selected the ssp585 (SSP5-RCP8.5) scenario, i.e. the scenario with the highest CO_2 concentration.

Since our study covers France, the reference data is the gridded "Systeme d'Analyze Fournissant des Renseignements Atmosphériques à la Neige" (SAFRAN) reanalysis dataset (Vidal et al., 2010). Daily time series of the same 5 variables have a 8 km $\times$ 8 km spatial resolution and divide France into 8981 contiguous continental grid cells. IPSL-CM6A-LR data, available at the 2.5řÖ1.3ř resolution, were regridded to the SAFRAN resolution using the nearest-neighbor technique.

Three very contrasted regions of France were selected: Brittany (North-West part of France, 259 grid cells), Ile de France (the region around Paris, 319 grid cells) and Provence (South-east part of France, 337 grid cells). In the latter, some grid cells are located in the Alps, with quite high mean elevation, up to 2900 m.

1.2.2 Impact models

The physical variables described above are used as input variables for several process models in order to compute indicators.

Evapo-transpiration

As a first indicator, the reference evapo-transpiration, ET0 (in mm), is computed directly from all variables, using the Penman–Monteith formula (Allen et al., 1998), independently to any chosen plant model. ET0 is computed every day of the year, separately at each grid cell.

Plant models

We use the generic framework presented in Caubel et al. (2015) for computing agroclimatic indicators over phenological periods. Different ecophysiological processes or cultural practices taking place during each of these phenological periods are modeled and translated into `R` scripts. Several indicators are then computed in response to the climatic signal described by the physical variables. We refer to Caubel et al. (2015) for an in-depth description. The output variables that have been selected are:

- A phenological stage. This indicator was chosen because, as it depends only on the accumulation of temperature, it allows us to assess the effect of multivariate bias correction methods on temperature only, which is the reference variable for one of the MBC method (see Section 1.3 below). Specifically, stage 3, which corresponds to flowering, was selected because it is the latest stage reached in most grid cells and years, except perhaps in the grid cells covering high mountains in the Provence domain. For one given year, the indicator FLO is thus the date, expressed in Julian days, at which flowering is reached for the considered plant. The computation is based on the Phenological Modeling Platform (Chuine et al., 2013) to simulate the different phenological stages.

- The Soil Water Content (SWC), which is an indicator in relation to the water balance, roughly equal to 'Precipitation − ET0'. SWC is the water content in the soil, expressed as a percentage of the total mass. The variable 'Water Reserve', expressed in mm was also computed. It lead to very similar result and it is not reported here. SWC involves all 5 variables and it has a strong temporal component relating to the temporal occurrence of precipitation. With this indicator, it is possible to assess whether or not the MBCs are able to correct a highly non-linear transformation of the 5 variables.

Following Caubel et al. (2015), three plant models, among the major crops cultivated in France, have been selected: wheat, maize and grapevine.

- Wheat is mostly cultivated in and around Ile-de-France, but wheat fields can be found anywhere in France, except at high elevations. Sowing date was set to October 1st, every year and for all grid cells.
- A short-cycle variety was chosen for maize in order to achieve late phenological stages in the Northern regions (Brittany and Ile-de-France). Since no irrigation was introduced, water deficit can be expected in the Southern region (Provence). Sowing date was set to April 10, every year and for all grid cells.
- Vineyards are very common in Provence (except in the Alps), possible in the Ile-de-France region (e.g. nearby Champagne) and are currently absent in Brittany. A rather ubiquitous variety, Chardonay, was chosen. There is no sowing date for grapewines, but all computations were re-initialized August 1st of the previous year.

A deep soil (140 cm), with more than 200 mm useful water reserve and moderate soil water capacity (28% at field capacity and 35% at saturation) was chosen for all grid cells in all regions.

Forest Weather Index

With nearly one third of Metropolitan France (mainland France and Corsica, without overseas territories) covered by woods and forests, France has among Europe's highest forest cover (MTES, 2021). Apart from providing resources and recreational activities, the forest plays a key role in climate regulation, the water cycle, and soil preservation including its role as biodiversity reservoir, carbon sink and in erosion control. However, weather conditions such as drought, temperature and wind have strong influence on the forests' vulnerability to fire and its potential for spreading. Between 2007 and 2019, wildfires destroyed around 11,500 ha of forest per year in Metropolitan France. In 2022, over 59,000 ha of forests were destroyed (`https://bdiff.agriculture.gouv.fr/incendies`). Climate change increases the weather-induced component of the forest fire risk across France and Europe (Dupuy et al., 2020; Fargeon et al., 2020; Ruffault et al., 2020). The Forest Weather Index (Van Wagner et al., 1987) summarizes the effects of wind, temperature, humidity and precipitation into a single index used by the national security services as a danger rating system for forest wildfires. In theory, the FWI is determined every day from the FWI value of the preceding day and from noon weather readings: temperature, relative humidity, wind speed, and rain (if any). In this work, FWI is computed based on simulation or reanalysis data instead of meteorological readings, using the `R` package `cffdrs` (Wang et al., 2017).

1.3 Multivariate bias correction methods

Multivariate Bias Correction methods (MBC) must be chosen for their capacity to correct the biases and their spatial properties over large geographical areas. Following the discussion in François et al. (2020), good candidates are dOCT (dynamical Optimal Transport Correction) and R2D2 (Rank Resampling for Distributions and Dependences). These methods are briefly recalled here and we refer to François et al. (2020) and the original papers referenced therein for a more in-depth presentation.

R2D2, proposed in Vrac (2018) consists in two steps. In the first step, each climate variable is adjusted using a univariate bias correction methods. In this work, CDF-t (described below) is used, but other methods could be used. The second step is essentially a re-ordering technique, called the Schaake Shuffle (Clark et al., 2004) which reorders a sample such that the rank structure corresponds to the rank structure of a reference sample. A reference dimension (i.e. one physical variable at one given site) is selected, for which the rank chronology of the simulations remains unchanged. Reconstruction of the inter-variable and spatial rank correlations of the reference is then performed, while preserving the rank temporal dynamics for the reference dimension. It must be emphasized that, by construction, R2D2 assumes the intervariable and spatial rank correlations to be stationary in time.

dOTC (Robin et al., 2019) corrects the marginal distributions and the multivariate dependence at the same time. It is a generaliztion of the univariate quantile mapping approach to the multivariate case. Based on optimal transport theory, it builds a transfer plan, which is a multivariate transfer function from one multivariate distribution to another, that minimizes a cost function based on an energy criterion. Two important differences between R2D2 and dOTC are that dOTC does not single out a particular 'reference dimension' and that dOTC does not assume the stationarity of copula structure between the calibration and the projection periods. dOTC is designed to transfer some of the multivariate properties' changes between the calibration and the projection periods from the model to bias corrected data.

As a benchmark, the multivariate dataset is also corrected using the univariate CDF-t correction method (Michelangeli et al., 2009). Independently for each variable and at each site, CDF-t estimates a univariate transfer function, denoted T, that links the Cumulative Distribution Function (CDF) of a climate variable of interest in the model simulations during calibration period to that of the same variable in the reference dataset. By assuming that T is also valid during the projection period, a quantile-quantile approach is performed between the new reference CDF and the CDF from the model simulations during the projection period. CDF-t is designed to take into account potential simulated changes (between calibration and projection periods) of the univariate distribution in the correction procedure. Thus, the bias-corrected data for the projection period incorporate the model's projected changes. In the specific case of precipitations, the "Singularity Stochastic Removal" version of CDF-t (Vrac et al., 2016) is applied, working the same way as CDF-t but specifically designed to account for rainfall occurrences.

1.4 Statistical analysis

Let us denote $Z(\boldsymbol{s}, t)$, one of the output variable, computed at site $\boldsymbol{s} \in \mathcal{S}$ and Julian day t. There is a total of n_S sites in $\mathcal{S}$ and n_T Julian days considered for the analysis every year. Measurements (or computations) are repeated during m years of a period whose climate is considered as being approximately constant. The m years are thus assumed to be independent and identically distributed repetitions of the same spatio-temmporal process. Several summary statistics, described below, are computed for visualization and hypothesis testing.

1.4.1 Univariate statistics

For a given spatio-temporal output $Z(\boldsymbol{s}, t)$, the mean and variances are computed at each site,

$$\hat{\mu}(\boldsymbol{s}) = (mn_T)^{-1} \sum_{i=1}^{m} \sum_{t_i=1}^{n_T} Z(\boldsymbol{s}, t_i); \qquad \hat{\sigma}^2(\boldsymbol{s}) = (mn_T)^{-1} \sum_{i=1}^{m} \sum_{t_i=1}^{n_T} \big(Z(\boldsymbol{s}, t_i - \hat{\mu}(\boldsymbol{s})\big)^2, \tag{1.1}$$

where t_i denotes the Julian day t in year i. From these, spatial maps of the biases $\hat{\mu}_M(\boldsymbol{s}) - \hat{\mu}_R(\boldsymbol{s})$ and variance ratios $\hat{\sigma}^2_M(\boldsymbol{s})/\hat{\sigma}^2_R(\boldsymbol{s})$ can be represented, where the index M refers to one of the models (with or without bias correction) and R stands for 'Reference'. Boxplots allow for a first simple visual assessment of the biases, but in this case the spatial information is lost.

1.4.2 Spatial covariance and Moran's I

In order to assess the spatial structure in $Z(\boldsymbol{s}, t)$, the spatial auto-covariance at short distances is computed assuming second-order stationarity. It is known that given the size of the domains under consideration (from 16,000 km^2 to 22,000 km^2) and the complex topographic structures, in particular in Provence, one must expect that the mean and variance of $Z(\boldsymbol{s}, t)$ vary in space. However a locally stationary assumption is possible, at least in Brittany and Ile de France, at the 30 km scale, which corresponds approximately to 4 SAFRAN grid meshes. For a given spatial lag $\boldsymbol{k} \in \{-4, -3, \ldots, 3, 4\} \times \{-4, -3, \ldots, 3, 4\}$ the empirical spatial covariance is

$$\hat{C}(\boldsymbol{k}) = (mn_T n_S(\boldsymbol{k}))^{-1} \sum_{i=1}^{m} \sum_{t_i=1}^{n_T} \sum_{\boldsymbol{s} \in \mathcal{S}_{\boldsymbol{k}}} \big(Z(\boldsymbol{s}, t_i) - \hat{\mu}(\boldsymbol{s})\big)\big(Z(\boldsymbol{s} + \boldsymbol{k}, t_i) - \hat{\mu}(\boldsymbol{s} + \boldsymbol{k})\big), \tag{1.2}$$

where $\mathcal{S}_{\boldsymbol{k}}$ is the restriction of $\mathcal{S}$ with $n_S(\boldsymbol{k})$ elements such that both $\boldsymbol{s}$ and $\boldsymbol{s} + \boldsymbol{k}$ are in $\mathcal{S}$.

Moran's I (Moran, 1950) is a widely used measure of spatial auto-correlation at short distances. We use here a local, un-normalized version of Moran's I given by

$$I = \frac{1}{mn_T \sum_{\boldsymbol{s}} \sum_{\boldsymbol{s}'} w_{\boldsymbol{s},\boldsymbol{s}'}} \sum_{i=1}^{m} \sum_{t=1}^{n_t} \sum_{\boldsymbol{s}} \sum_{\boldsymbol{s}'} w_{\boldsymbol{s},\boldsymbol{s}'} \big(Z(\boldsymbol{s},t_i) - \hat{\mu}(\boldsymbol{s})\big)\big(Z(\boldsymbol{s}',t_i) - \hat{\mu}(\boldsymbol{s}')\big), \tag{1.3}$$

where $w(\boldsymbol{s},\boldsymbol{s}')$ is a binary indicator that characterizes the neighborhood structure with $w(\boldsymbol{s},\boldsymbol{s}) = 0$. The 'rook' (resp. 'queen') neighborhood corresponds to $||\boldsymbol{s} - \boldsymbol{s}'|| \leq 1$ (resp. to $||\boldsymbol{s} - \boldsymbol{s}'|| \leq \sqrt{2}$), where the distance is expressed in mesh units. The measure I in (1.3) is local because local means $\hat{\mu}(\boldsymbol{s})$ are used, and contrarily to the usual Moran's I it is not normalized by the variance, for an easier implementation of the hypothesis testing presented below. Using the symmetry of the covariance function, direct manipulations of (1.3) show that

$$I_{\text{rook}} = \frac{\hat{C}(0,1) + \hat{C}(1,0)}{2} \quad \text{and} \quad I_{\text{queen}} = \frac{\hat{C}(0,1) + \hat{C}(1,0) + \hat{C}(1,1) + \hat{C}(-1,1)}{4}, \tag{1.4}$$

which shows that Moran's I is a summary of the short distance behavior of the spatial covariance function.

1.4.3 Spatio-temporal correlation

At larger scales, the spatio-temporal non-stationarity must be acknowledged. We thus decompose $Z(\boldsymbol{s},t)$ according to

$$Z(\boldsymbol{s},t) = \mu(\boldsymbol{s},t) + \sigma(\boldsymbol{s},t)\varepsilon(\boldsymbol{s},t), \tag{1.5}$$

where $\varepsilon(\boldsymbol{s},t)$ is a standardized residual and where the mean $\mu(\boldsymbol{s},t)$ and standard deviation $\sigma(\boldsymbol{s},t)$ vary in space and time. They are estimated with their empirical versions:

$$\hat{\mu}(\boldsymbol{s},t) = m^{-1} \sum_{i=1}^{m} Z(\boldsymbol{s},t_i); \qquad \hat{\sigma}^2(\boldsymbol{s},t) = m^{-1} \sum_{i=1}^{m} \big(Z(\boldsymbol{s},t_i) - \hat{\mu}(\boldsymbol{s},t)\big)^2. \tag{1.6}$$

In all generality, the spatio-temporal correlation function $\text{Cor}\big(\varepsilon(\boldsymbol{s},t), \varepsilon(\boldsymbol{s}',t')\big) = \rho(\boldsymbol{s},\boldsymbol{s}',t,t')$ is any positive definite function of $(\boldsymbol{s},\boldsymbol{s}',t,t')$ (Chen et al., 2021). However, motivated by the absence of complex space-time interactions in $\varepsilon(\boldsymbol{s},t)$, such as diffusion or transport, the spatio-temporal correlation function for ε is assumed to be space-time separable with

$$\text{Cor}\big(\varepsilon(\boldsymbol{s},t), \varepsilon(\boldsymbol{s}',t')\big) = \rho(\boldsymbol{s},\boldsymbol{s}',t,t') = \rho_S(\boldsymbol{s},\boldsymbol{s}')\rho_T(t,t'). \tag{1.7}$$

The spatial and temporal correlations are estimated using temporal and spatial repetitions, respectively:

$$\hat{\rho}_S(\boldsymbol{s},\boldsymbol{s}') = (mn_T)^{-1} \sum_{i=1}^{n} \sum_{t=1}^{n_T} \text{Cor}\big(\varepsilon(\boldsymbol{s},t), \varepsilon(\boldsymbol{s}',t)\big) \tag{1.8}$$

$$\rho_T(t,t') = (mn_S)^{-1} \sum_{i=1}^{n} \sum_{\boldsymbol{s}\in\mathcal{S}} \text{Cor}\big(\varepsilon(\boldsymbol{s},t), \varepsilon(\boldsymbol{s},t')\big). \tag{1.9}$$

We refer the reader to Chen et al. (2021) and references therein for an in-depth discussion on separability for spatio-temporal correlation functions, its application and testing.

1.4.4 Effective Sample Size

When the sample values are spatially correlated, the actual number of data cannot be taken as such for computing the degrees of freedom for hypothesis testing. One must instead assess the correlation between the values and derive an Effective Sample Size (ESS), which quantifies the number of independent and identically distributed observations within the sample under consideration. Let us consider a sample $\boldsymbol{Z}$ of size n with expectation μ, variance σ^2 and correlation matrix $\boldsymbol{R}$. Then, under the assumption that $\boldsymbol{R}$ is invertible, Vallejos and Osorio (2014) define the ESS as $\text{ESS} = \mathbf{1}_n^\top \boldsymbol{R}^{-1} \mathbf{1}_n$, where $^\top$ is the transpose operator and $\mathbf{1}_n$ is a vector of 1s of length n. There is a enlightening interpretation to the ESS, in relation to the estimation of μ when $\boldsymbol{R}$ is known. It can be shown that in this case the best (i.e. unbiased and with minimum variance) estimator of μ is $\hat{\mu} = \mathbf{1}_n^\top \boldsymbol{R}^{-1} \boldsymbol{Z}$ and that its variance is $\text{Var}(\hat{\mu}) = \sigma^2/\text{ESS}$ (Chiles and Delfiner, 2012, Section 3.4). ESS depends on n and on the correlation structure of $\boldsymbol{Z}$ which, in a spatio-temporal context, depends on the space and time coordinates of the samples and

on the spatio-temporal correlation function. ESS decreases from n to 1 as the correlation strength decreases from no correlation (i.e. $\boldsymbol{R}$ is the identity matrix of size $n \times n$) to perfect correlation (i.e. $\boldsymbol{R}$ is the $n \times n$ matrix of 1s).

In the spatio-temporal context above, the correlation matrix to be considered is of size $n_S n_T \times n_S n_T$, which can be too large for an easy inversion (for example, the summer season in Provence would yield to a $31,004 \times 31,004$ matrix). However, under the separability assumption in (1.7), the computation of the SSE corresponding to one year of data simplifies to $\mathrm{SSE}_1 = \mathrm{SSE}_S \times \mathrm{SSE}_\mathrm{T}$, with $\mathrm{SSE}_S = \mathbf{1}_n^\top \boldsymbol{R}_S^{-1} \mathbf{1}_n$ and $\boldsymbol{R}_{S,ij} = \hat{\rho}_S(\boldsymbol{s}_i, \boldsymbol{s}_j)$, with $1 \leq i, j \leq n_S$, and with a similar expression for SSE_T. As an illustration, for the summer season in Provence, $n_S = 337$ and $n_T = 92$. Finally, the SSE of a period (e.g. the summer season) for m independent years is simply $\mathrm{SSE}_m = m\mathrm{SSE}_1$.

1.4.5 Hypothesis testing

Two types of statistical tests are performed. The first type aims at testing the absence of bias or differences on global averages. The basis for this is the Welch's t-test, or unequal variances t-test (Welch, 1947). The second family aims at testing whether variances and Moran's I are equal or unequal. Fort this, the Fisher's F-tests of equality of variances, based on the ratio of the variances is used. In all cases, an important parameter for these tests are the 'degrees of freedom', equal to $n-1$ when the n samples are independent. Here, following the discussion in the paragraph above, the degrees of freedom is set to $\mathrm{SSE}_m - 1$ to take into account the spatio-temporal auto-correlation.

1.5 Experiments

All indicators (ET0, FLO, SWC, FWI) are computed using the 5 physical variables described in Section 1.2.1 (tas, pr, scfWind, rsds and hurs) given by the IPSL model gridded to the SAFRAN 8 km × 8 km mesh (hence, with no correction) or corrected on the same grid using one of the bias correction methods: CDFt, dOTC and R2D2. The MBC methods dOTC and R2D2 are applied according to the three following configurations:

- The Intervar configuration (I) aims at correcting inter-variable correlations only: the MBC method corrects jointly the 5 physical variables at each grid cell of the domain independently on all other grid cells. In this configuration, the pivot dimension is Temperature at the considered grid cell.
- The Spatial configuration (S) aims at correcting the spatial correlations for each physical variable separately: each variable is corrected independently, and for each variable the N_S vector of all values in the domain is corrected. Here, the pivot dimension is the considered physical variable at the center of the region.
- The Spatial-Intervar configuration (SI) intents to correct simultaneously the inter-variable and the spatial correlations of the simulations: the complete $5N_S$ vector of all variables in the domain are corrected at once. In this configuration, the pivot is the Temperature at the center of the region.

In addition to the historical reference data SAFRAN, for each of the three regions, there is thus a total of 8 climate datasets with the physical variables described in Section 1.2.1 (tas, pr, scfWind, rsds and hurs): IPSL (gridded to the SAFRAN 8 km × 8 km mesh) and 7 bias corrected datasets. Using those 9 datasets as input variables, ET0 and FWI are computed every day at all grid cells. Then, for each plant model and at all grid cells, SWC and WR are computed every day and FLO is determined for each year.

The summer season (92 days in June, July and August) has been selected for analysis because variations of ET0, SWC and FWI are expected to be amplified and differences between MBC configurations largest. In particular, the Provence region is characterized by high temperatures and low precipitations in Summer.

Local biases and variance ratio are computed at each grid cell. Specifically, for a given indicator Z at grid cell $[i, j]$, the local bias and variance ratio are:

$$\mathrm{BIAS}[i,j] = \bar{Z}_{\mathrm{BC}}[i,j] - \bar{Z}_{\mathrm{SAFRAN}}[i,j]; \quad \mathrm{RATIO[i,j]} = \mathrm{S^2(Z_{BC})[i,j]} \,/\, \mathrm{S^2(Z_{SAFRAN})[i,j]},$$

where BC is any Bias Correction method (including none), $\bar{Z}[i,j]$ is the average of $Z[i,j]$ over the time window considered and $S^2(Z)[i,j]$ is the corresponding empirical variance. These local statistics can be represented as maps and summarized using boxplots. The spatial covariances and Moran's I are then computed using (1.2) and (1.4). Hypothesis testing is done on global biases and variance ratios, which are the spatial average of the local biases and local variances, respectively.

Chapter 2

ET0 in the past: 1984-2015

ET0 depends only on climate variables. It is therefore identical for all plant models. We consider here the average computed over the meteorological summer, i.e. from June 1st to August 31st.

2.1 Boxplots

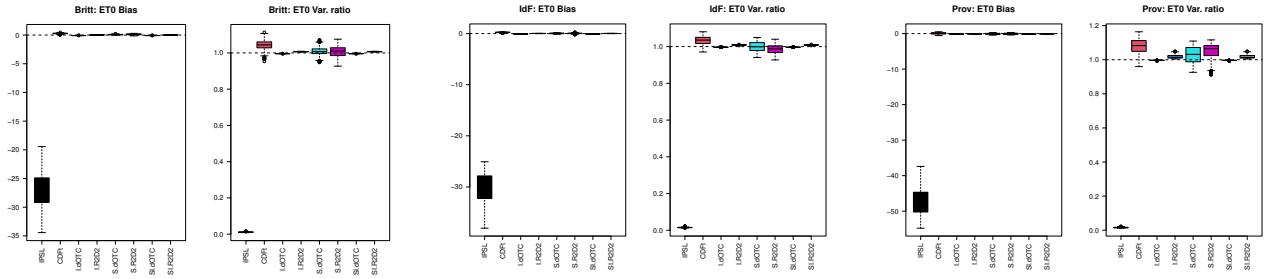

Figure 2.1: Overall summer ET0 bias to SAFRAN and summer ET0's variance ratio to SAFRAN for all bias correction methods. Left column: Bretagne. Middle column: Ile de France. Right column: Provence. In each panel, from left to right: IPSL (no correction), CDF-t, Intervar-dOTC, Intervar-R2D2, spatial-dOTC, spatial R2D2, spatial-intervar-dOTC, spatial-intervar-R2D2.

2.2 Covariances

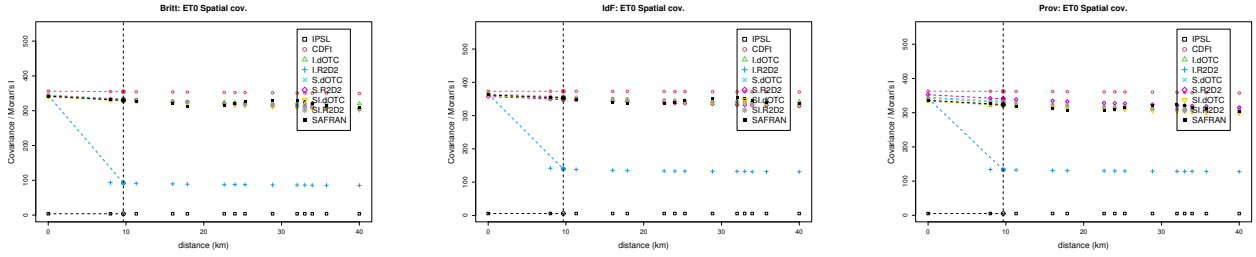

Figure 2.2: Spatial covariance and Moran's I of summer ET0 in the past for all bias correction methods. Left column: Bretagne. Middle column: Ile de France. Right column: Provence.

2.3 p-values

	IPSL	CDFt	I.dOTC	I.R2D2	S.dOTC	S.R2D2	SI.dOTC	SI.R2D2
p-values for "equality-of-means" tests								
Britt.	0.000	**0.396**	**0.826**	**0.967**	**0.817**	**0.773**	**0.828**	**0.966**
IdF	0.000	**0.468**	**0.820**	**0.958**	**0.923**	**0.931**	**0.822**	**0.951**
Prov.	0.000	**0.812**	**0.664**	**0.804**	**0.808**	**0.932**	**0.609**	**0.749**
p-values for "equality-of-variances" tests								
Britt.	0.000	**0.101**	**0.883**	**0.803**	**0.729**	**0.877**	**0.885**	**0.795**
IdF	0.000	**0.212**	**0.891**	**0.779**	**0.940**	**0.625**	**0.892**	**0.746**
Prov.	0.000	0.000	**0.860**	**0.439**	**0.163**	0.011	**0.834**	**0.324**
p-values for "equality-of-Moran's I" tests								
Britt.	0.000	0.004	**0.962**	0.000	**0.673**	**0.771**	**0.885**	**0.795**
IdF	0.000	0.024	**0.706**	0.000	**0.928**	**0.631**	**0.893**	**0.744**
Prov.	0.000	0.000	**0.604**	0.000	**0.120**	0.007	**0.837**	**0.330**

Table 2.1: Statistical analysis for summer ET0 in the past: p-values for the Welsh t-test of absence of bias on the average (first block); Fisher F-test of equality of variance (second block) and its adaptation to testing the equality of Moran's I (third block). Non rejection at the confidence level 0.90 is indicated in bold font.

2.4 Maps for bias

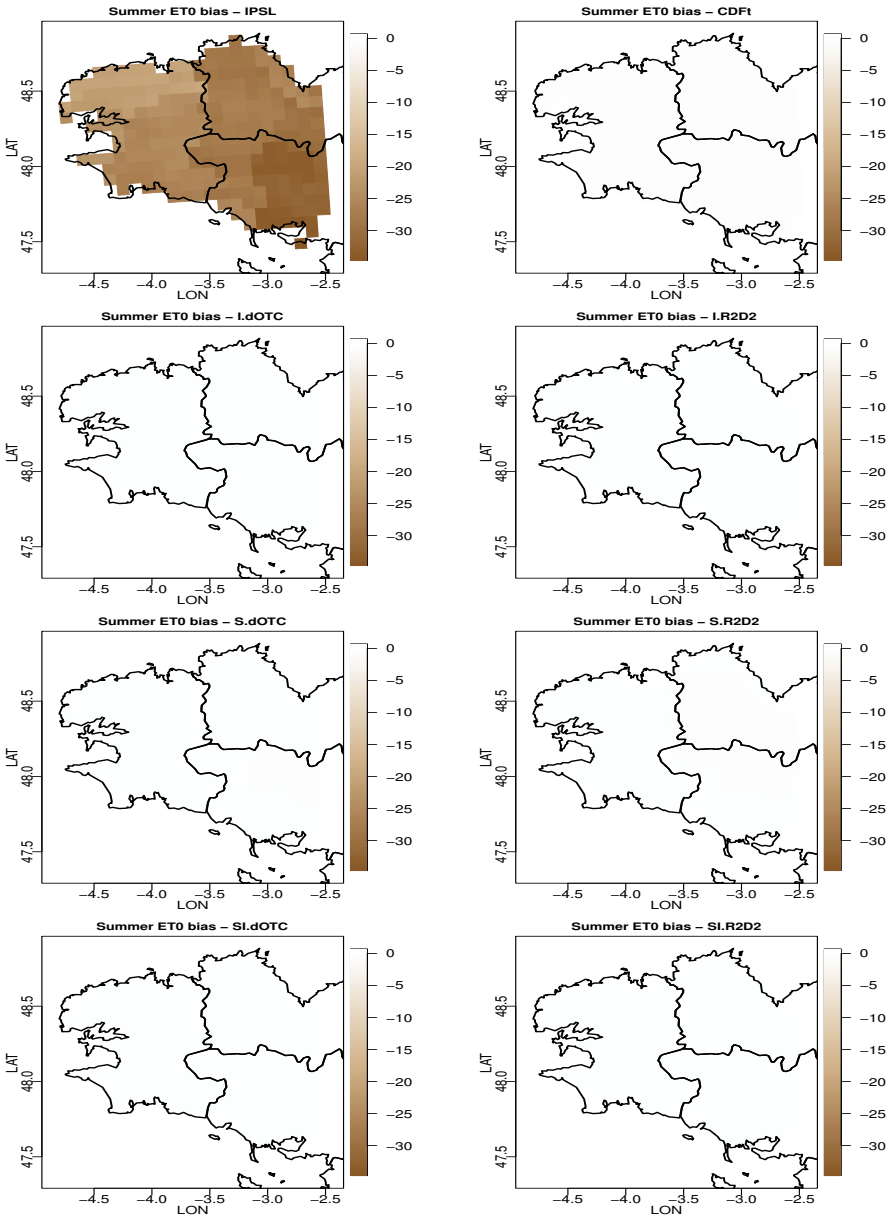

Figure 2.3: For each bias correction method: map of summer ET0 bias to SAFRAN in Bretagne. From top to bottom and from left to right: IPSL (no correction), CDF-t, Intervar-dOTC, Intervar-R2D2, spatial-dOTC, spatial R2D2, spatial-intervar-dOTC, spatial-intervar-R2D2.

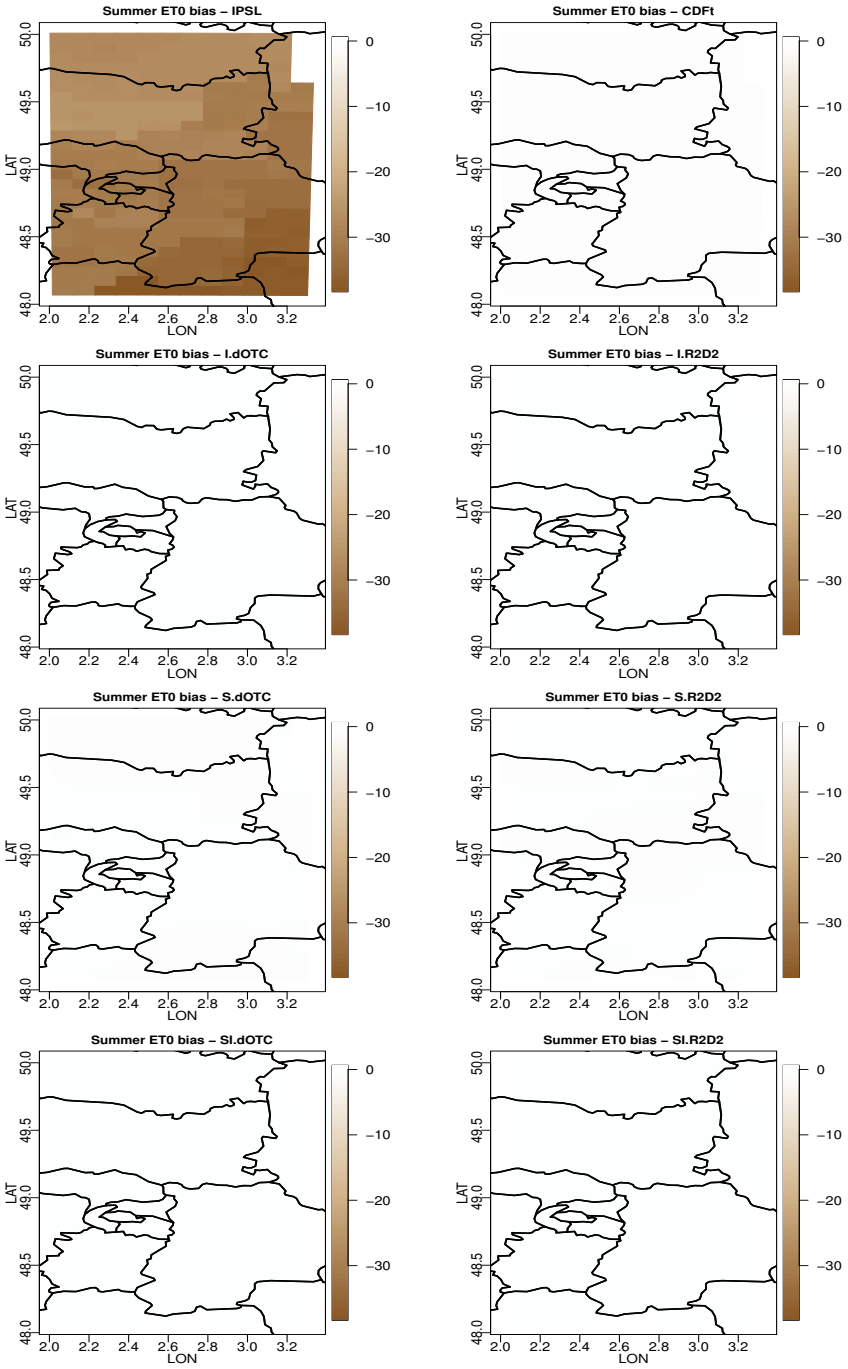

Figure 2.4: For each bias correction method: map of summer ET0 bias to SAFRAN in Ile de France. From top to bottom and from left to right: IPSL (no correction), CDF-t, Intervar-dOTC, Intervar-R2D2, spatial-dOTC, spatial R2D2, spatial-intervar-dOTC, spatial-intervar-R2D2.

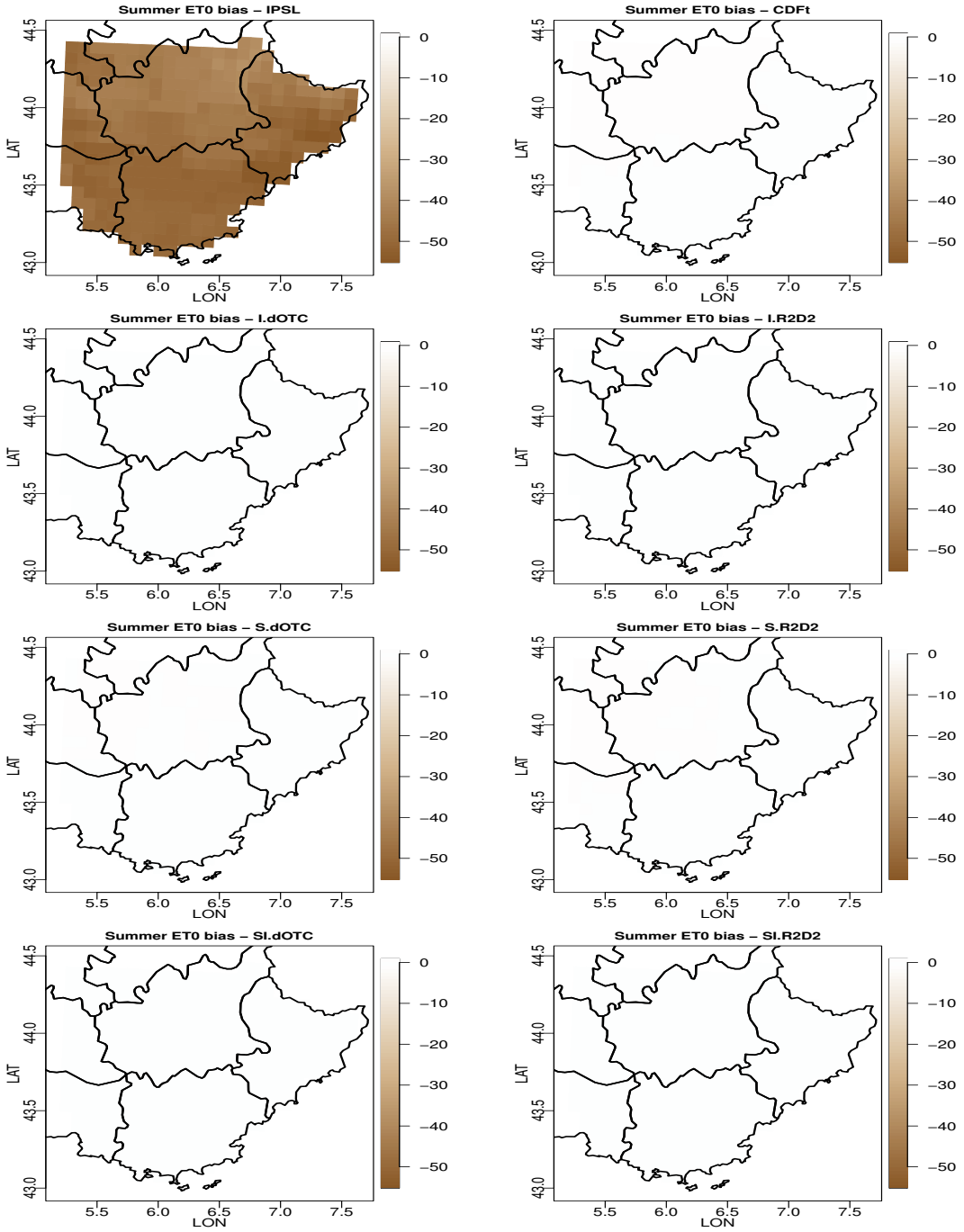

Figure 2.5: For each bias correction method: map of summer ET0 bias to SAFRAN in Provence. From top to bottom and from left to right: IPSL (no correction), CDF-t, Intervar-dOTC, Intervar-R2D2, spatial-dOTC, spatial R2D2, spatial-intervar-dOTC, spatial-intervar-R2D2.

2.5 Maps for variance ratio

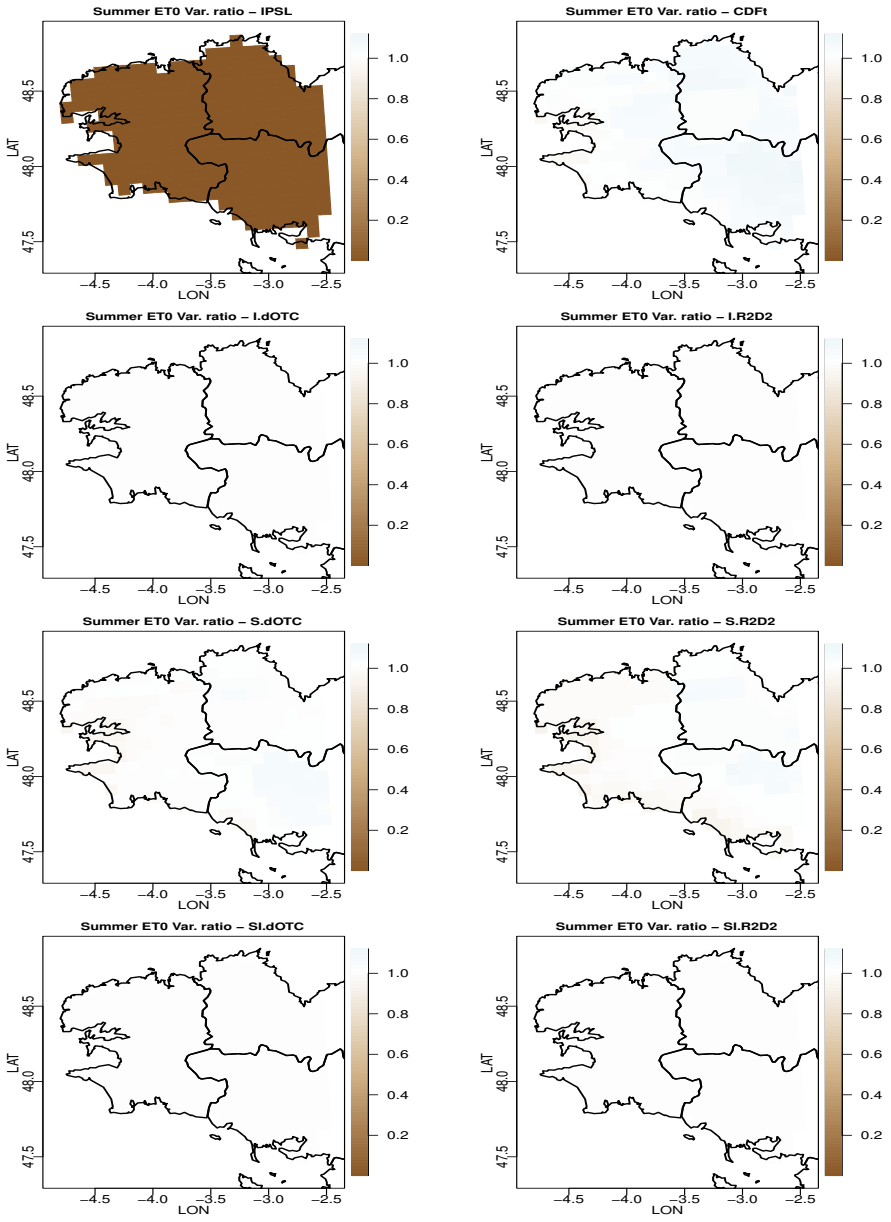

Figure 2.6: For each bias correction method: map of summer ET0 variance divided by summer ET0 variance for SAFRAN in Bretagne. From top to bottom and from left to right: IPSL (no correction), CDF-t, Intervar-dOTC, Intervar-R2D2, spatial-dOTC, spatial R2D2, spatial-intervar-dOTC, spatial-intervar-R2D2.

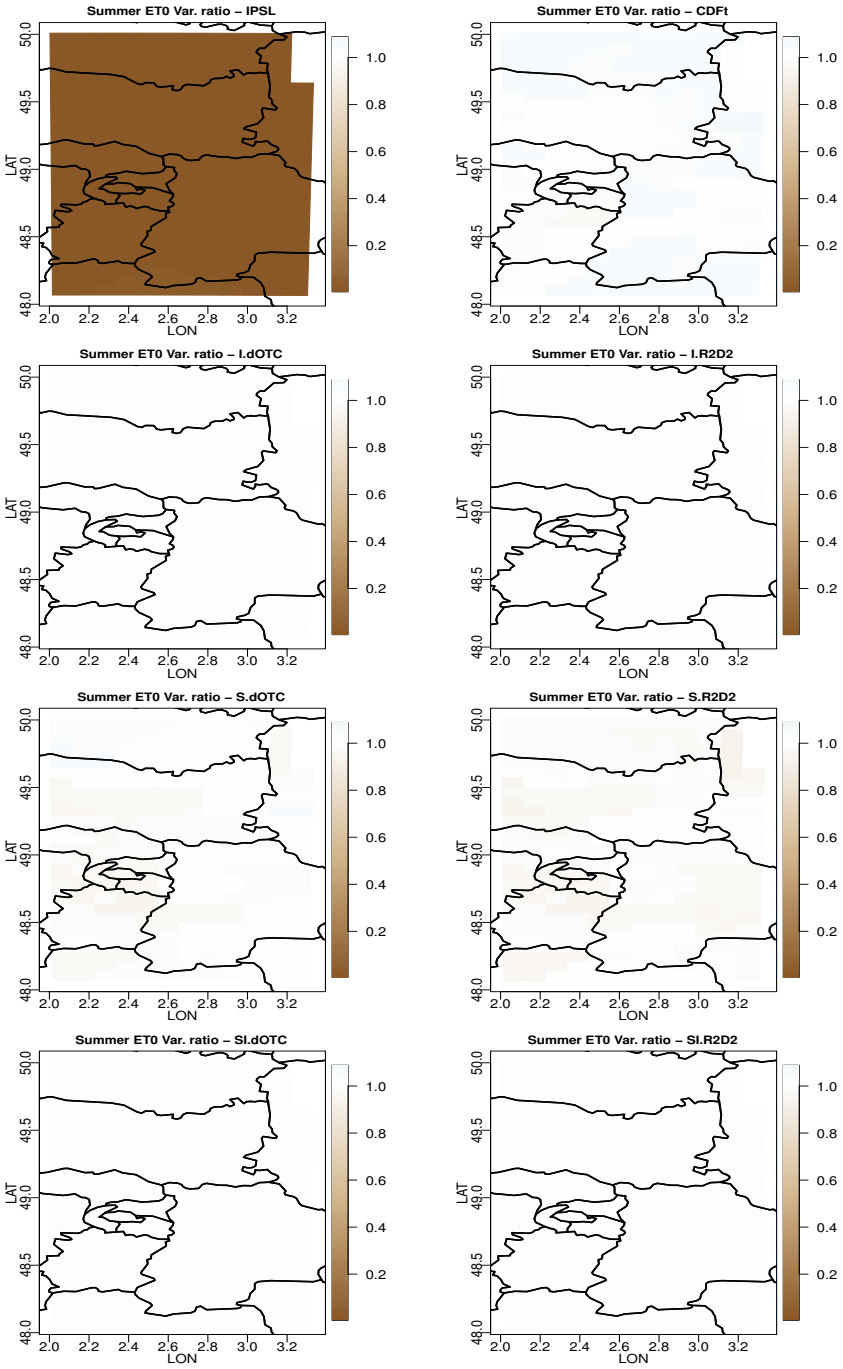

Figure 2.7: For each bias correction method: map of summer ET0 variance divided by summer ET0 variance for SAFRAN in Ile de France. From top to bottom and from left to right: IPSL (no correction), CDF-t, Intervar-dOTC, Intervar-R2D2, spatial-dOTC, spatial R2D2, spatial-intervar-dOTC, spatial-intervar-R2D2.

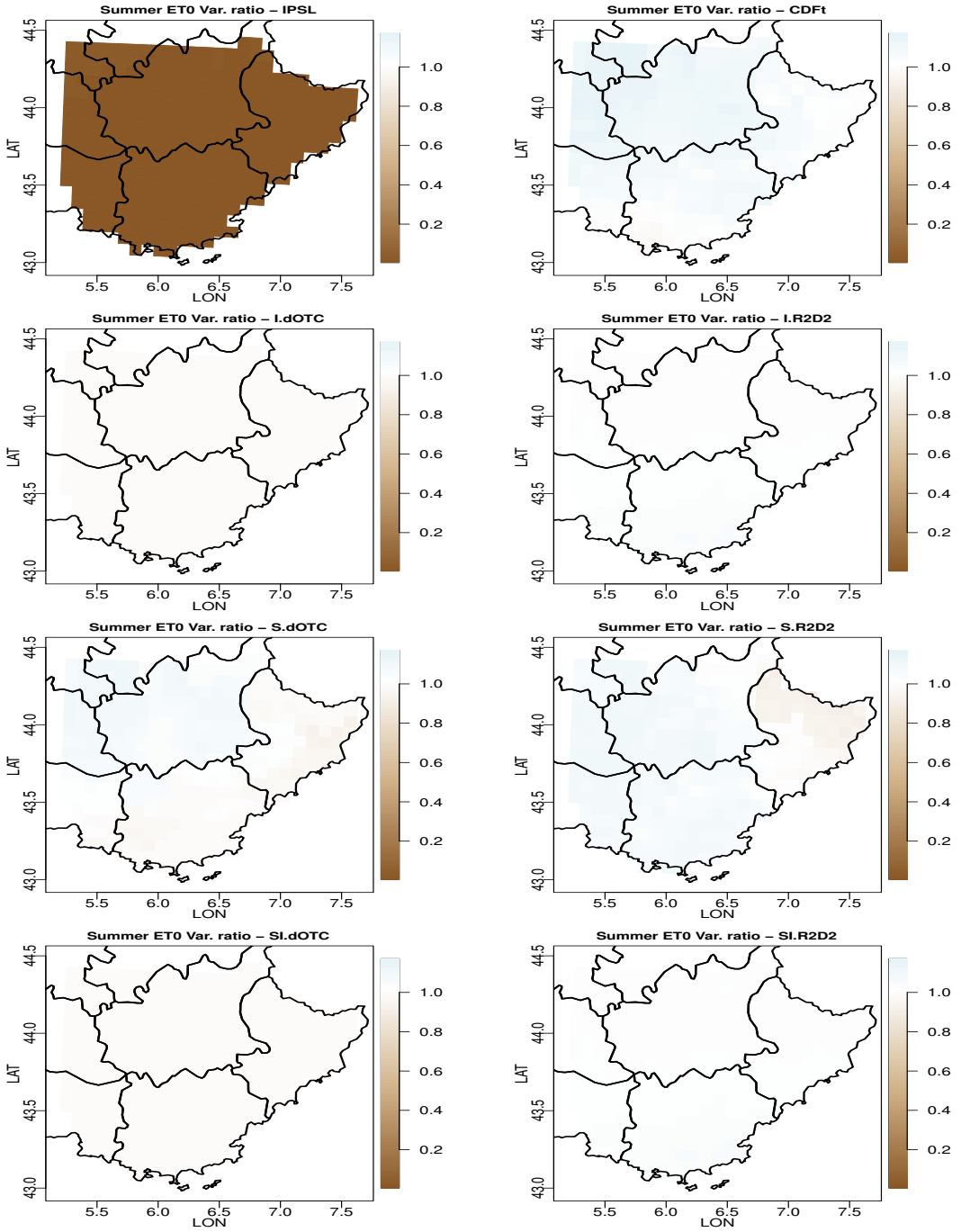

Figure 2.8: For each bias correction method and for: map of summer ET0 variance divided by summer ET0 variance for SAFRAN in Provence. From top to bottom and from left to right: IPSL (no correction), CDF-t, Intervar-dOTC, Intervar-R2D2, spatial-dOTC, spatial R2D2, spatial-intervar-dOTC, spatial-intervar-R2D2.

Chapter 3

ET0 in the future: 2036-2065

ET0 depends only on climate variables. It is therefore identical for all plant models. We consider here the average computed over the meteorological summer, i.e. from June 1st to August 31st.

3.1 Boxplots

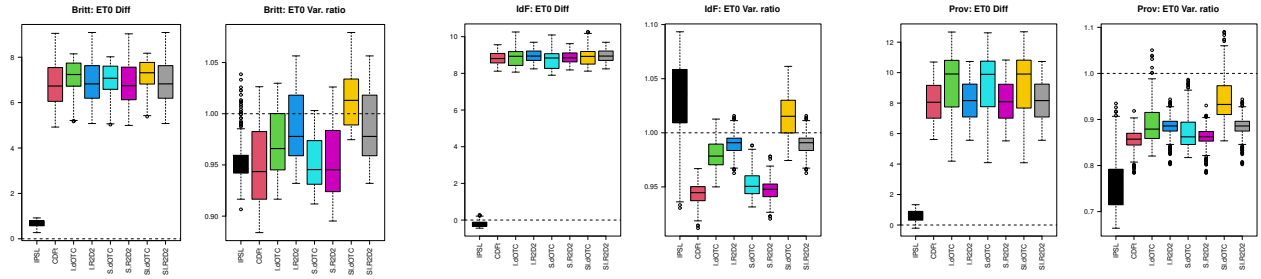

Figure 3.1: Overall summer ET0 difference between future and past and summer ET0's variance ratio between future and past for all bias correction methods. Left column: Bretagne. Middle column: Ile de France. Right column: Provence. In each panel, from left to right: IPSL (no correction), CDF-t, Intervar-dOTC, Intervar-R2D2, spatial-dOTC, spatial R2D2, spatial-intervar-dOTC, spatial-intervar-R2D2.

3.2 Covariances

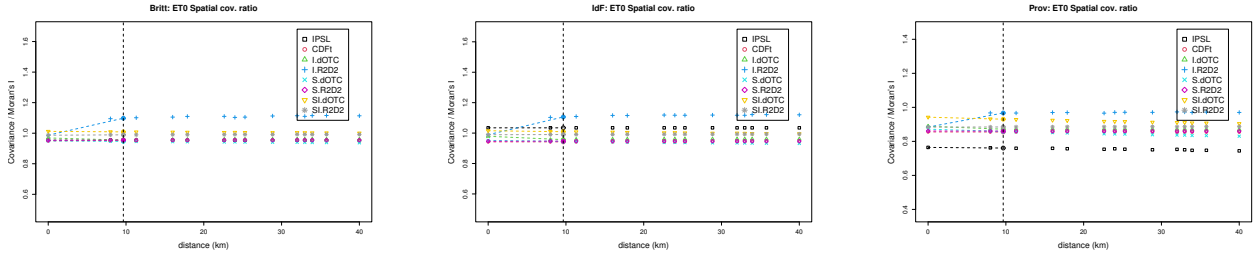

Figure 3.2: Spatial covariance and Moran's I ratio between future and past of summer ET0 for all bias correction methods. Left column: Bretagne. Middle column: Ile de France. Right column: Provence.

3.3 p-values

	IPSL	CDFt	I.dOTC	I.R2D2	S.dOTC	S.R2D2	SI.dOTC	SI.R2D2
p-values for "equality-of-means" tests								
Britt.	0.000	0.000	0.000	0.000	0.000	0.000	0.000	0.000
IdF	0.000	0.000	0.000	0.000	0.000	0.000	0.000	0.000
Prov.	0.000	0.000	0.000	0.000	0.000	0.000	0.000	0.000
p-values for "equality-of-variances" tests								
Britt.	0.000	0.000	**0.219**	**0.560**	0.032	0.060	**0.527**	**0.465**
IdF	0.000	0.000	**0.381**	**0.770**	0.027	0.018	**0.432**	**0.599**
Prov	0.000	0.000	0.000	0.000	0.001	0.000	0.001	0.000
p-values for "equality-of-Moran's I" tests								
Britt.	0.000	0.000	0.000	0.000	0.000	0.000	0.000	0.000
IdF	0.000	0.000	0.000	0.000	0.000	0.000	0.000	0.000
Prov.	0.000	0.000	0.000	0.000	0.000	0.000	0.000	0.000

Table 3.1: Statistical analysis for summer ET0, comparing future to past: p-values for the Welsh t-test of absence of bias on the average (first block); Fisher F-test of equality of variance (second block) and its adaptation to testing the equality of Moran's I (third block). Non rejection at the confidence level 0.90 is indicated in bold font.

3.4 Maps for average differences

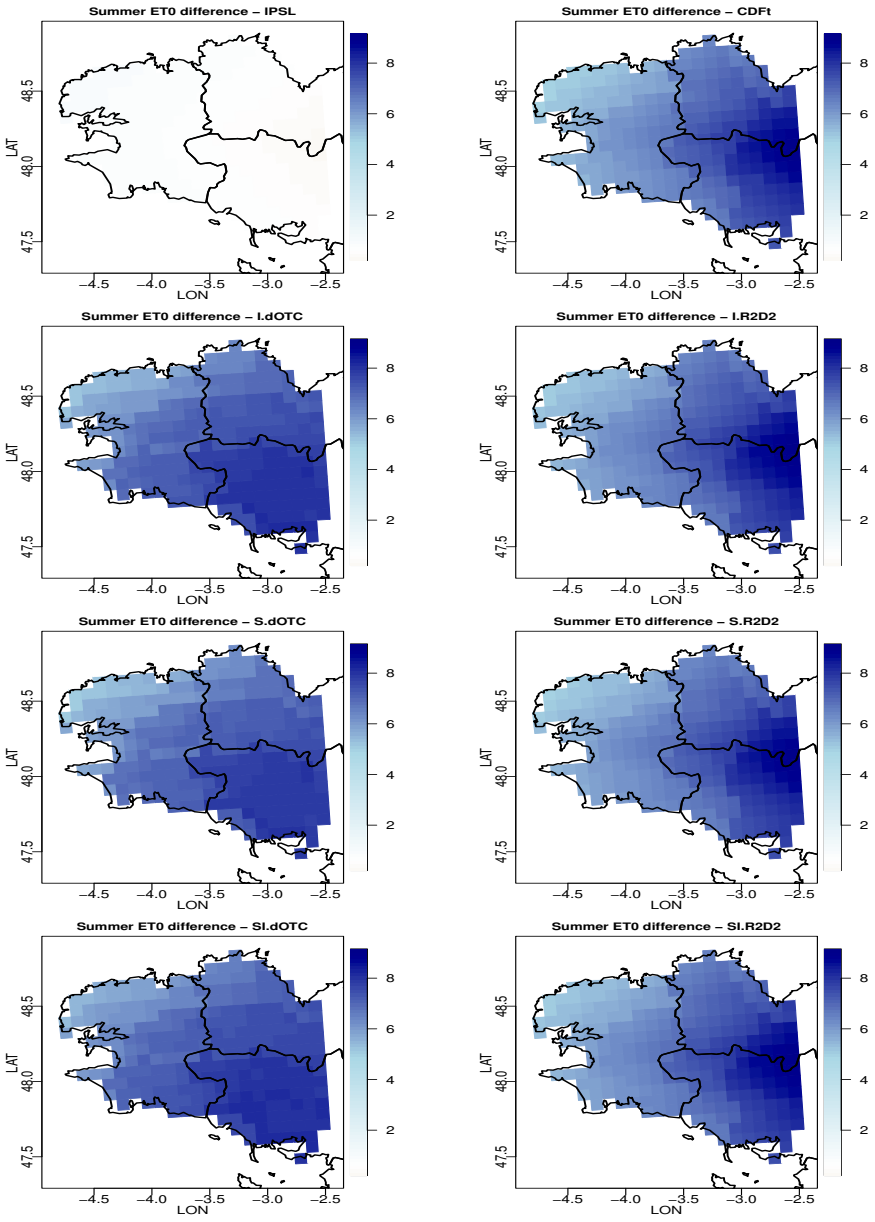

Figure 3.3: For each bias correction method: map of summer ET0 difference between future and past in Brittany. From top to bottom and from left to right: IPSL (no correction), CDF-t, Intervar-dOTC, Intervar-R2D2, spatial-dOTC, spatial R2D2, spatial-intervar-dOTC, spatial-intervar-R2D2.

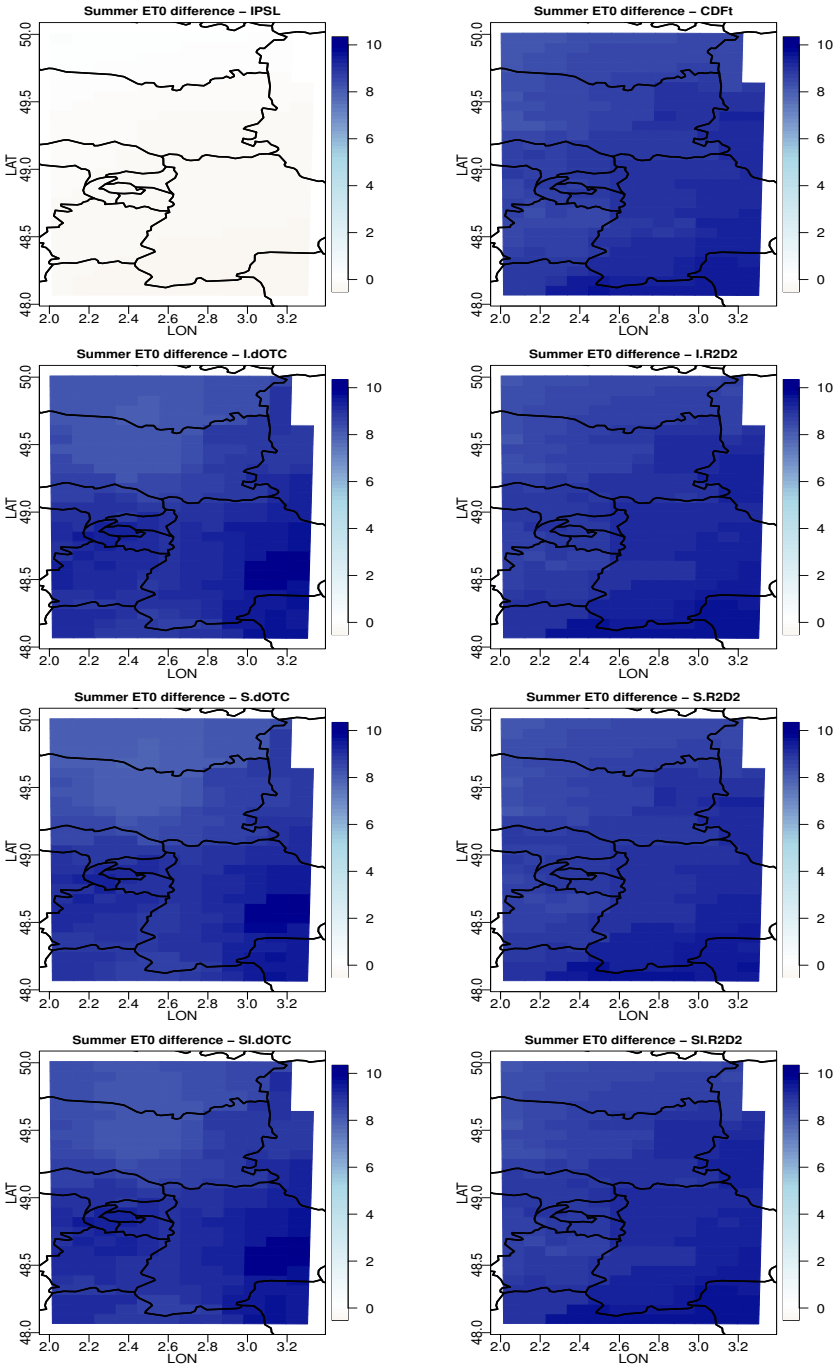

Figure 3.4: For each bias correction method: map of summer ET0 difference between future and past in Ile de France. From top to bottom and from left to right: IPSL (no correction), CDF-t, Intervar-dOTC, Intervar-R2D2, spatial-dOTC, spatial R2D2, spatial-intervar-dOTC, spatial-intervar-R2D2.

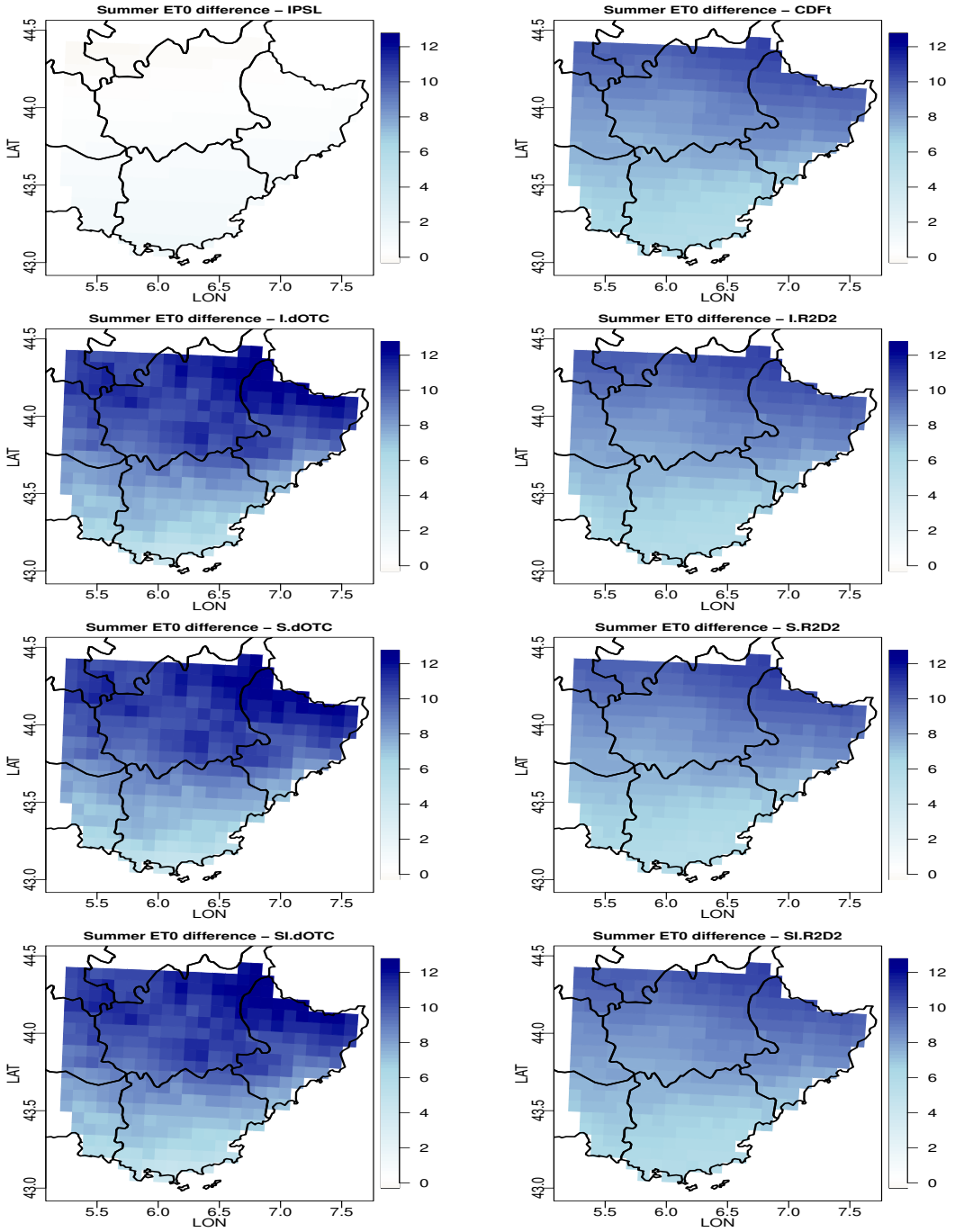

Figure 3.5: For each bias correction method: map of summer ET0 difference between future and past in Provence. From top to bottom and from left to right: IPSL (no correction), CDF-t, Intervar-dOTC, Intervar-R2D2, spatial-dOTC, spatial R2D2, spatial-intervar-dOTC, spatial-intervar-R2D2.

3.5 Maps for variance ratio

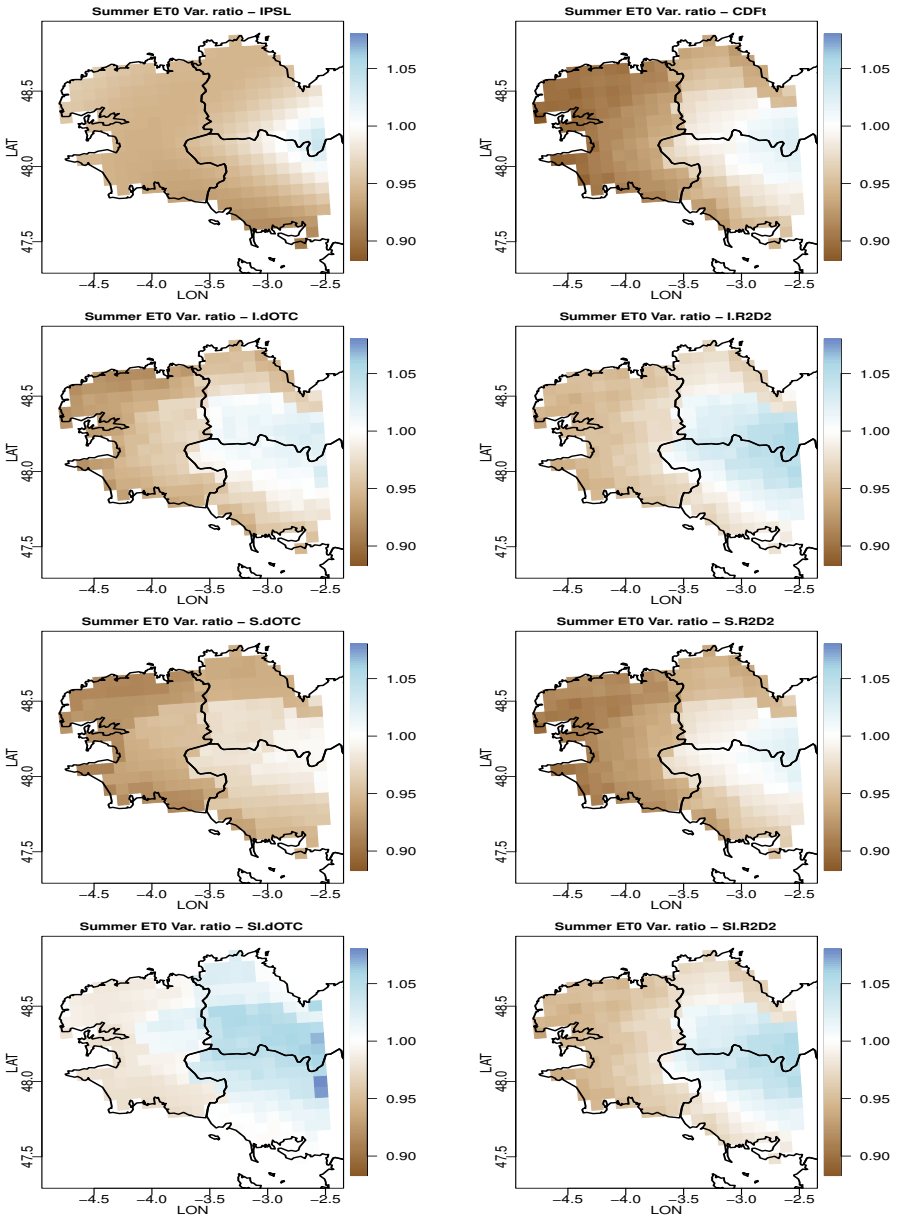

Figure 3.6: For each bias correction method: map of summer ET0 variance ratio between future and past in Brittany. From top to bottom and from left to right: IPSL (no correction), CDF-t, Intervar-dOTC, Intervar-R2D2, spatial-dOTC, spatial R2D2, spatial-intervar-dOTC, spatial-intervar-R2D2.

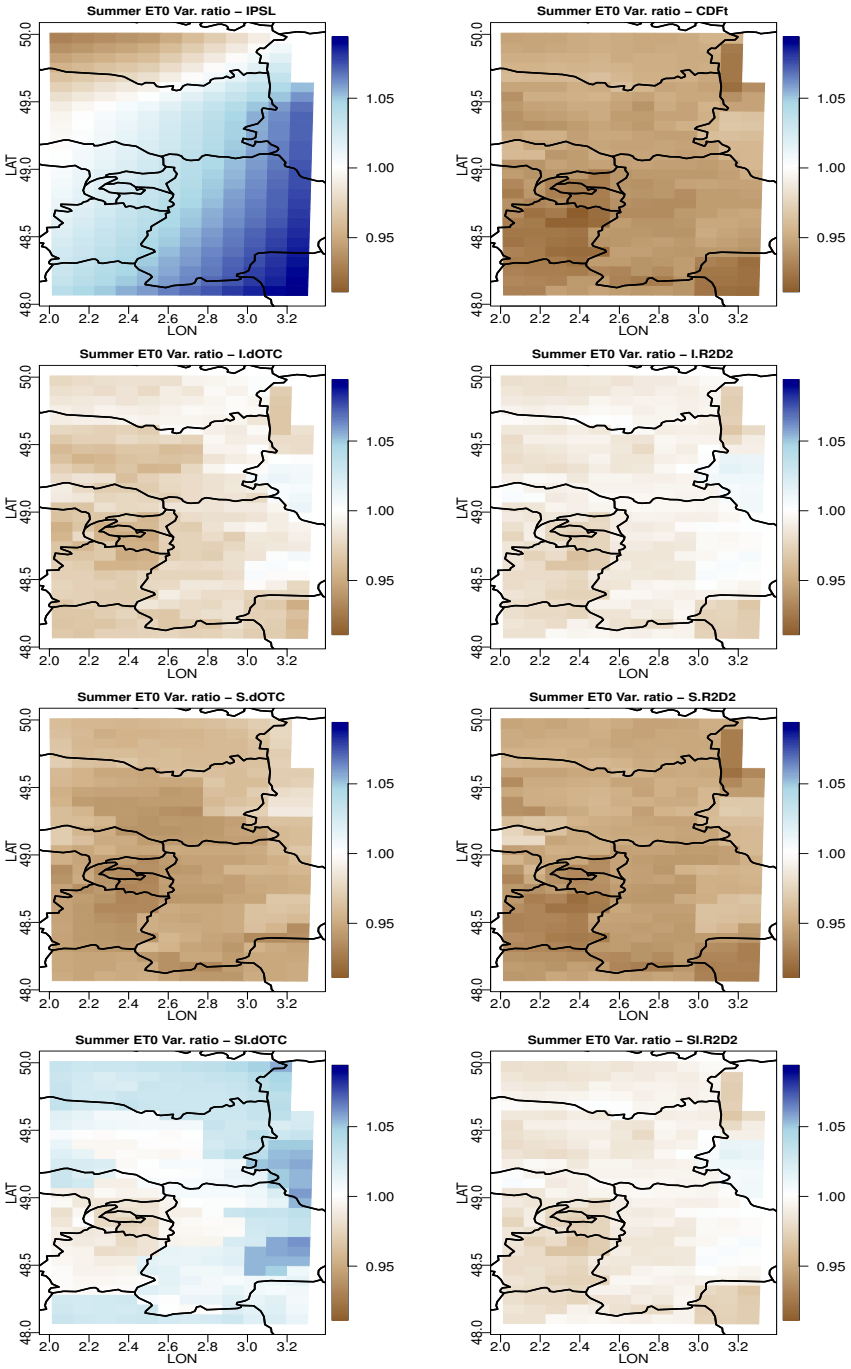

Figure 3.7: For each bias correction method: map of summer ET0 variance ratio between future and past in Ile de France. From top to bottom and from left to right: IPSL (no correction), CDF-t, Intervar-dOTC, Intervar-R2D2, spatial-dOTC, spatial R2D2, spatial-intervar-dOTC, spatial-intervar-R2D2.

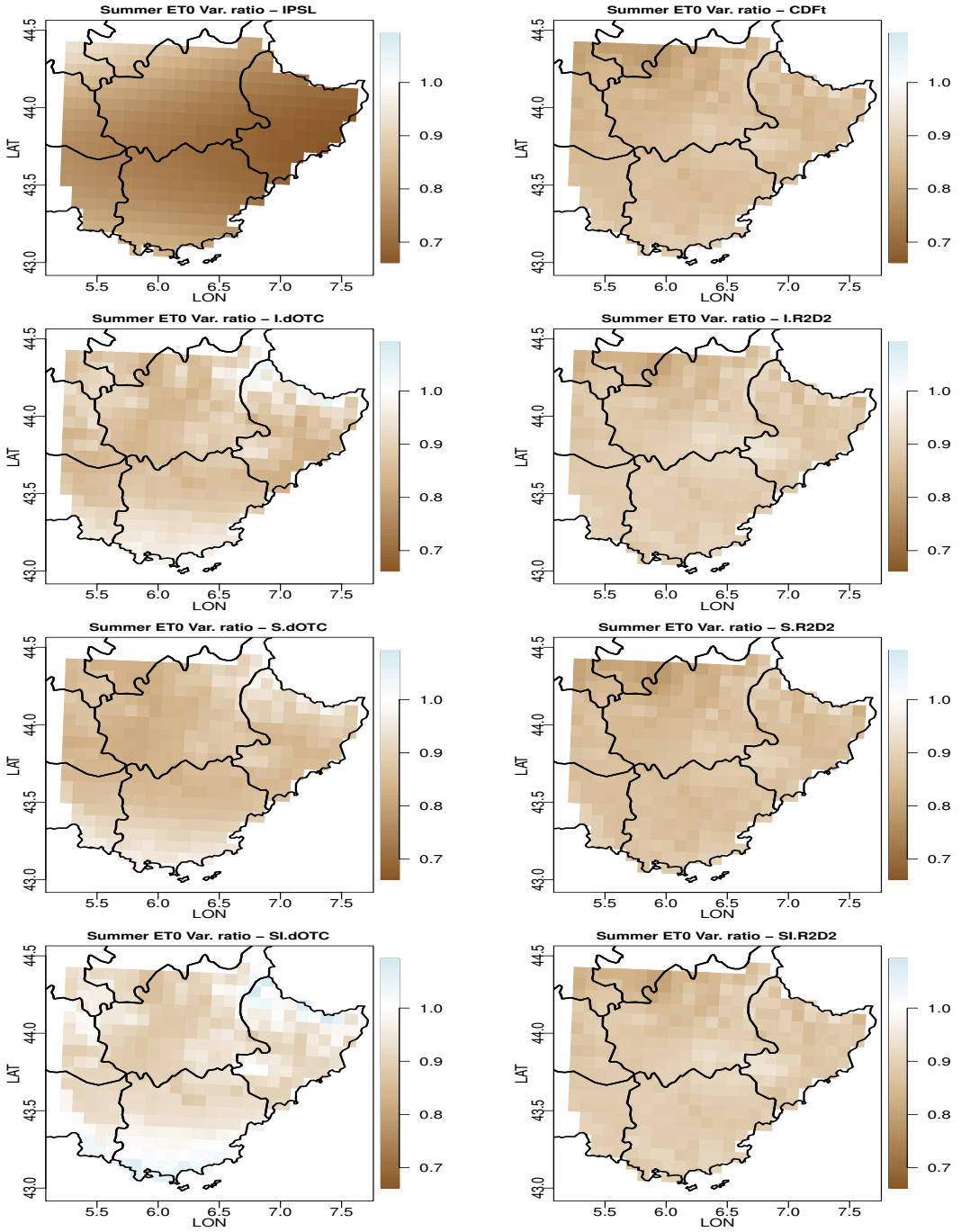

Figure 3.8: For each bias correction method and for: map of summer ET0 variance ratio between future and past in Provence. From top to bottom and from left to right: IPSL (no correction), CDF-t, Intervar-dOTC, Intervar-R2D2, spatial-dOTC, spatial R2D2, spatial-intervar-dOTC, spatial-intervar-R2D2.

Chapter 4

Pheno: FLO in the past: 1984-2015

FLO is the Julian day for the third phenology stage computed as described in Caubel et al. (2015). In some cases, FLO is not attained, in which case a NaN value is produced. All statistics are computed after removing NaN values.

4.1 Boxplots

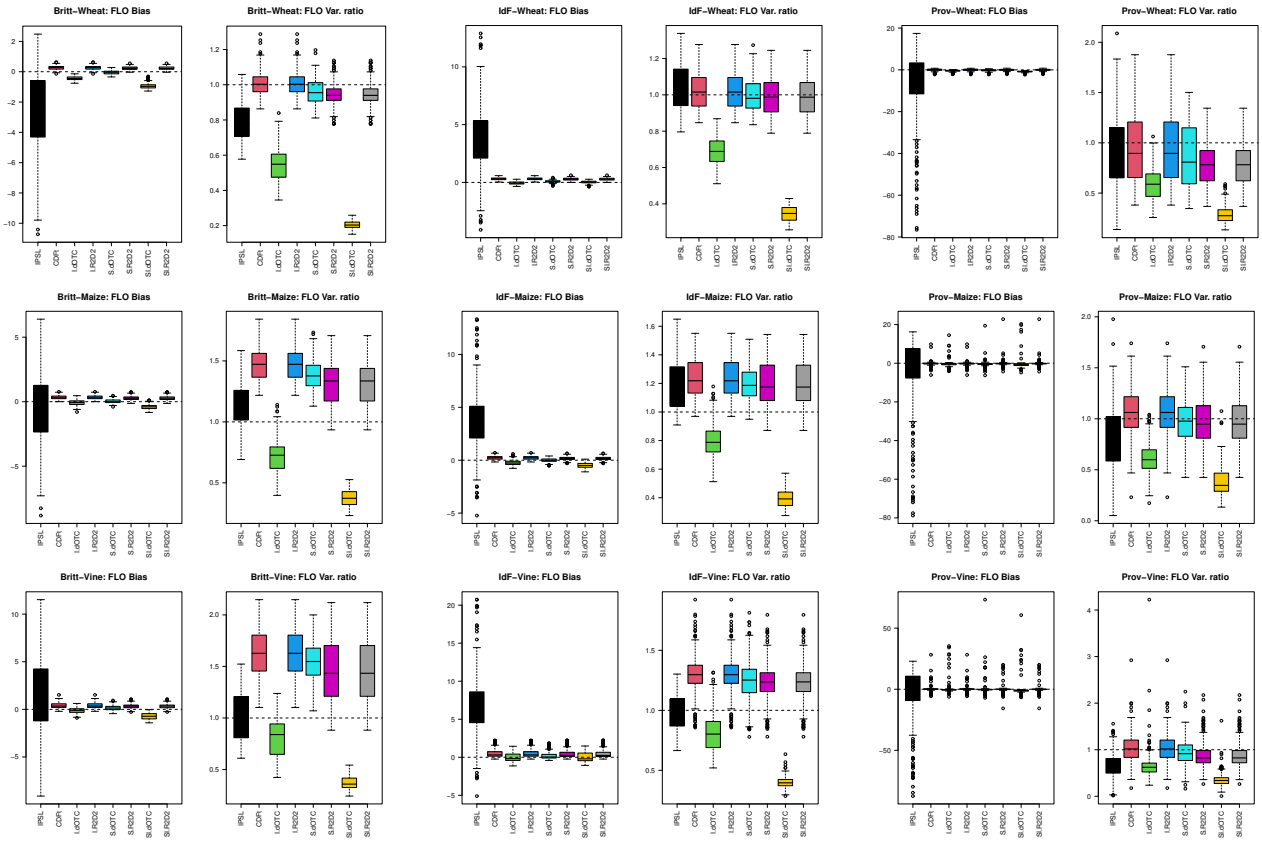

Figure 4.1: Overall FLO bias to SAFRAN and FLO's variance ratio to SAFRAN for all bias correction methods. Top row: wheat. Middle row: Maize. Bottom row: Vine. Left column: Bretagne. Middle column: Ile de France. Right column: Provence. In each panel, from left to right: IPSL (no correction), CDF-t, Intervar-dOTC, Intervar-R2D2, spatial-dOTC, spatial R2D2, spatial-intervar-dOTC, spatial-intervar-R2D2.

4.2 Covariances

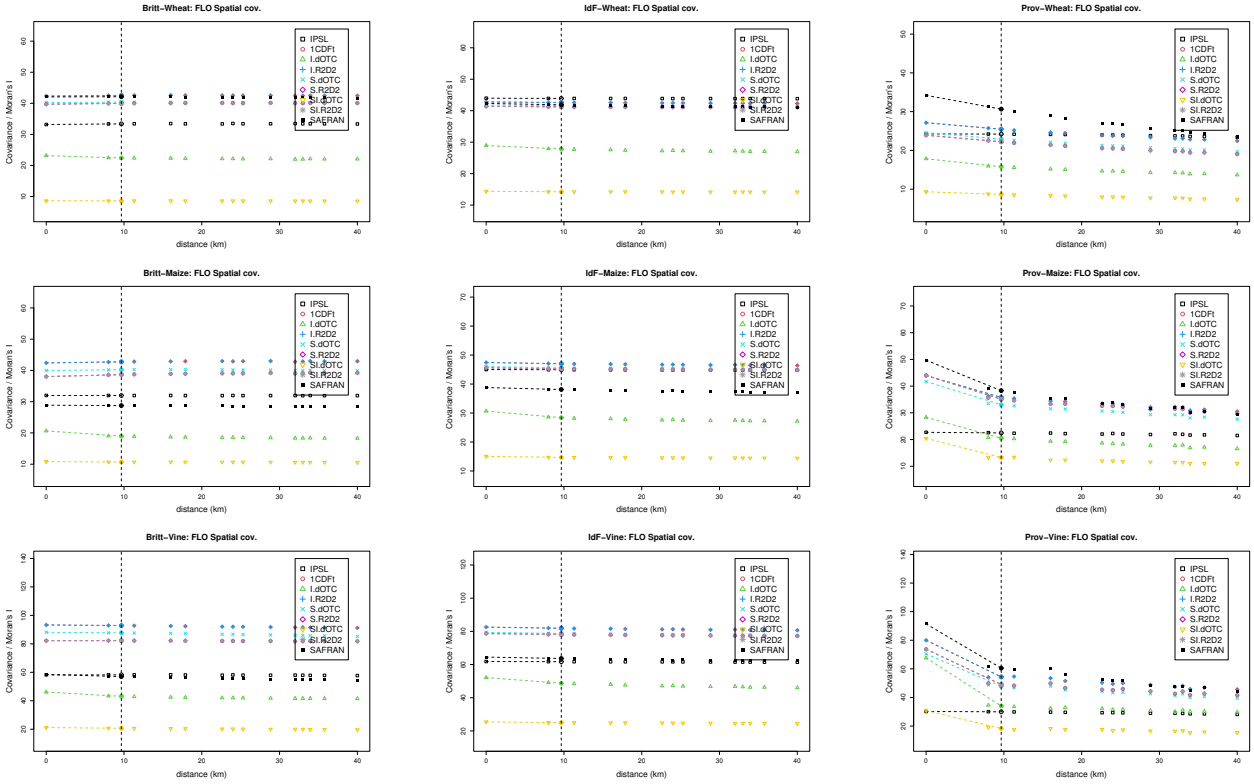

Figure 4.2: Spatial covariance and Moran's I of FLO in the past for all bias correction methods. Top row: wheat. Middle row: Maize. Bottom row: Vine. Left column: Bretagne. Middle column: Ile de France. Right column: Provence.

4.3 p-values

		IPSL	CDFt	I.dOTC	I.R2D2	S.dOTC	S.R2D2	SI.dOTC	SI.R2D2
p-values for "equality-of-means" tests									
Britt.	wheat	0.052	**0.856**	**0.676**	**0.856**	**0.976**	**0.872**	**0.371**	**0.872**
	maize	**0.626**	**0.788**	**0.909**	**0.788**	**0.981**	**0.828**	**0.578**	**0.828**
	vine	**0.363**	**0.807**	**0.906**	**0.807**	**0.931**	**0.850**	**0.465**	**0.850**
IdF	wheat	0.016	**0.820**	**0.953**	**0.820**	**0.953**	**0.837**	**0.978**	**0.837**
	maize	0.009	**0.866**	**0.765**	**0.866**	**1.000**	**0.897**	**0.583**	**0.897**
	vine	0.000	**0.759**	**0.993**	**0.759**	**0.891**	**0.785**	**0.988**	**0.785**
Prov.	wheat	0.000	**0.831**	0.001	**0.831**	**0.243**	**0.894**	0.000	**0.894**
	maize	0.000	**0.106**	0.003	**0.106**	0.018	**0.114**	0.004	**0.114**
	vine	0.001	0.000	0.000	0.000	0.001	0.002	0.000	0.002
p-values for "equality-of-variances" tests									
Britt.	wheat	**0.439**	**0.973**	0.006	**0.973**	**0.899**	**0.869**	0.000	**0.869**
	maize	**0.699**	**0.160**	0.056	**0.160**	**0.214**	**0.334**	0.000	**0.334**
	vine	**1.000**	0.062	**0.159**	0.062	**0.110**	**0.195**	0.000	**0.195**
IdF	wheat	**0.887**	**0.961**	0.096	**0.961**	**0.975**	**0.951**	0.000	**0.951**
	maize	**0.594**	**0.452**	**0.195**	**0.452**	**0.520**	**0.548**	0.000	**0.548**
	vine	**0.900**	**0.341**	**0.210**	**0.341**	**0.405**	**0.446**	0.000	**0.446**
Prov.	wheat	0.018	0.002	0.000	0.002	0.000	0.000	0.000	0.000
	maize	0.000	**0.368**	0.000	**0.368**	**0.117**	**0.397**	0.000	**0.397**
	vine	0.000	0.058	0.000	0.058	0.014	0.033	0.000	0.033
p-values for "equality-of-Moran's I" tests									
Britt.	wheat	**0.448**	**0.964**	0.003	**0.964**	**0.901**	**0.882**	0.000	**0.882**
	maize	**0.688**	**0.147**	0.017	**0.147**	**0.199**	**0.299**	0.000	**0.299**
	vine	**0.918**	0.051	0.099	0.051	0.093	**0.163**	0.000	**0.163**
IdF	wheat	**0.865**	**0.947**	0.072	**0.947**	**0.990**	**0.968**	0.000	**0.968**
	maize	**0.556**	**0.432**	**0.105**	**0.432**	**0.502**	**0.526**	0.000	**0.526**
	vine	**0.933**	**0.333**	**0.115**	**0.333**	**0.395**	**0.434**	0.000	**0.434**
Prov.	wheat	**0.101**	0.012	0.000	0.012	0.000	0.000	0.000	0.000
	maize	0.006	**0.655**	0.000	**0.655**	**0.209**	**0.577**	0.000	**0.577**
	vine	0.000	**0.282**	0.000	**0.282**	0.078	**0.115**	0.000	**0.115**

Table 4.1: Statistical analysis for FLO in the past: p-values for the Welsh t-test of absence of bias on the average (first block); Fisher F-test of equality of variance (second block) and its adaptation to testing the equality of Moran's I (third block). Non rejection at the confidence level 0.90 is indicated in bold font.

4.4 Maps for bias

4.4.1 Wheat

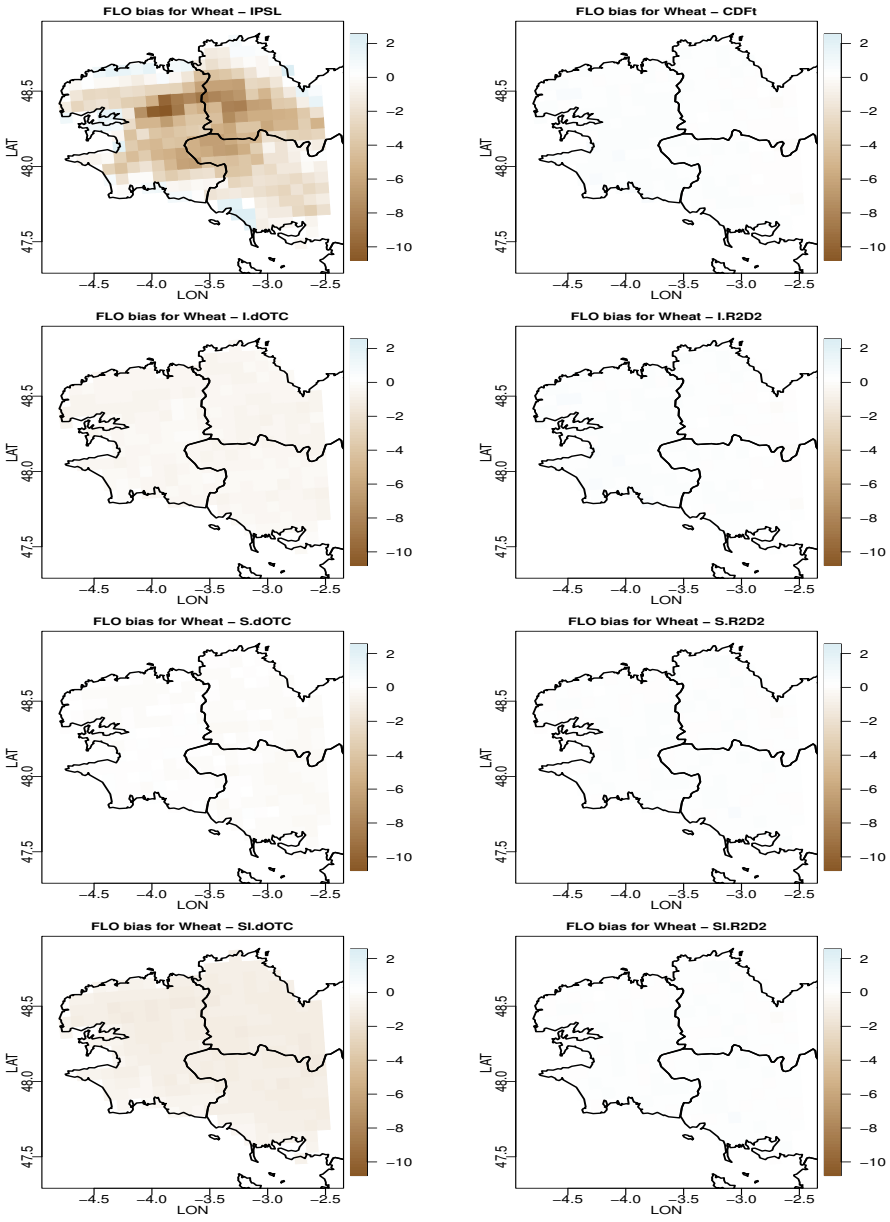

Figure 4.3: For each bias correction method and for wheat: map of FLO bias to SAFRAN in Brittany. From top to bottom and from left to right: IPSL (no correction), CDF-t, Intervar-dOTC, Intervar-R2D2, spatial-dOTC, spatial R2D2, spatial-intervar-dOTC, spatial-intervar-R2D2.

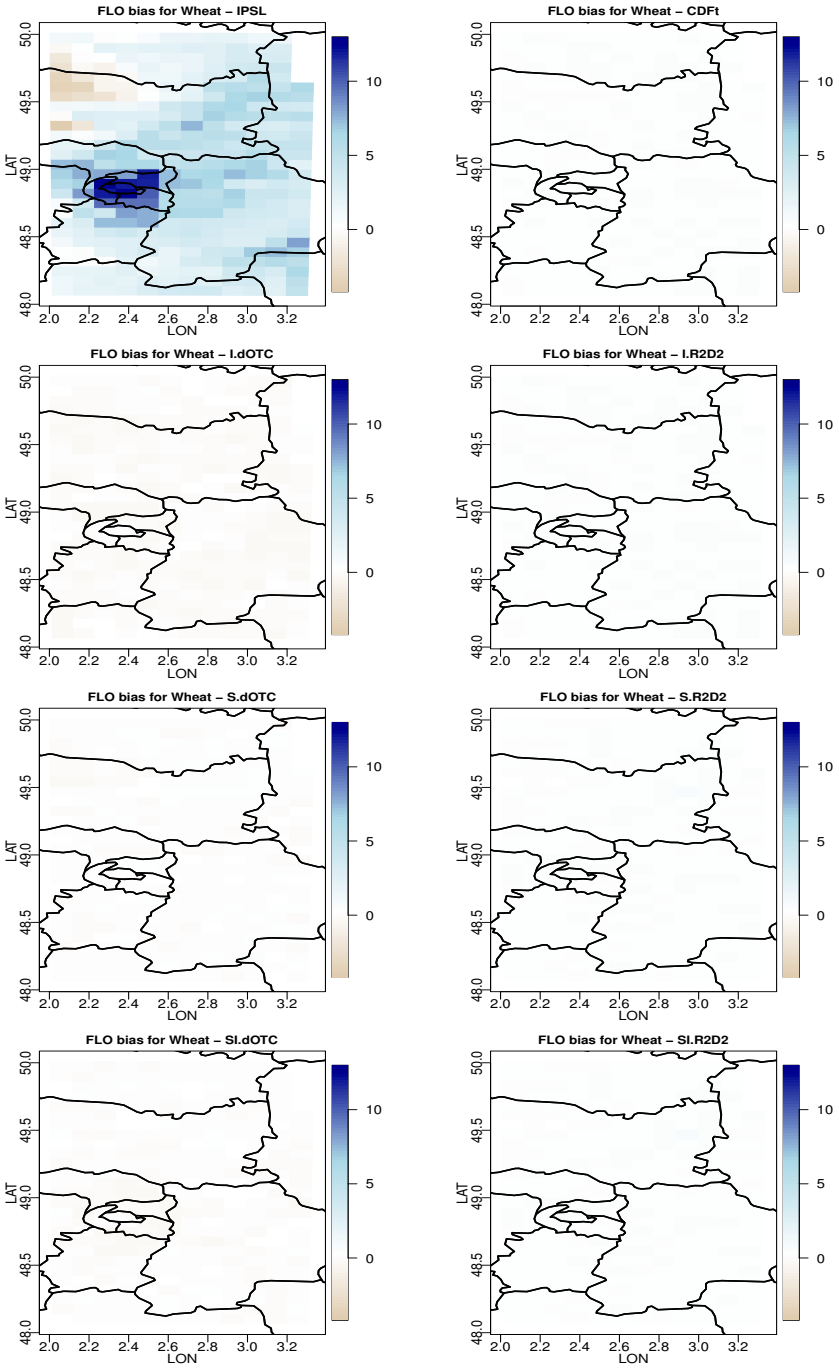

Figure 4.4: For each bias correction method and for wheat: map of FLO bias to SAFRAN in Ile de France. From top to bottom and from left to right: IPSL (no correction), CDF-t, Intervar-dOTC, Intervar-R2D2, spatial-dOTC, spatial R2D2, spatial-intervar-dOTC, spatial-intervar-R2D2.

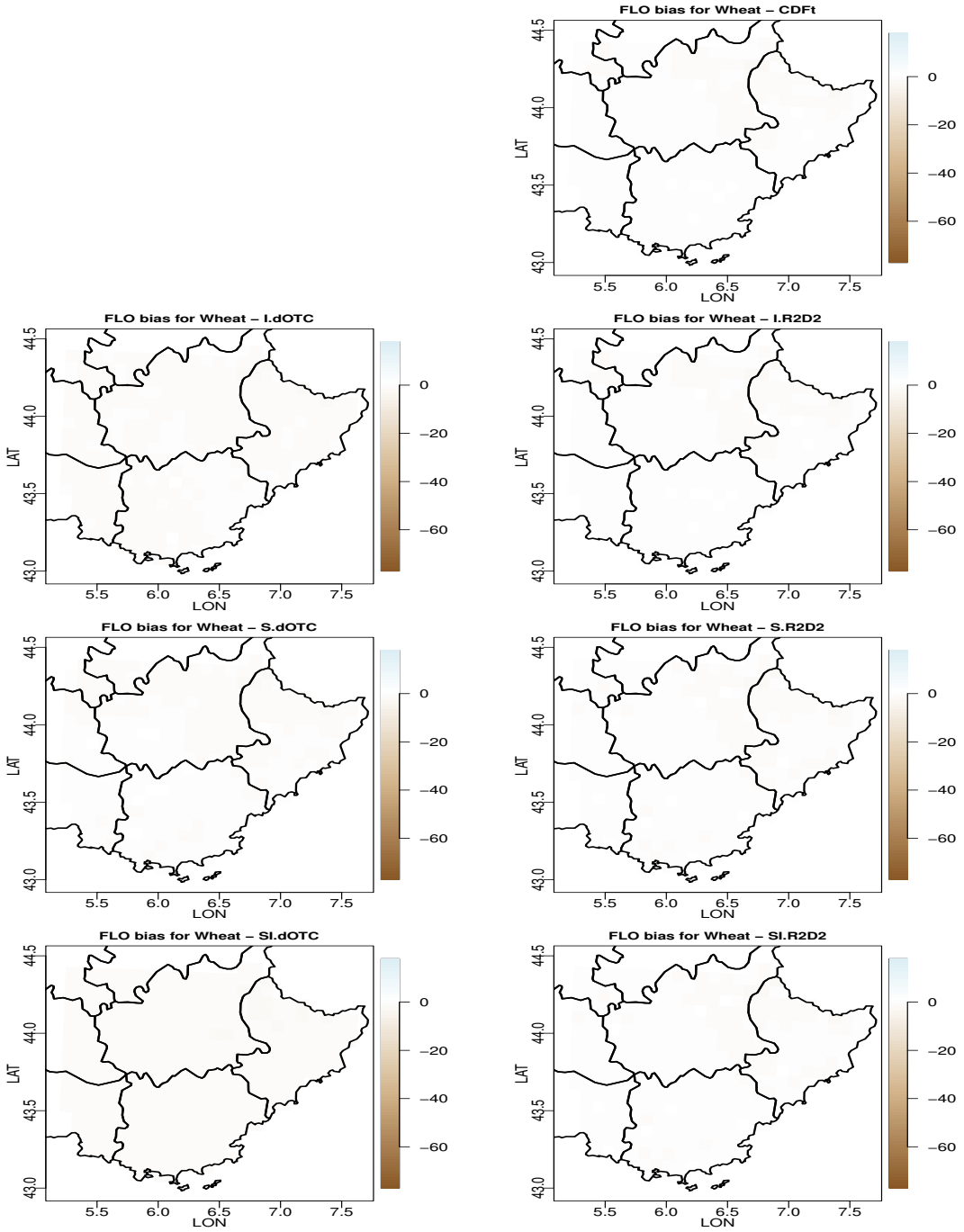

Figure 4.5: For each bias correction method and for wheat: map of FLO bias to SAFRAN in Provence. From top to bottom and from left to right: IPSL (no correction), CDF-t, Intervar-dOTC, Intervar-R2D2, spatial-dOTC, spatial R2D2, spatial-intervar-dOTC, spatial-intervar-R2D2.

4.4.2 Maize

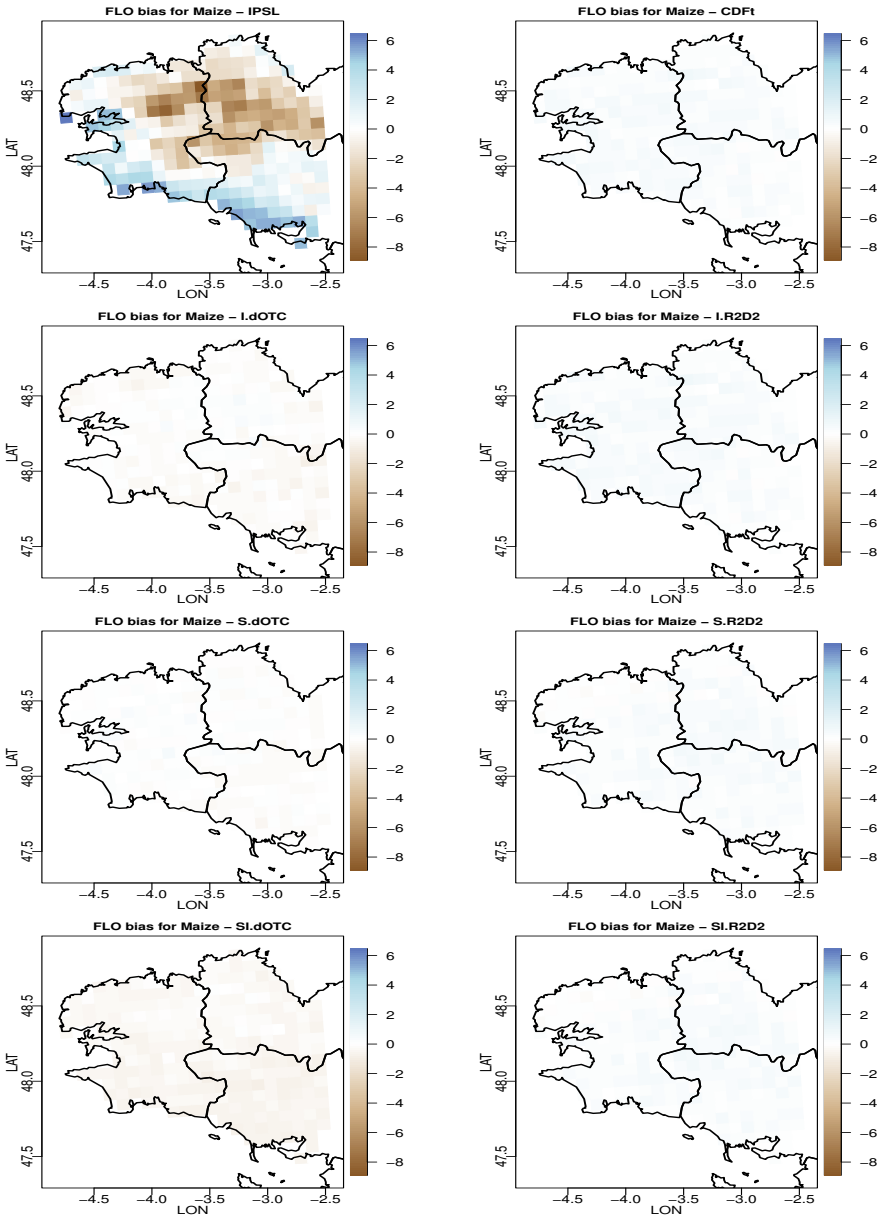

Figure 4.6: For each bias correction method and for maize: map of FLO bias to SAFRAN in Brittany. From top to bottom and from left to right: IPSL (no correction), CDF-t, Intervar-dOTC, Intervar-R2D2, spatial-dOTC, spatial R2D2, spatial-intervar-dOTC, spatial-intervar-R2D2.

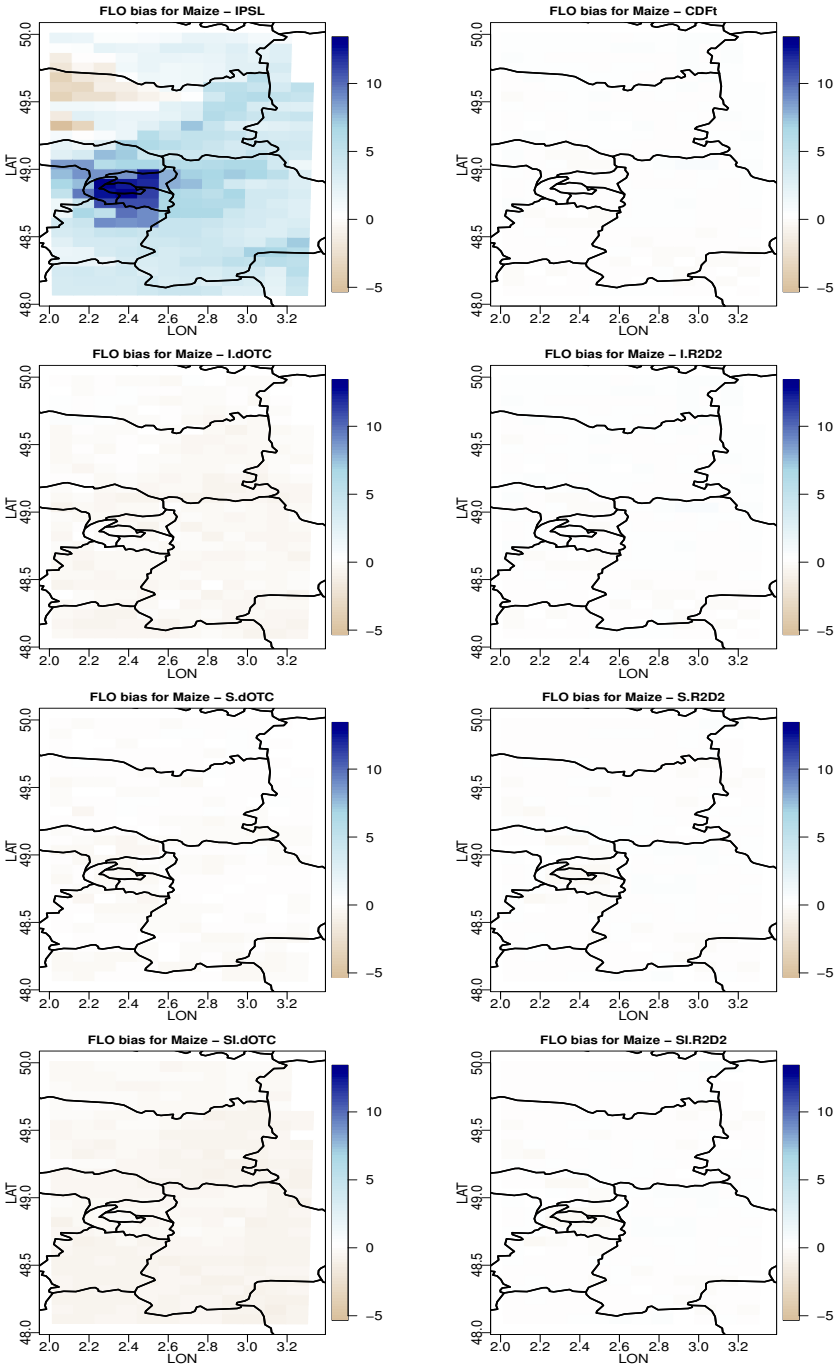

Figure 4.7: For each bias correction method and for maize: map of FLO bias to SAFRAN in Ile de France. From top to bottom and from left to right: IPSL (no correction), CDF-t, Intervar-dOTC, Intervar-R2D2, spatial-dOTC, spatial R2D2, spatial-intervar-dOTC, spatial-intervar-R2D2.

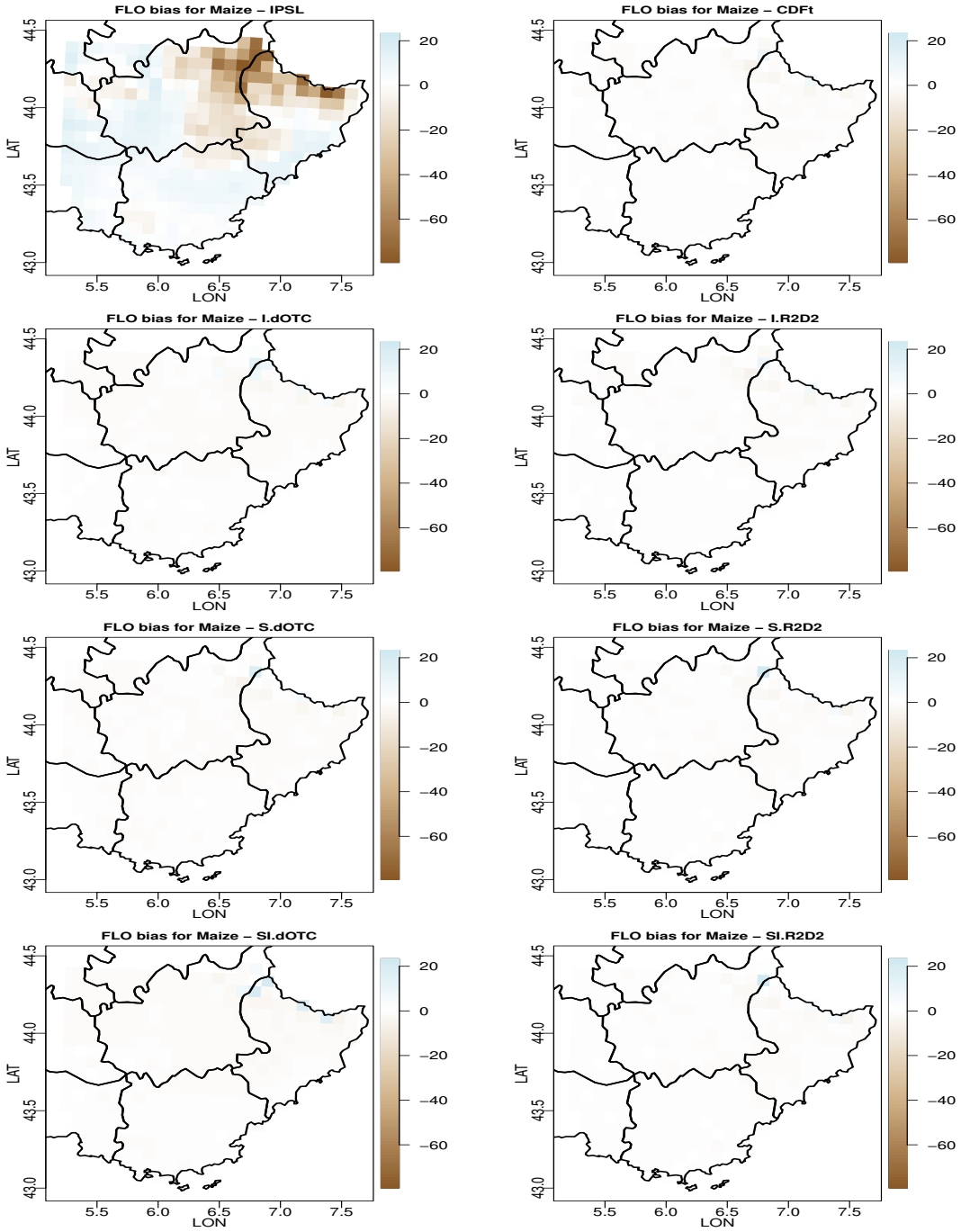

Figure 4.8: For each bias correction method and for maize: map of FLO bias to SAFRAN in Provence. From top to bottom and from left to right: IPSL (no correction), CDF-t, Intervar-dOTC, Intervar-R2D2, spatial-dOTC, spatial R2D2, spatial-intervar-dOTC, spatial-intervar-R2D2.

4.4.3 Vine

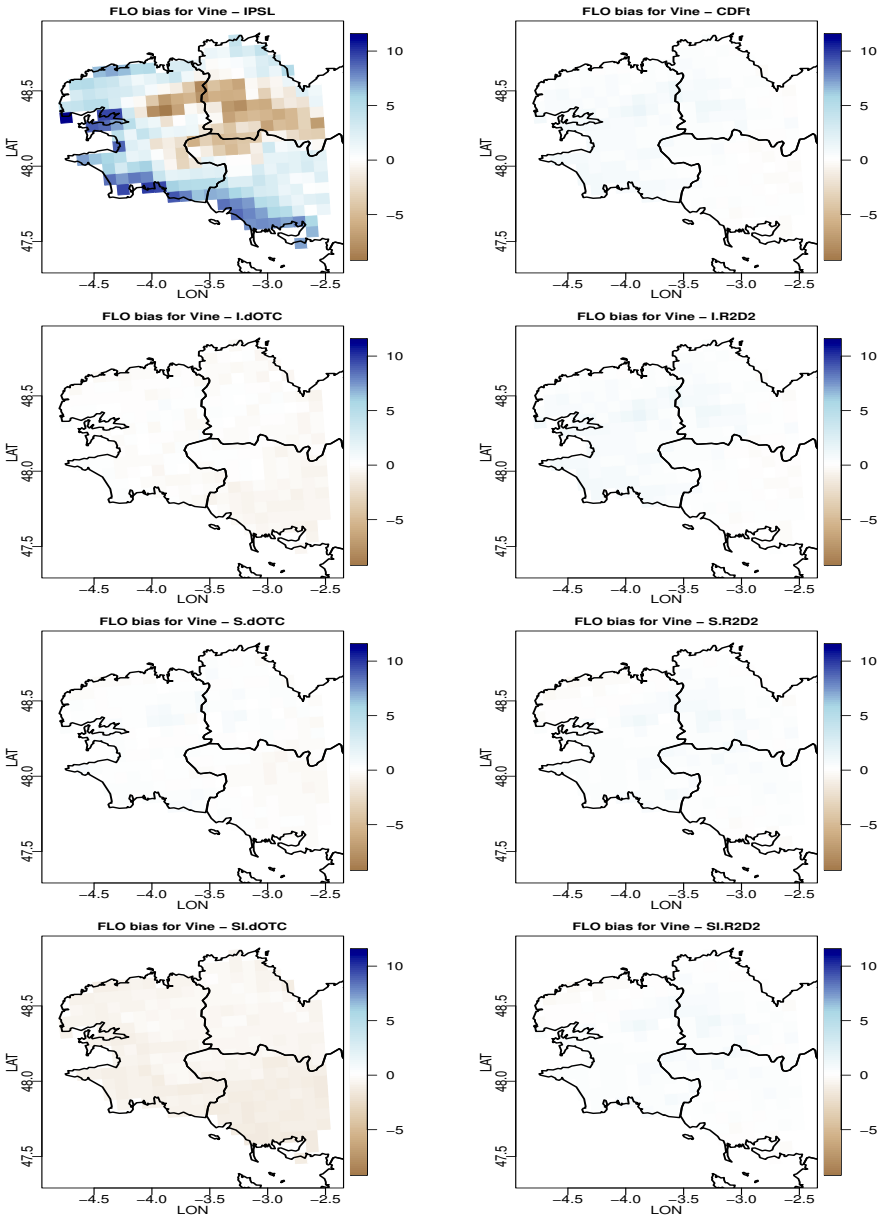

Figure 4.9: For each bias correction method and for vine: map of FLO bias to SAFRAN in Brittany. From top to bottom and from left to right: IPSL (no correction), CDF-t, Intervar-dOTC, Intervar-R2D2, spatial-dOTC, spatial R2D2, spatial-intervar-dOTC, spatial-intervar-R2D2.

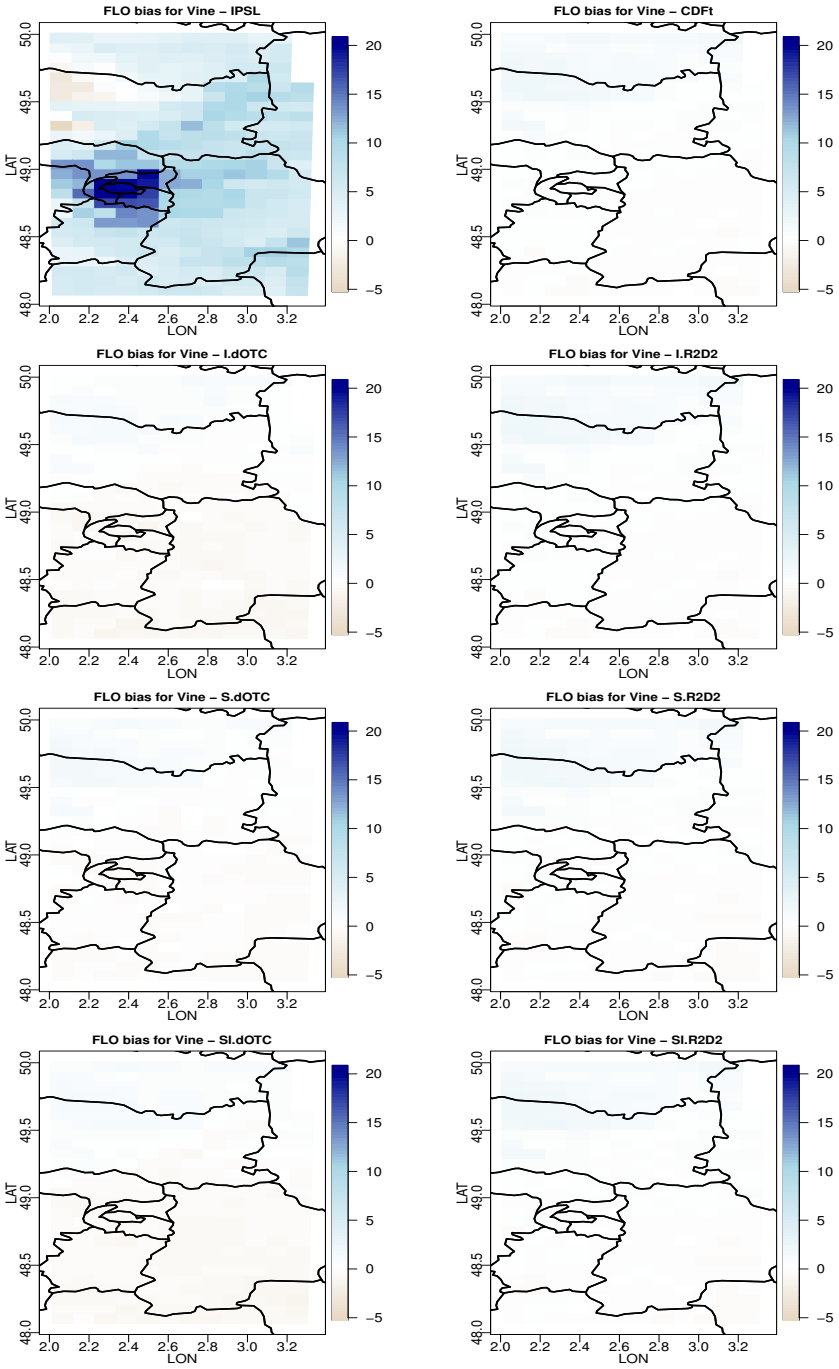

Figure 4.10: For each bias correction method and for vine: map of FLO bias to SAFRAN in Ile de France. From top to bottom and from left to right: IPSL (no correction), CDF-t, Intervar-dOTC, Intervar-R2D2, spatial-dOTC, spatial R2D2, spatial-intervar-dOTC, spatial-intervar-R2D2.

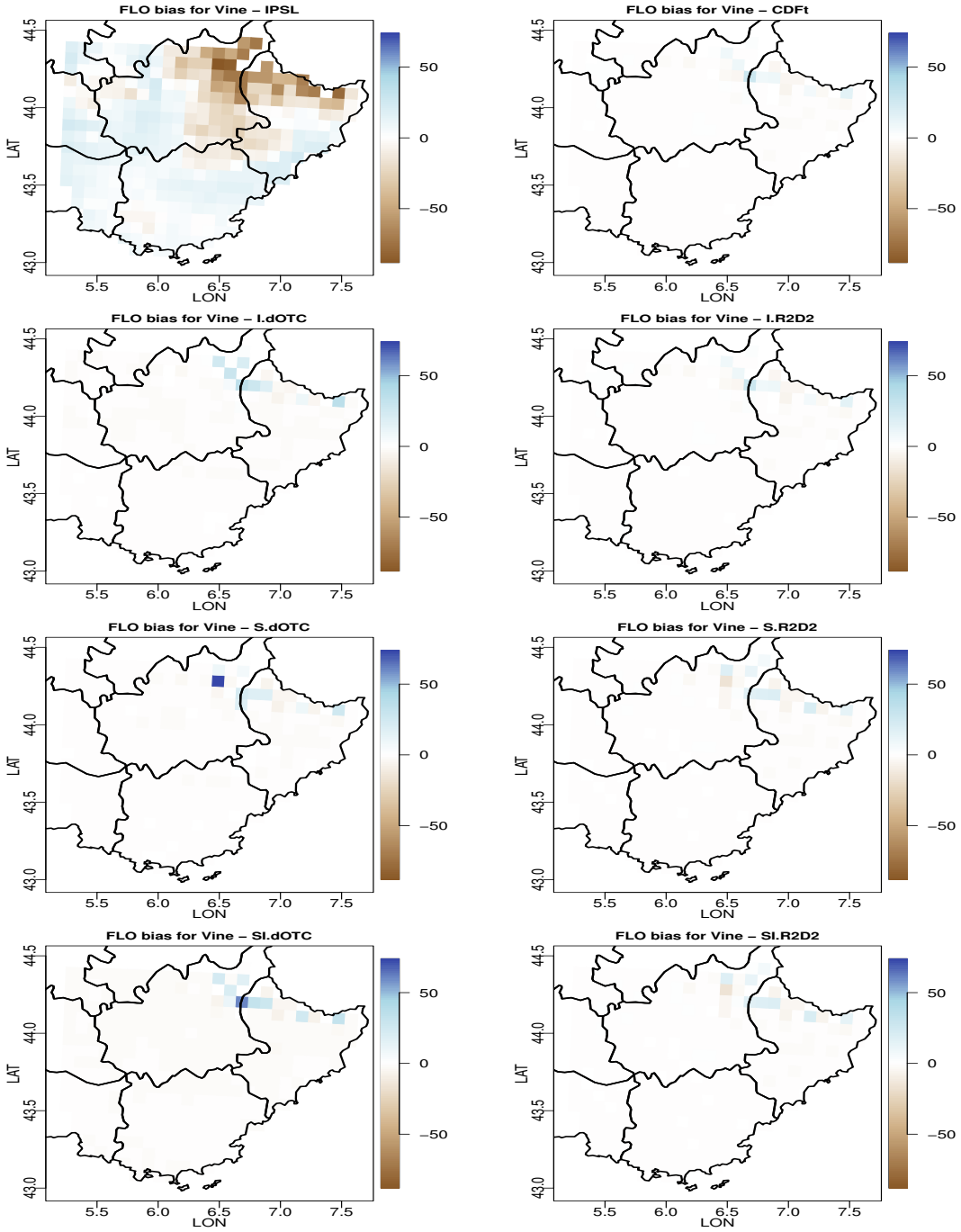

Figure 4.11: For each bias correction method and for vine: map of FLO bias to SAFRAN in Provence. From top to bottom and from left to right: IPSL (no correction), CDF-t, Intervar-dOTC, Intervar-R2D2, spatial-dOTC, spatial R2D2, spatial-intervar-dOTC, spatial-intervar-R2D2.

4.5 Maps for variance ratio

4.5.1 Wheat

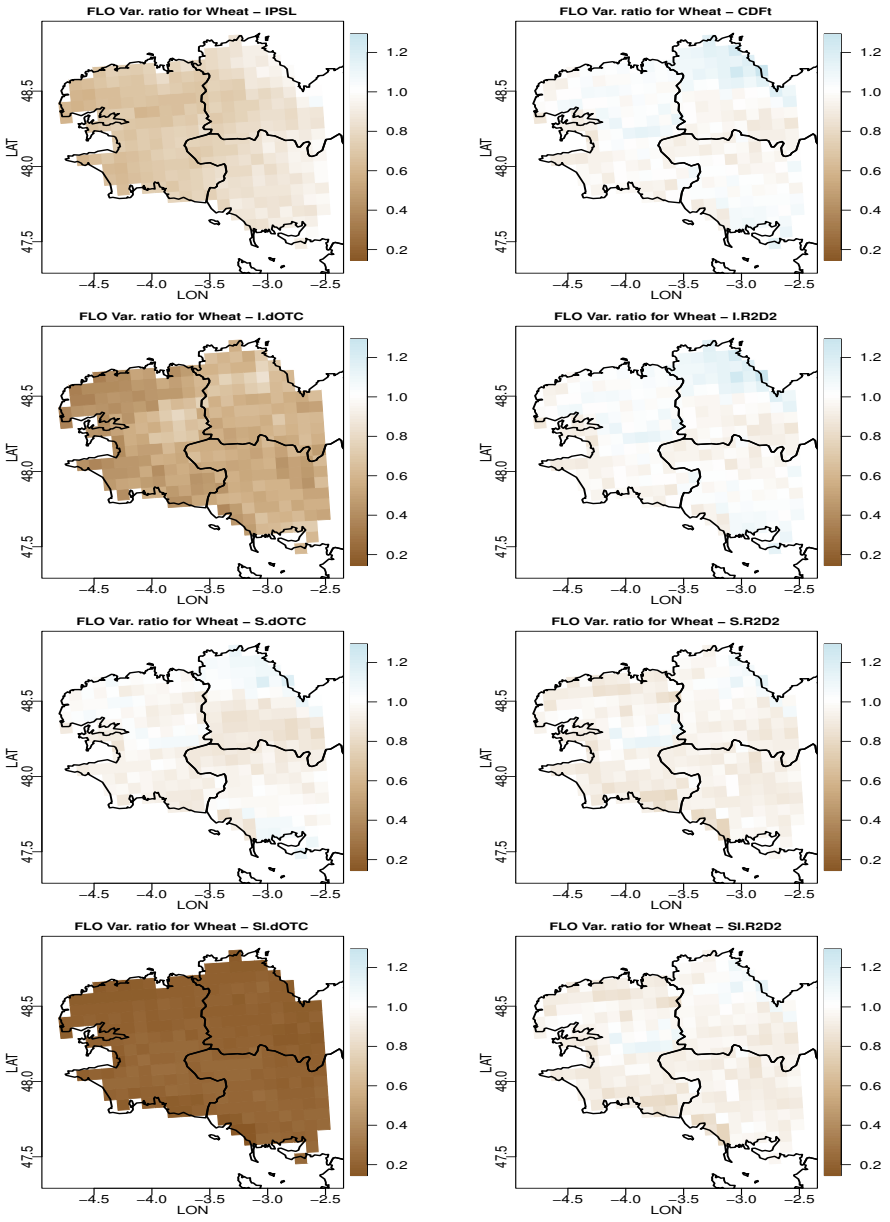

Figure 4.12: For each bias correction method and for wheat: map of FLO variance divided by the FLO variance for SAFRAN in Brittany. From top to bottom and from left to right: IPSL (no correction), CDF-t, Intervar-dOTC, Intervar-R2D2, spatial-dOTC, spatial R2D2, spatial-intervar-dOTC, spatial-intervar-R2D2.

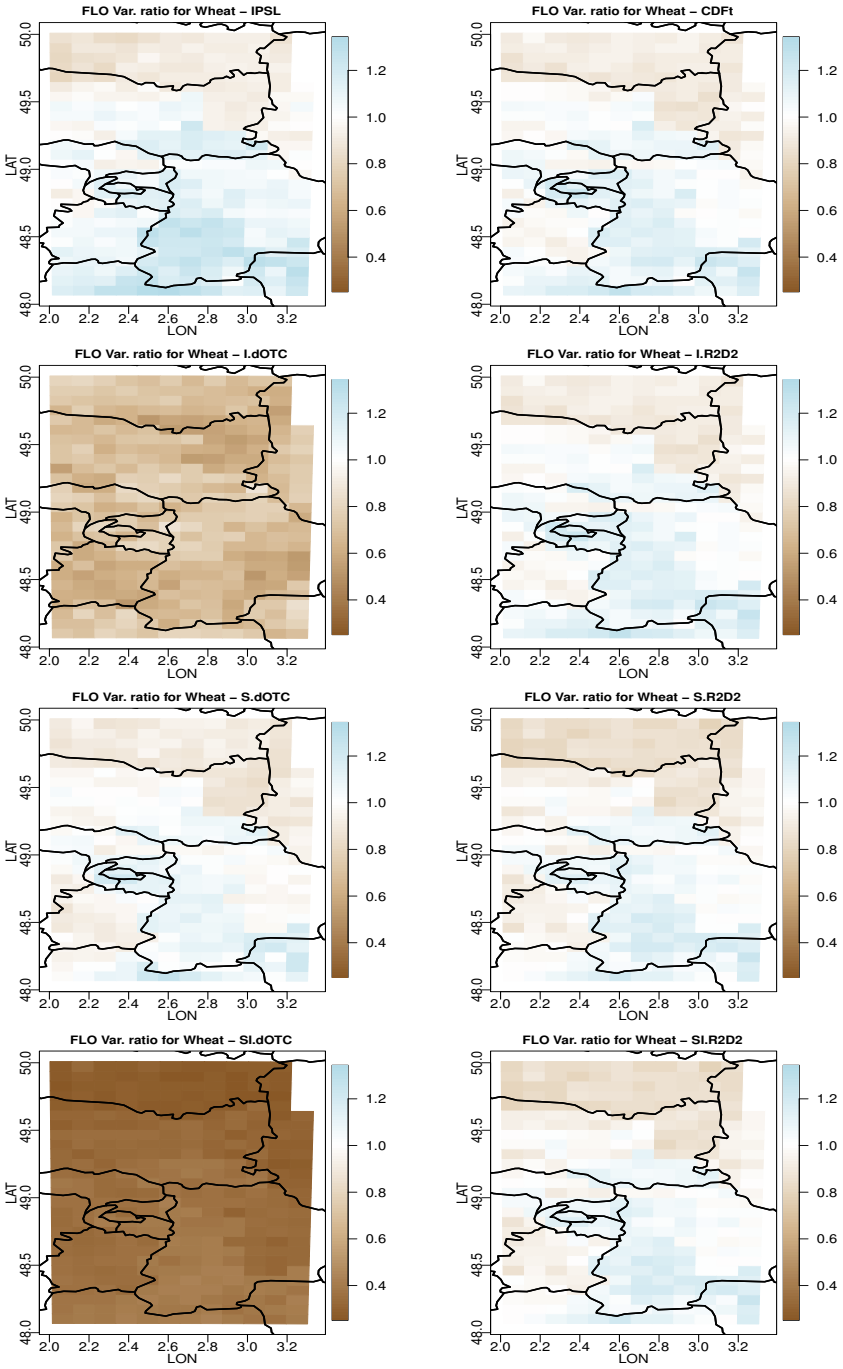

Figure 4.13: For each bias correction method and for wheat: map of FLO variance divided by the FLO variance for SAFRAN in Ile de France. From top to bottom and from left to right: IPSL (no correction), CDF-t, Intervar-dOTC, Intervar-R2D2, spatial-dOTC, spatial R2D2, spatial-intervar-dOTC, spatial-intervar-R2D2.

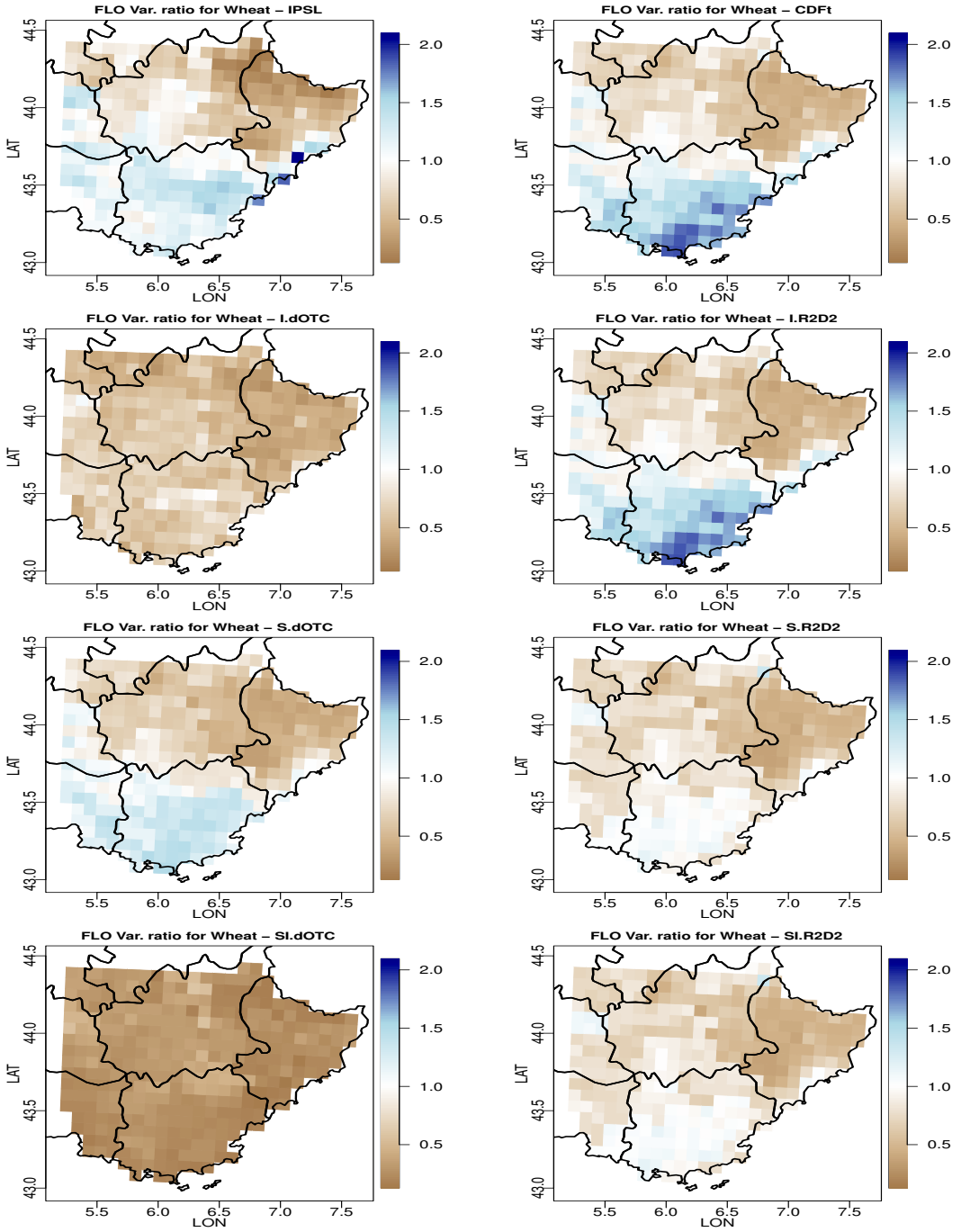

Figure 4.14: For each bias correction method and for wheat: map of FLO variance divided by the FLO variance for SAFRAN in Provence. From top to bottom and from left to right: IPSL (no correction), CDF-t, Intervar-dOTC, Intervar-R2D2, spatial-dOTC, spatial R2D2, spatial-intervar-dOTC, spatial-intervar-R2D2.

4.5.2 Maize

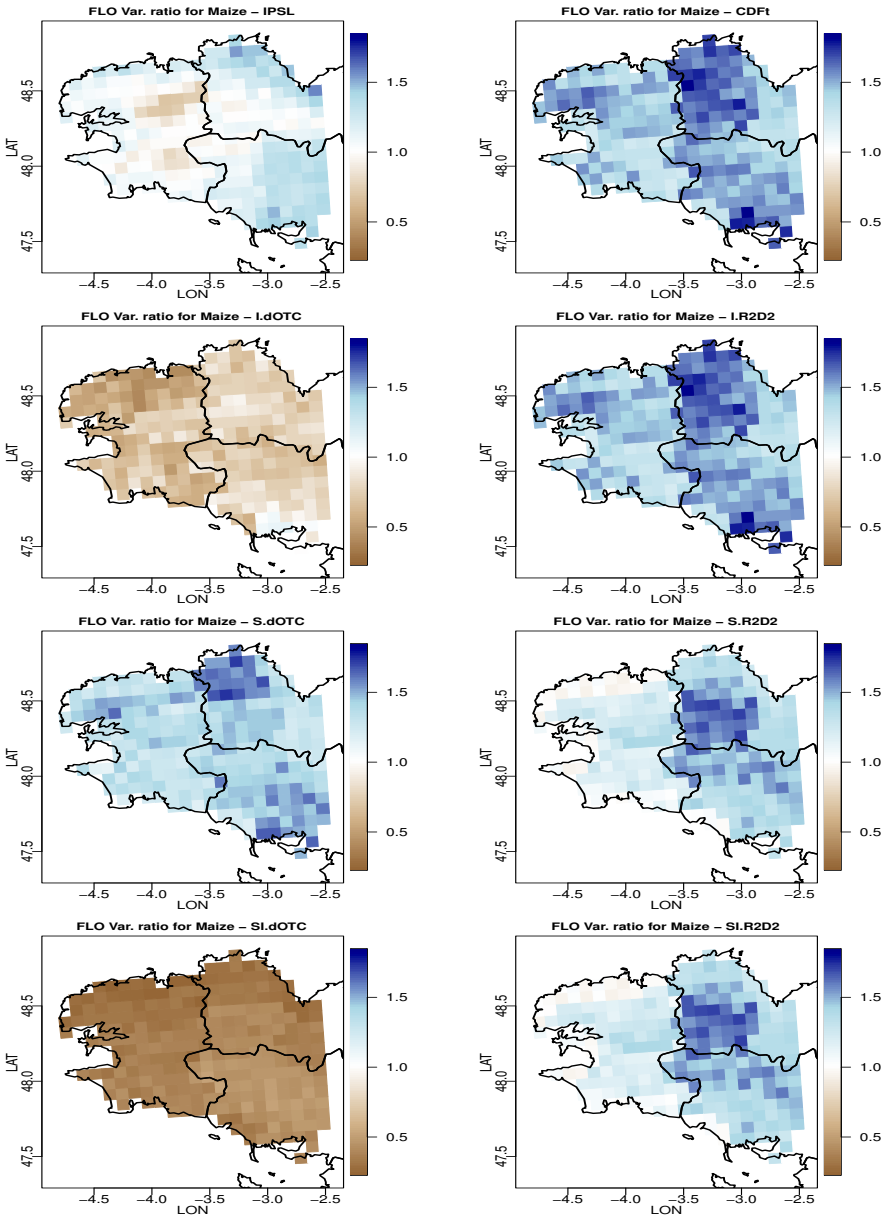

Figure 4.15: For each bias correction method and for maize: map of FLO variance divided by the FLO variance for SAFRAN in Brittany. From top to bottom and from left to right: IPSL (no correction), CDF-t, Intervar-dOTC, Intervar-R2D2, spatial-dOTC, spatial R2D2, spatial-intervar-dOTC, spatial-intervar-R2D2.

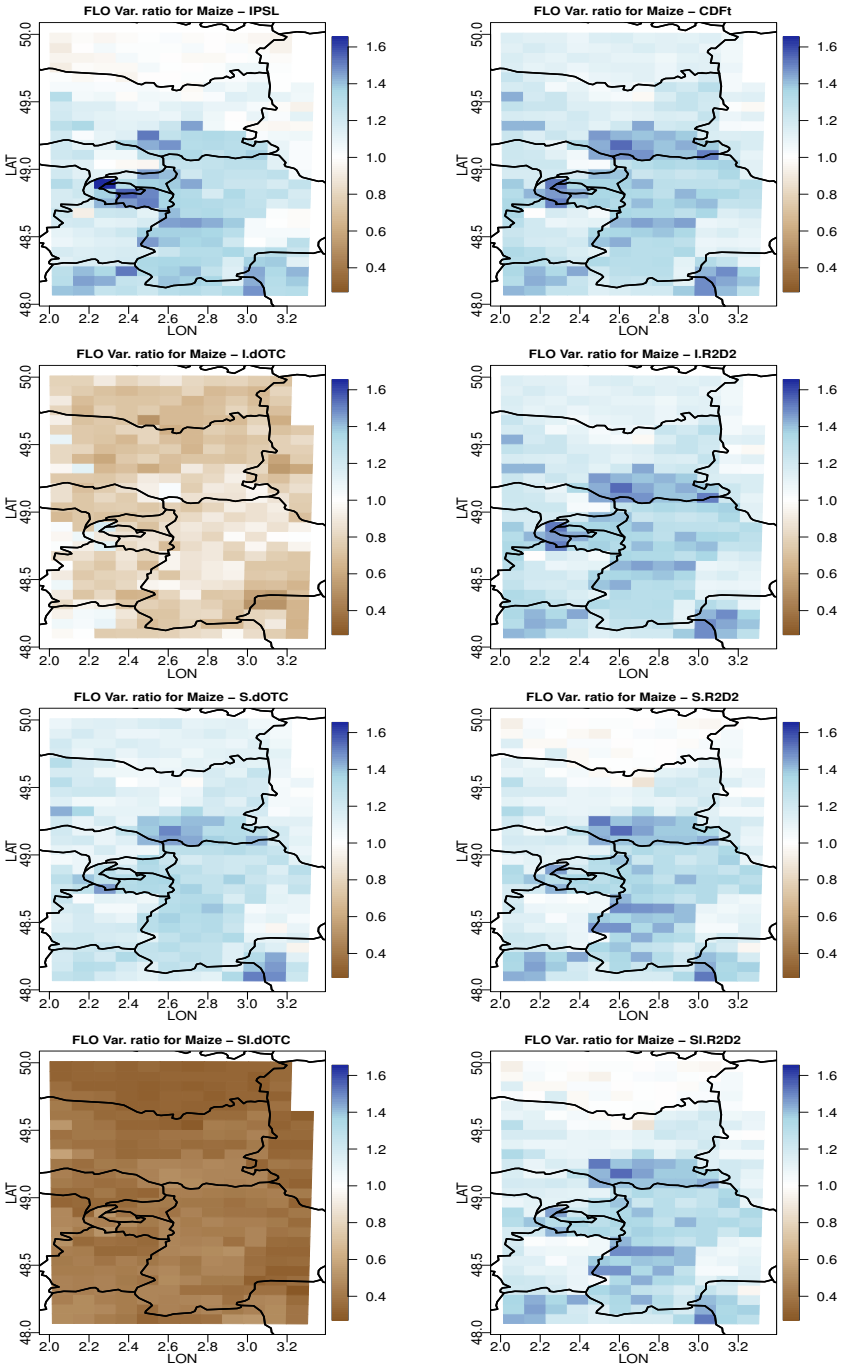

Figure 4.16: For each bias correction method and for maize: map of FLO variance divided by the FLO variance for SAFRAN in Ile de France. From top to bottom and from left to right: IPSL (no correction), CDF-t, Intervar-dOTC, Intervar-R2D2, spatial-dOTC, spatial R2D2, spatial-intervar-dOTC, spatial-intervar-R2D2.

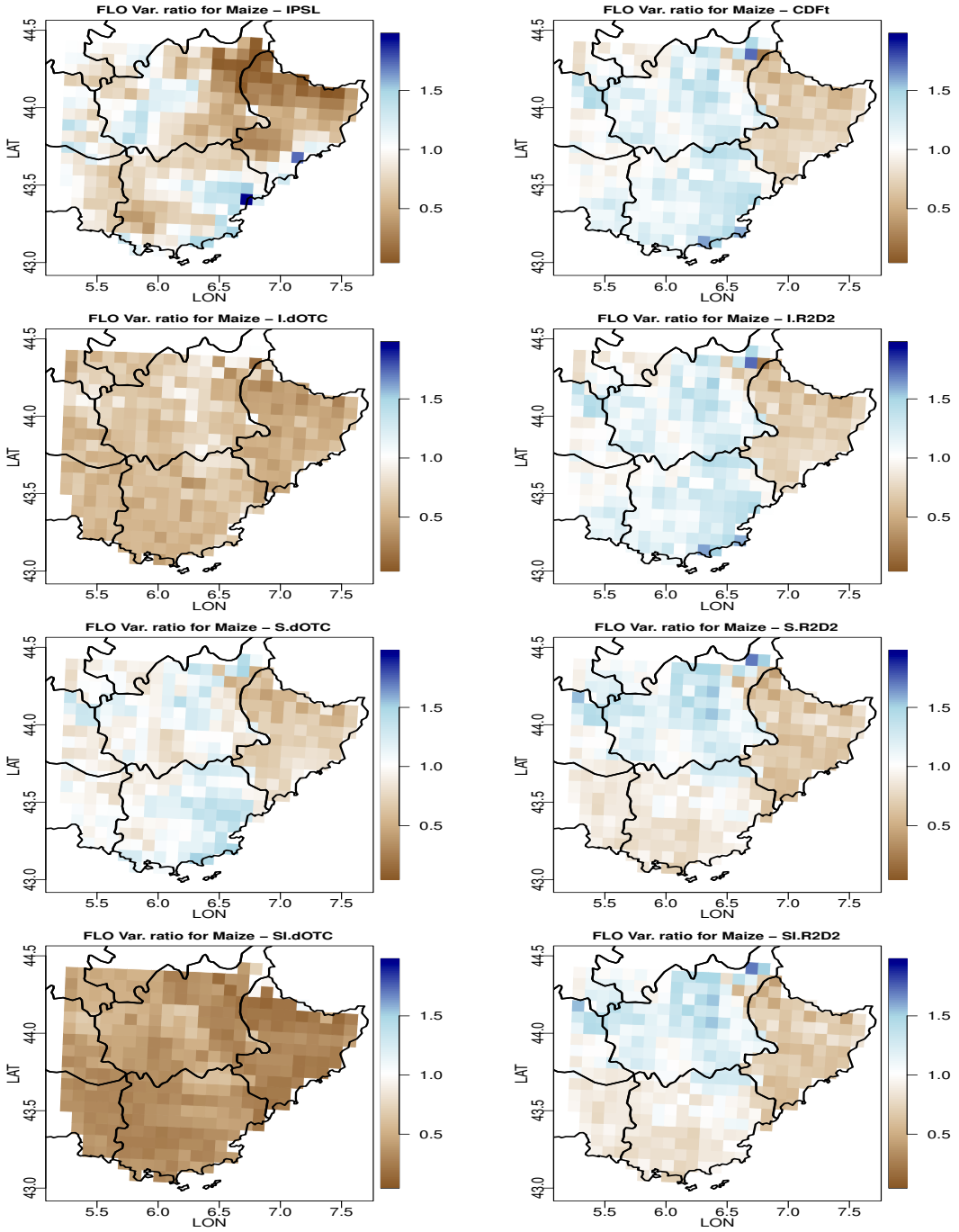

Figure 4.17: For each bias correction method and for maize: map of FLO variance divided by the FLO variance for SAFRAN in Provence. From top to bottom and from left to right: IPSL (no correction), CDF-t, Intervar-dOTC, Intervar-R2D2, spatial-dOTC, spatial R2D2, spatial-intervar-dOTC, spatial-intervar-R2D2.

4.5.3 Vine

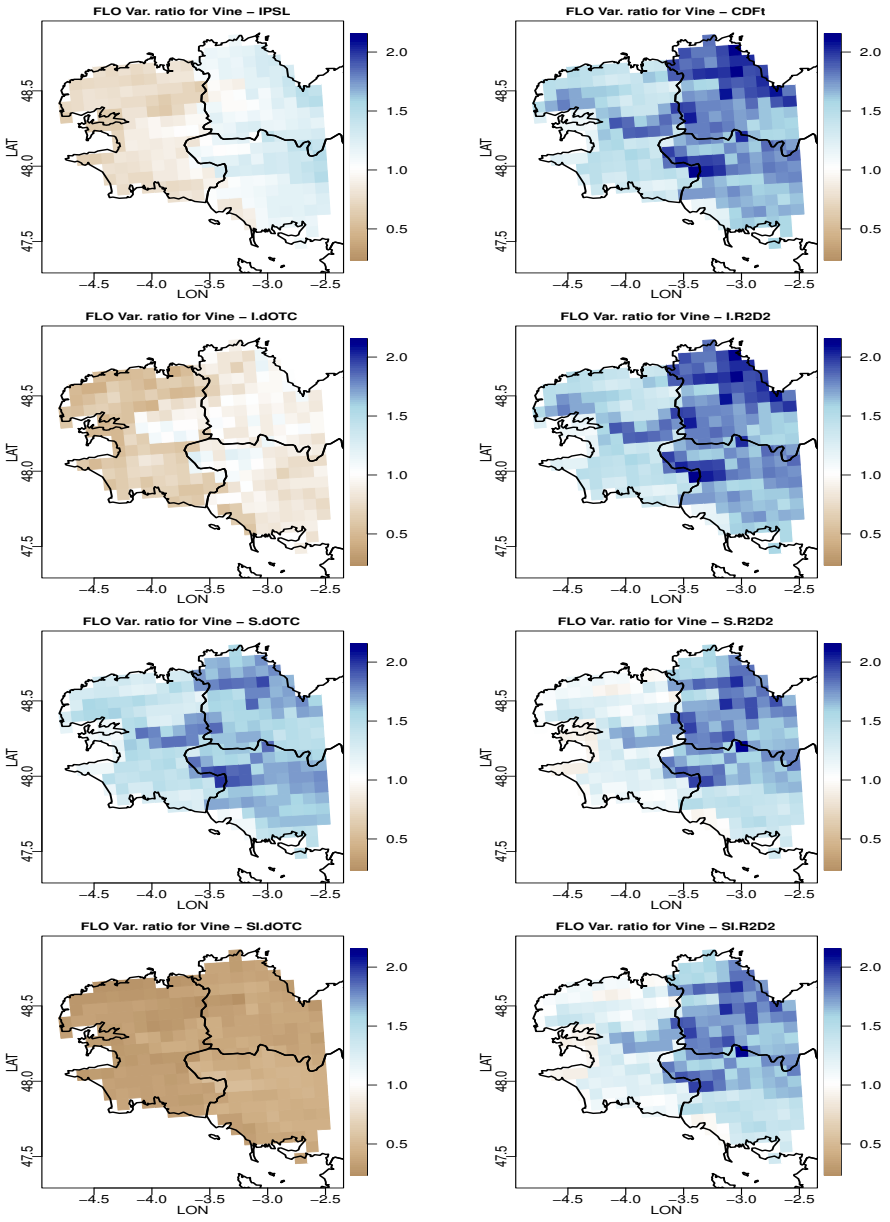

Figure 4.18: For each bias correction method and for vine: map of FLO variance divided by the FLO variance for SAFRAN in Brittany. From top to bottom and from left to right: IPSL (no correction), CDF-t, Intervar-dOTC, Intervar-R2D2, spatial-dOTC, spatial R2D2, spatial-intervar-dOTC, spatial-intervar-R2D2.

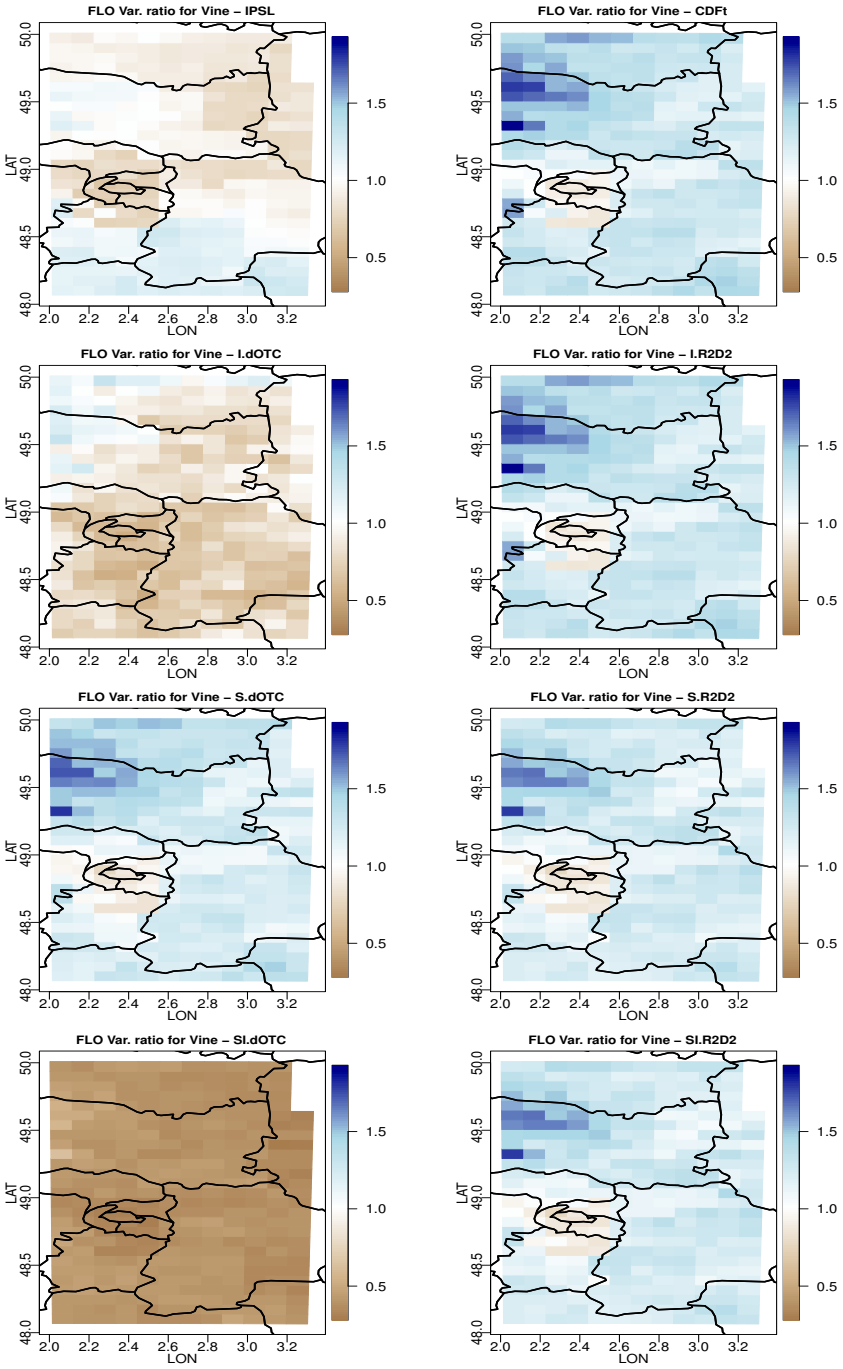

Figure 4.19: For each bias correction method and for vine: map of FLO variance divided by the FLO variance for SAFRAN in Ile de France. From top to bottom and from left to right: IPSL (no correction), CDF-t, Intervar-dOTC, Intervar-R2D2, spatial-dOTC, spatial R2D2, spatial-intervar-dOTC, spatial-intervar-R2D2.

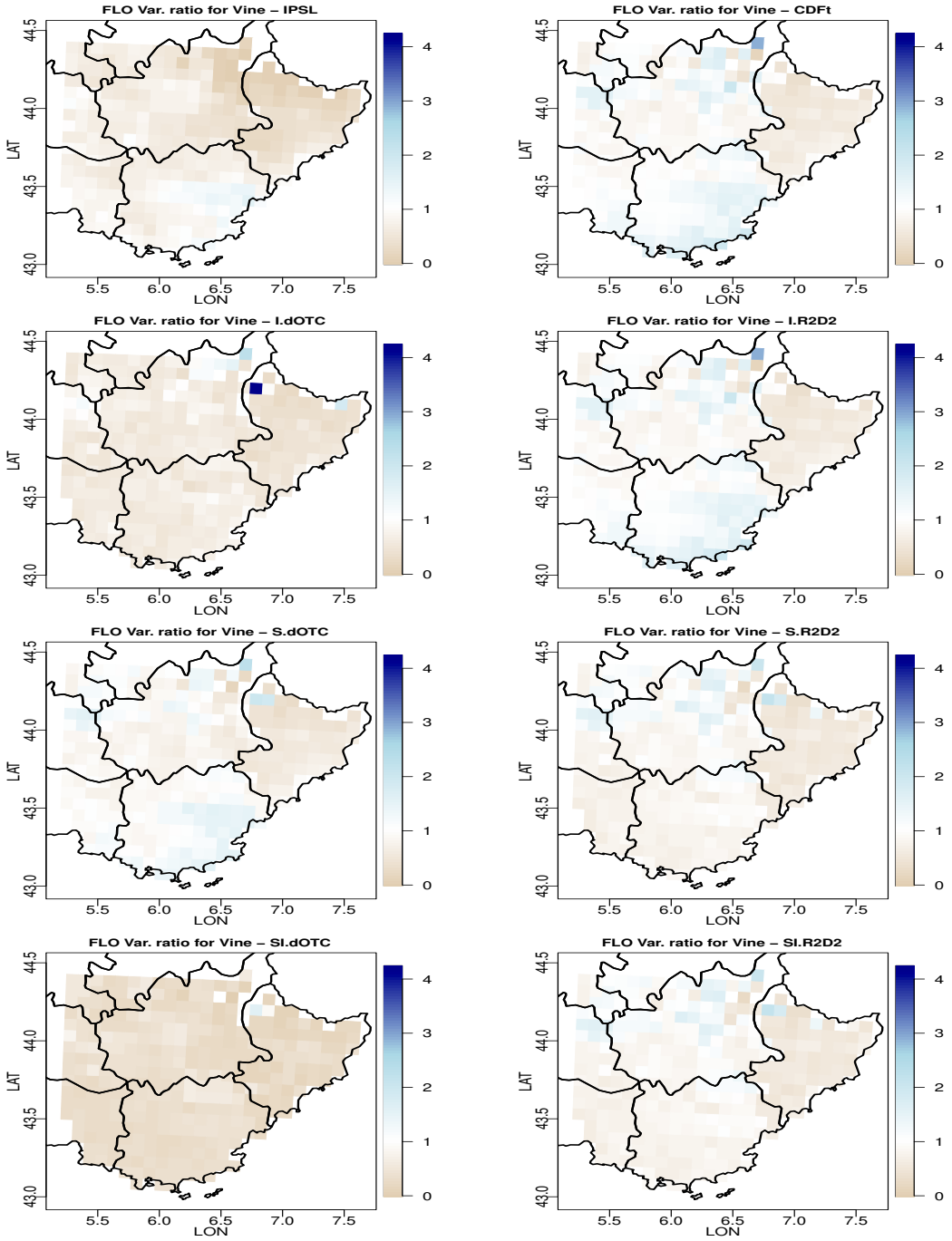

Figure 4.20: For each bias correction method and for vine: map of FLO variance divided by the FLO variance for SAFRAN in Provence. From top to bottom and from left to right: IPSL (no correction), CDF-t, Intervar-dOTC, Intervar-R2D2, spatial-dOTC, spatial R2D2, spatial-intervar-dOTC, spatial-intervar-R2D2.

Chapter 5

Pheno: FLO in the future: 2036-2065

FLO is the Julian day for the third phenology stage computed as described in Caubel et al. (2015). In some cases, FLO is not attained, in which case a NaN value is produced. All statistics are computed after removing NaN values.

5.1 Boxplots

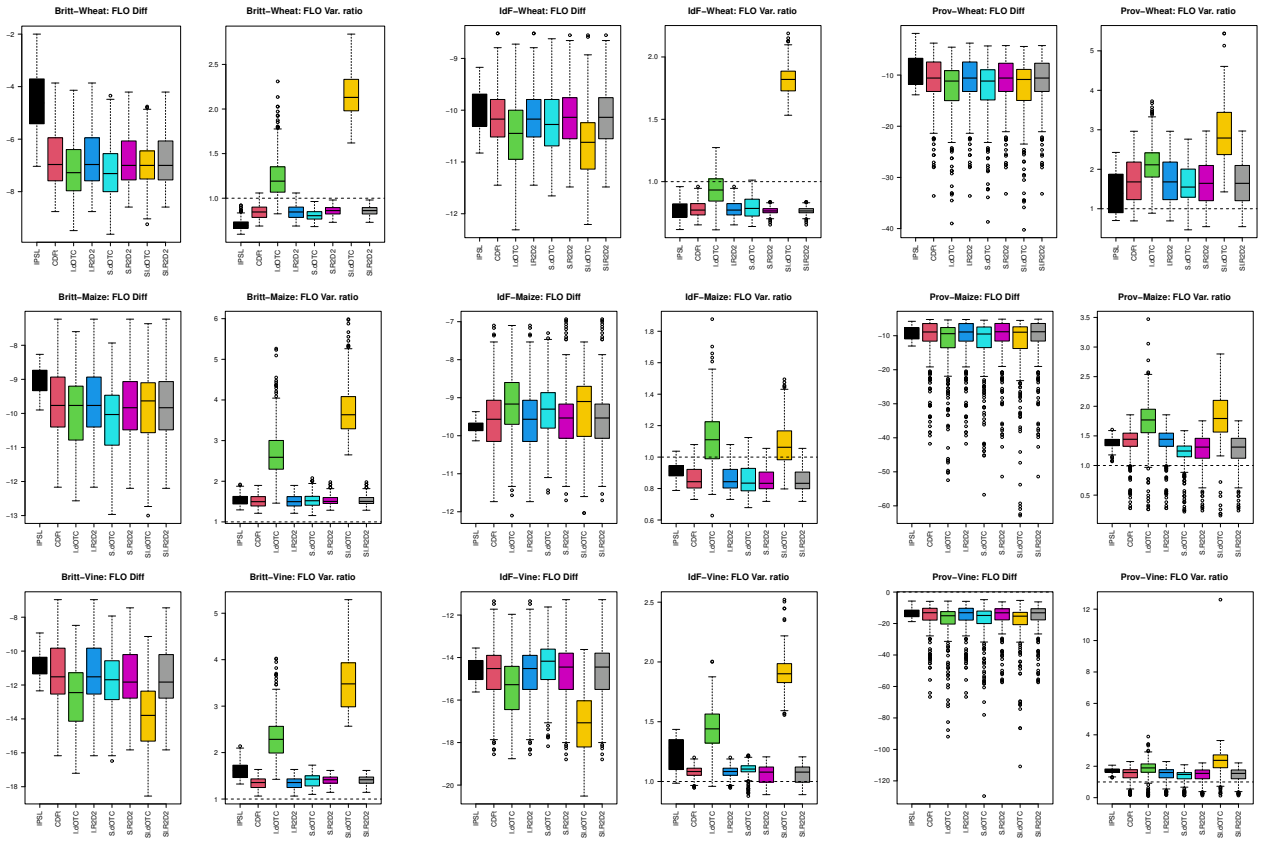

Figure 5.1: Overall FLO difference between future and past and FLO's variance ratio between future and past for all bias correction methods. Top row: wheat. Middle row: Maize. Bottom row: Vine. Left column: Bretagne. Middle column: Ile de France. Right column: Provence. In each panel, from left to right: IPSL (no correction), CDF-t, Intervar-dOTC, Intervar-R2D2, spatial-dOTC, spatial R2D2, spatial-intervar-dOTC, spatial-intervar-R2D2.

5.2 Covariances

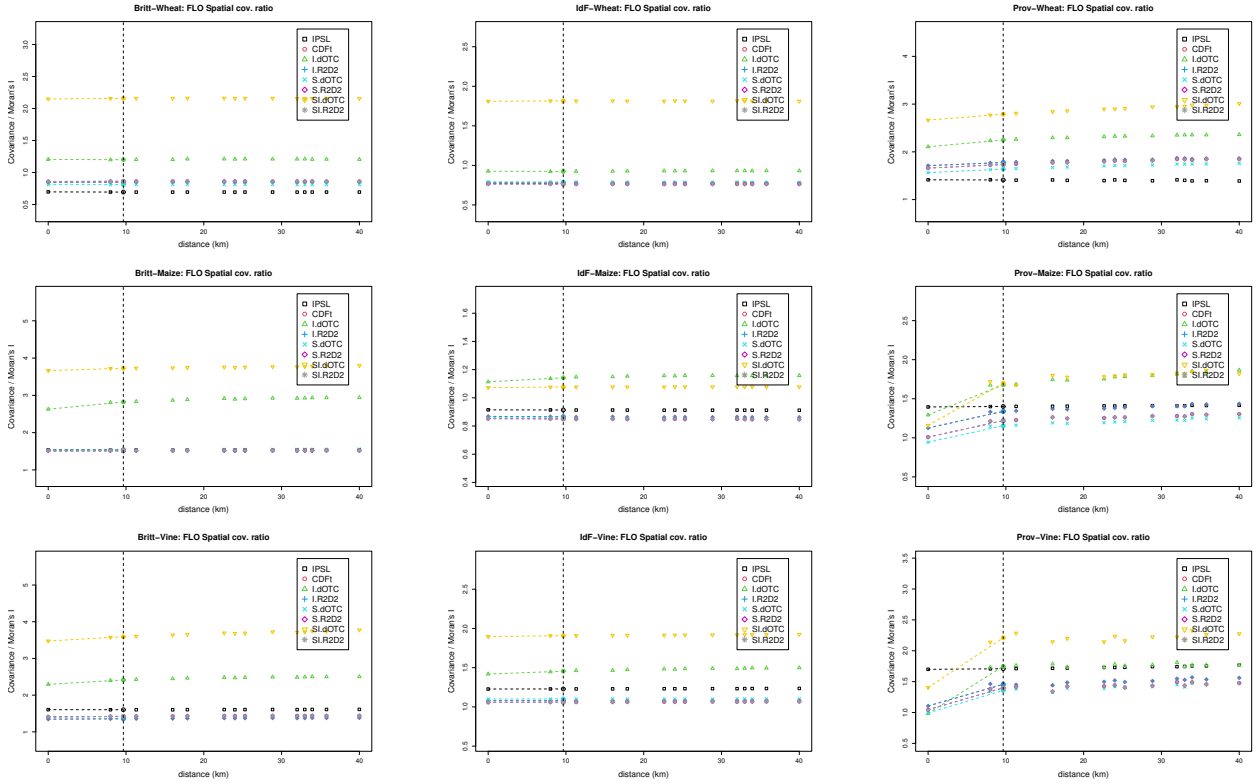

Figure 5.2: Spatial covariance and Moran's I ratio between future and past of FLO for all bias correction methods. Top row: wheat. Middle row: Maize. Bottom row: Vine. Left column: Bretagne. Middle column: Ile de France. Right column: Provence.

5.3 p-values

		IPSL	CDFt	I.dOTC	I.R2D2	S.dOTC	S.R2D2	SI.dOTC	SI.R2D2
p-values for "equality-of-means" tests									
Britt.	wheat	0.000	0.000	0.000	0.000	0.000	0.000	0.000	0.000
	maize	0.000	0.000	0.000	0.000	0.000	0.000	0.000	0.000
	vine	0.000	0.000	0.000	0.000	0.000	0.000	0.000	0.000
IdF	wheat	0.000	0.000	0.000	0.000	0.000	0.000	0.000	0.000
	maize	0.000	0.000	0.000	0.000	0.000	0.000	0.000	0.000
	vine	0.000	0.000	0.000	0.000	0.000	0.000	0.000	0.000
Prov.	wheat	0.000	0.000	0.000	0.000	0.000	0.000	0.000	0.000
	maize	0.000	0.000	0.000	0.000	0.000	0.000	0.000	0.000
	vine	0.000	0.000	0.000	0.000	0.000	0.000	0.000	0.000
p-values for "equality-of-variances" tests									
Britt.	wheat	**0.217**	**0.573**	**0.217**	**0.573**	**0.480**	**0.639**	0.003	**0.639**
	maize	**0.195**	**0.213**	0.000	**0.213**	**0.159**	**0.229**	0.000	**0.229**
	vine	**0.159**	**0.330**	0.000	**0.330**	**0.276**	**0.284**	0.000	**0.284**
IdF	wheat	**0.468**	**0.452**	**0.694**	**0.452**	**0.477**	**0.422**	0.046	**0.422**
	maize	**0.798**	**0.660**	**0.478**	**0.660**	**0.619**	**0.616**	**0.769**	**0.616**
	vine	**0.535**	**0.807**	0.008	**0.807**	**0.739**	**0.861**	0.009	**0.861**
Prov.	wheat	0.056	0.000	0.000	0.000	0.000	0.000	0.000	0.000
	maize	**0.152**	**0.535**	0.000	**0.535**	**0.653**	**0.993**	0.062	**0.993**
	vine	0.020	**0.213**	0.007	**0.213**	**0.540**	**0.422**	0.000	**0.422**
p-values for "equality-of-Moran's I" tests									
Britt.	wheat	0.000	0.000	0.000	0.000	0.000	0.000	0.000	0.000
	maize	0.000	0.000	0.000	0.000	0.000	0.000	0.000	0.000
	vine	0.000	0.000	0.000	0.000	0.000	0.000	0.000	0.000
IdF	wheat	0.000	0.000	0.000	0.000	0.000	0.000	0.000	0.000
	maize	0.000	0.000	0.000	0.000	0.000	0.000	0.000	0.000
	vine	0.000	0.000	0.000	0.000	0.000	0.000	0.000	0.000
Prov.	wheat	0.000	0.000	0.000	0.000	0.000	0.000	0.000	0.000
	maize	0.000	0.000	0.000	0.000	0.000	0.000	0.000	0.000
	vine	0.000	0.000	0.000	0.000	0.000	0.000	0.000	0.000

Table 5.1: Statistical analysis for FLO in the future: p-values for the Welsh t-test of absence of bias on the average (first block); Fisher F-test of equality of variance (second block) and its adaptation to testing the equality of Moran's I (third block). Non rejection at the confidence level 0.90 is indicated in bold font.

5.4 Maps for average differences

5.4.1 Wheat

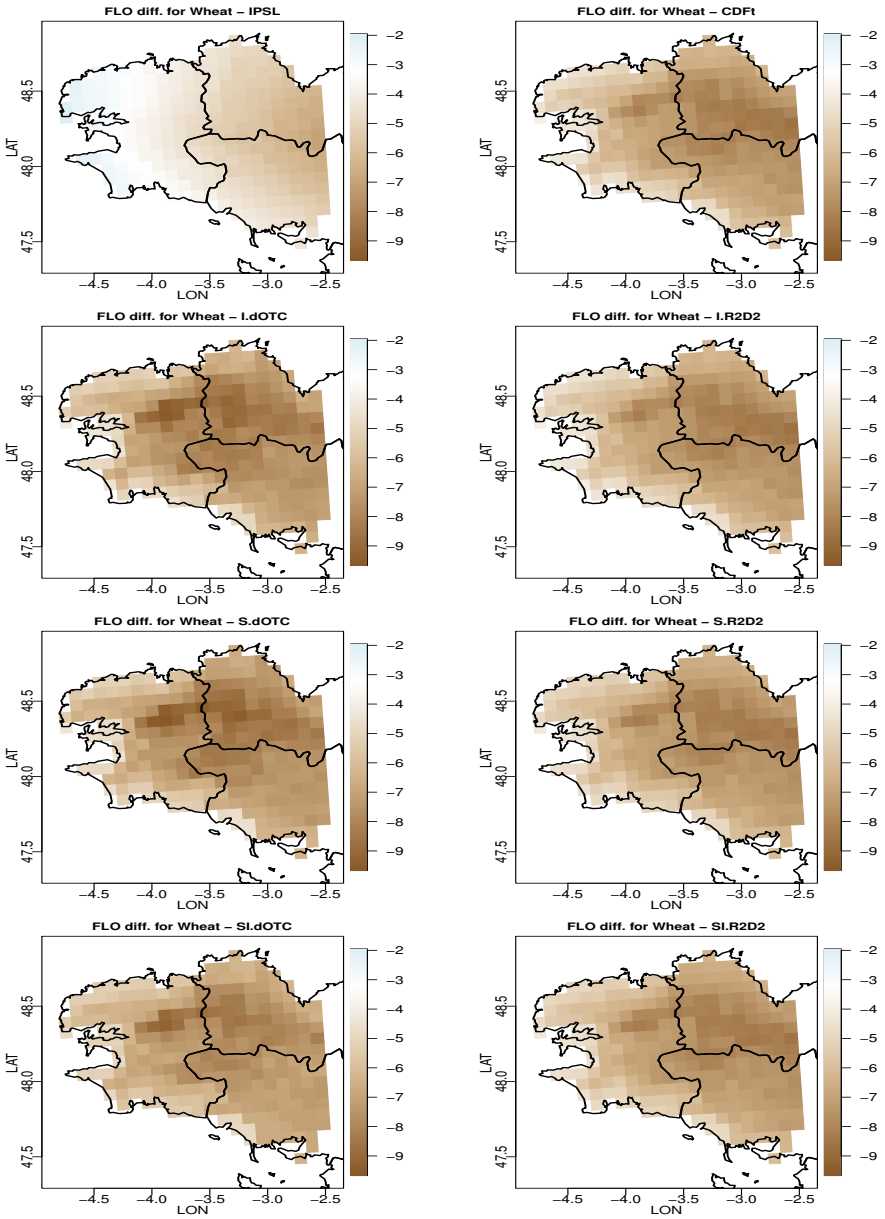

Figure 5.3: For each bias correction method and for wheat: map of the FLO difference between future and past in Brittany. From top to bottom and from left to right: IPSL (no correction), CDF-t, Intervar-dOTC, Intervar-R2D2, spatial-dOTC, spatial R2D2, spatial-intervar-dOTC, spatial-intervar-R2D2.

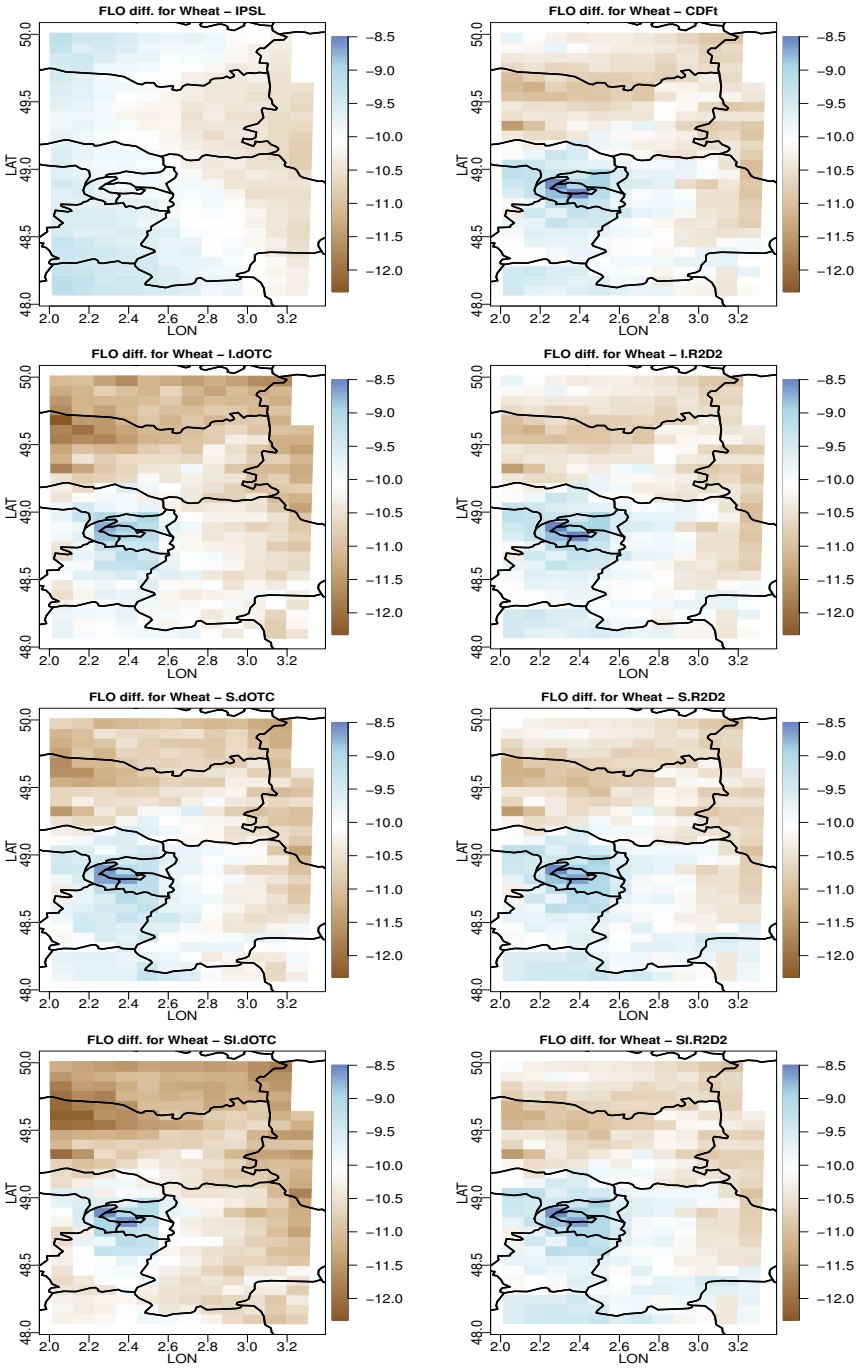

Figure 5.4: For each bias correction method and for wheat: map of the FLO difference between future and past in Ile de France. From top to bottom and from left to right: IPSL (no correction), CDF-t, Intervar-dOTC, Intervar-R2D2, spatial-dOTC, spatial R2D2, spatial-intervar-dOTC, spatial-intervar-R2D2.

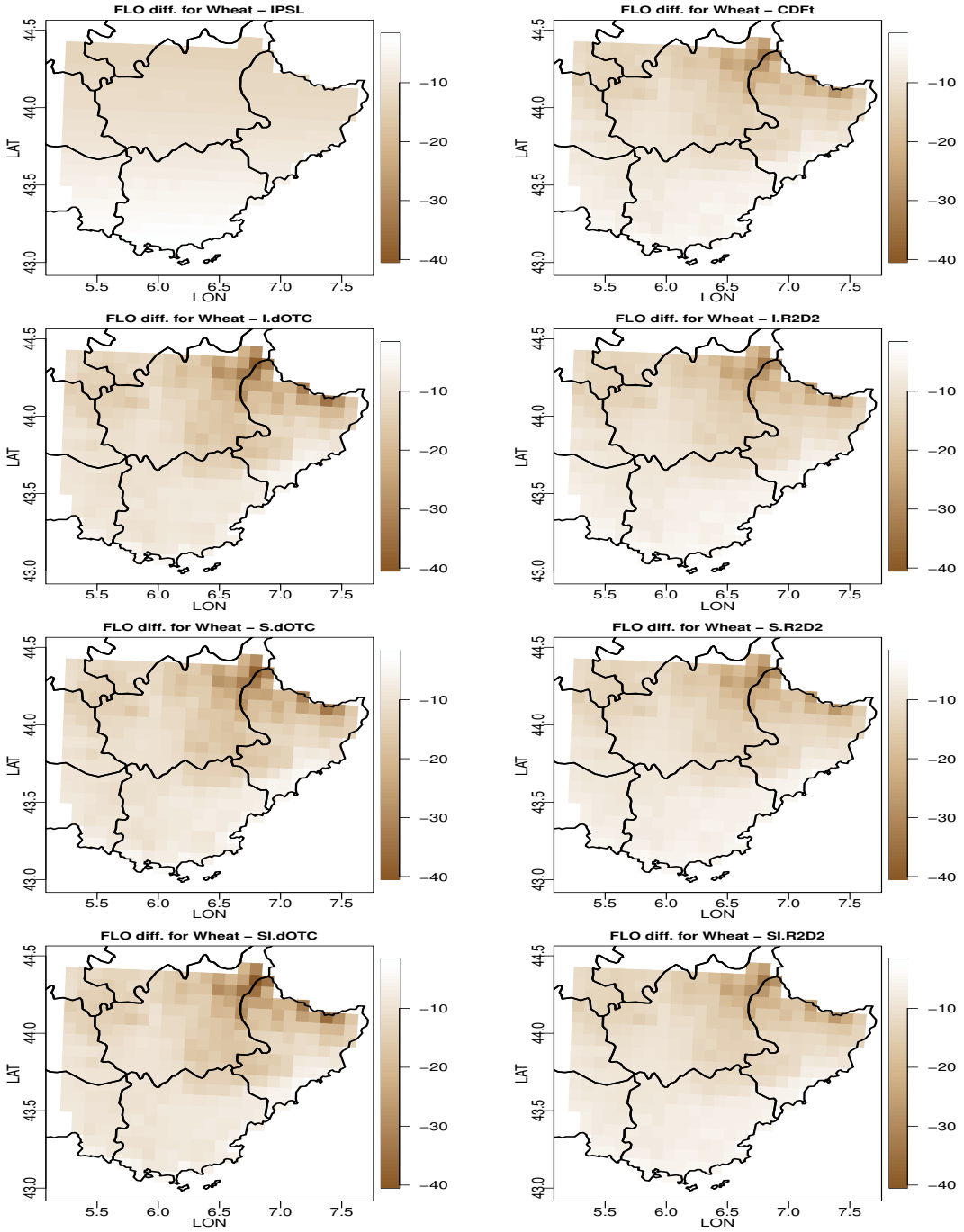

Figure 5.5: For each bias correction method and for wheat: map of the FLO difference between future and past in Provence. From top to bottom and from left to right: IPSL (no correction), CDF-t, Intervar-dOTC, Intervar-R2D2, spatial-dOTC, spatial R2D2, spatial-intervar-dOTC, spatial-intervar-R2D2.

5.4.2 Maize

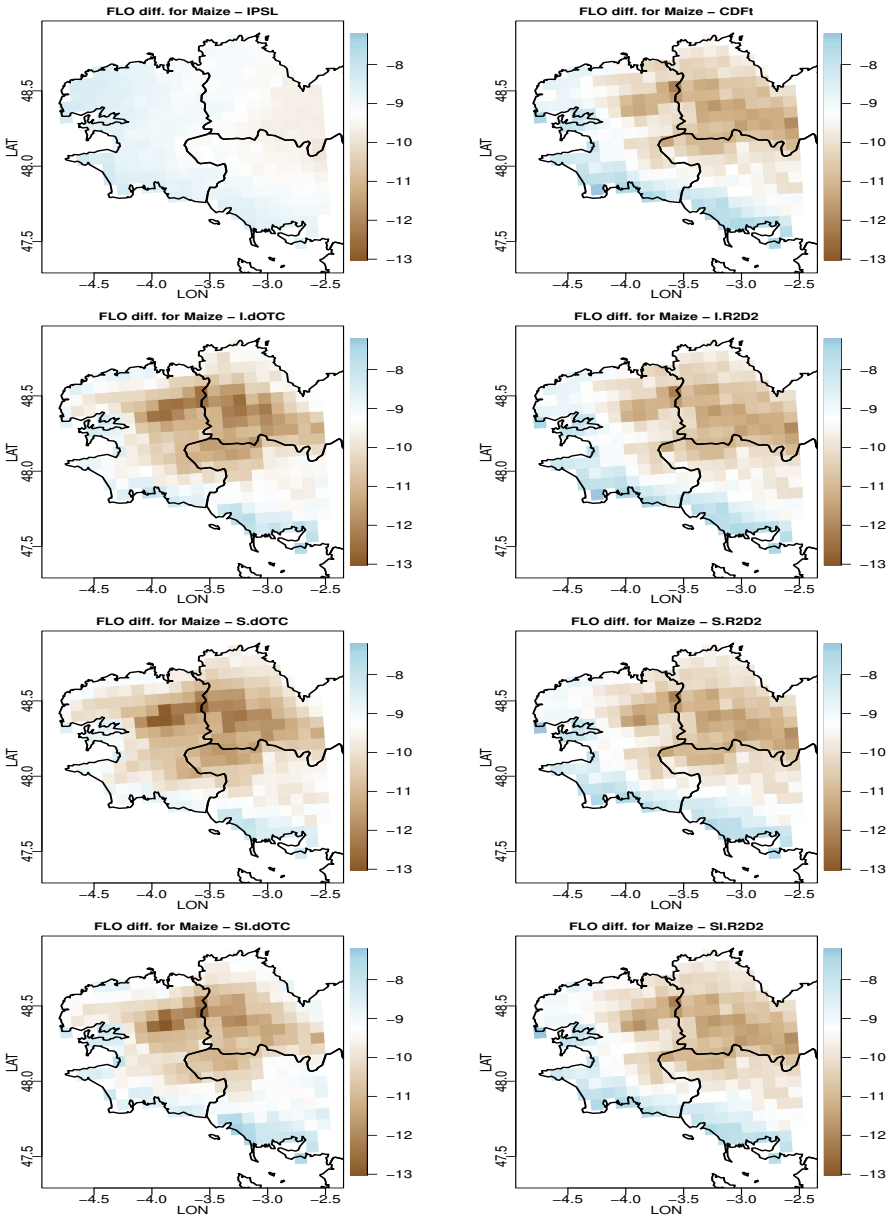

Figure 5.6: For each bias correction method and for maize: map of the FLO difference between future and past in Brittany. From top to bottom and from left to right: IPSL (no correction), CDF-t, Intervar-dOTC, Intervar-R2D2, spatial-dOTC, spatial R2D2, spatial-intervar-dOTC, spatial-intervar-R2D2.

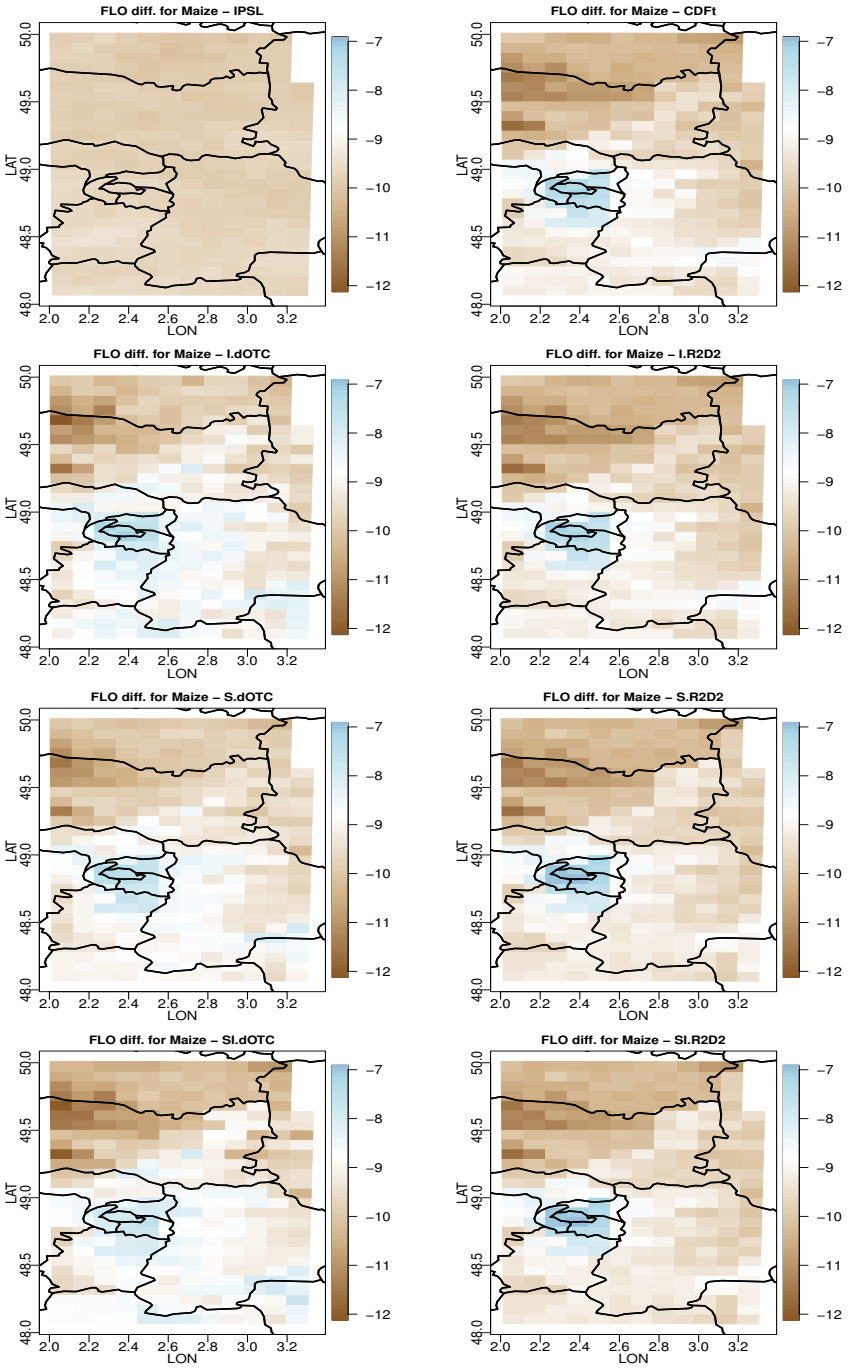

Figure 5.7: For each bias correction method and for maize: map of the FLO difference between future and past in Ile de France. From top to bottom and from left to right: IPSL (no correction), CDF-t, Intervar-dOTC, Intervar-R2D2, spatial-dOTC, spatial R2D2, spatial-intervar-dOTC, spatial-intervar-R2D2.

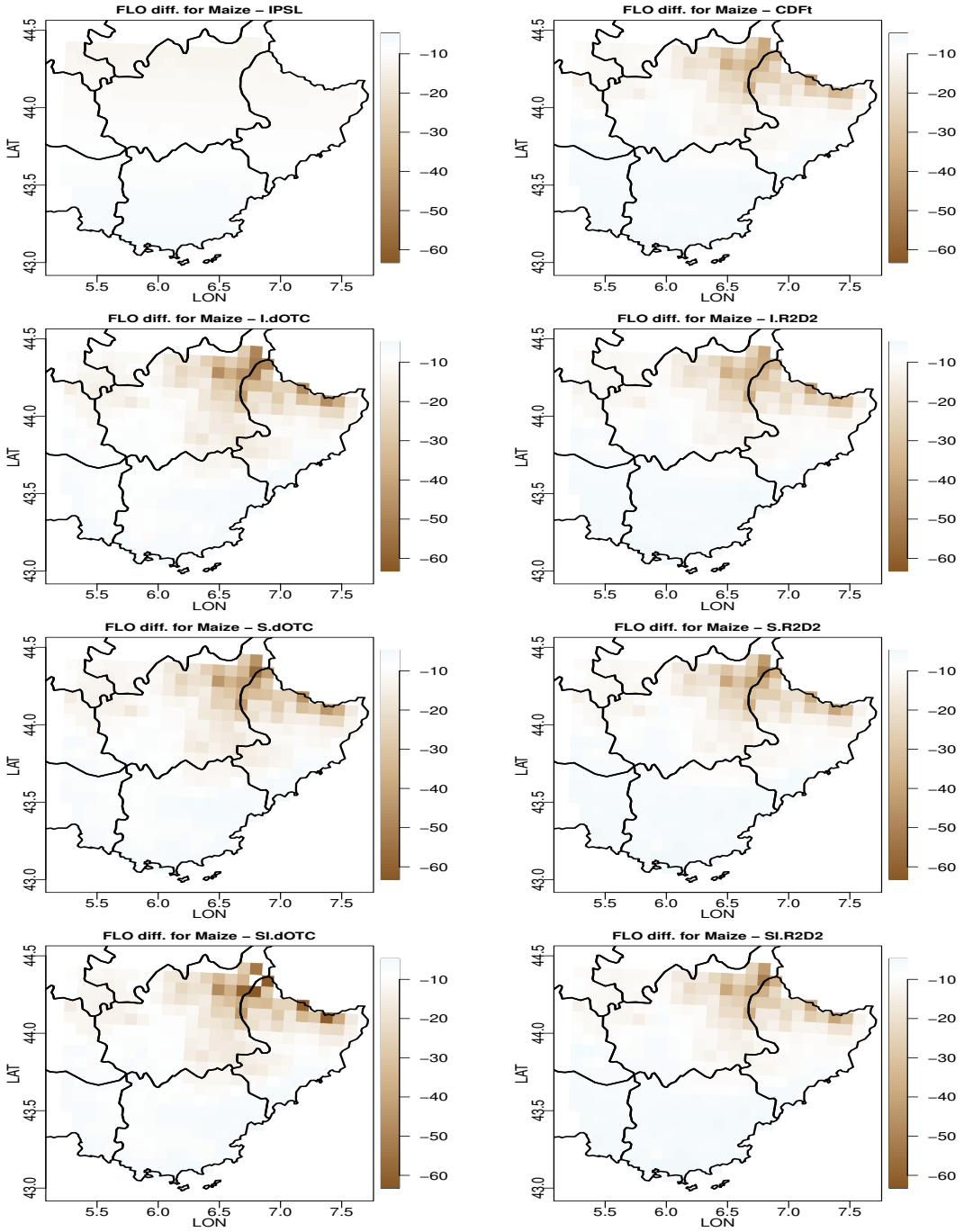

Figure 5.8: For each bias correction method and for maize: map of the FLO difference between future and past in Provence. From top to bottom and from left to right: IPSL (no correction), CDF-t, Intervar-dOTC, Intervar-R2D2, spatial-dOTC, spatial R2D2, spatial-intervar-dOTC, spatial-intervar-R2D2.

5.4.3 Vine

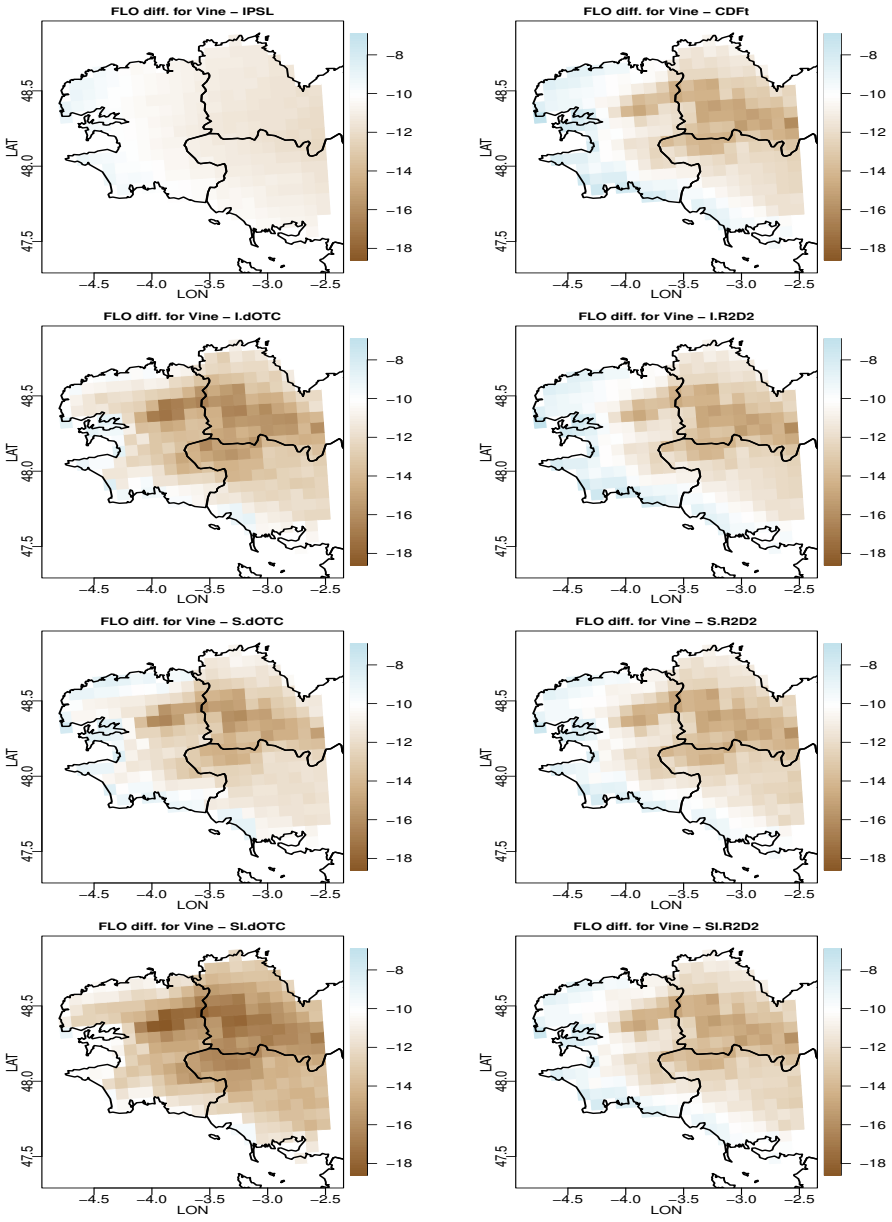

Figure 5.9: For each bias correction method and for vine: map of the FLO difference between future and past in Brittany. From top to bottom and from left to right: IPSL (no correction), CDF-t, Intervar-dOTC, Intervar-R2D2, spatial-dOTC, spatial R2D2, spatial-intervar-dOTC, spatial-intervar-R2D2.

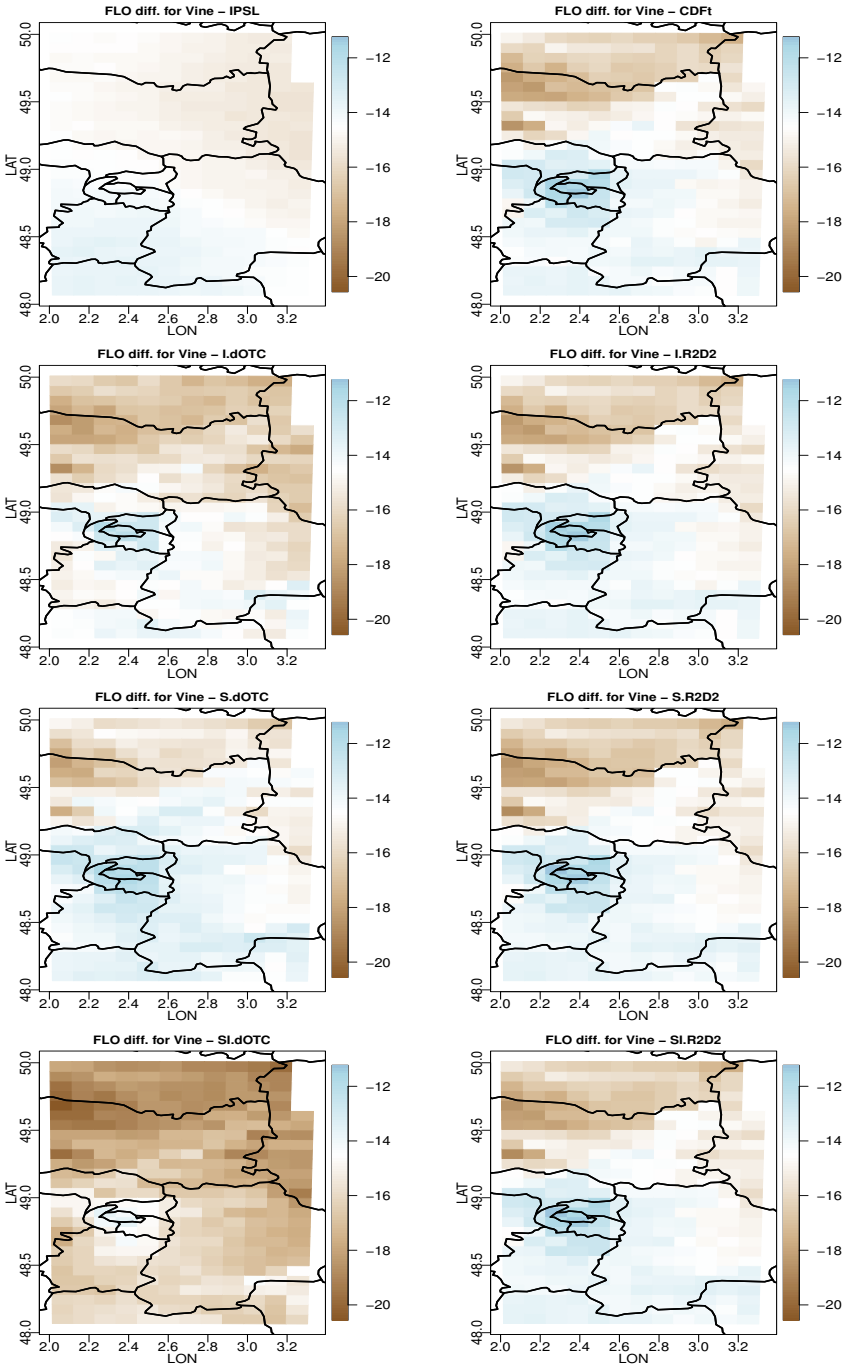

Figure 5.10: For each bias correction method and for vine: map of the FLO difference between future and past in Ile de France. From top to bottom and from left to right: IPSL (no correction), CDF-t, Intervar-dOTC, Intervar-R2D2, spatial-dOTC, spatial R2D2, spatial-intervar-dOTC, spatial-intervar-R2D2.

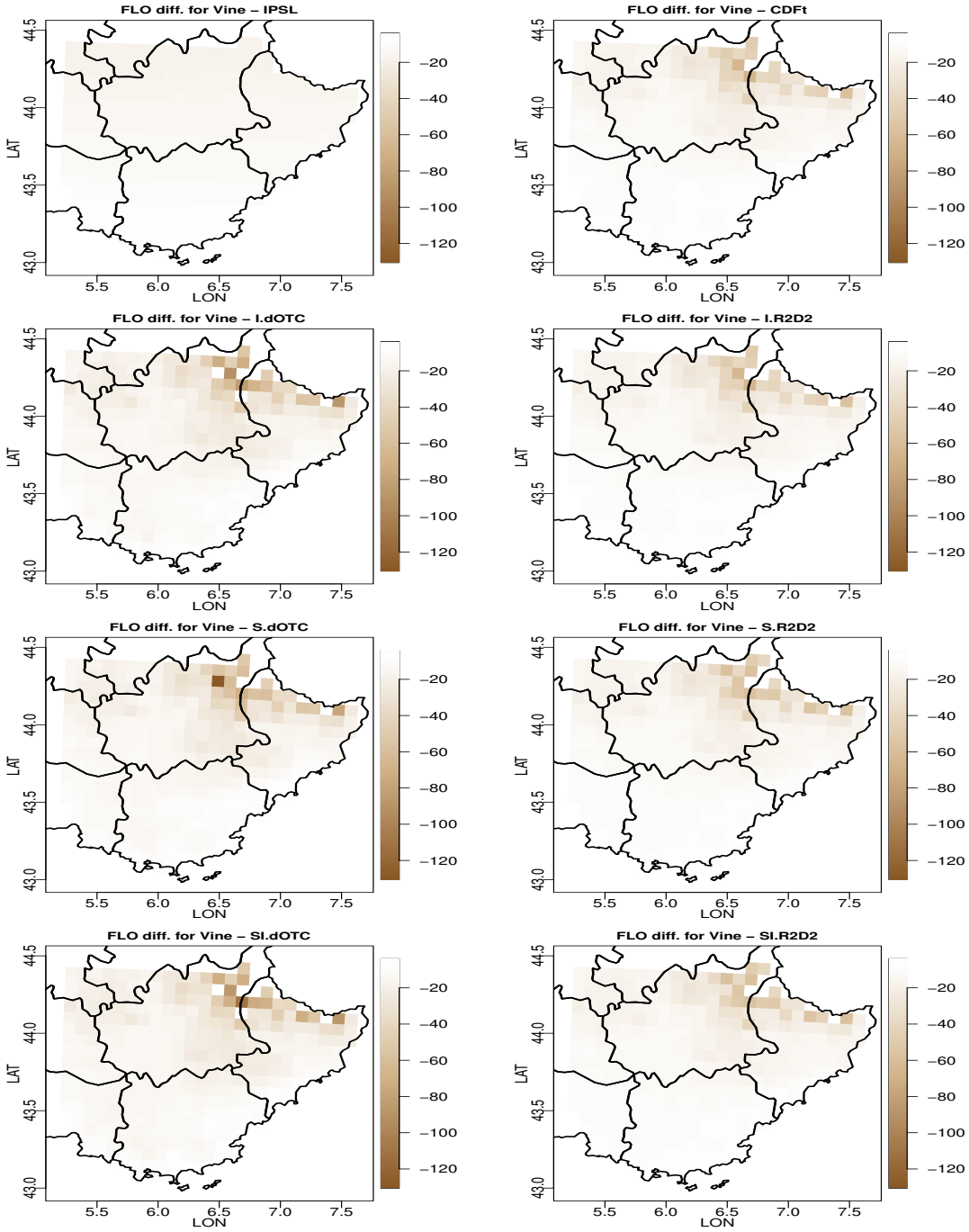

Figure 5.11: For each bias correction method and for vine: map of the FLO difference between future and past in Provence. From top to bottom and from left to right: IPSL (no correction), CDF-t, Intervar-dOTC, Intervar-R2D2, spatial-dOTC, spatial R2D2, spatial-intervar-dOTC, spatial-intervar-R2D2.

5.5 Maps for variance ratio

5.5.1 Wheat

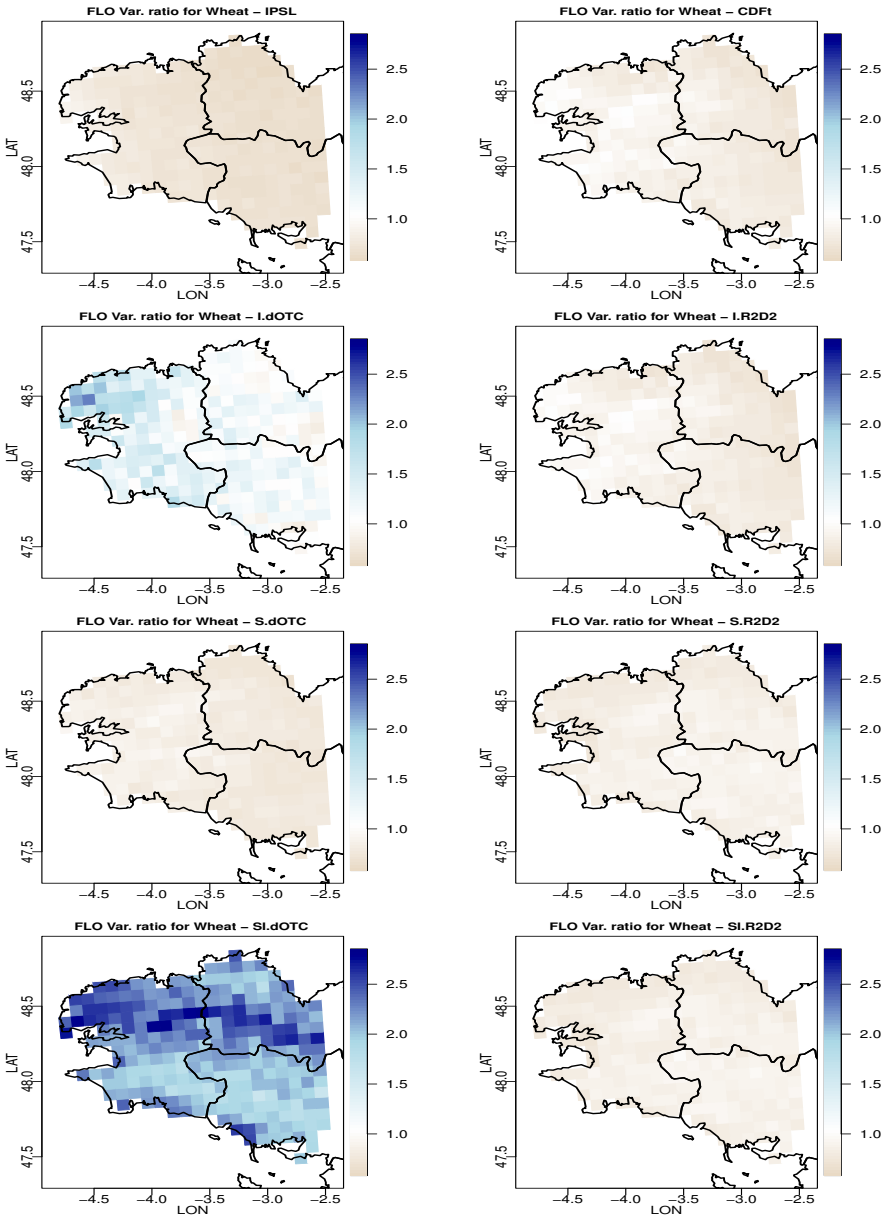

Figure 5.12: For each bias correction method and for wheat: map of the FLO variance ratio between future and past in Brittany. From top to bottom and from left to right: IPSL (no correction), CDF-t, Intervar-dOTC, Intervar-R2D2, spatial-dOTC, spatial R2D2, spatial-intervar-dOTC, spatial-intervar-R2D2.

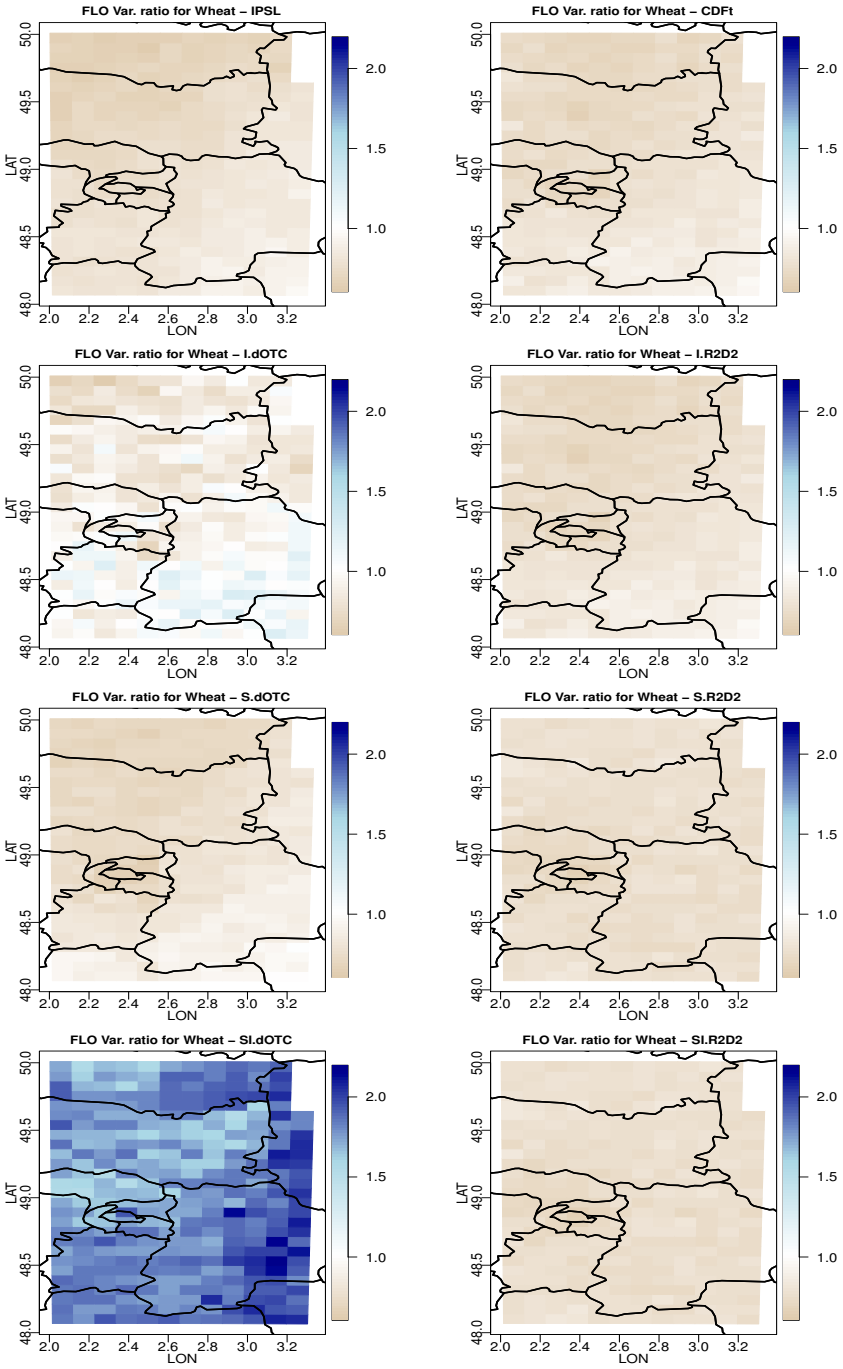

Figure 5.13: For each bias correction method and for wheat: map of the FLO variance ratio between future and past in ile de France. From top to bottom and from left to right: IPSL (no correction), CDF-t, Intervar-dOTC, Intervar-R2D2, spatial-dOTC, spatial R2D2, spatial-intervar-dOTC, spatial-intervar-R2D2.

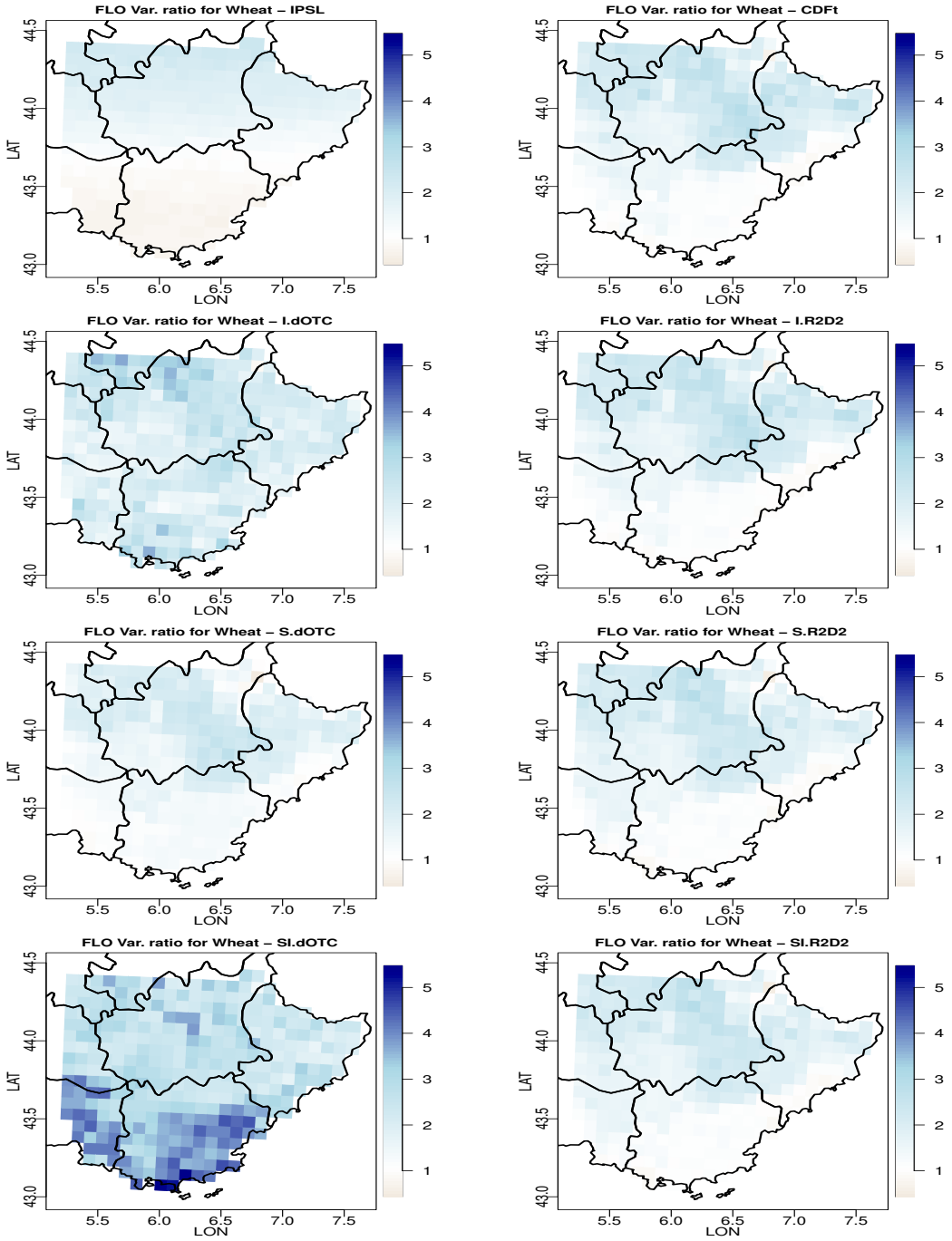

Figure 5.14: For each bias correction method and for wheat: map of the FLO variance ratio between future and past in Provence. From top to bottom and from left to right: IPSL (no correction), CDF-t, Intervar-dOTC, Intervar-R2D2, spatial-dOTC, spatial R2D2, spatial-intervar-dOTC, spatial-intervar-R2D2.

5.5.2 Maize

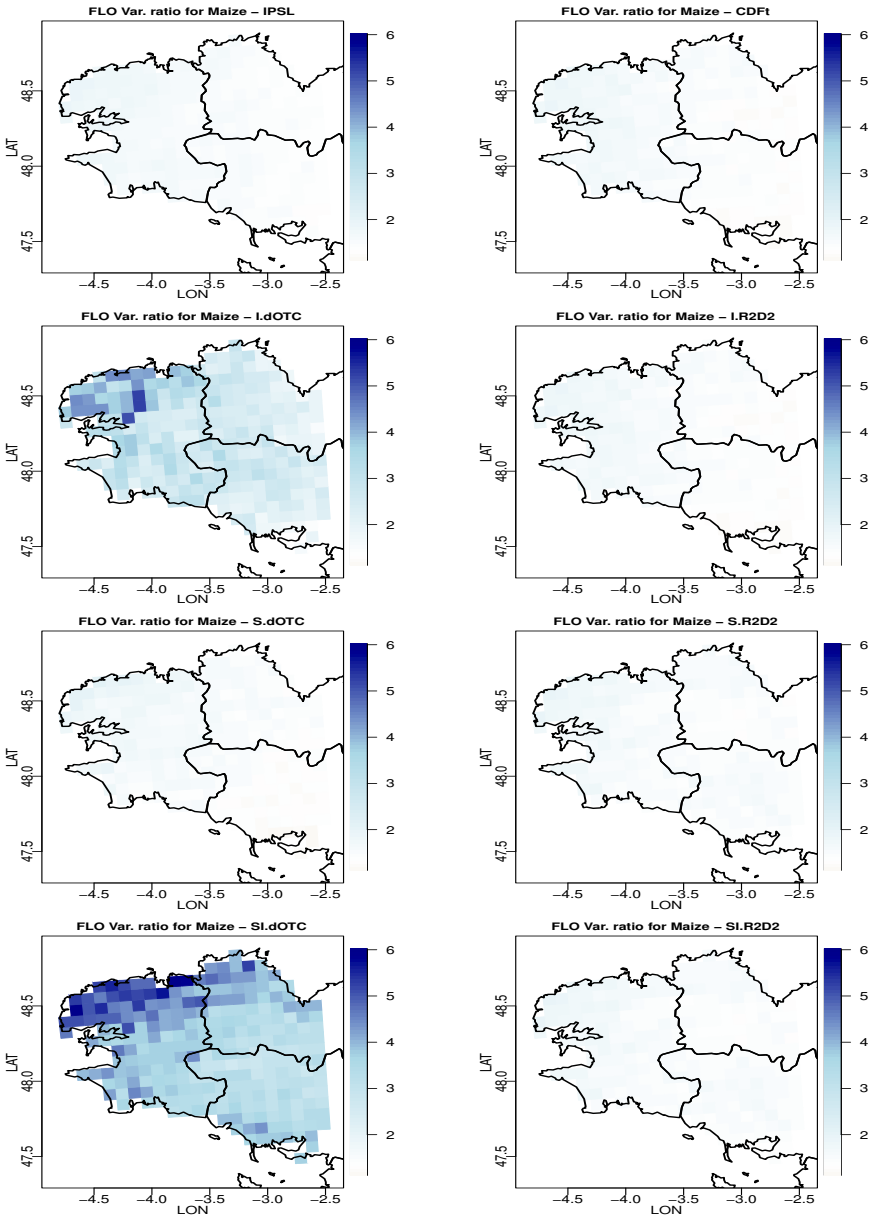

Figure 5.15: For each bias correction method and for maize: map of the FLO variance ratio between future and past in Brittany. From top to bottom and from left to right: IPSL (no correction), CDF-t, Intervar-dOTC, Intervar-R2D2, spatial-dOTC, spatial R2D2, spatial-intervar-dOTC, spatial-intervar-R2D2.

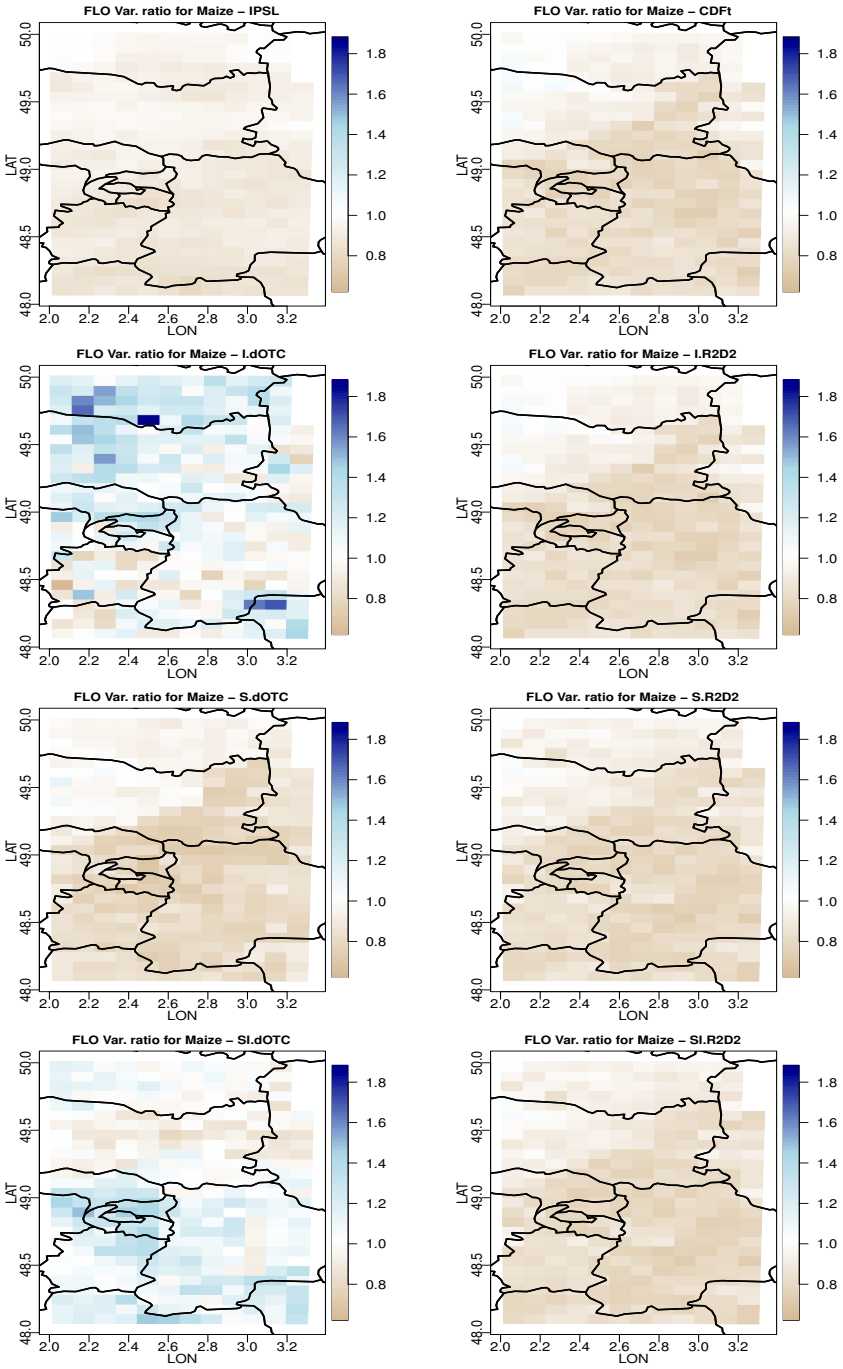

Figure 5.16: For each bias correction method and for maize: map of the FLO variance ratio between future and past in Ile de France. From top to bottom and from left to right: IPSL (no correction), CDF-t, Intervar-dOTC, Intervar-R2D2, spatial-dOTC, spatial R2D2, spatial-intervar-dOTC, spatial-intervar-R2D2.

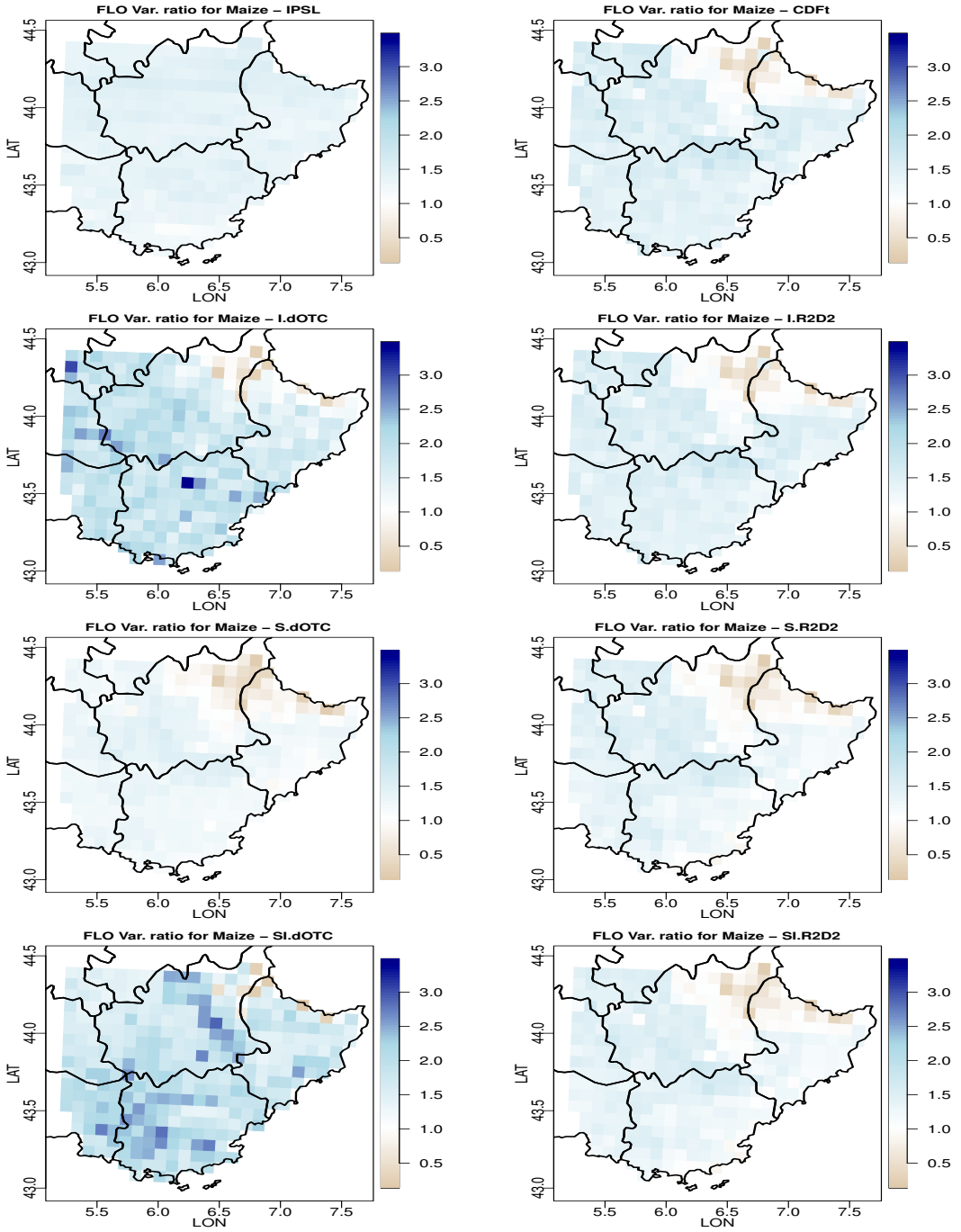

Figure 5.17: For each bias correction method and for maize: map of the FLO variance ratio between future and past in Provence. From top to bottom and from left to right: IPSL (no correction), CDF-t, Intervar-dOTC, Intervar-R2D2, spatial-dOTC, spatial R2D2, spatial-intervar-dOTC, spatial-intervar-R2D2.

5.5.3 Vine

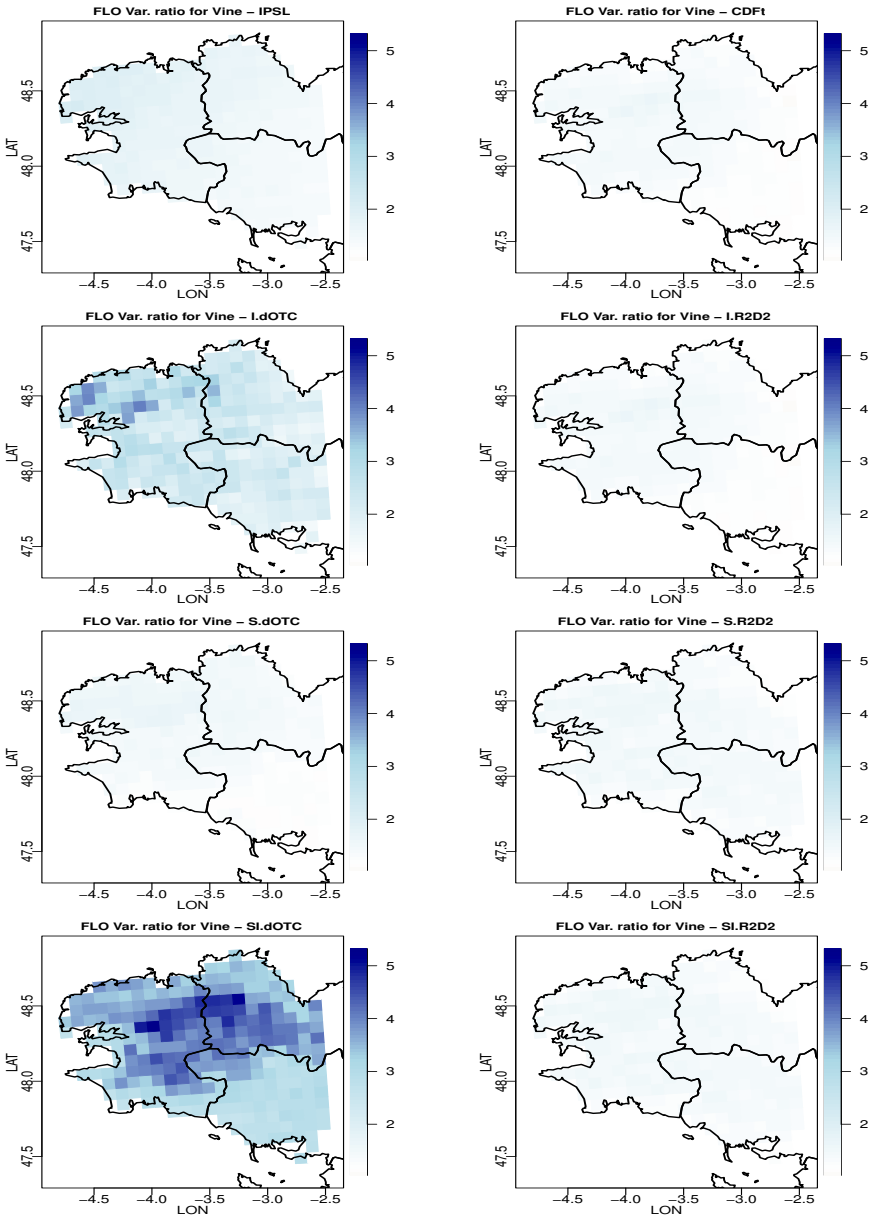

Figure 5.18: For each bias correction method and for vine: map of the FLO variance ratio between future and past in Brittany. From top to bottom and from left to right: IPSL (no correction), CDF-t, Intervar-dOTC, Intervar-R2D2, spatial-dOTC, spatial R2D2, spatial-intervar-dOTC, spatial-intervar-R2D2.

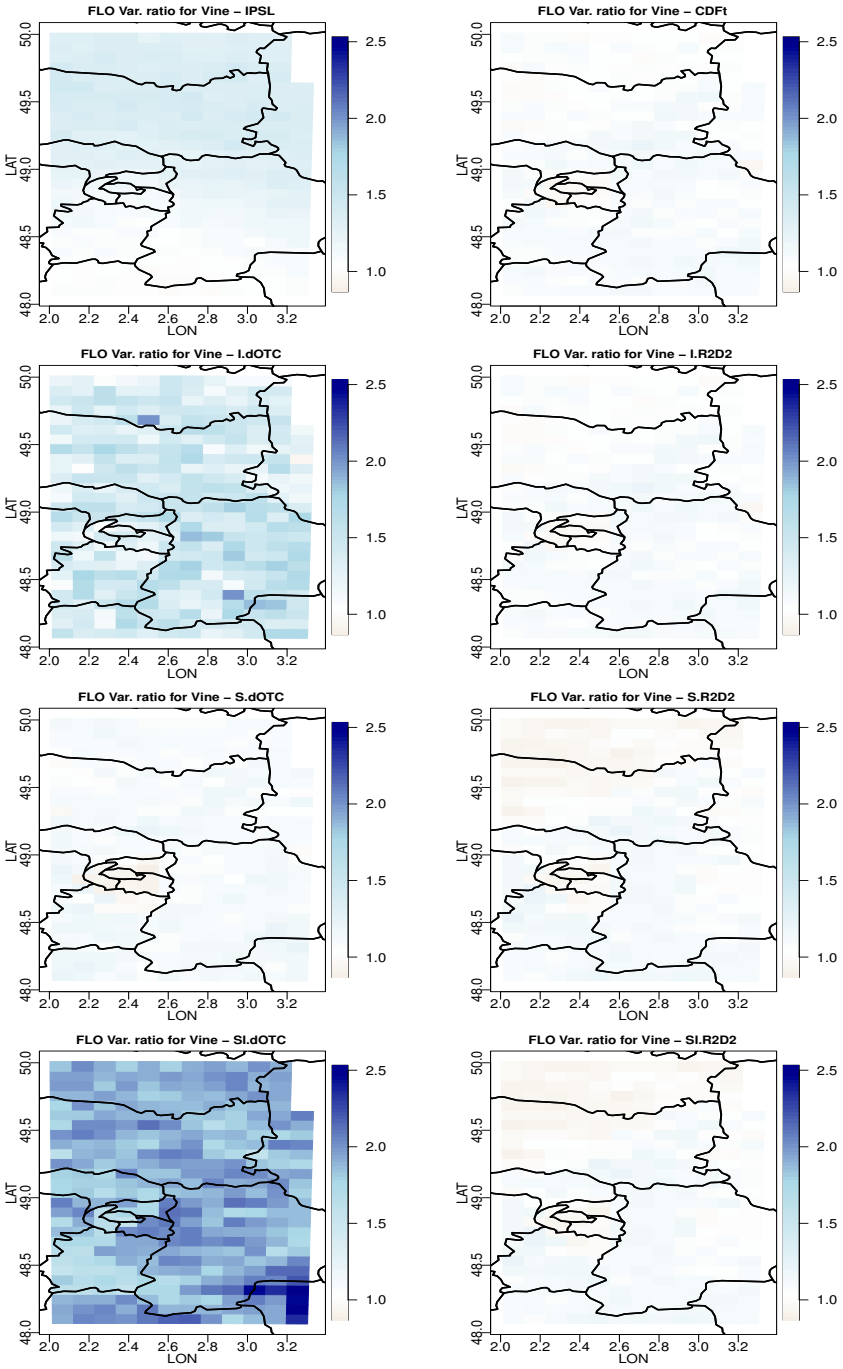

Figure 5.19: For each bias correction method and for vine: map of the FLO variance ratio between future and past in Ile de France. From top to bottom and from left to right: IPSL (no correction), CDF-t, Intervar-dOTC, Intervar-R2D2, spatial-dOTC, spatial R2D2, spatial-intervar-dOTC, spatial-intervar-R2D2.

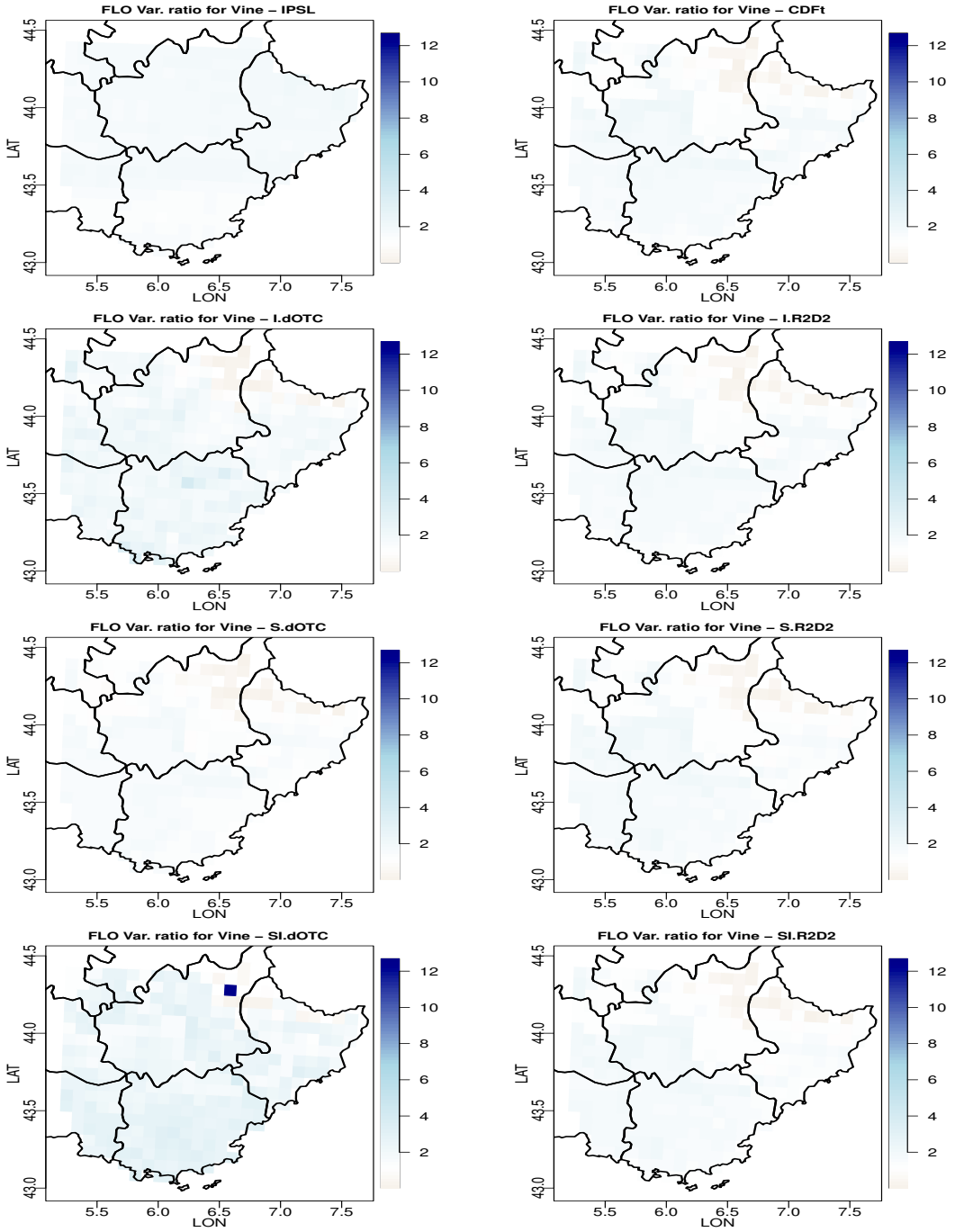

Figure 5.20: For each bias correction method and for vine: map of the FLO variance ratio between future and past in Provence. From top to bottom and from left to right: IPSL (no correction), CDF-t, Intervar-dOTC, Intervar-R2D2, spatial-dOTC, spatial R2D2, spatial-intervar-dOTC, spatial-intervar-R2D2.

Chapter 6

Soil Water Content in the past: 1984-2014

We consider here the average of the Soil Water Content computed over the meteorological summer, i.e. from June 1st to August 31st. We obtain similar results with Reserve, which are therefore not not shown.

6.1 Boxplots

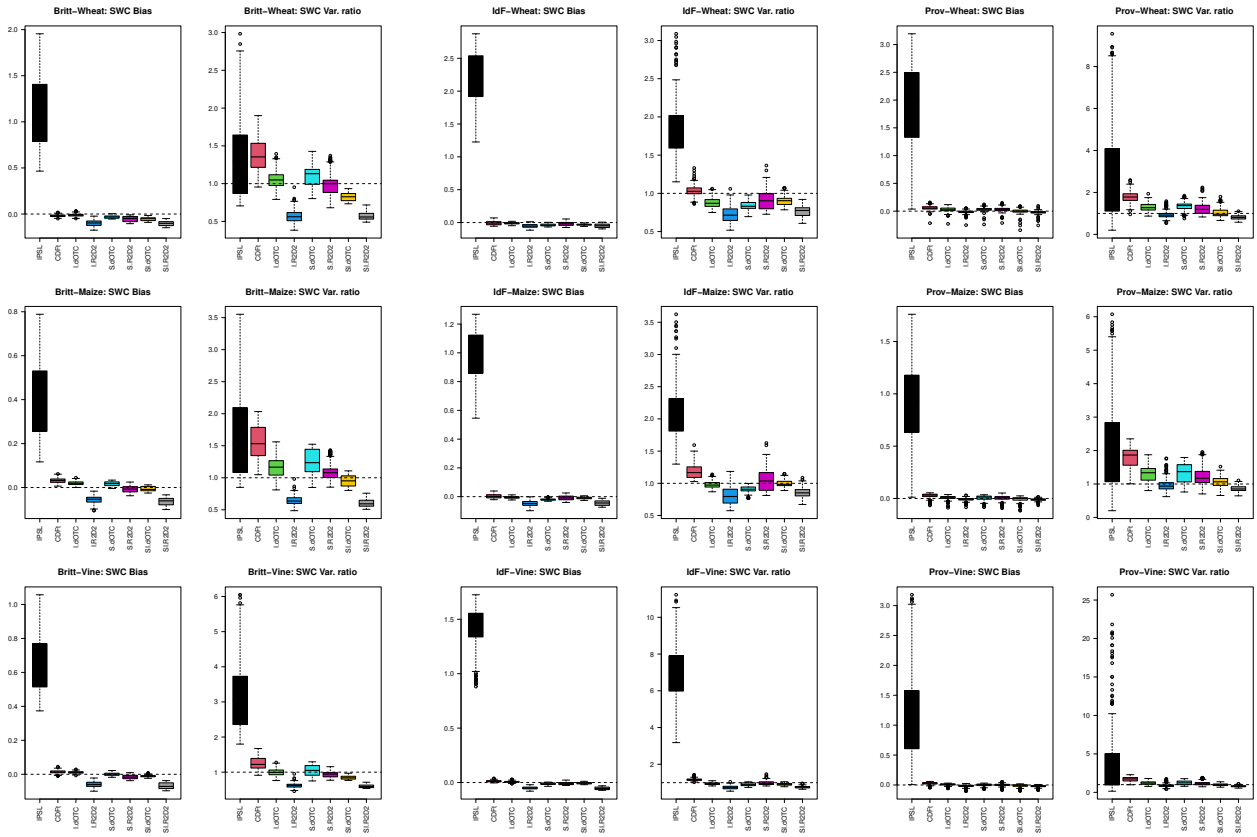

Figure 6.1: Overall summer SWC bias to SAFRAN and summer SWC's variance ratio to SAFRAN for all bias correction methods. Top row: wheat. Middle row: Maize. Bottom row: Vine. Left column: Bretagne. Middle column: Ile de France. Right column: Provence. In each panel, from left to right: IPSL (no correction), CDF-t, Intervar-dOTC, Intervar-R2D2, spatial-dOTC, spatial R2D2, spatial-intervar-dOTC, spatial-intervar-R2D2.

6.2 Covariances

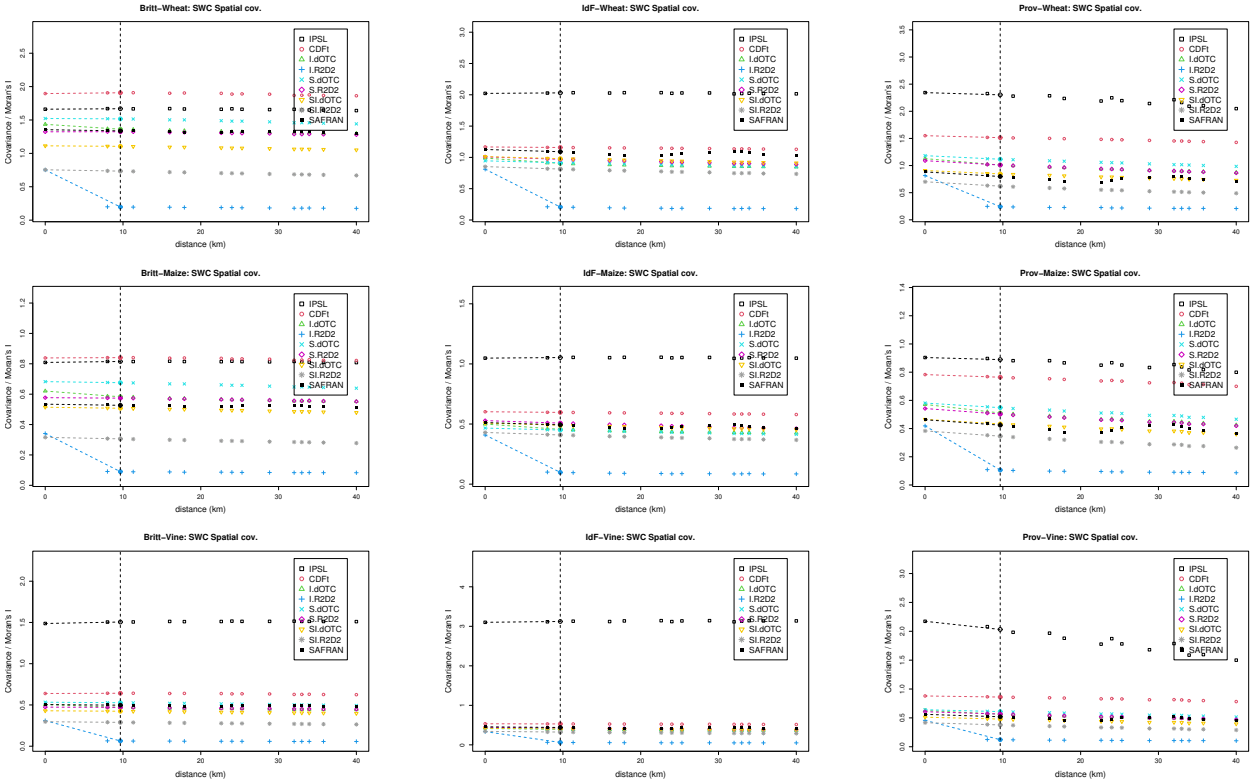

Figure 6.2: Spatial covariance and Moran's I of summer SWC in the past for all bias correction methods. Top row: wheat. Middle row: Maize. Bottom row: Vine. Left column: Bretagne. Middle column: Ile de France. Right column: Provence.

6.3 p-values

		IPSL	CDFt	I.dOTC	I.R2D2	S.dOTC	S.R2D2	SI.dOTC	SI.R2D2
p-values for "equality-of-means" tests									
Britt.	wheat	0.000	**0.570**	**0.798**	0.005	**0.467**	**0.137**	**0.151**	0.002
	maize	0.000	0.053	**0.370**	0.000	**0.446**	**0.661**	**0.766**	0.000
	vine	0.000	**0.312**	**0.634**	0.000	**0.983**	**0.335**	**0.570**	0.000
IdF	wheat	0.000	**0.773**	**0.770**	**0.131**	**0.339**	**0.567**	**0.441**	**0.133**
	maize	0.000	**0.884**	**0.778**	0.002	**0.290**	**0.634**	**0.620**	0.006
	vine	0.000	**0.407**	**0.724**	0.002	**0.503**	**0.577**	**0.749**	0.000
Prov.	wheat	0.000	0.024	**0.342**	**0.598**	**0.387**	**0.343**	**0.982**	**0.409**
	maize	0.000	0.091	**0.688**	**0.550**	**0.728**	**0.841**	**0.685**	0.000
	vine	0.000	0.071	**0.726**	**0.269**	**0.944**	**0.988**	**0.492**	**0.176**
p-values for "equality-of-variances" tests									
Britt.	wheat	0.000	0.000	**0.304**	0.000	0.024	**0.596**	0.000	0.000
	maize	0.000	0.000	0.000	0.000	0.000	0.027	**0.276**	0.000
	vine	0.000	0.000	**0.955**	0.000	**0.130**	0.053	0.000	0.000
IdF	wheat	0.000	**0.392**	0.016	0.000	0.001	0.016	0.051	0.000
	maize	0.000	0.000	**0.520**	0.000	0.013	**0.352**	**0.825**	0.000
	vine	0.000	0.000	**0.214**	0.000	0.007	**0.461**	0.020	0.000
Prov.	wheat	0.000	0.000	0.000	0.050	0.000	0.000	**0.526**	0.000
	maize	0.000	0.000	0.000	0.003	0.000	0.000	**0.880**	0.000
	vine	0.000	0.000	0.012	0.000	0.000	0.007	0.007	0.000
p-values for "equality-of-Moran's I" tests									
Britt.	wheat	0.000	0.000	**0.737**	0.000	0.015	**0.828**	0.000	0.000
	maize	0.000	0.000	0.015	0.000	0.000	0.014	**0.282**	0.000
	vine	0.000	0.000	**0.214**	0.000	**0.116**	0.090	0.000	0.000
IdF	wheat	0.000	**0.143**	0.001	0.000	0.001	0.011	0.051	0.007
	maize	0.000	0.000	0.036	0.000	0.014	**0.403**	**0.863**	0.000
	vine	0.000	0.000	0.007	0.000	0.007	**0.331**	0.017	0.000
Prov.	wheat	0.000	0.000	0.000	0.000	0.000	0.000	**0.203**	0.000
	maize	0.000	0.000	0.000	0.003	0.000	0.000	**0.570**	0.000
	vine	0.000	0.000	0.012	0.000	0.000	0.006	0.008	0.000

Table 6.1: Statistical analysis for summer SWC: p-values for the Welsh t-test of absence of bias on the average (first block); Fisher F-test of equality of variance (second block) and its adaptation to testing the equality of Moran's I (third block). Non rejection at the confidence level 0.90 is indicated in bold font.

6.4 Maps for bias

6.4.1 Wheat

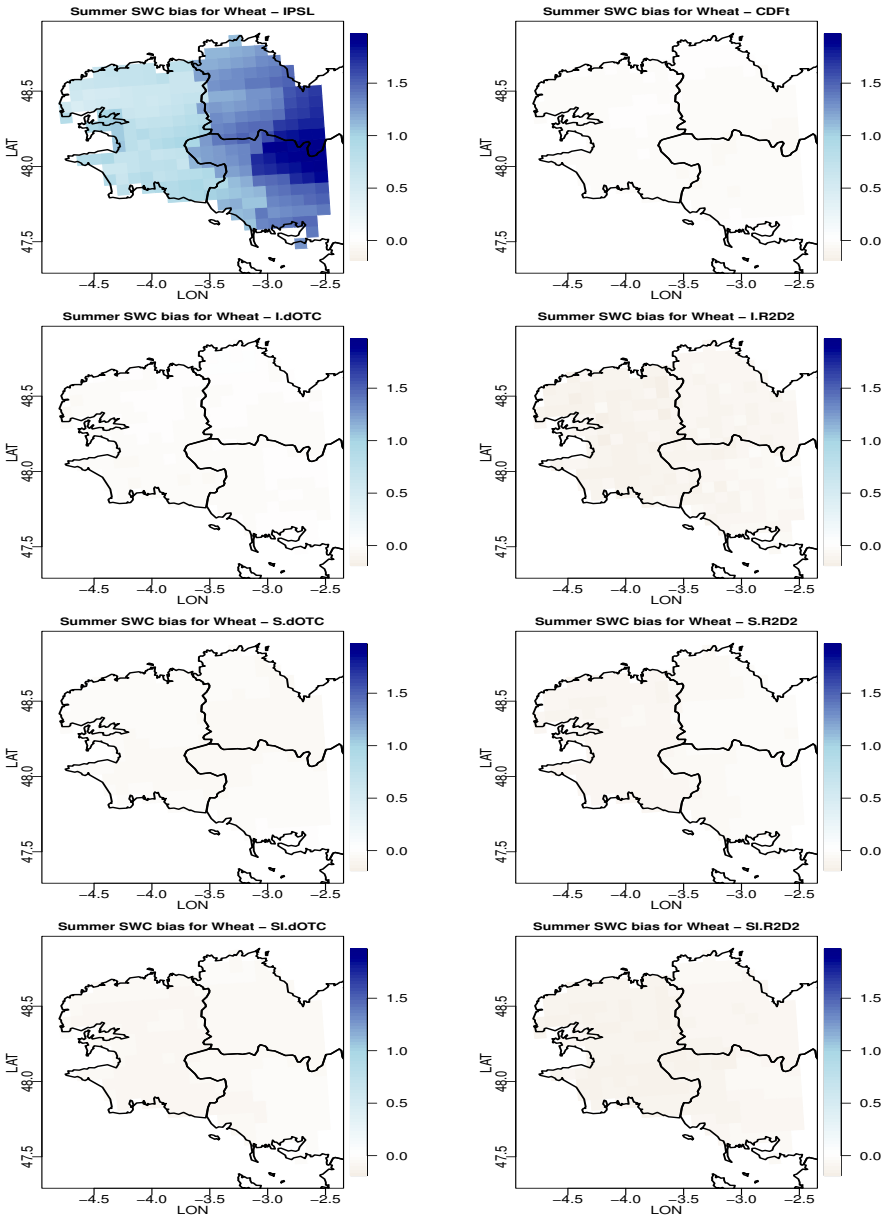

Figure 6.3: For each bias correction method and for wheat: map of summer SWC bias to SAFRAN in Brittany. From top to bottom and from left to right: IPSL (no correction), CDF-t, Intervar-dOTC, Intervar-R2D2, spatial-dOTC, spatial R2D2, spatial-intervar-dOTC, spatial-intervar-R2D2.

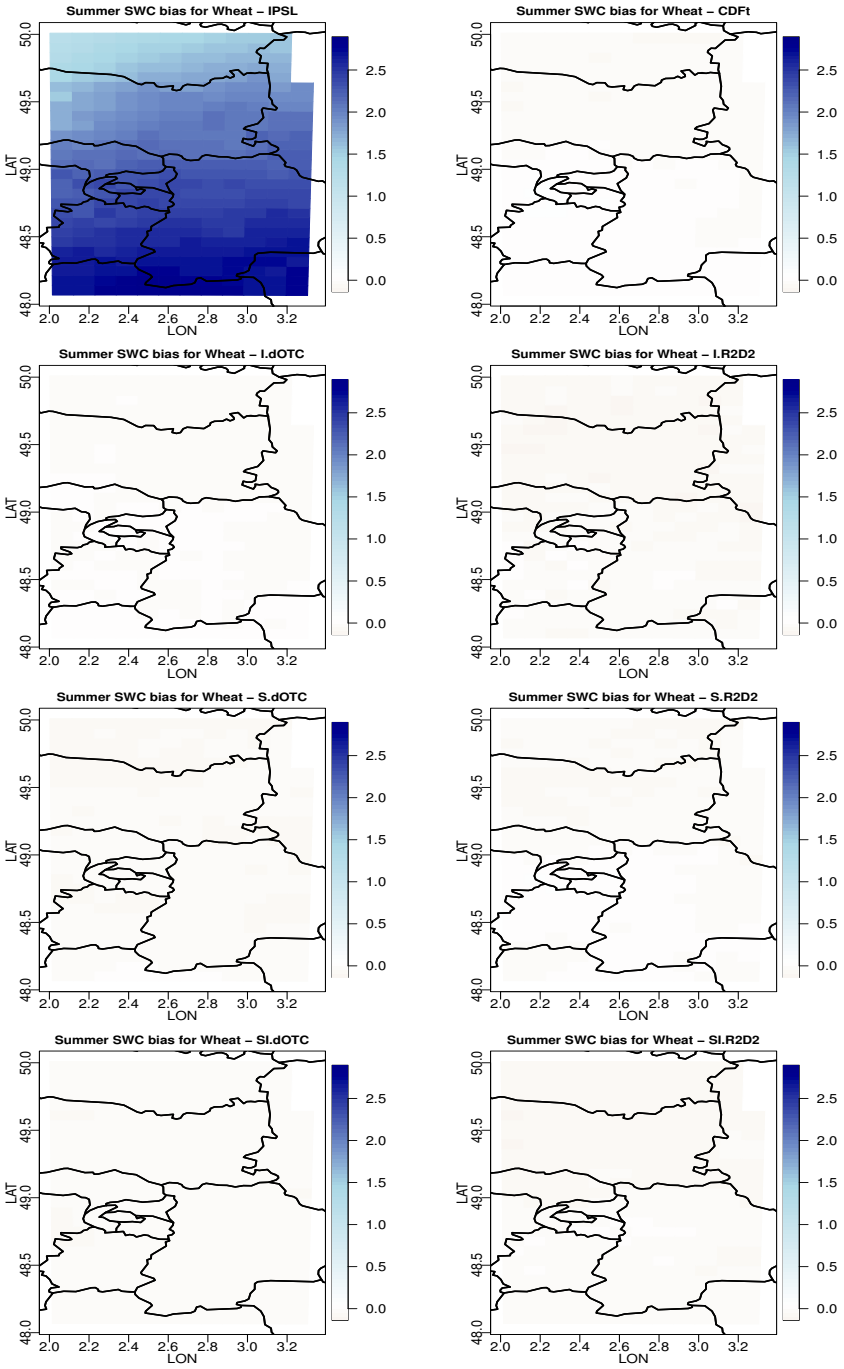

Figure 6.4: For each bias correction method and for wheat: map of summer SWC bias to SAFRAN in Ile-de-France. From top to bottom and from left to right: IPSL (no correction), CDF-t, Intervar-dOTC, Intervar-R2D2, spatial-dOTC, spatial R2D2, spatial-intervar-dOTC, spatial-intervar-R2D2.

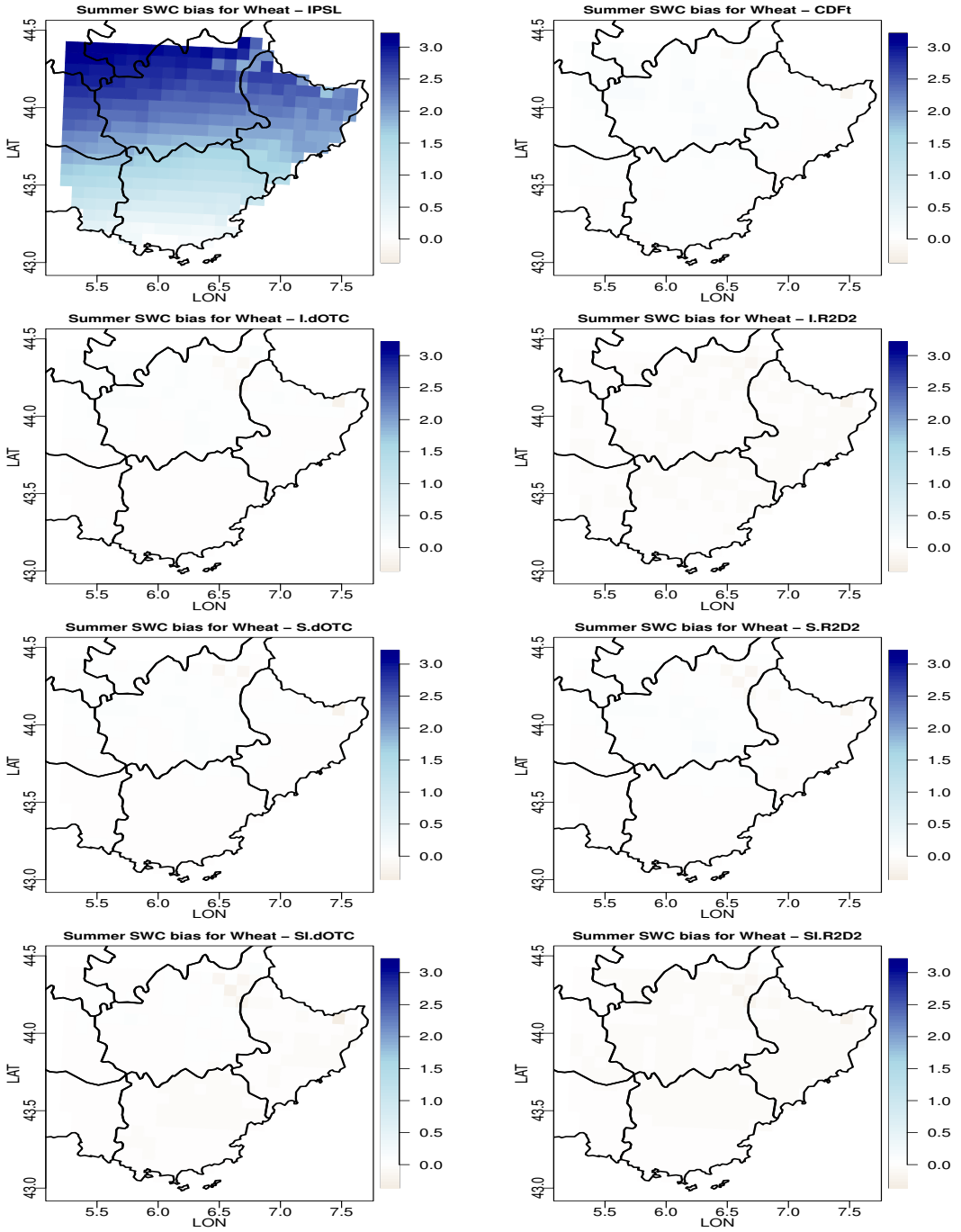

Figure 6.5: For each bias correction method and for wheat: map of summer SWC bias to SAFRAN in Provence. From top to bottom and from left to right: IPSL (no correction), CDF-t, Intervar-dOTC, Intervar-R2D2, spatial-dOTC, spatial R2D2, spatial-intervar-dOTC, spatial-intervar-R2D2.

6.4.2 Maize

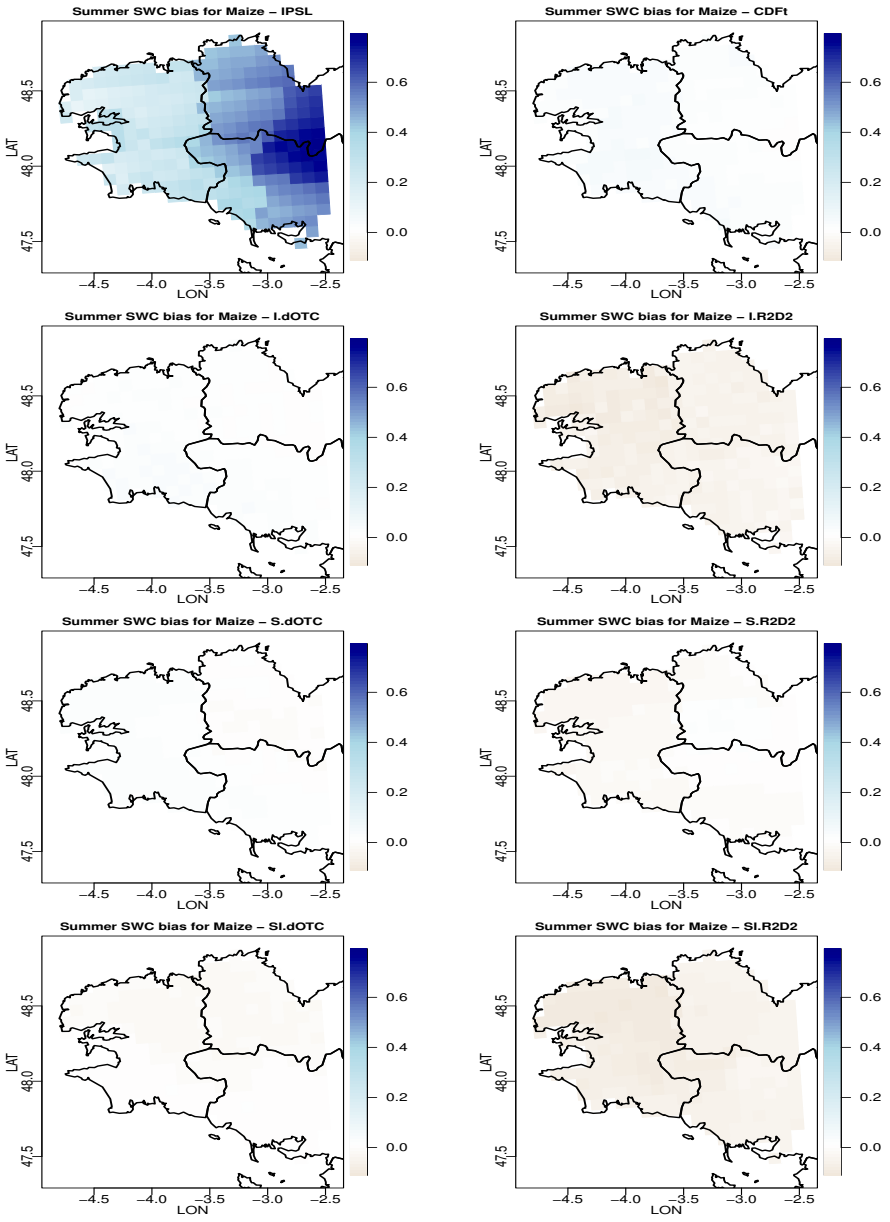

Figure 6.6: For each bias correction method and for maize: map of summer SWC bias to SAFRAN in Brittany. From top to bottom and from left to right: IPSL (no correction), CDF-t, Intervar-dOTC, Intervar-R2D2, spatial-dOTC, spatial R2D2, spatial-intervar-dOTC, spatial-intervar-R2D2.

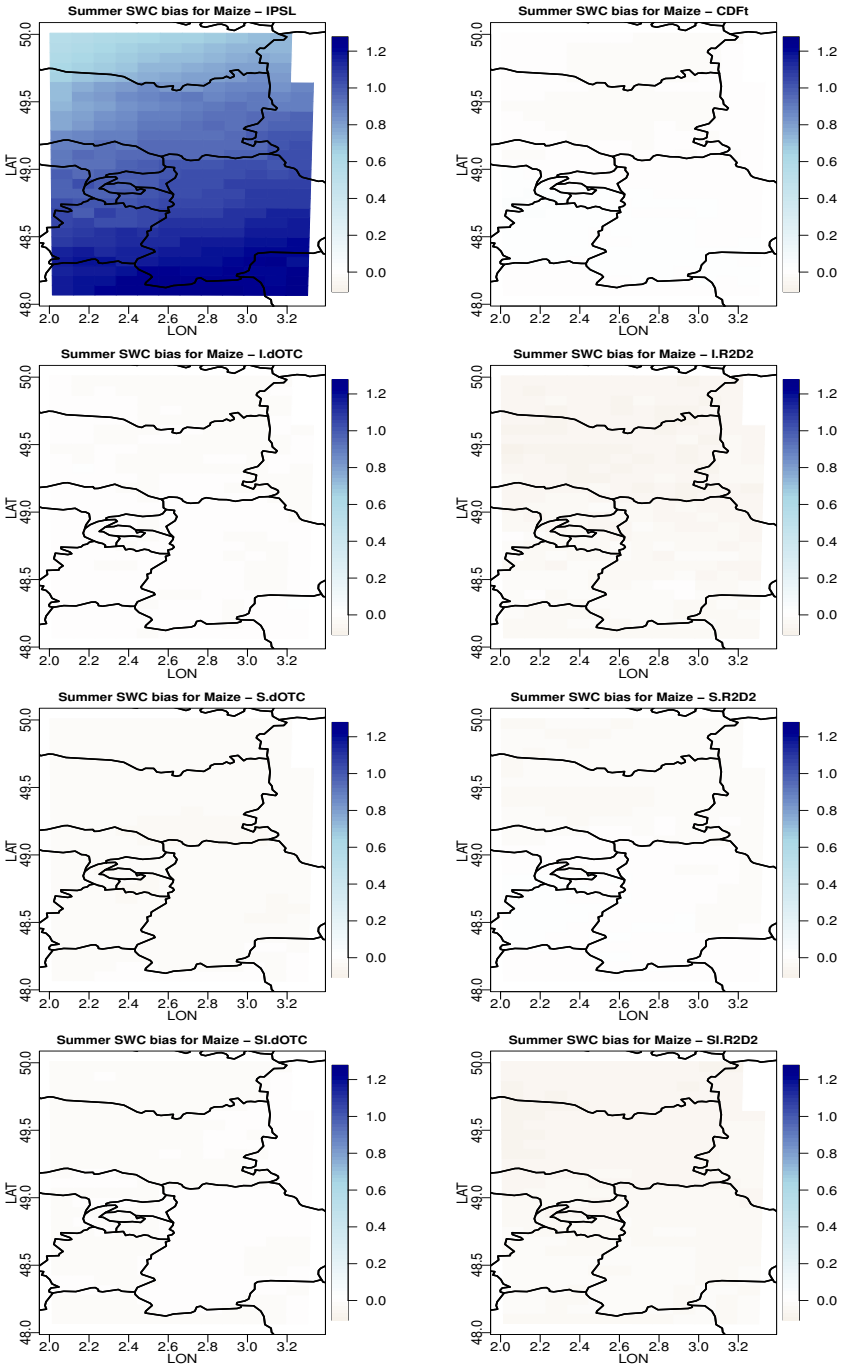

Figure 6.7: For each bias correction method and for maize: map of SWC bias to SAFRAN in Ile-de-France. From top to bottom and from left to right: IPSL (no correction), CDF-t, Intervar-dOTC, Intervar-R2D2, spatial-dOTC, spatial R2D2, spatial-intervar-dOTC, spatial-intervar-R2D2.

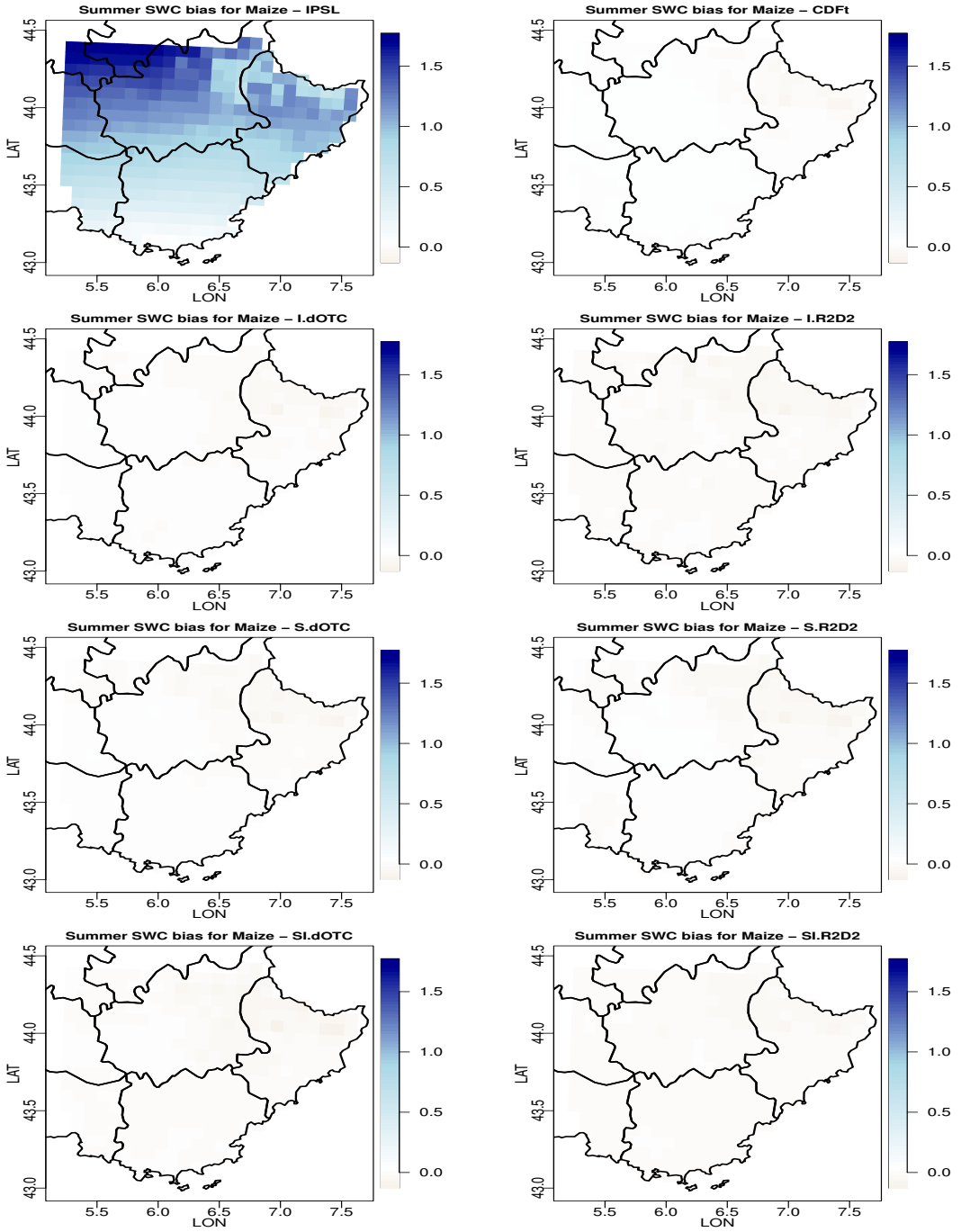

Figure 6.8: For each bias correction method and for maize: map of summer SWC bias to SAFRAN in Provence. From top to bottom and from left to right: IPSL (no correction), CDF-t, Intervar-dOTC, Intervar-R2D2, spatial-dOTC, spatial R2D2, spatial-intervar-dOTC, spatial-intervar-R2D2.

6.4.3 Vine

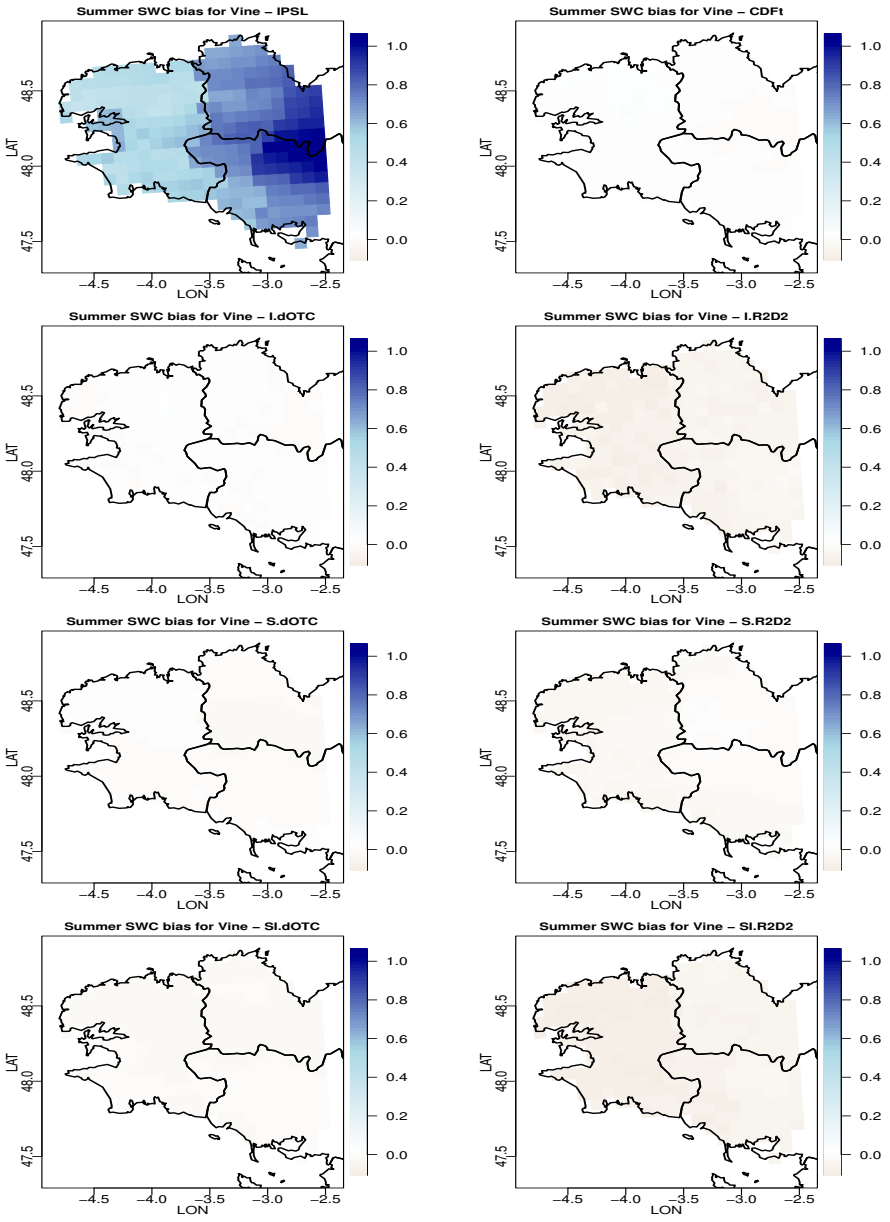

Figure 6.9: For each bias correction method and for vine: map of summer SWC bias to SAFRAN in Brittany. From top to bottom and from left to right: IPSL (no correction), CDF-t, Intervar-dOTC, Intervar-R2D2, spatial-dOTC, spatial R2D2, spatial-intervar-dOTC, spatial-intervar-R2D2.

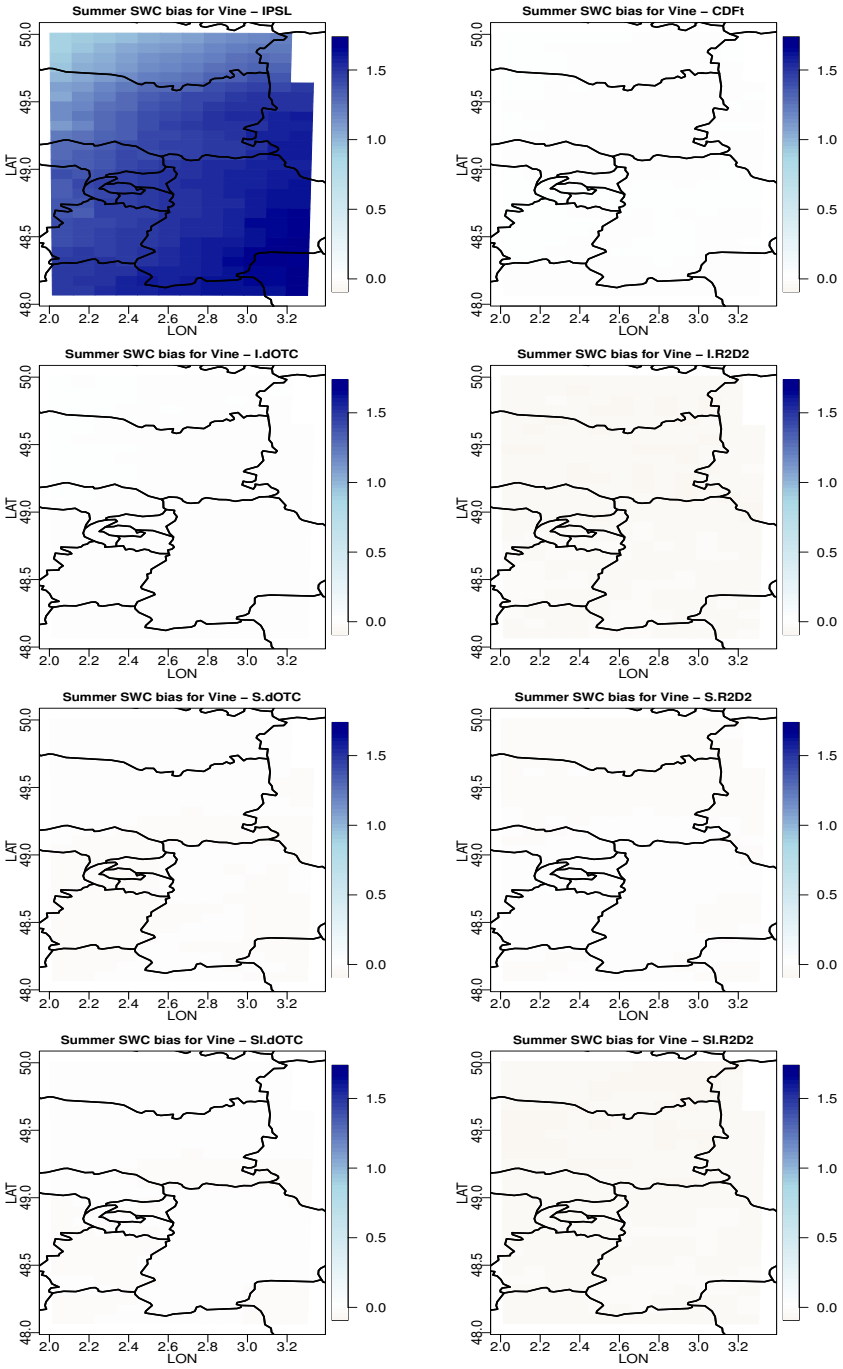

Figure 6.10: For each bias correction method and for vine: map of summer SWC bias to SAFRAN in Ile-de-France. From top to bottom and from left to right: IPSL (no correction), CDF-t, Intervar-dOTC, Intervar-R2D2, spatial-dOTC, spatial R2D2, spatial-intervar-dOTC, spatial-intervar-R2D2.

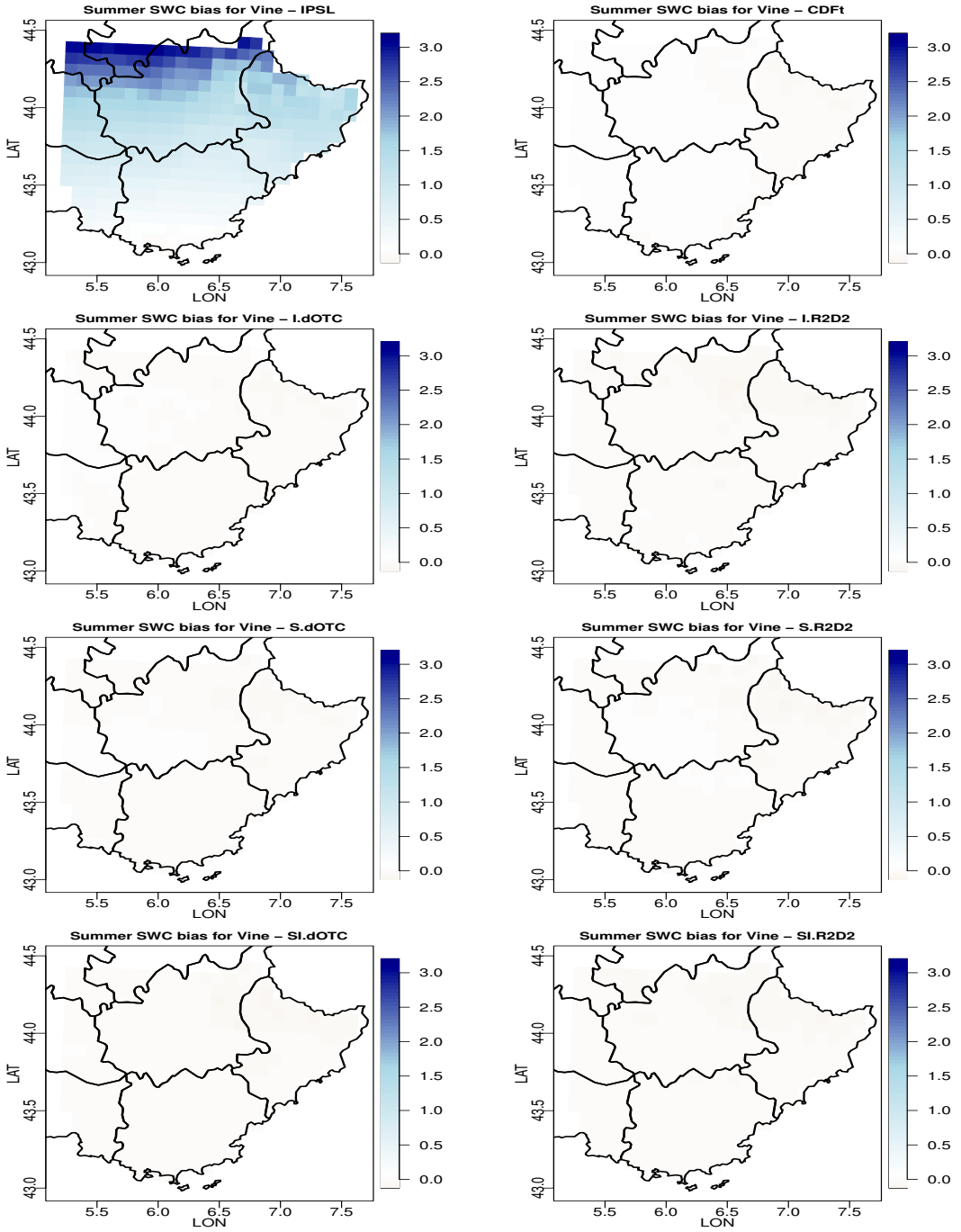

Figure 6.11: For each bias correction method and for vine: map of summer SWC bias to SAFRAN in Provence. From top to bottom and from left to right: IPSL (no correction), CDF-t, Intervar-dOTC, Intervar-R2D2, spatial-dOTC, spatial R2D2, spatial-intervar-dOTC, spatial-intervar-R2D2.

6.5 Maps for variance ratio

6.5.1 Wheat

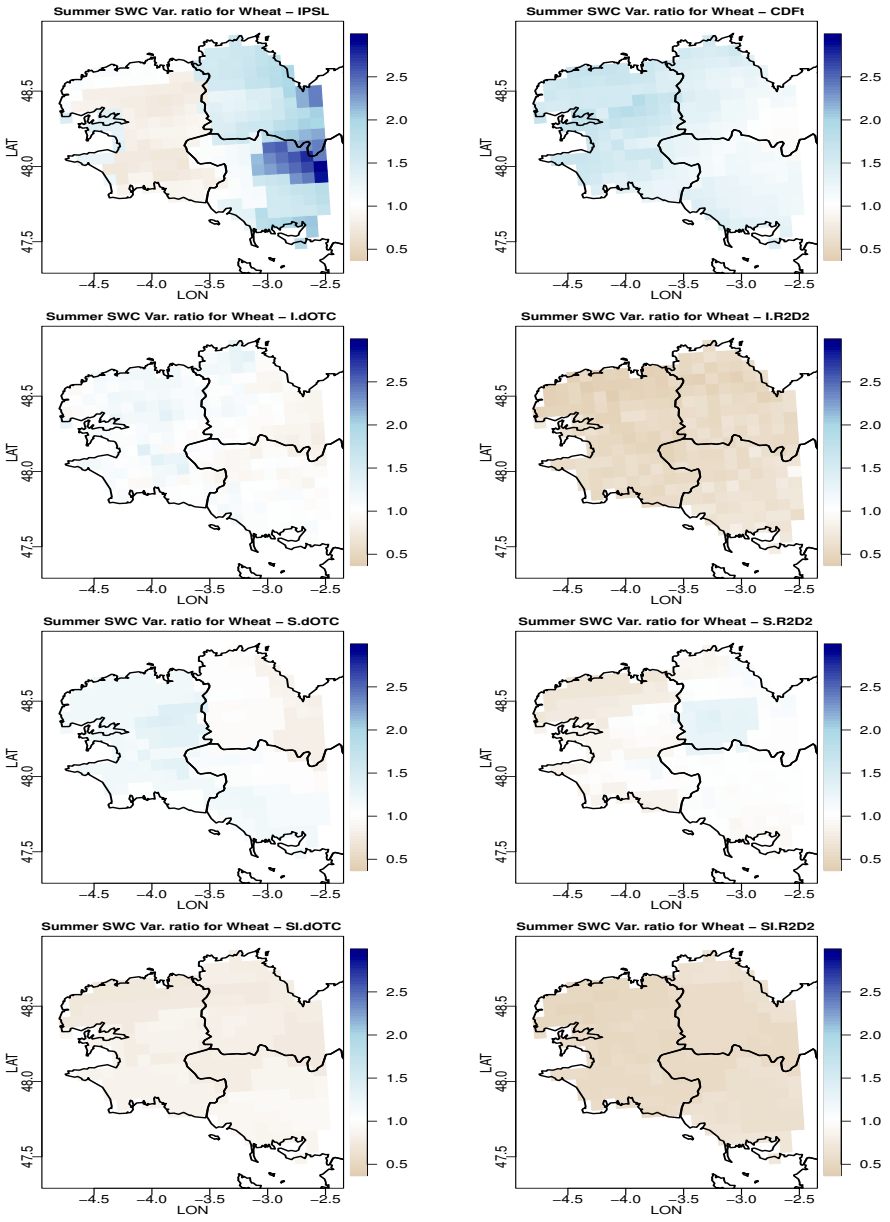

Figure 6.12: For each bias correction method and for wheat: map of summer SWC variance divided by summer SWC variance for SAFRAN in Brittany. From top to bottom and from left to right: IPSL (no correction), CDF-t, Intervar-dOTC, Intervar-R2D2, spatial-dOTC, spatial R2D2, spatial-intervar-dOTC, spatial-intervar-R2D2.

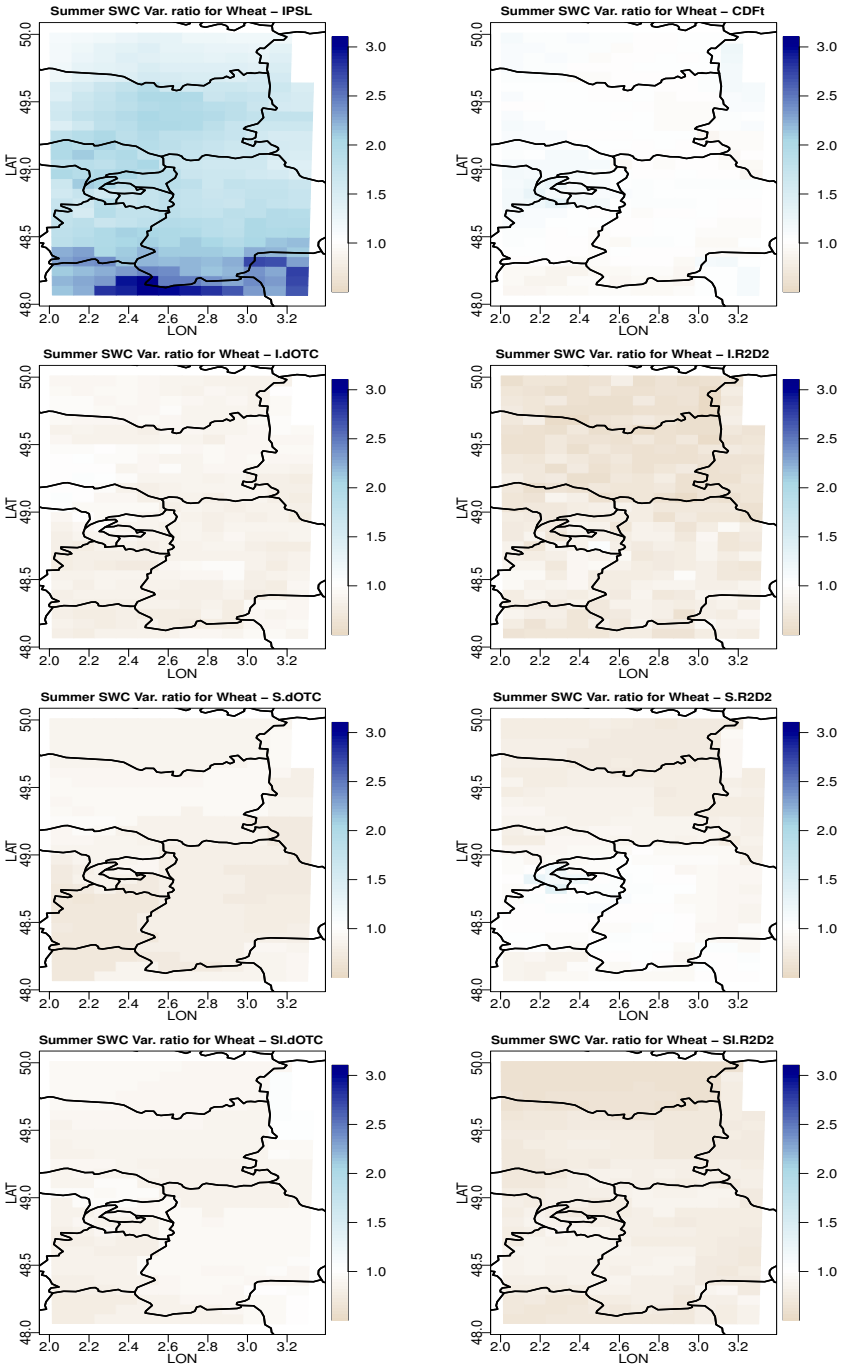

Figure 6.13: For each bias correction method and for wheat: map of summer SWC variance divided by summer SWC variance for SAFRAN in Ile-de-France. From top to bottom and from left to right: IPSL (no correction), CDF-t, Intervar-dOTC, Intervar-R2D2, spatial-dOTC, spatial R2D2, spatial-intervar-dOTC, spatial-intervar-R2D2.

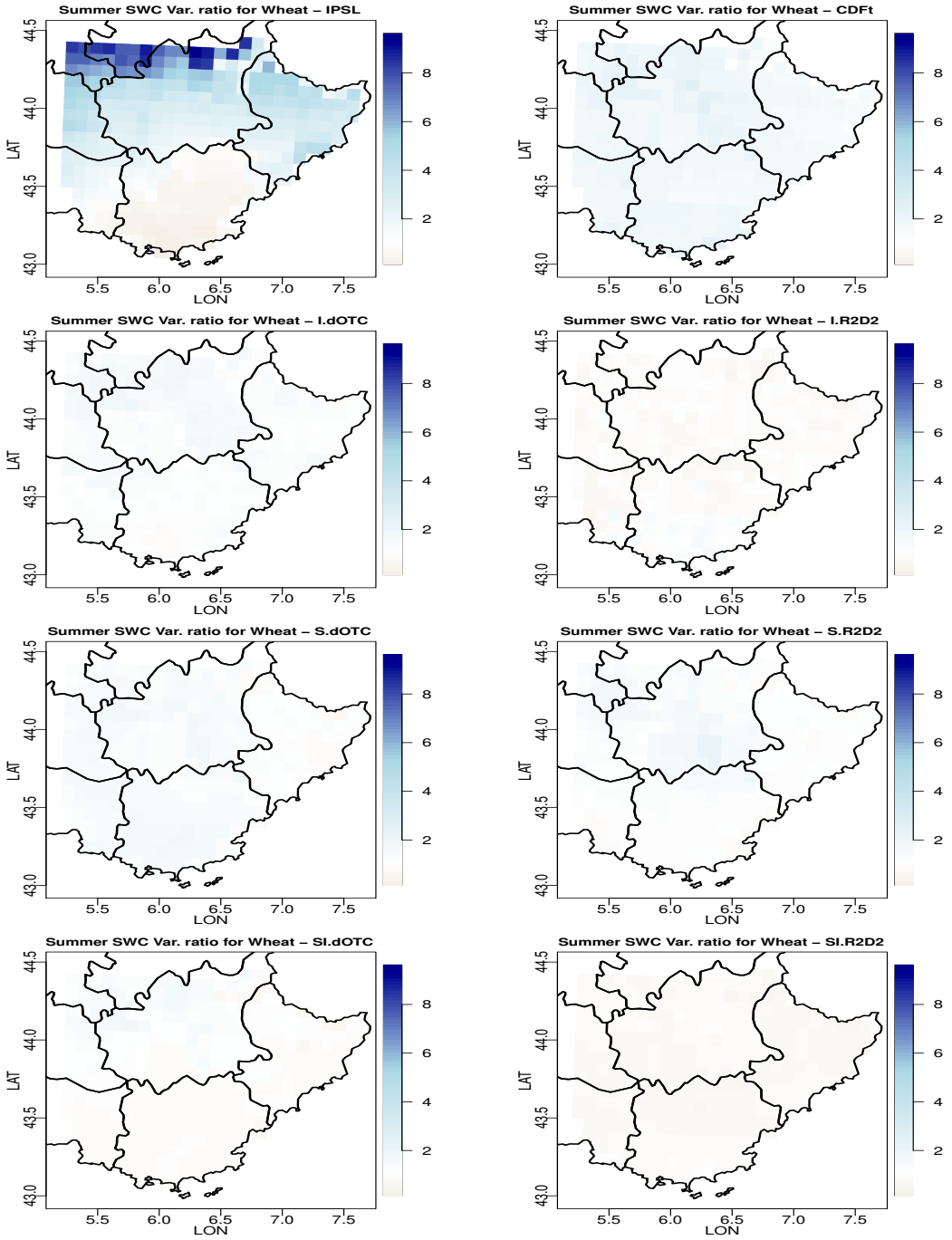

Figure 6.14: For each bias correction method and for wheat: map of summer SWC variance divided by summer SWC variance for SAFRAN in Provence. From top to bottom and from left to right: IPSL (no correction), CDF-t, Intervar-dOTC, Intervar-R2D2, spatial-dOTC, spatial R2D2, spatial-intervar-dOTC, spatial-intervar-R2D2.

6.5.2 Maize

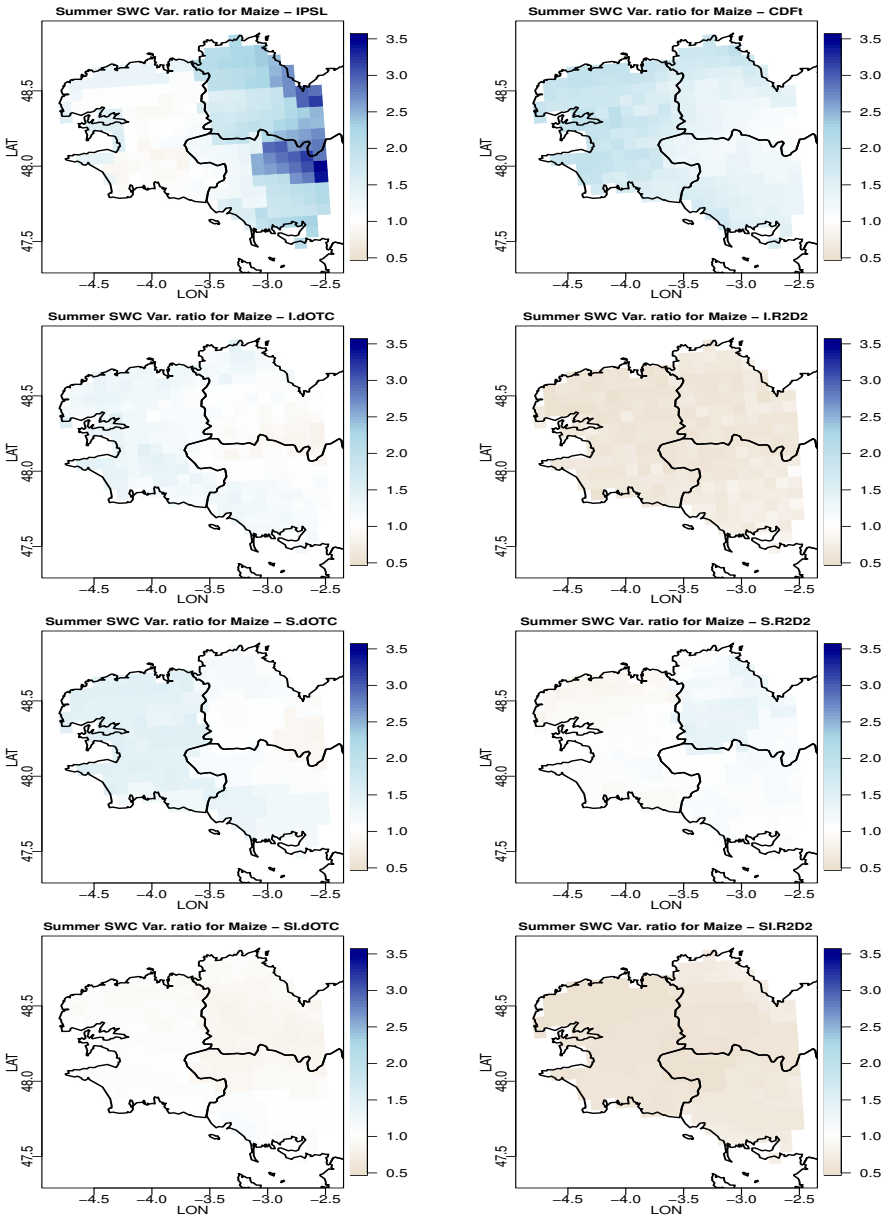

Figure 6.15: For each bias correction method and for maize: map of summer SWC variance divided by summer SWC variance for SAFRAN in Brittany. From top to bottom and from left to right: IPSL (no correction), CDF-t, Intervar-dOTC, Intervar-R2D2, spatial-dOTC, spatial R2D2, spatial-intervar-dOTC, spatial-intervar-R2D2.

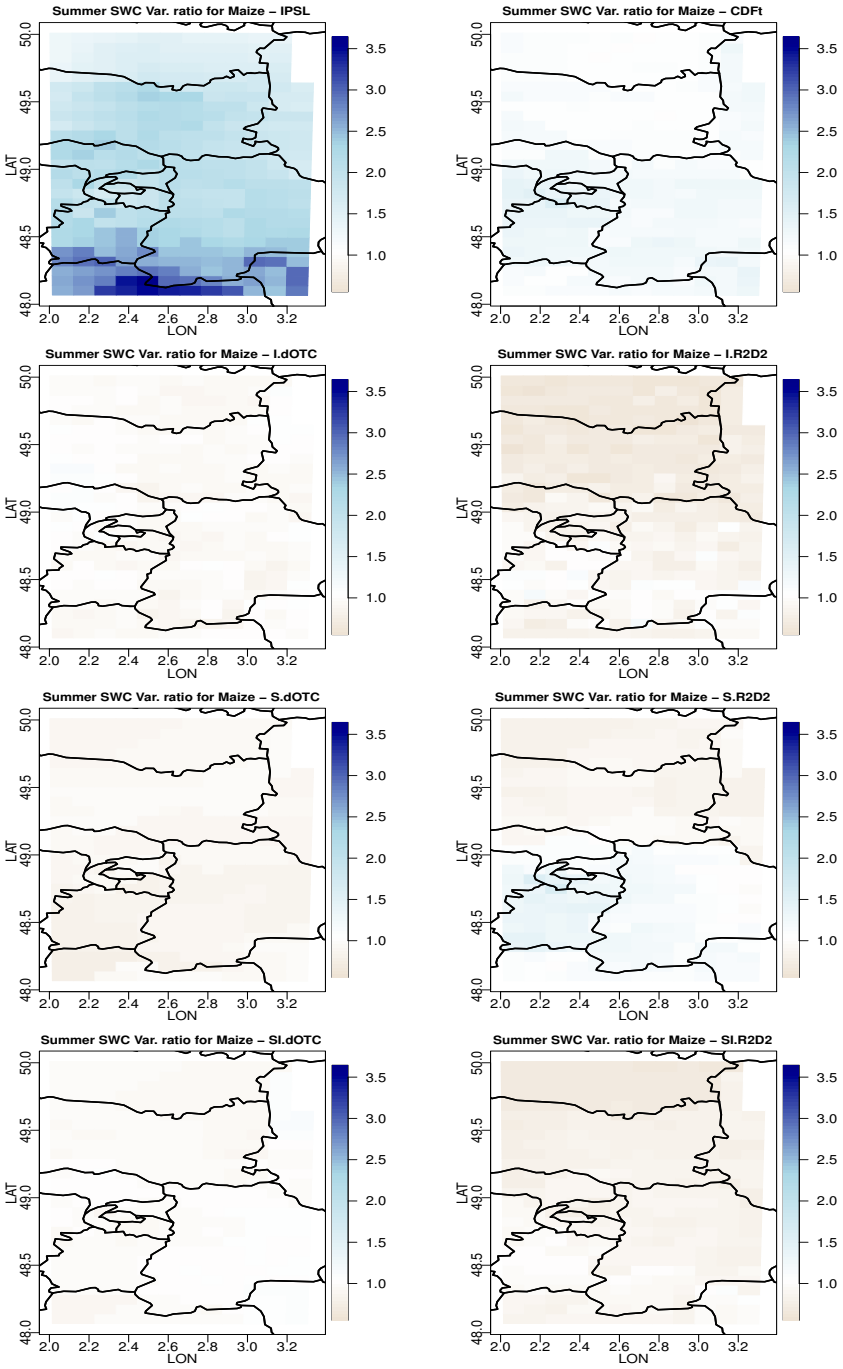

Figure 6.16: For each bias correction method and for maize: map of summer SWC variance divided by summer SWC variance for SAFRAN in Ile-de-France. From top to bottom and from left to right: IPSL (no correction), CDF-t, Intervar-dOTC, Intervar-R2D2, spatial-dOTC, spatial R2D2, spatial-intervar-dOTC, spatial-intervar-R2D2.

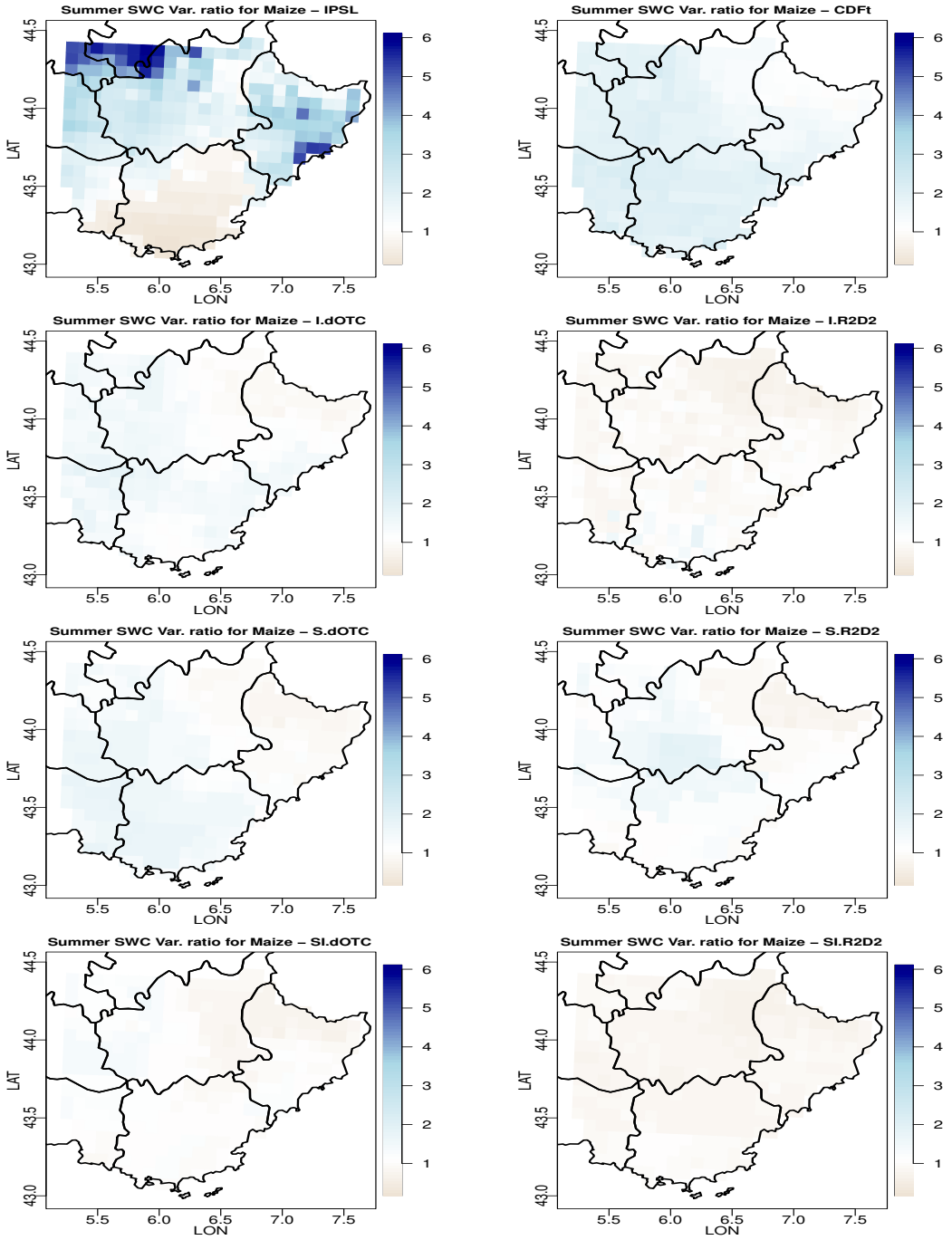

Figure 6.17: For each bias correction method and for maize: map of summer SWC variance divided by summer SWC variance for SAFRAN in Provence. From top to bottom and from left to right: IPSL (no correction), CDF-t, Intervar-dOTC, Intervar-R2D2, spatial-dOTC, spatial R2D2, spatial-intervar-dOTC, spatial-intervar-R2D2.

6.5.3 Vine

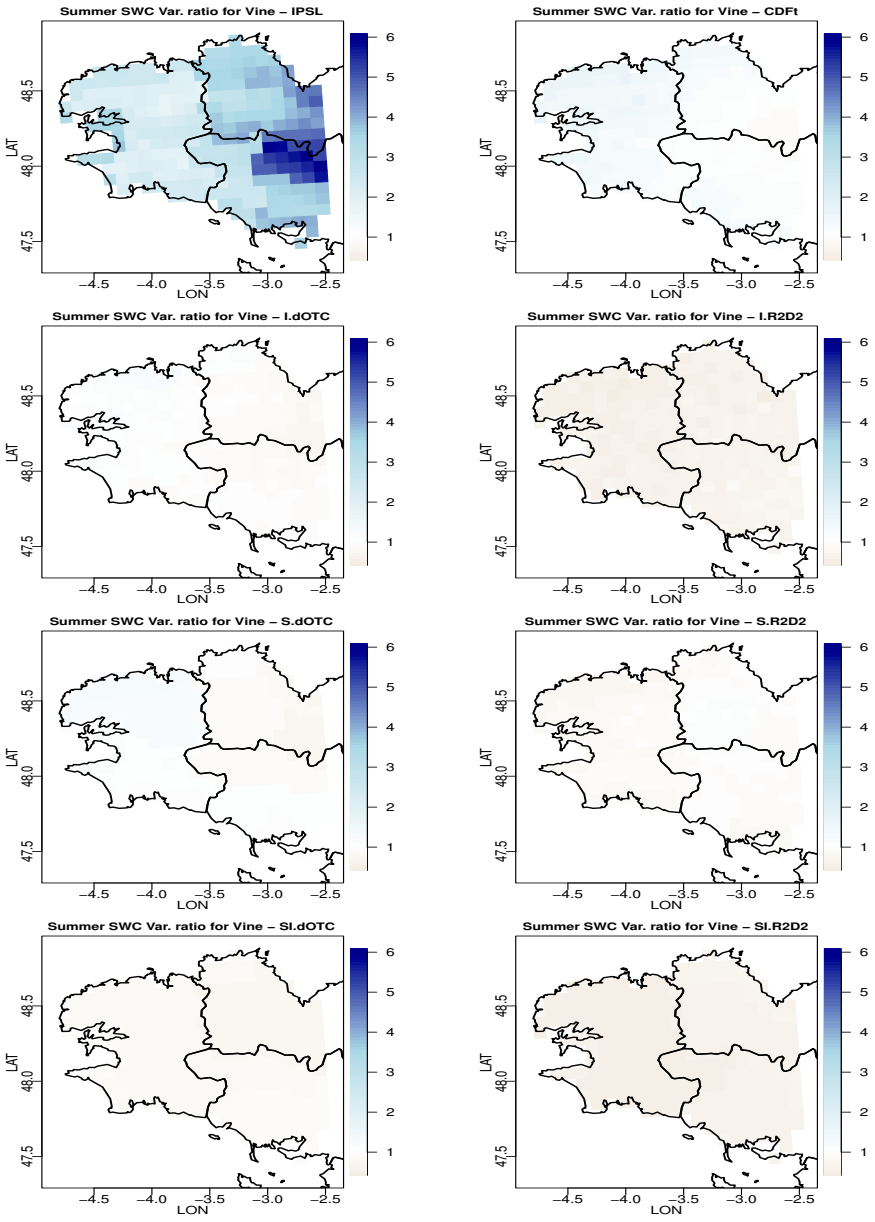

Figure 6.18: For each bias correction method and for vine: map of summer SWC variance divided by summer SWC variance for SAFRAN in Brittany. From top to bottom and from left to right: IPSL (no correction), CDF-t, Intervar-dOTC, Intervar-R2D2, spatial-dOTC, spatial R2D2, spatial-intervar-dOTC, spatial-intervar-R2D2.

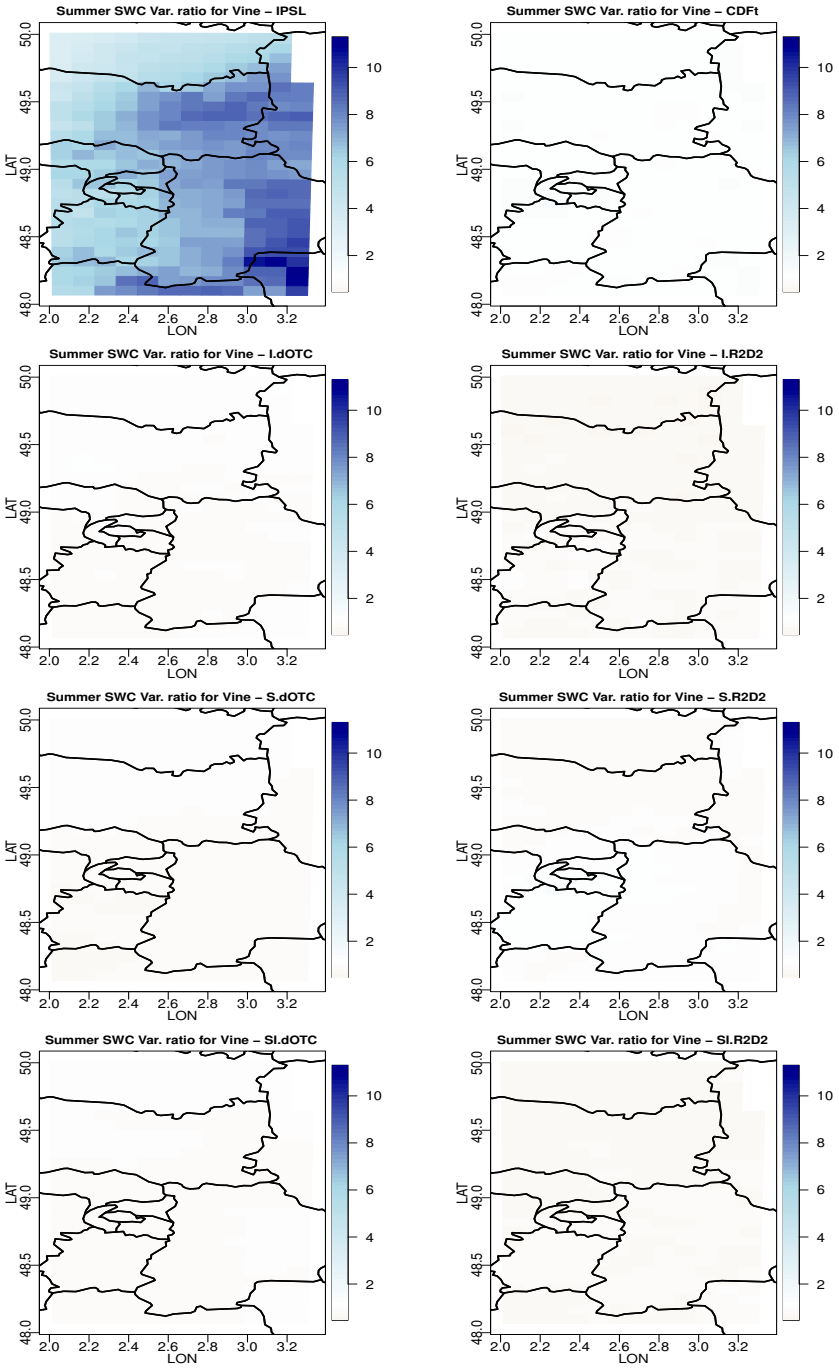

Figure 6.19: For each bias correction method and for vine: map of summer SWC variance divided by summer SWC variance for SAFRAN in Ile-de-France. From top to bottom and from left to right: IPSL (no correction), CDF-t, Intervar-dOTC, Intervar-R2D2, spatial-dOTC, spatial R2D2, spatial-intervar-dOTC, spatial-intervar-R2D2.

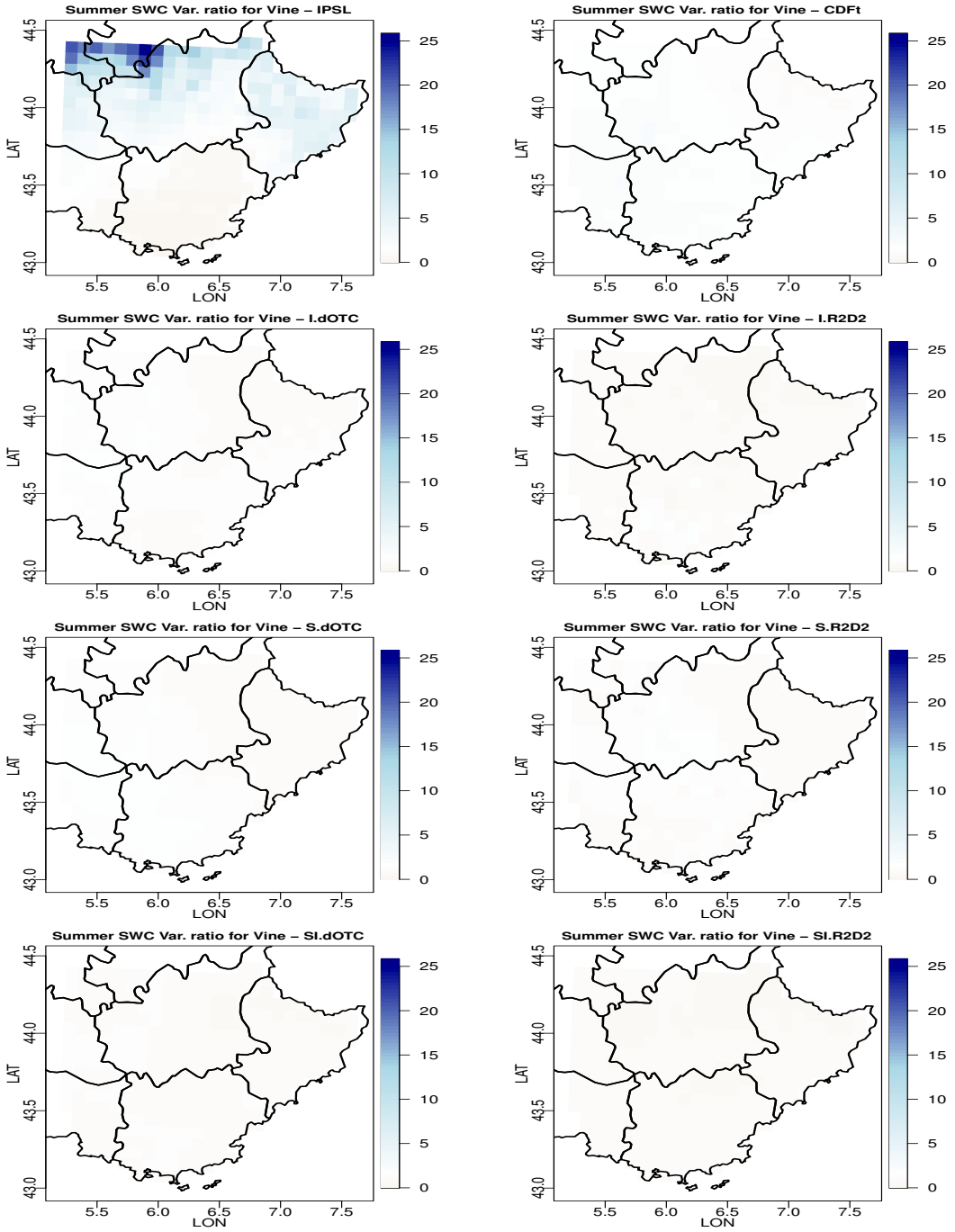

Figure 6.20: For each bias correction method and for vine: map of summer SWC variance divided by summer SWC variance for SAFRAN in Provence. From top to bottom and from left to right: IPSL (no correction), CDF-t, Intervar-dOTC, Intervar-R2D2, spatial-dOTC, spatial R2D2, spatial-intervar-dOTC, spatial-intervar-R2D2.

Chapter 7

Soil Water Content in the future: 2036-2065

We consider here the average of the Soil Water Content computed over the meteorological summer, i.e. from June 1st to August 31st. We obtain similar results with Reserve, which are therefore not not shown.

7.1 Boxplots

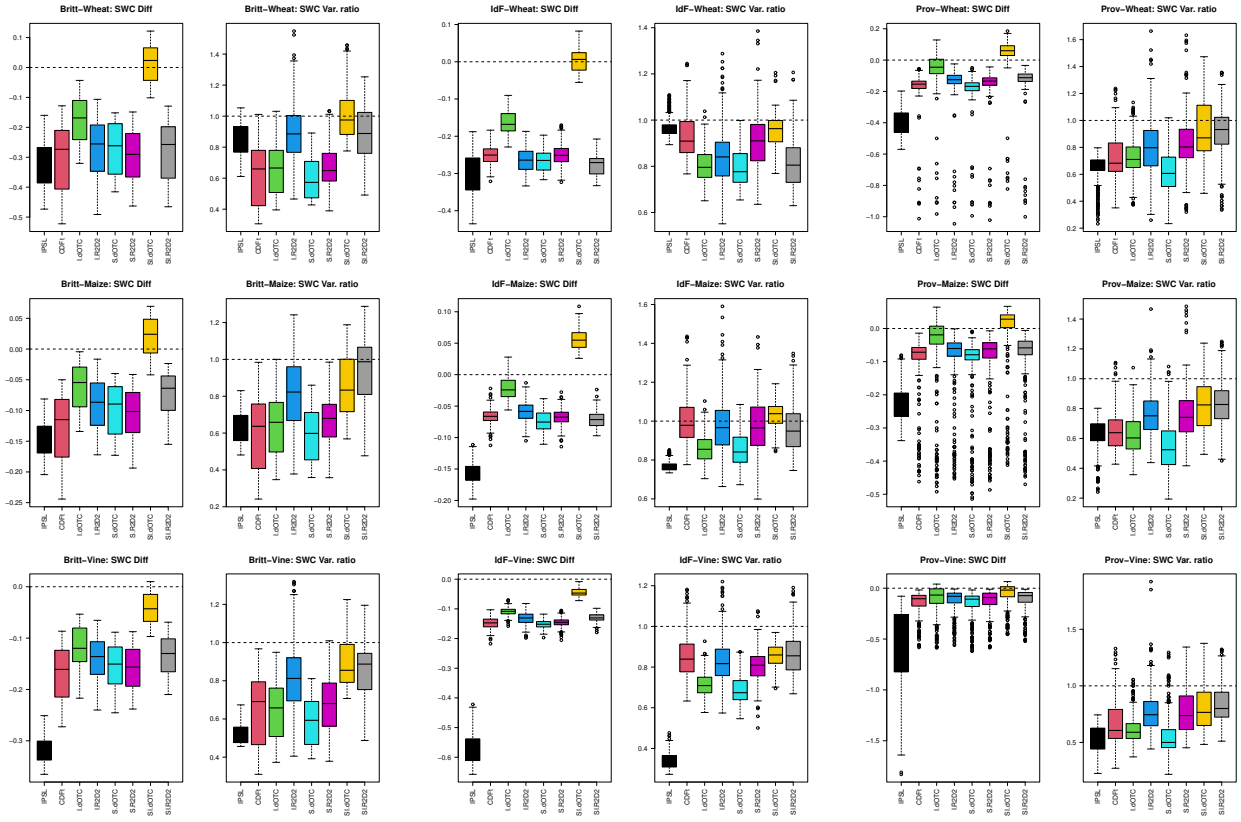

Figure 7.1: Overall summer SWC difference between future and past and summer SWC's variance ratio between future and past for all bias correction methods. Top row: wheat. Middle row: Maize. Bottom row: Vine. Left column: Bretagne. Middle column: Ile de France. Right column: Provence. In each panel, from left to right: IPSL (no correction), CDF-t, Intervar-dOTC, Intervar-R2D2, spatial-dOTC, spatial R2D2, spatial-intervar-dOTC, spatial-intervar-R2D2.

7.2 Covariances

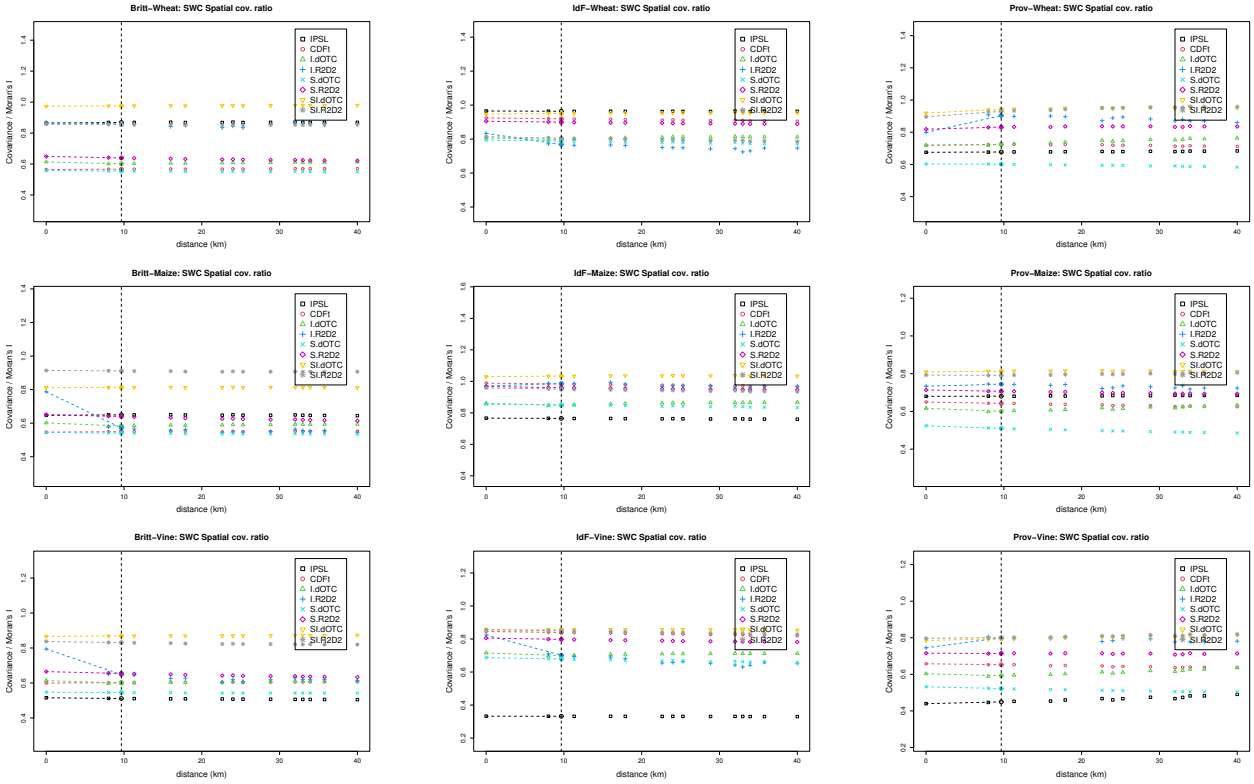

Figure 7.2: Spatial covariance and Moran's I ratio between future and past of summer SWC for all bias correction methods. Top row: wheat. Middle row: Maize. Bottom row: Vine. Left column: Bretagne. Middle column: Ile de France. Right column: Provence.

7.3 p-values

		IPSL	CDFt	I.dOTC	I.R2D2	S.dOTC	S.R2D2	SI.dOTC	SI.R2D2
p-values for "equality-of-means" tests									
Britt.	wheat	0.000	0.000	0.000	0.000	0.000	0.000	**0.666**	0.000
	maize	0.000	0.000	0.005	0.000	0.000	0.000	**0.166**	0.000
	vine	0.000	0.000	0.000	0.000	0.000	0.000	0.007	0.000
IdF	wheat	0.000	0.000	0.000	0.000	0.000	0.000	**0.918**	0.000
	maize	0.000	0.000	**0.276**	0.000	0.000	0.000	0.001	0.000
	vine	0.000	0.000	0.000	0.000	0.000	0.000	0.002	0.000
Prov.	wheat	0.000	0.000	0.054	0.000	0.000	0.000	**0.122**	0.000
	maize	0.000	0.000	0.000	0.000	0.000	0.000	**0.518**	0.000
	vine	0.000	0.000	0.000	0.000	0.000	0.000	0.000	0.000
p-values for "equality-of-variances" tests									
Britt.	wheat	0.000	0.000	0.000	0.002	0.000	0.000	**0.491**	0.000
	maize	0.000	0.000	0.000	0.000	0.000	0.000	0.000	0.001
	vine	0.000	0.000	0.000	0.000	0.000	0.000	0.000	0.000
IdF	wheat	0.000	0.000	0.000	0.000	0.001	0.0005	**0.255**	0.000
	maize	0.000	**0.405**	0.000	**0.192**	0.000	**0.275**	**0.370**	0.089
	vine	0.000	0.000	0.000	0.000	0.000	0.000	0.000	0.000
Prov.	wheat	0.000	0.000	0.000	0.050	0.000	0.000	0.041	0.008
	maize	0.000	0.000	0.000	0.000	0.000	0.000	0.000	0.000
	vine	0.000	0.000	0.000	0.000	0.000	0.000	0.000	0.000
p-values for "equality-of-Moran's I" tests									
Britt.	wheat	0.000	0.000	0.000	0.000	0.000	0.000	0.002	0.000
	maize	0.000	0.000	**0.984**	0.000	0.000	0.000	0.000	0.000
	vine	0.000	0.000	0.000	0.000	**0.386**	0.000	0.000	0.000
IdF	wheat	0.000	0.000	0.032	0.000	0.002	0.034	**0.528**	**0.750**
	maize	0.000	0.000	0.000	0.000	0.000	0.000	0.000	0.000
	vine	0.000	0.000	0.000	0.000	0.000	0.000	0.000	0.000
Prov.	wheat	0.000	0.000	0.000	0.000	0.000	0.000	0.009	0.000
	maize	0.000	0.000	0.000	0.000	0.053	0.000	0.000	0.000
	vine	0.000	0.000	0.051	0.000	0.000	0.000	0.000	0.000

Table 7.1: Statistical analysis for summer SWC in the future: p-values for the Welsh t-test of absence of differences on the average (first block); Fisher F-test of equality of variance between future and past (second block) and its adaptation to testing the equality of Moran's I (third block). Non rejection at the confidence level 0.90 is indicated in bold font.

7.4 Maps for average differences

7.4.1 Wheat

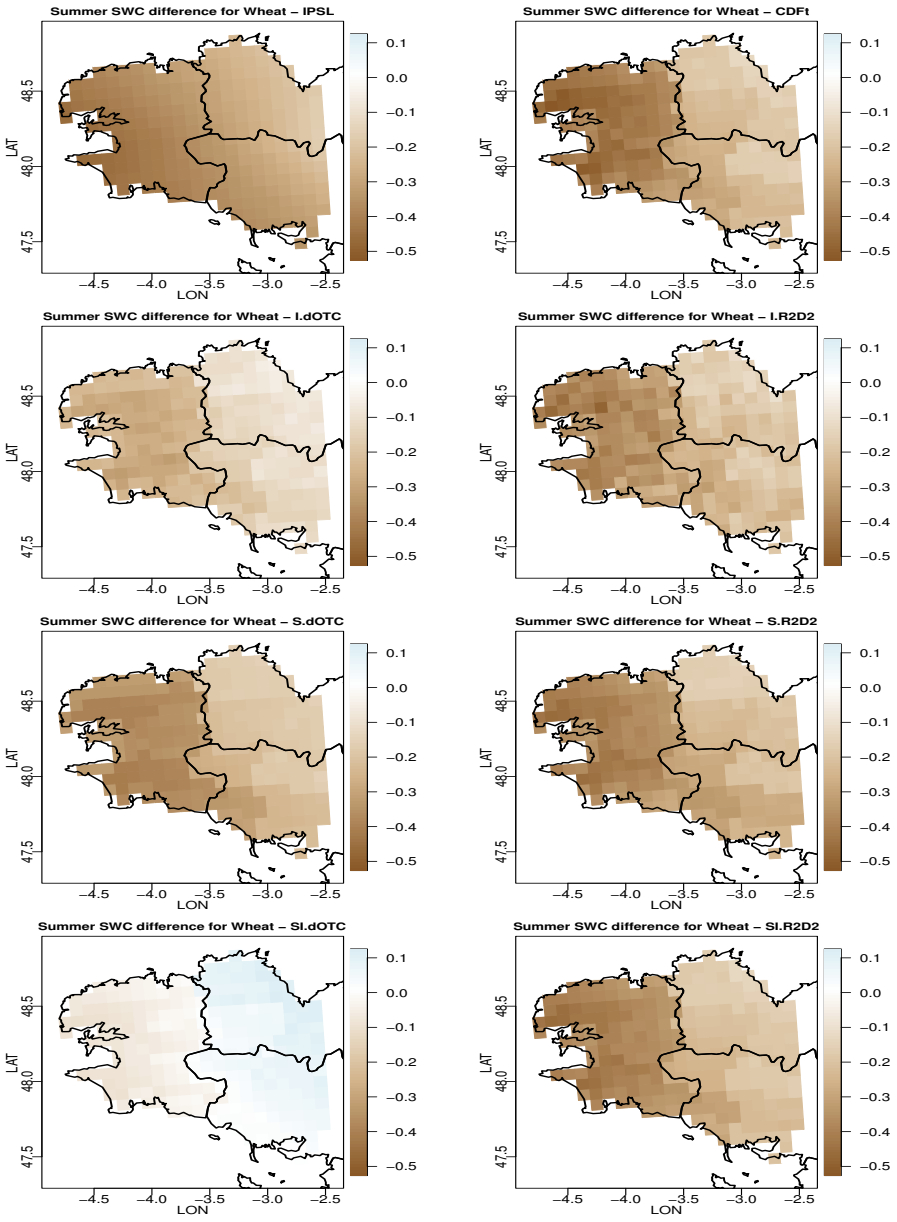

Figure 7.3: For each bias correction method and for wheat: map of summer SWC difference between future and past in Brittany. From top to bottom and from left to right: IPSL (no correction), CDF-t, Intervar-dOTC, Intervar-R2D2, spatial-dOTC, spatial R2D2, spatial-intervar-dOTC, spatial-intervar-R2D2.

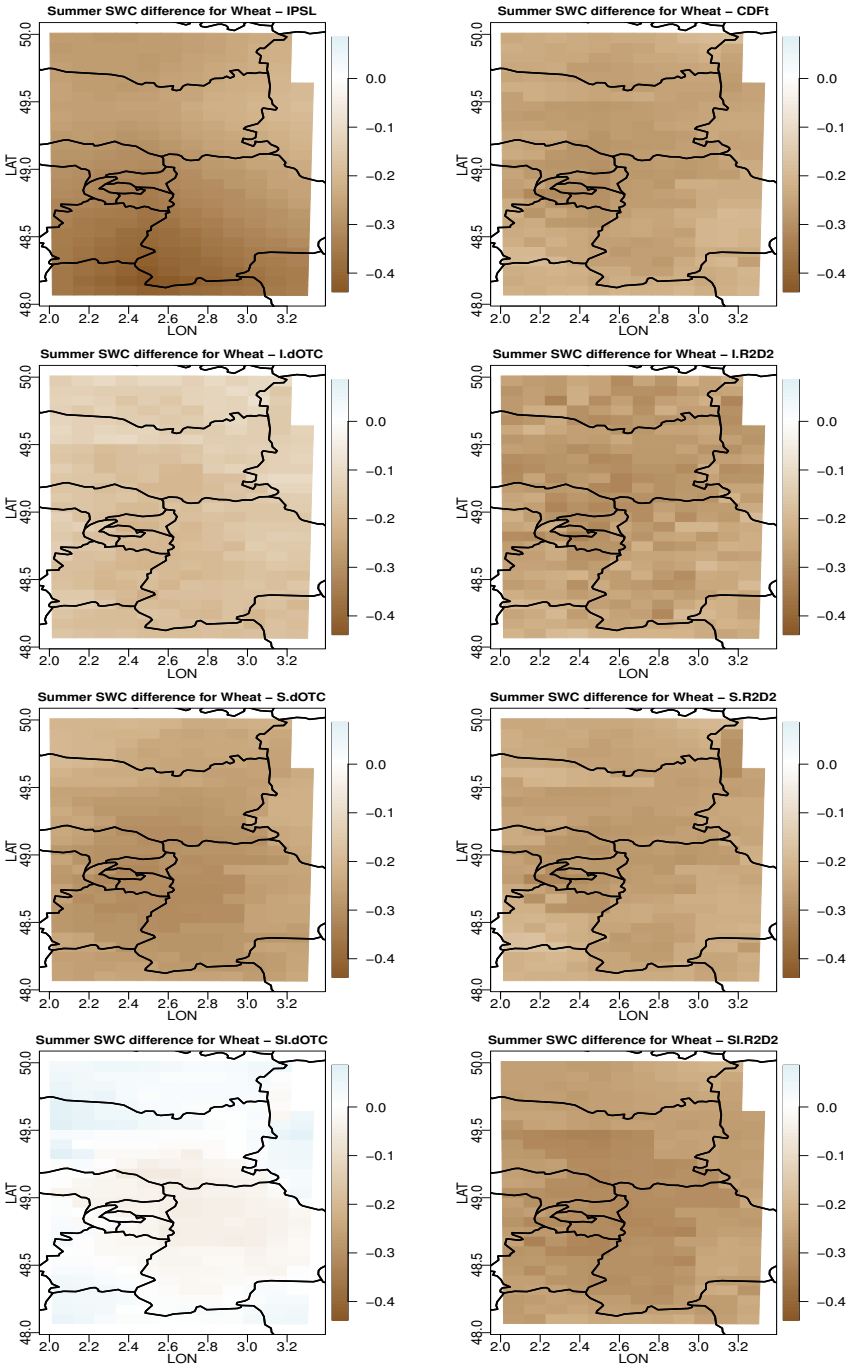

Figure 7.4: For each bias correction method and for wheat: map of summer SWC difference between future and past in Ile de France. From top to bottom and from left to right: IPSL (no correction), CDF-t, Intervar-dOTC, Intervar-R2D2, spatial-dOTC, spatial R2D2, spatial-intervar-dOTC, spatial-intervar-R2D2.

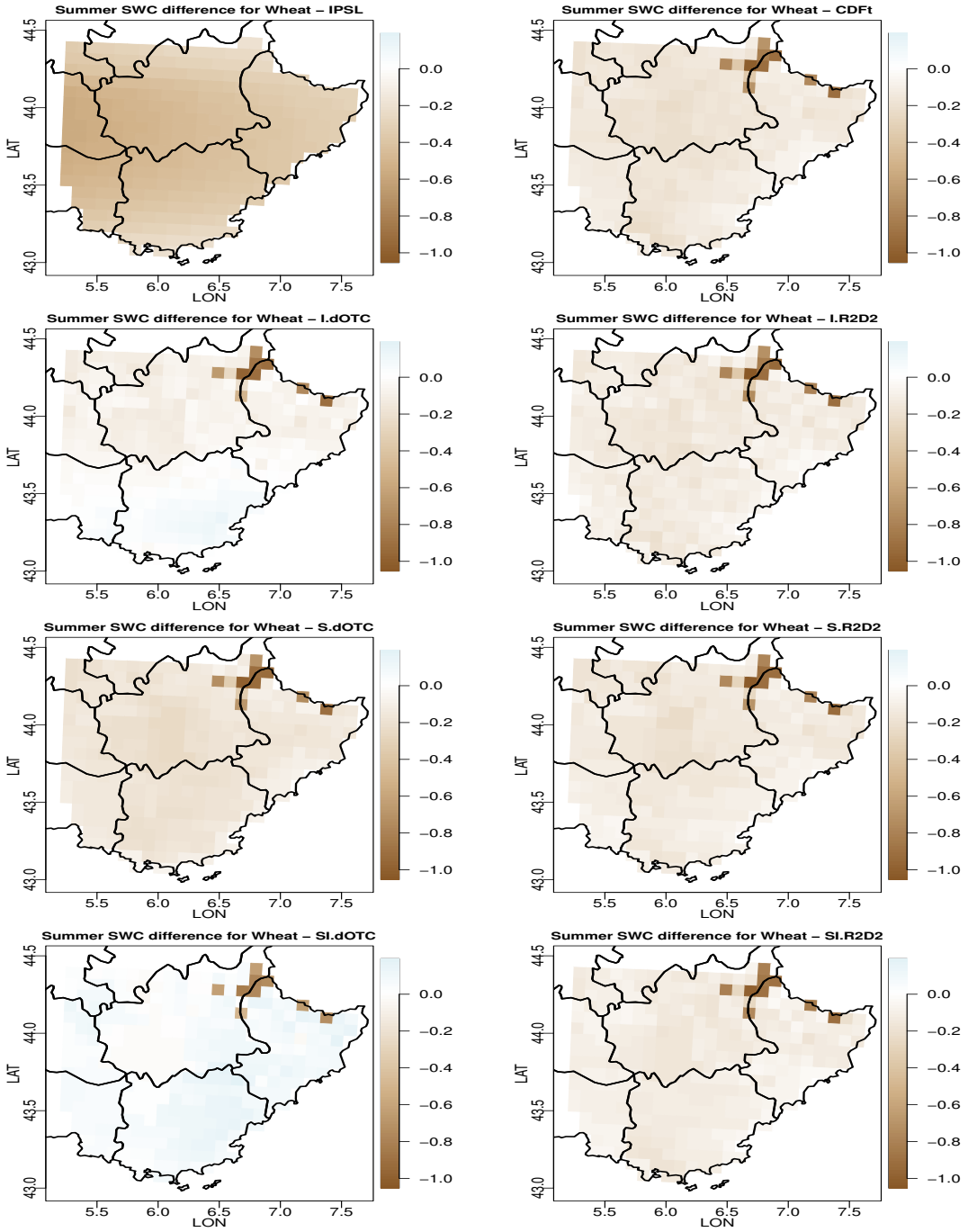

Figure 7.5: For each bias correction method and for wheat: map of summer SWC difference between future and past in Provence. From top to bottom and from left to right: IPSL (no correction), CDF-t, Intervar-dOTC, Intervar-R2D2, spatial-dOTC, spatial R2D2, spatial-intervar-dOTC, spatial-intervar-R2D2.

7.4.2 Maize

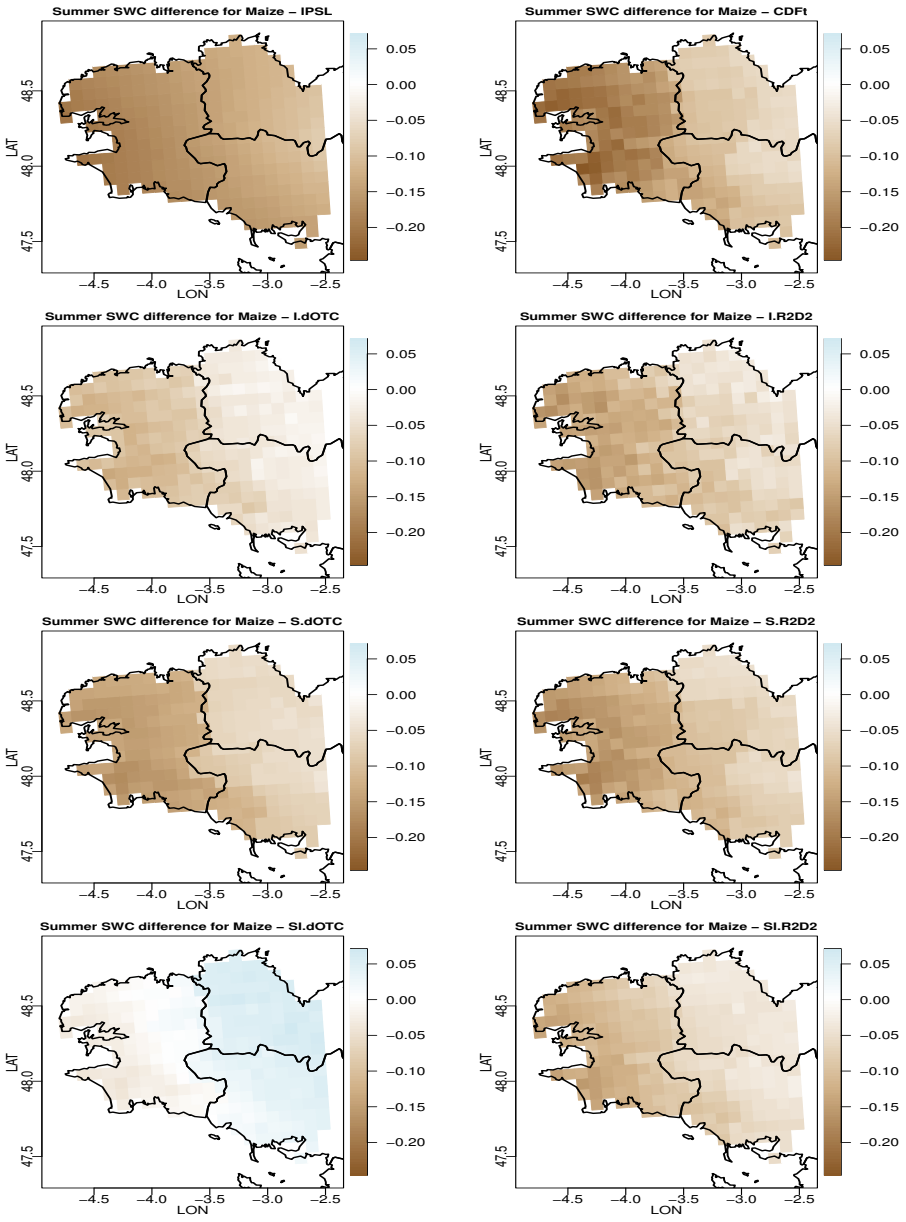

Figure 7.6: For each bias correction method and for maize: map of summer SWC difference between future and past in Brittany. From top to bottom and from left to right: IPSL (no correction), CDF-t, Intervar-dOTC, Intervar-R2D2, spatial-dOTC, spatial R2D2, spatial-intervar-dOTC, spatial-intervar-R2D2.

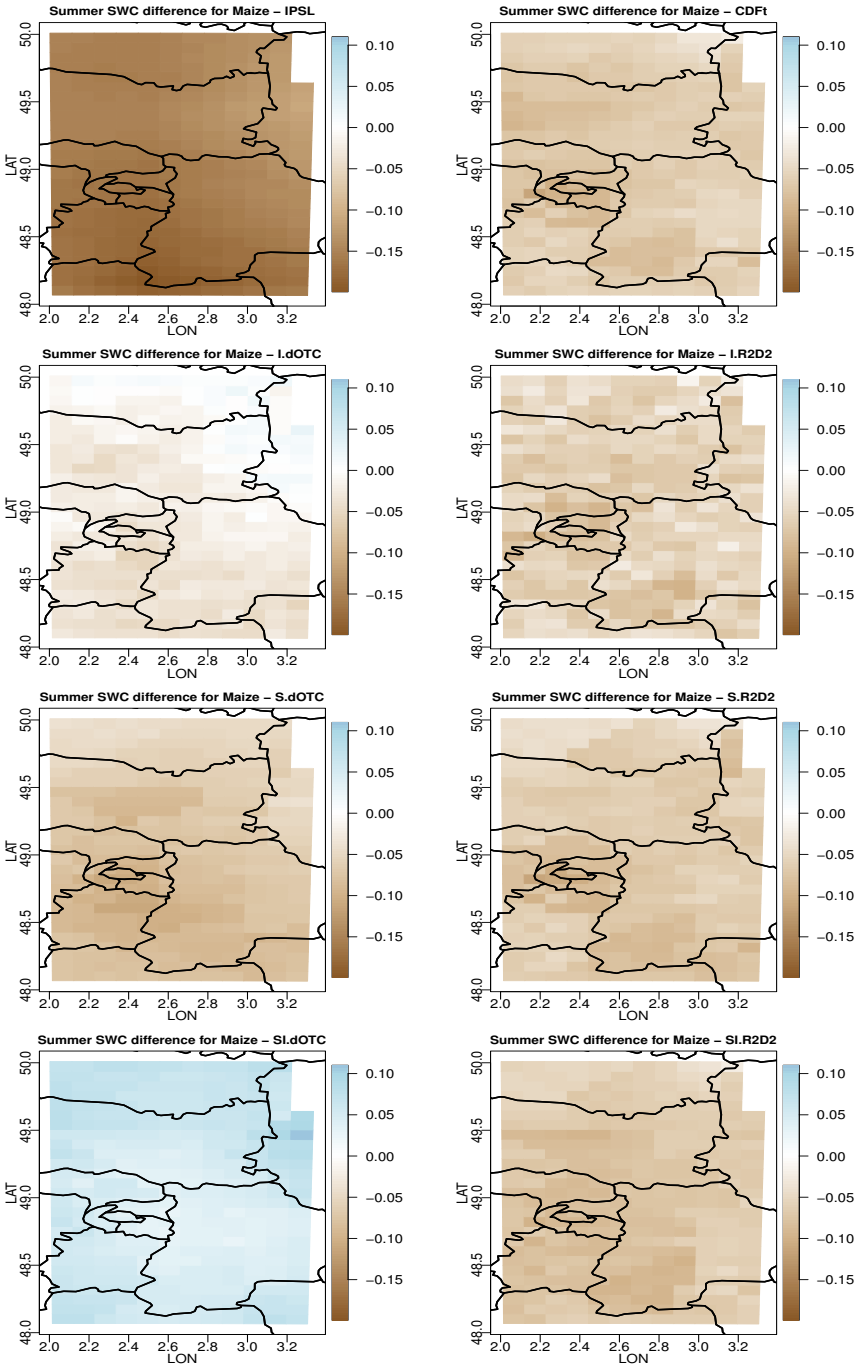

Figure 7.7: For each bias correction method and for maize: map of summer SWC difference between future and past in Ile de France. From top to bottom and from left to right: IPSL (no correction), CDF-t, Intervar-dOTC, Intervar-R2D2, spatial-dOTC, spatial R2D2, spatial-intervar-dOTC, spatial-intervar-R2D2.

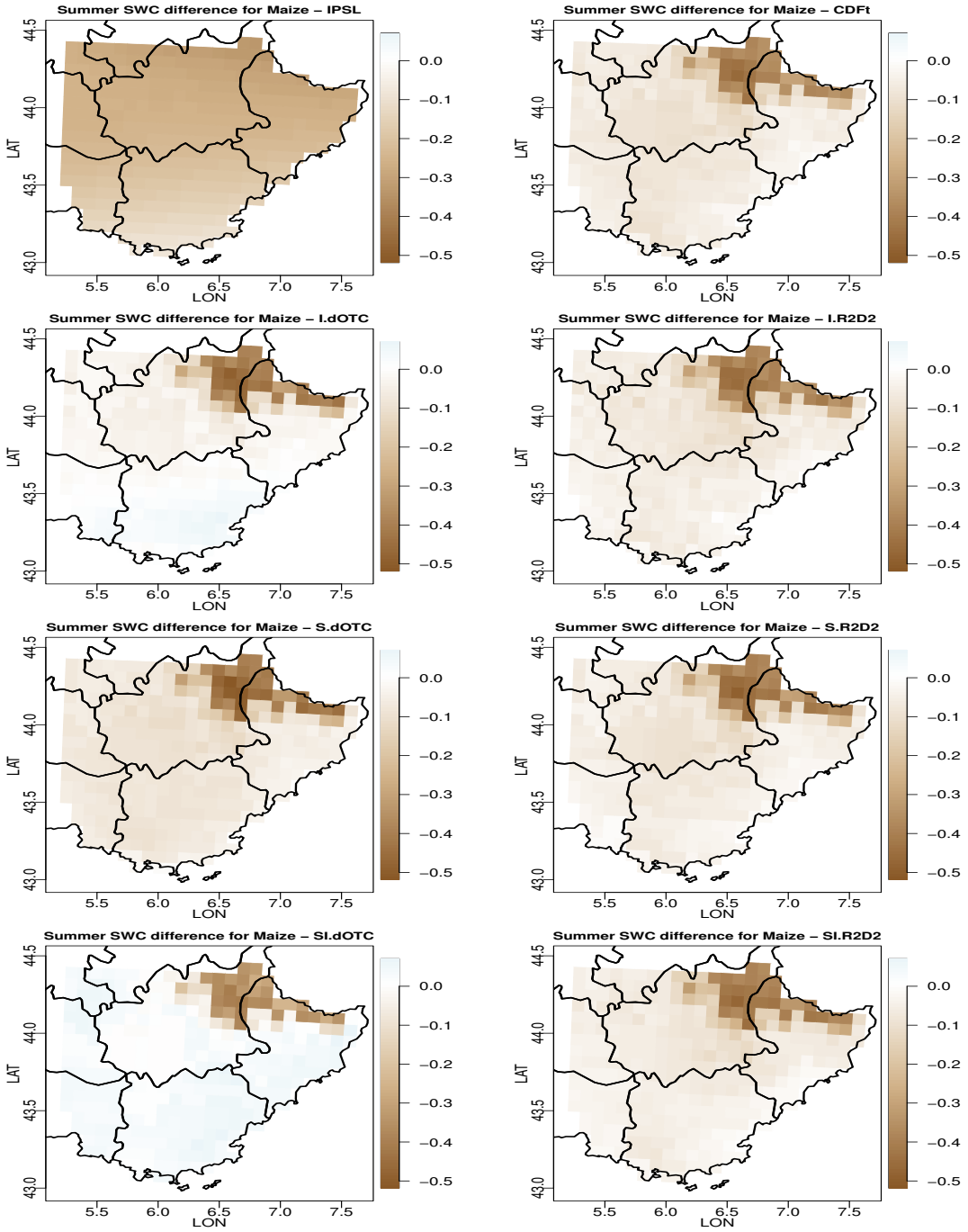

Figure 7.8: For each bias correction method and for maize: map of summer SWC difference between future and past in Provence. From top to bottom and from left to right: IPSL (no correction), CDF-t, Intervar-dOTC, Intervar-R2D2, spatial-dOTC, spatial R2D2, spatial-intervar-dOTC, spatial-intervar-R2D2.

7.4.3 Vine

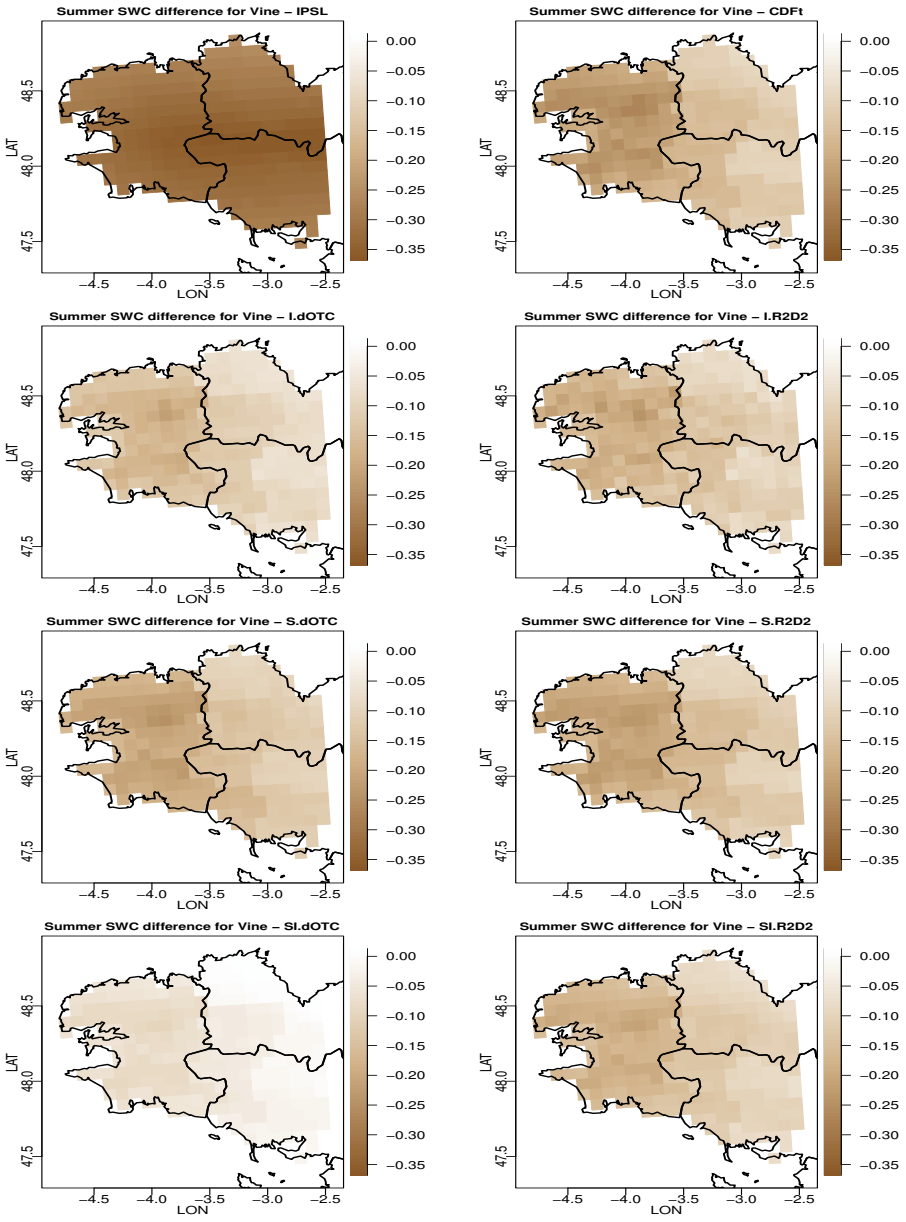

Figure 7.9: For each bias correction method and for vine: map of summer SWC difference between future and past in Brittany. From top to bottom and from left to right: IPSL (no correction), CDF-t, Intervar-dOTC, Intervar-R2D2, spatial-dOTC, spatial R2D2, spatial-intervar-dOTC, spatial-intervar-R2D2.

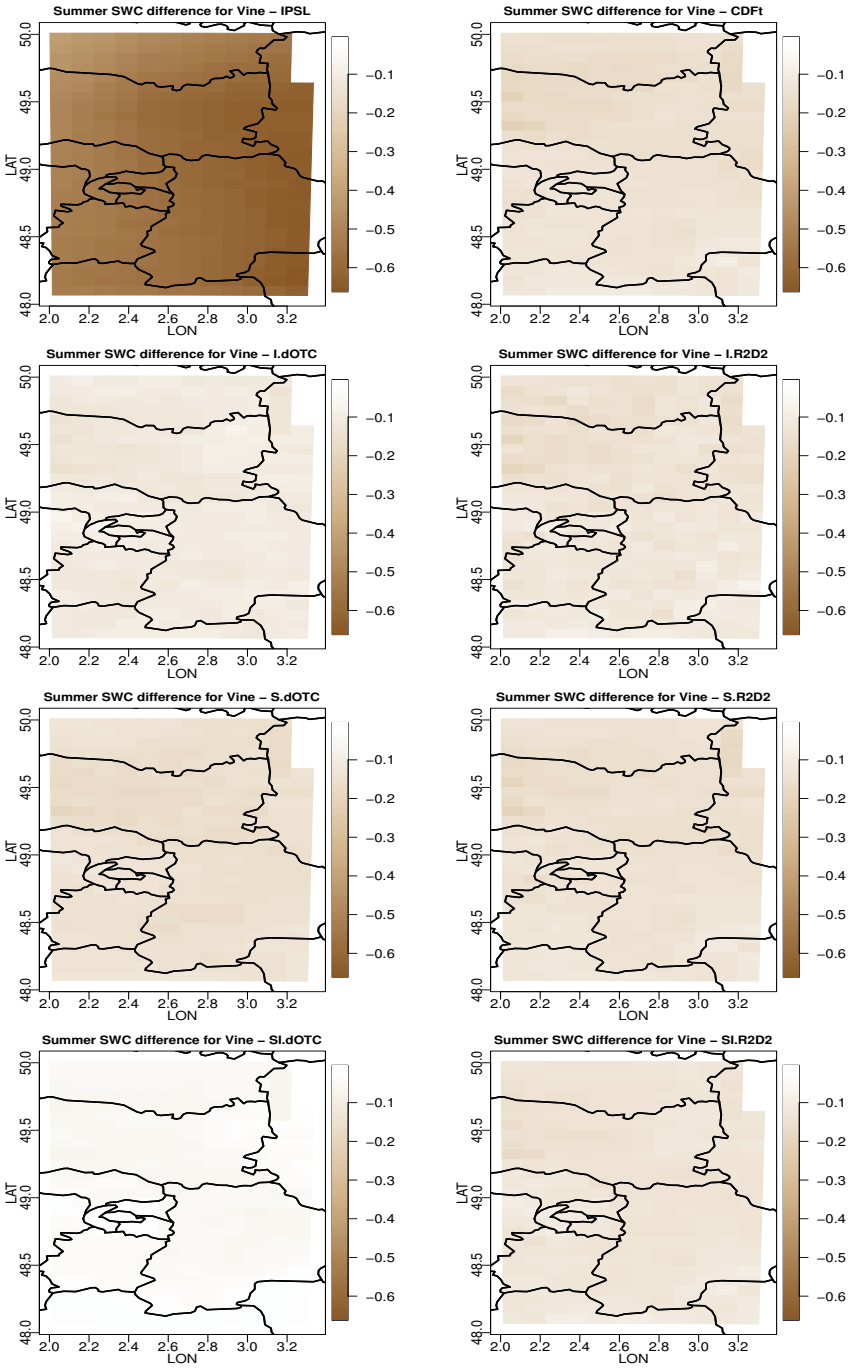

Figure 7.10: For each bias correction method and for vine: map of summer SWC difference between future and past in Ile de France. From top to bottom and from left to right: IPSL (no correction), CDF-t, Intervar-dOTC, Intervar-R2D2, spatial-dOTC, spatial R2D2, spatial-intervar-dOTC, spatial-intervar-R2D2.

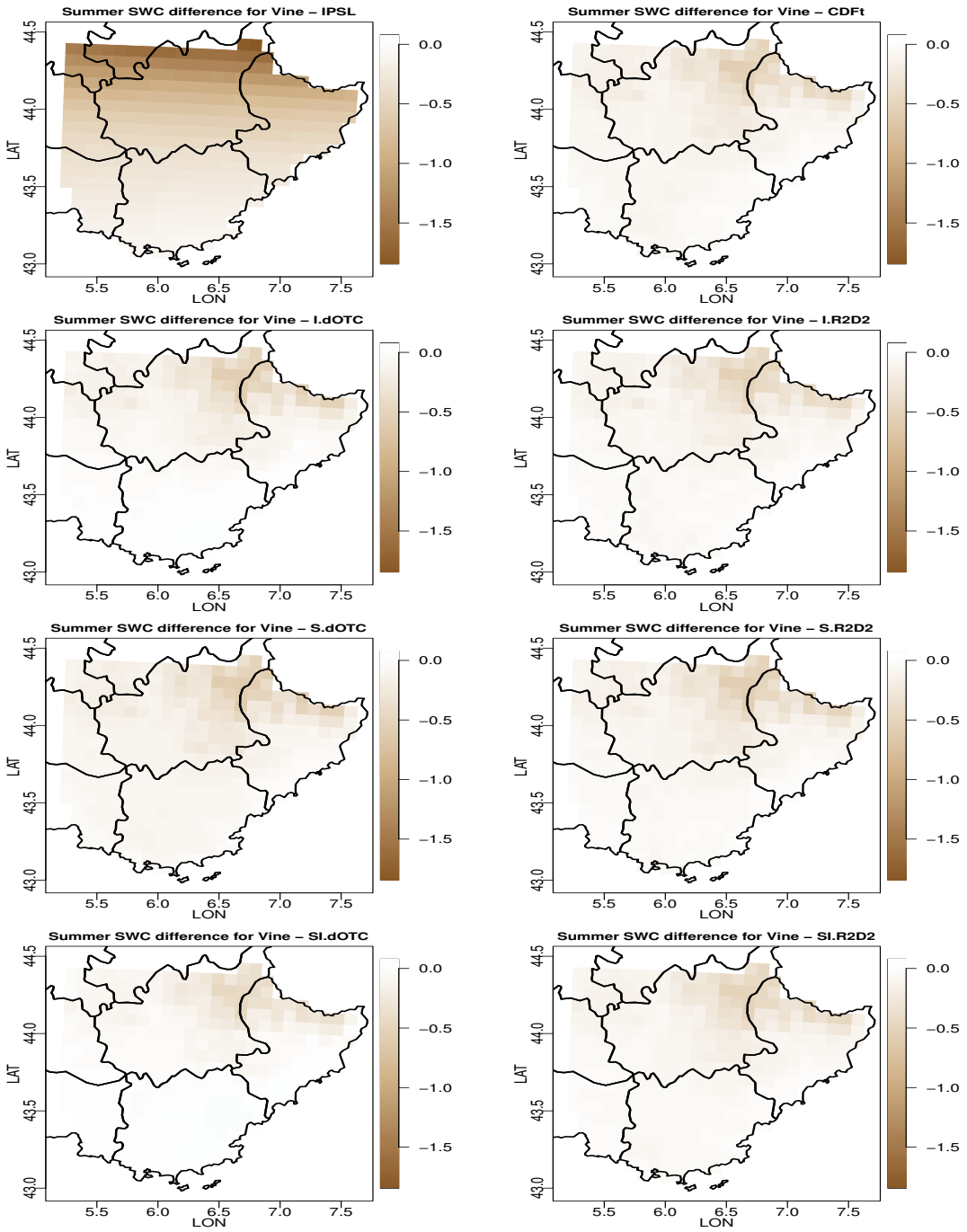

Figure 7.11: For each bias correction method and for vine: map of summer SWC difference between future and past in Provence. From top to bottom and from left to right: IPSL (no correction), CDF-t, Intervar-dOTC, Intervar-R2D2, spatial-dOTC, spatial R2D2, spatial-intervar-dOTC, spatial-intervar-R2D2.

7.5 Maps for variance ratio

7.5.1 Wheat

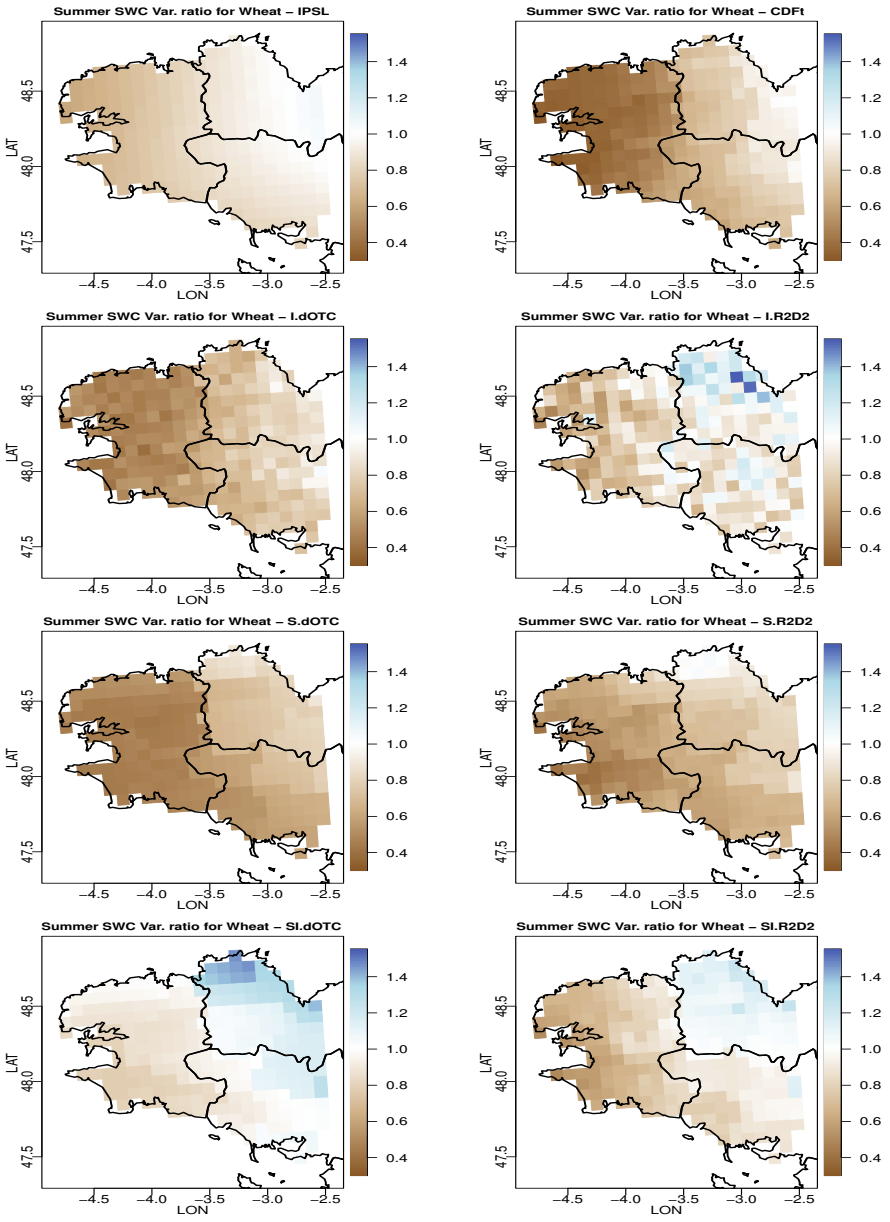

Figure 7.12: For each bias correction method and for wheat: map of summer SWC variance ratio between future and past in Brittany. From top to bottom and from left to right: IPSL (no correction), CDF-t, Intervar-dOTC, Intervar-R2D2, spatial-dOTC, spatial R2D2, spatial-intervar-dOTC, spatial-intervar-R2D2.

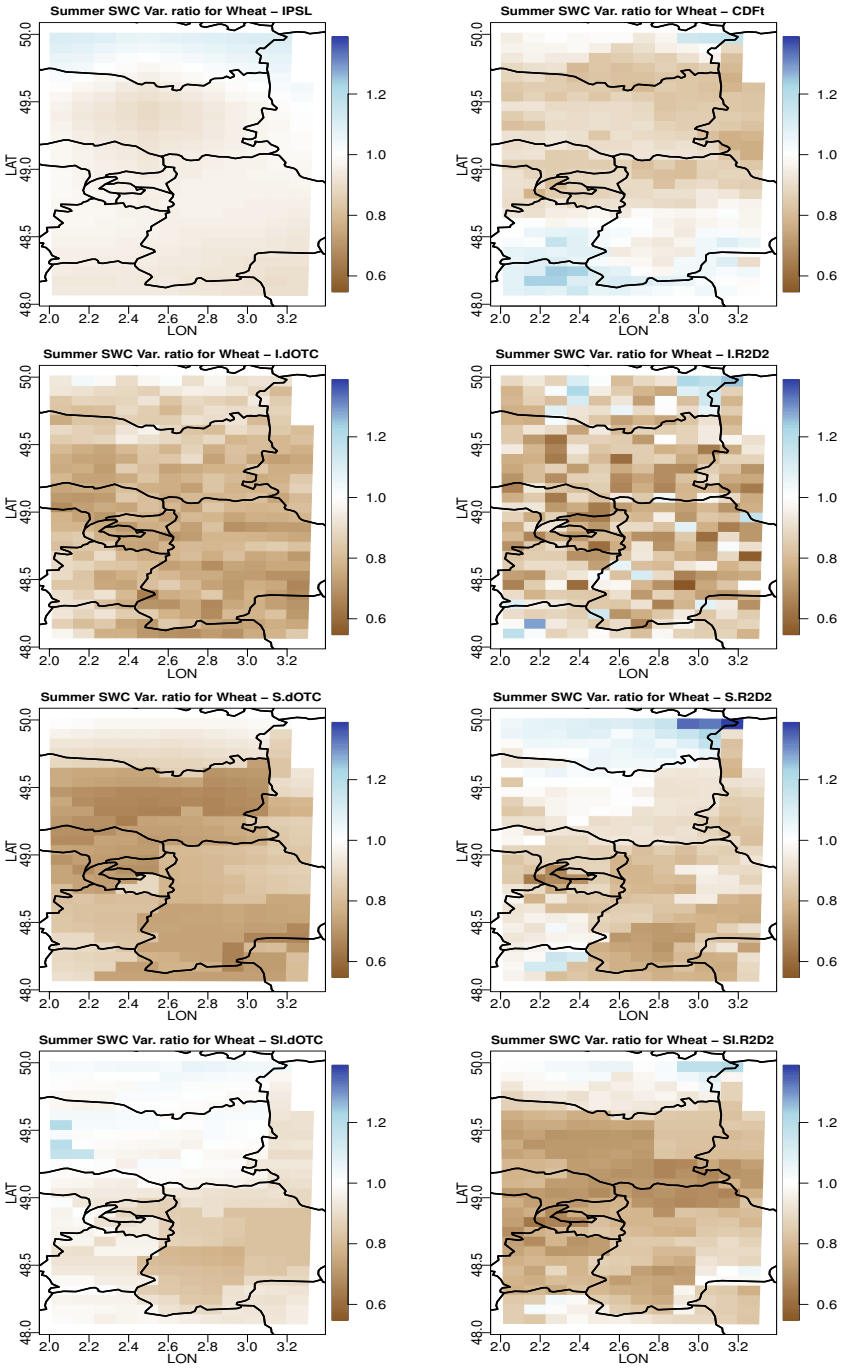

Figure 7.13: For each bias correction method and for wheat: map of summer SWC variance ratio between future and past in Ile de France. From top to bottom and from left to right: IPSL (no correction), CDF-t, Intervar-dOTC, Intervar-R2D2, spatial-dOTC, spatial R2D2, spatial-intervar-dOTC, spatial-intervar-R2D2.

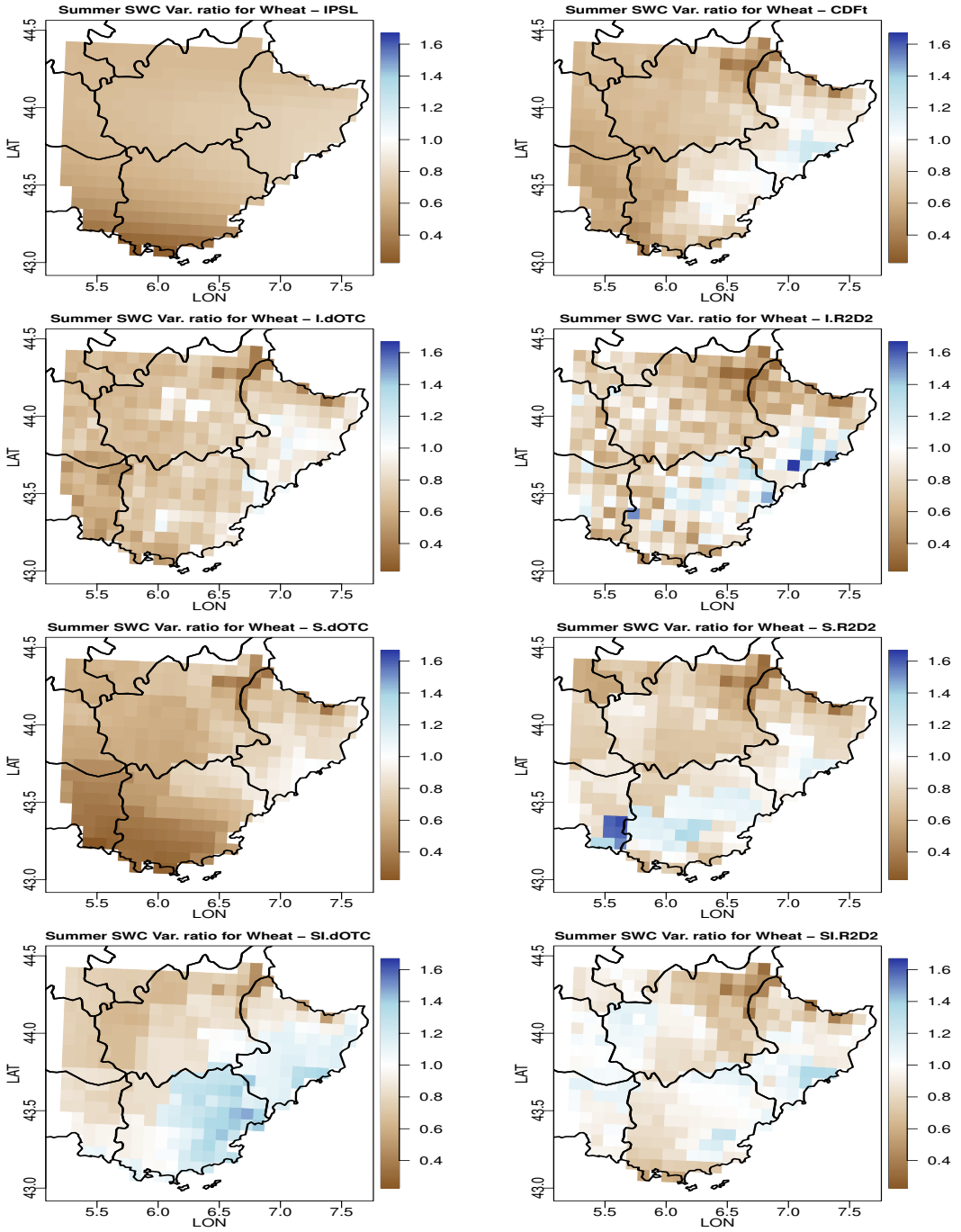

Figure 7.14: For each bias correction method and for wheat: map of summer SWC variance ratio between future and past in Provence. From top to bottom and from left to right: IPSL (no correction), CDF-t, Intervar-dOTC, Intervar-R2D2, spatial-dOTC, spatial R2D2, spatial-intervar-dOTC, spatial-intervar-R2D2.

7.5.2 Maize

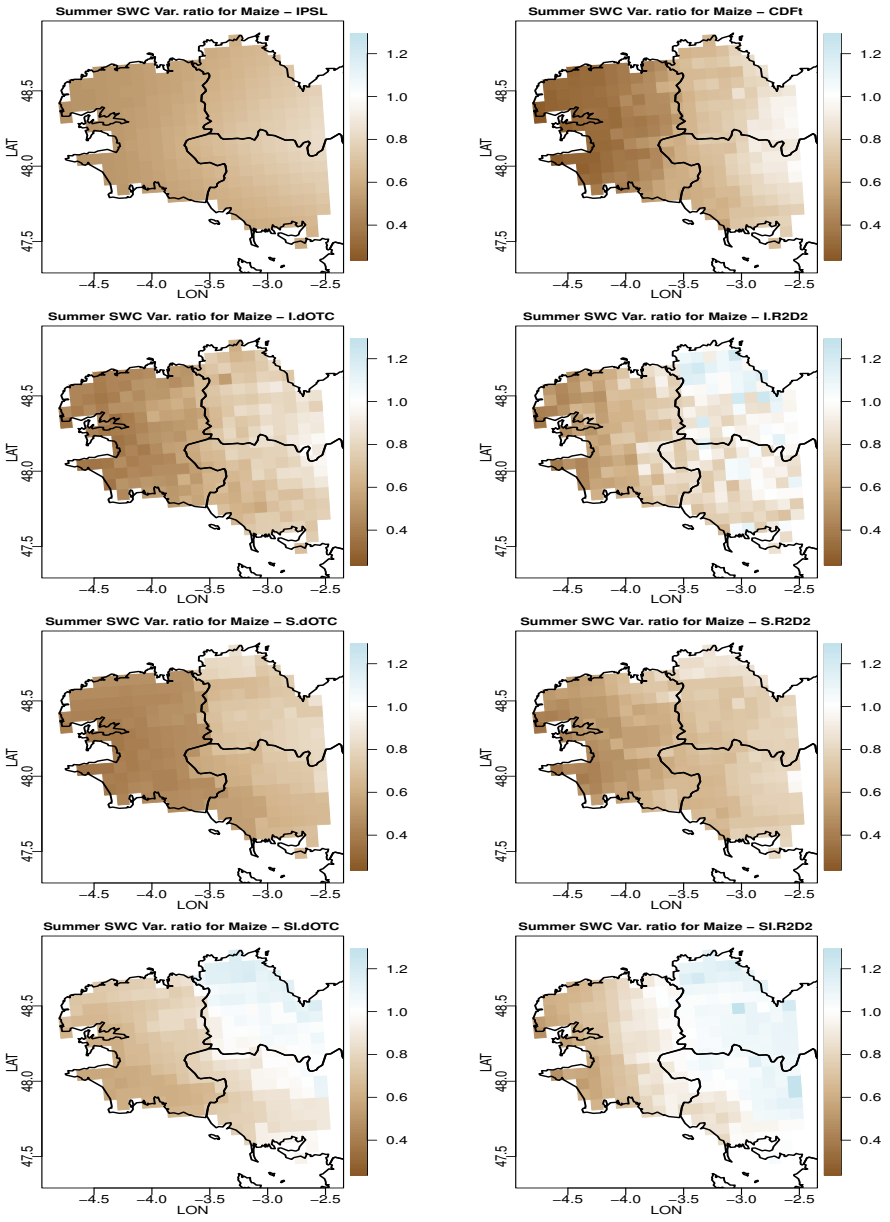

Figure 7.15: For each bias correction method and for maize: map of summer SWC variance ratio between future and past in Brittany. From top to bottom and from left to right: IPSL (no correction), CDF-t, Intervar-dOTC, Intervar-R2D2, spatial-dOTC, spatial R2D2, spatial-intervar-dOTC, spatial-intervar-R2D2.

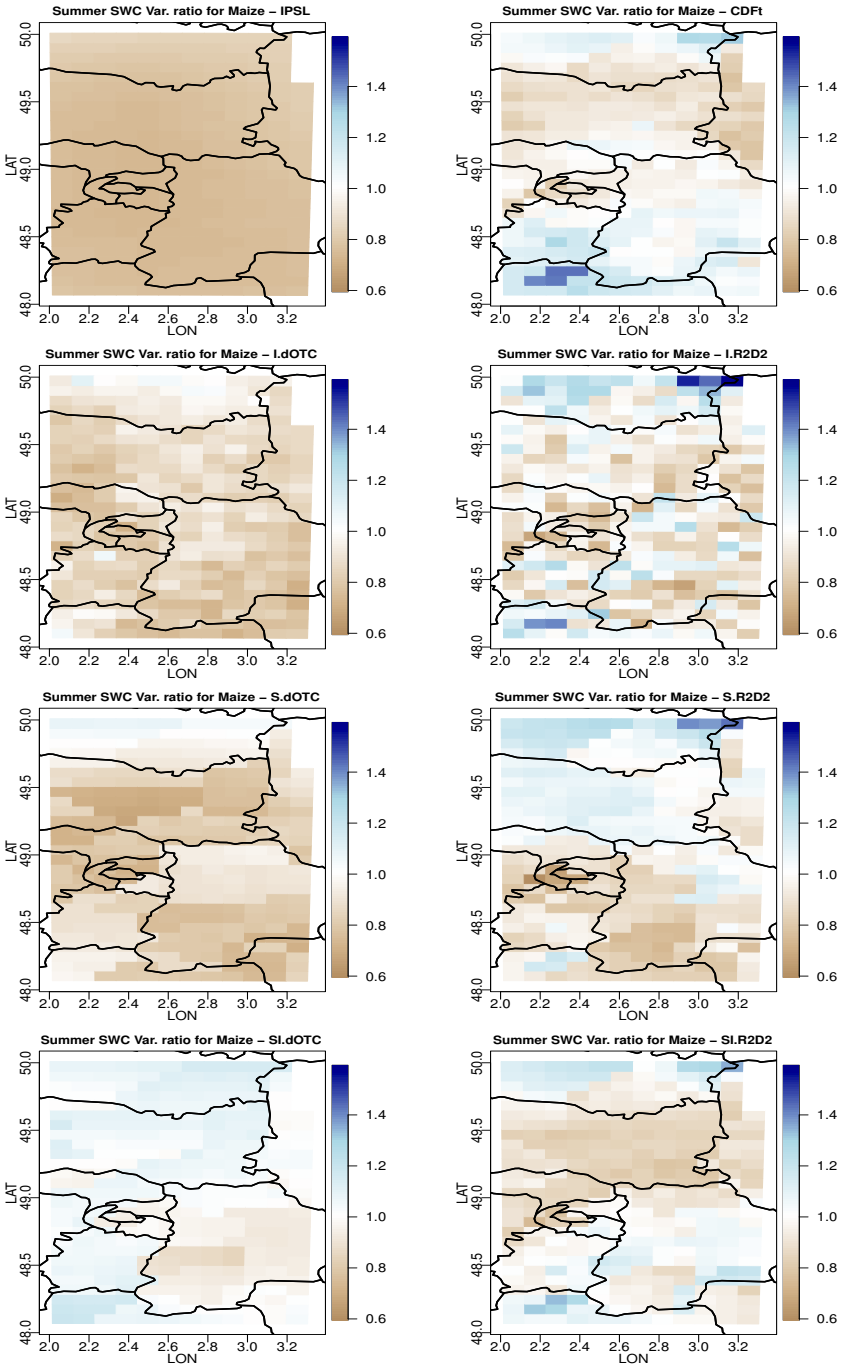

Figure 7.16: For each bias correction method and for maize: map of summer SWC variance ratio between future and past in Ile de France. From top to bottom and from left to right: IPSL (no correction), CDF-t, Intervar-dOTC, Intervar-R2D2, spatial-dOTC, spatial R2D2, spatial-intervar-dOTC, spatial-intervar-R2D2.

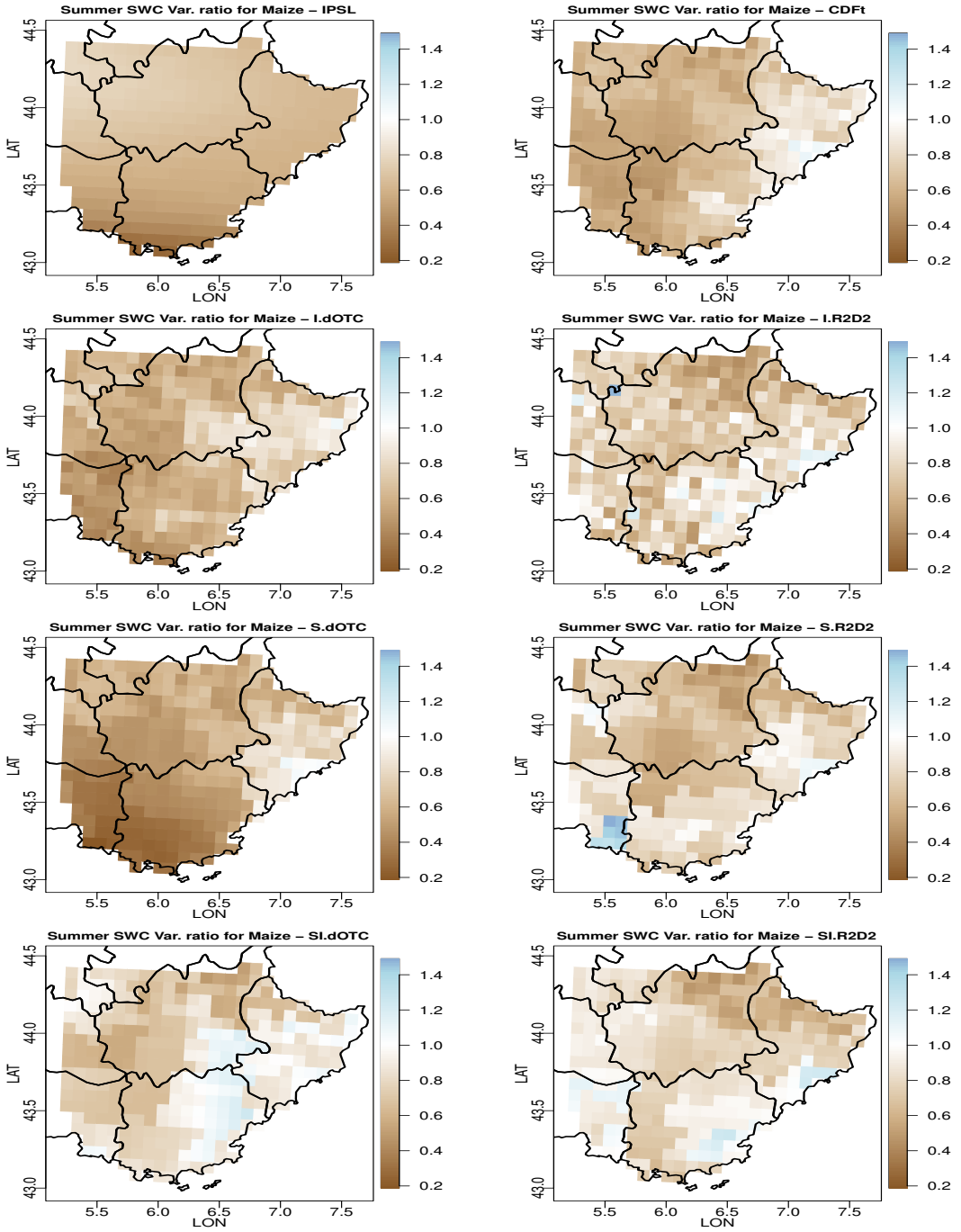

Figure 7.17: For each bias correction method and for maize: map of summer SWC variance ratio between future and past in Provence. From top to bottom and from left to right: IPSL (no correction), CDF-t, Intervar-dOTC, Intervar-R2D2, spatial-dOTC, spatial R2D2, spatial-intervar-dOTC, spatial-intervar-R2D2.

7.5.3 Vine

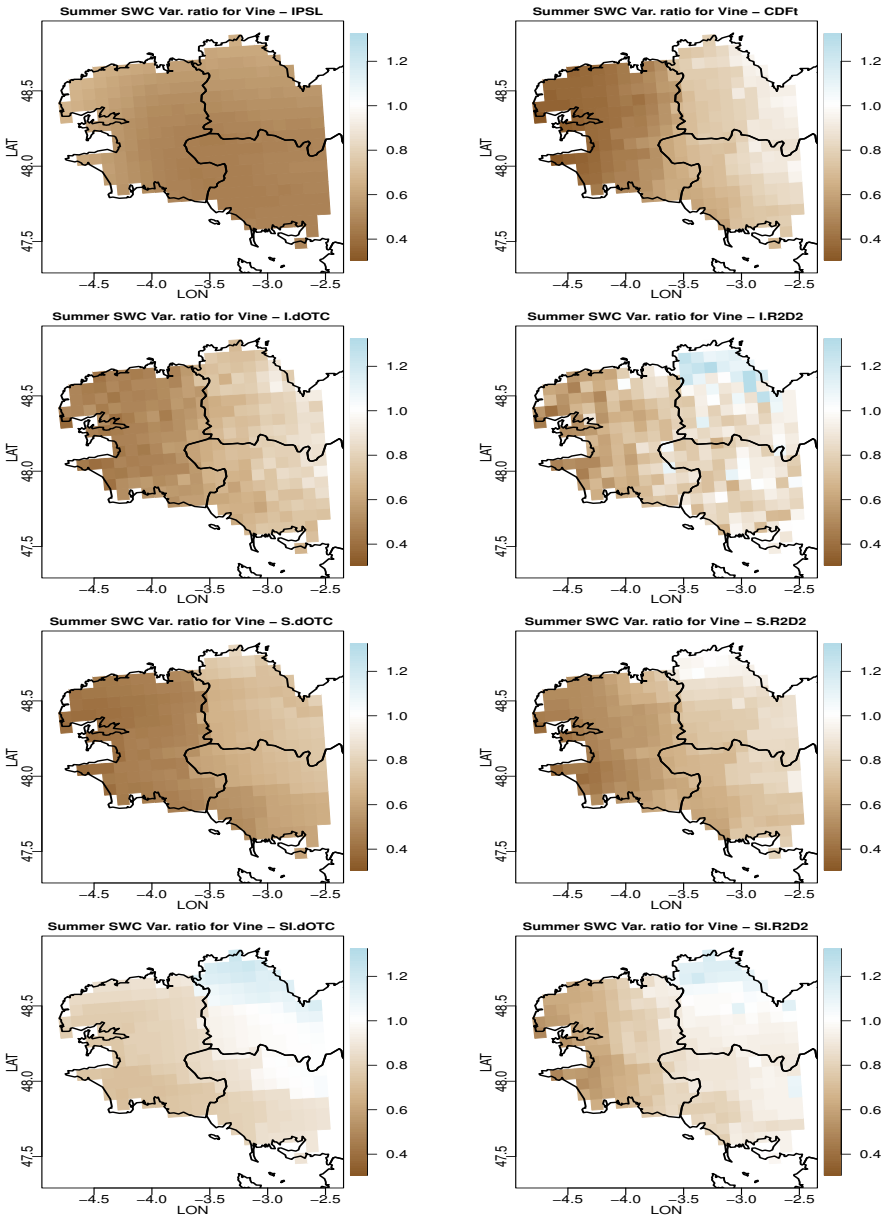

Figure 7.18: For each bias correction method and for vine: map of summer SWC variance ratio between future and past in Bretagne. From top to bottom and from left to right: IPSL (no correction), CDF-t, Intervar-dOTC, Intervar-R2D2, spatial-dOTC, spatial R2D2, spatial-intervar-dOTC, spatial-intervar-R2D2.

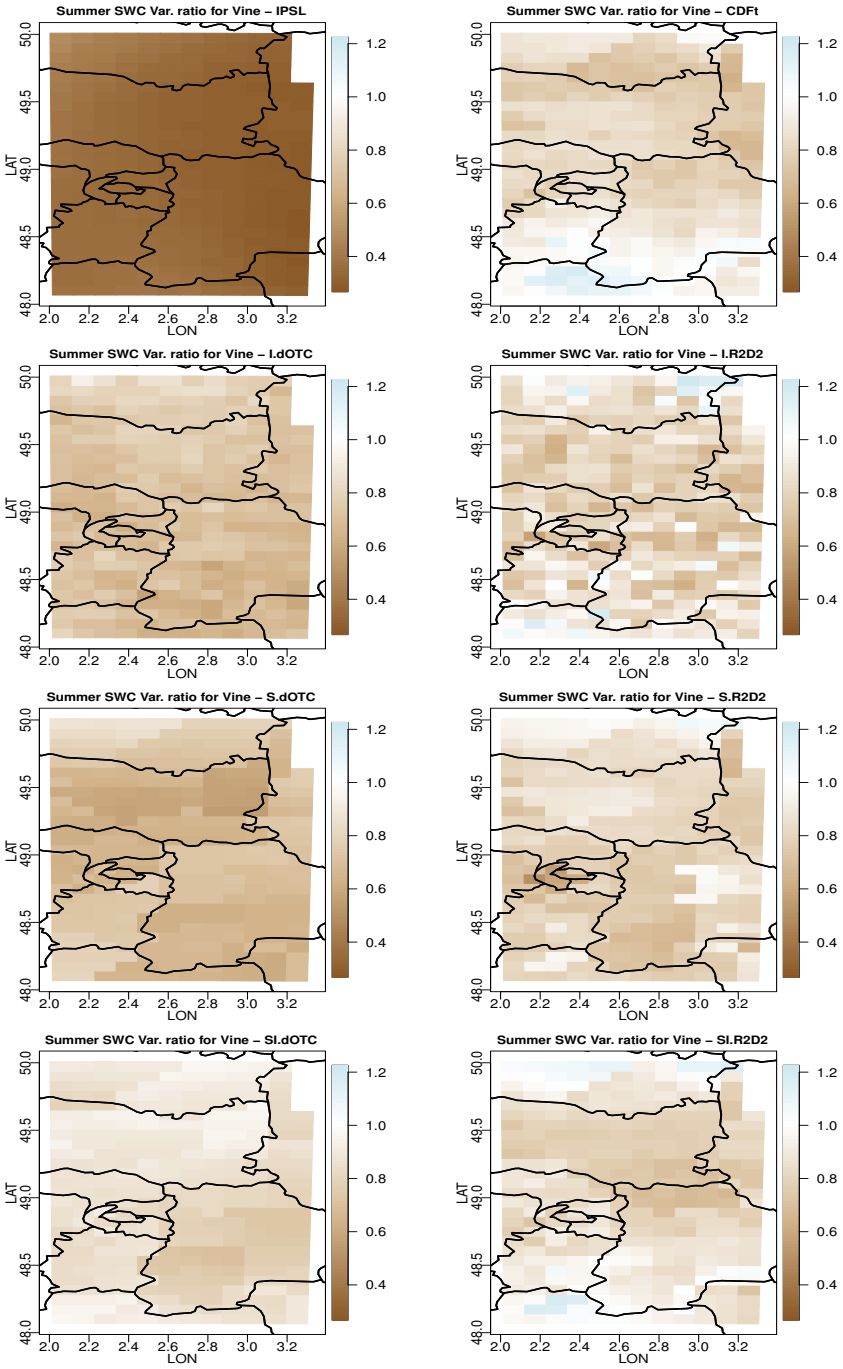

Figure 7.19: For each bias correction method and for vine: map of summer SWC variance ratio between future and past in Ile de France. From top to bottom and from left to right: IPSL (no correction), CDF-t, Intervar-dOTC, Intervar-R2D2, spatial-dOTC, spatial R2D2, spatial-intervar-dOTC, spatial-intervar-R2D2.

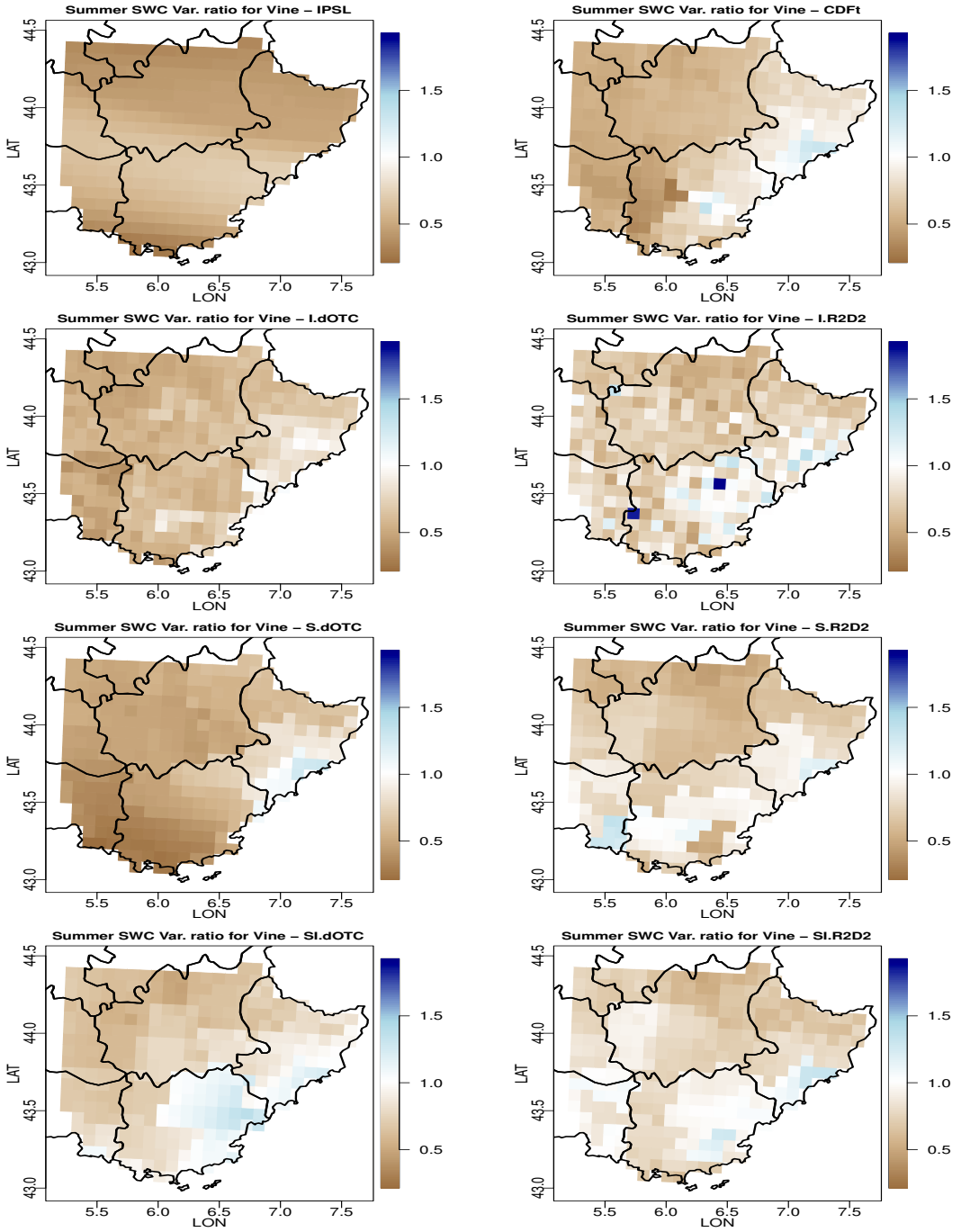

Figure 7.20: For each bias correction method and for vine: map of summer SWC variance ratio between future and past in Provence. From top to bottom and from left to right: IPSL (no correction), CDF-t, Intervar-dOTC, Intervar-R2D2, spatial-dOTC, spatial R2D2, spatial-intervar-dOTC, spatial-intervar-R2D2.

Chapter 8

Fire Weather Index in the past: 1986-2014

We consider the average of the Fire Weather Index computed during the meteorological summer, i.e. from June 1st to August 31st.

8.1 Boxplots

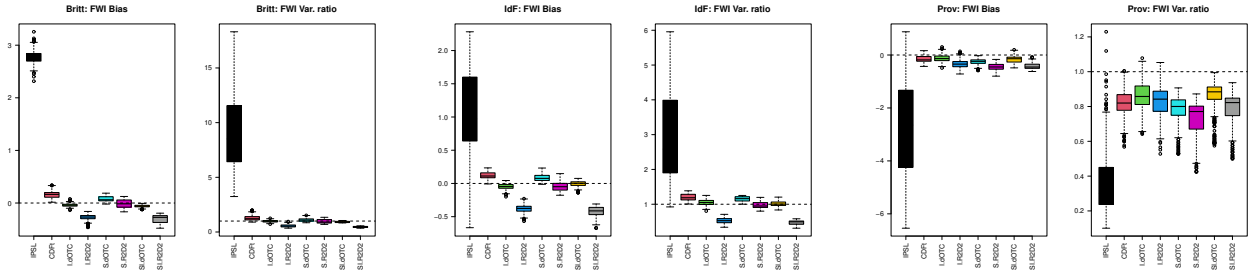

Figure 8.1: Overall summer FWI bias to SAFRAN and summer FWI's variance ratio to SAFRAN for all bias correction methods. Left column: Bretagne. Middle column: Ile de France. Right column: Provence. In each panel, from left to right: IPSL (no correction), CDF-t, Intervar-dOTC, Intervar-R2D2, spatial-dOTC, spatial R2D2, spatial-intervar-dOTC, spatial-intervar-R2D2.

8.2 Covariances

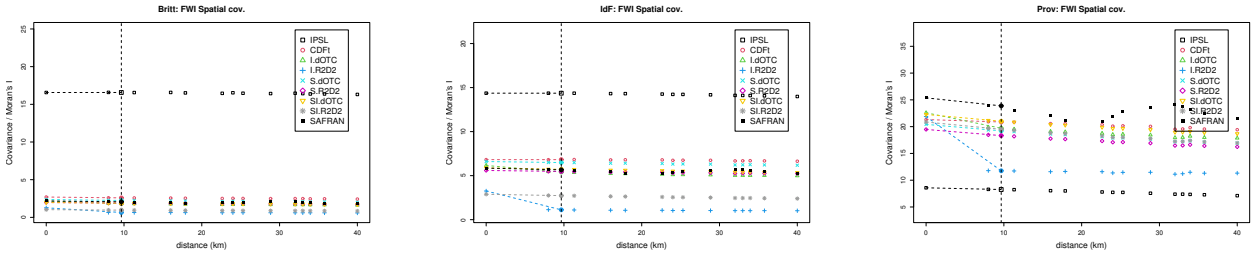

Figure 8.2: Spatial covariance and Moran's I of summer FWI in the past for all bias correction methods. Left column: Bretagne. Middle column: Ile de France. Right column: Provence.

8.3 p-values

	IPSL	CDFt	I.dOTC	I.R2D2	S.dOTC	S.R2D2	SI.dOTC	SI.R2D2
p-values for "equality-of-means" tests								
Britt.	0.000	0.000	**0.494**	0.000	**0.144**	**0.830**	**0.178**	0.000
IdF	0.000	0.058	**0.573**	0.000	**0.232**	**0.605**	**0.930**	0.000
Prov.	0.000	**0.303**	**0.482**	0.040	**0.124**	0.008	**0.265**	0.011
p-values for "equality-of-variances" tests								
Britt.	0.000	0.000	**0.976**	0.000	0.071	0.043	0.021	0.000
IdF	0.000	0.000	**0.298**	0.000	0.004	**0.299**	**0.915**	0.000
Prov.	0.000	0.000	0.021	0.002	0.000	0.000	0.004	0.000
p-values for "equality-of-Moran's I" tests								
Britt.	0.000	0.000	0.035	0.000	0.084	0.059	0.028	0.000
IdF	0.000	0.000	**0.354**	0.000	0.001	**0.466**	**0.803**	0.000
Prov.	0.000	0.001	0.000	0.000	0.000	0.000	0.004	0.000

Table 8.1: Statistical analysis for Summer FWI in the past: p-values for the Welsh t-test of absence of bias on the average (first block); Fisher F-test of equality of variance between future and past (second block) and its adaptation to testing the equality of Moran's I (third block). Non rejection at the confidence level 0.90 is indicated in bold font.

8.4 Maps for bias

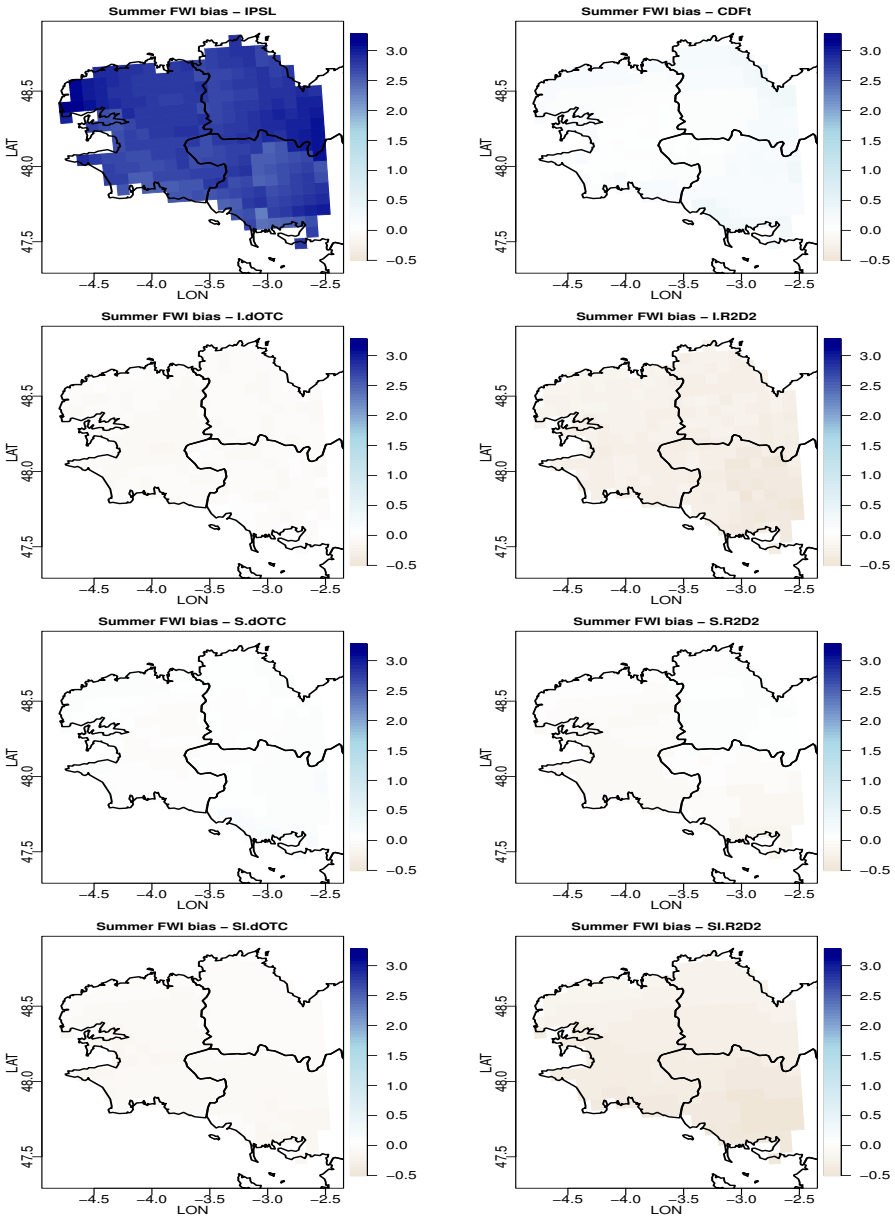

Figure 8.3: For each bias correction method: map of the summer FWI bias to SAFRAN in Brittany. From top to bottom and from left to right: IPSL (no correction), CDF-t, Intervar-dOTC, Intervar-R2D2, spatial-dOTC, spatial R2D2, spatial-intervar-dOTC, spatial-intervar-R2D2.

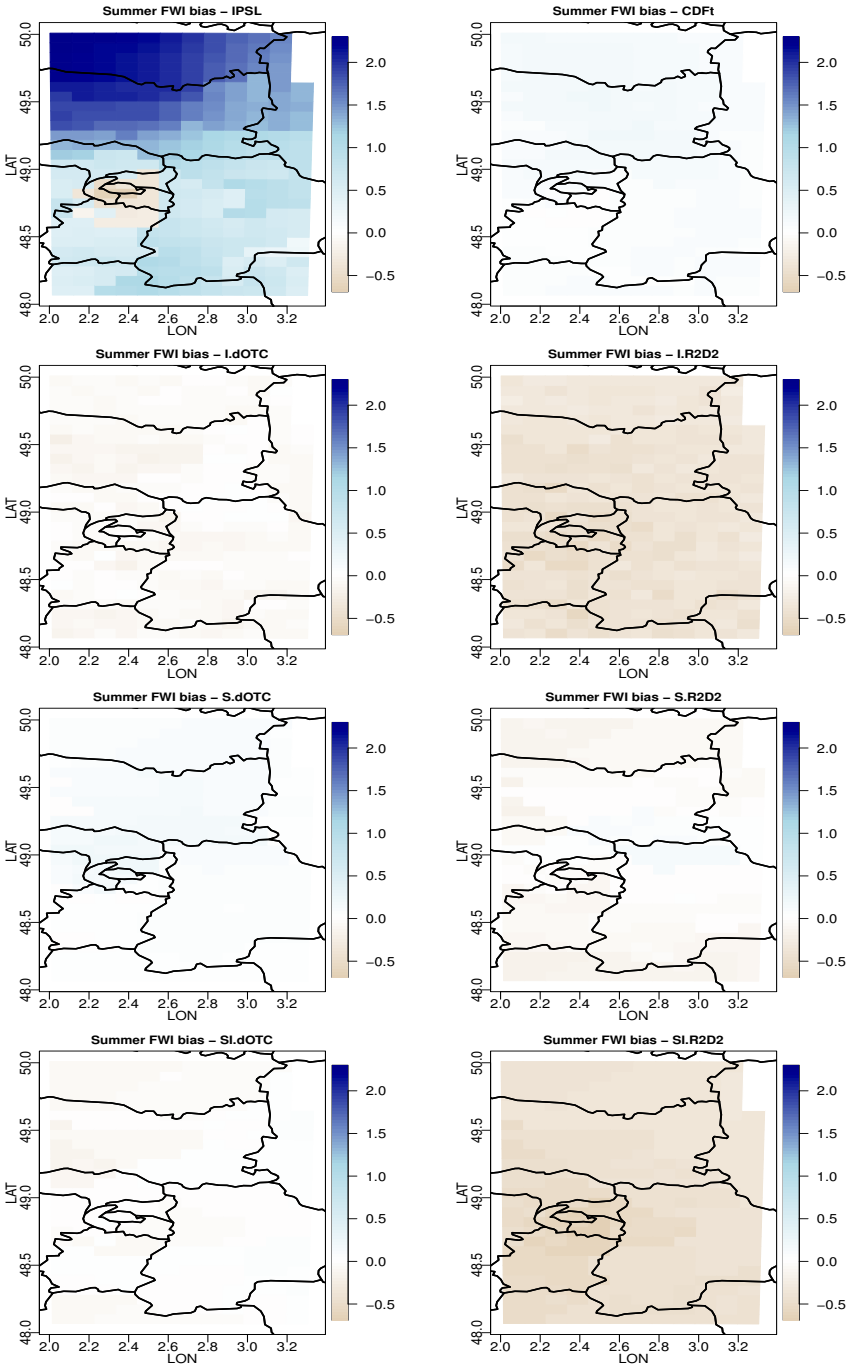

Figure 8.4: For each bias correction method: map of FWI bias to SAFRAN in Ile de France. From top to bottom and from left to right: IPSL (no correction), CDF-t, Intervar-dOTC, Intervar-R2D2, spatial-dOTC, spatial R2D2, spatial-intervar-dOTC, spatial-intervar-R2D2.

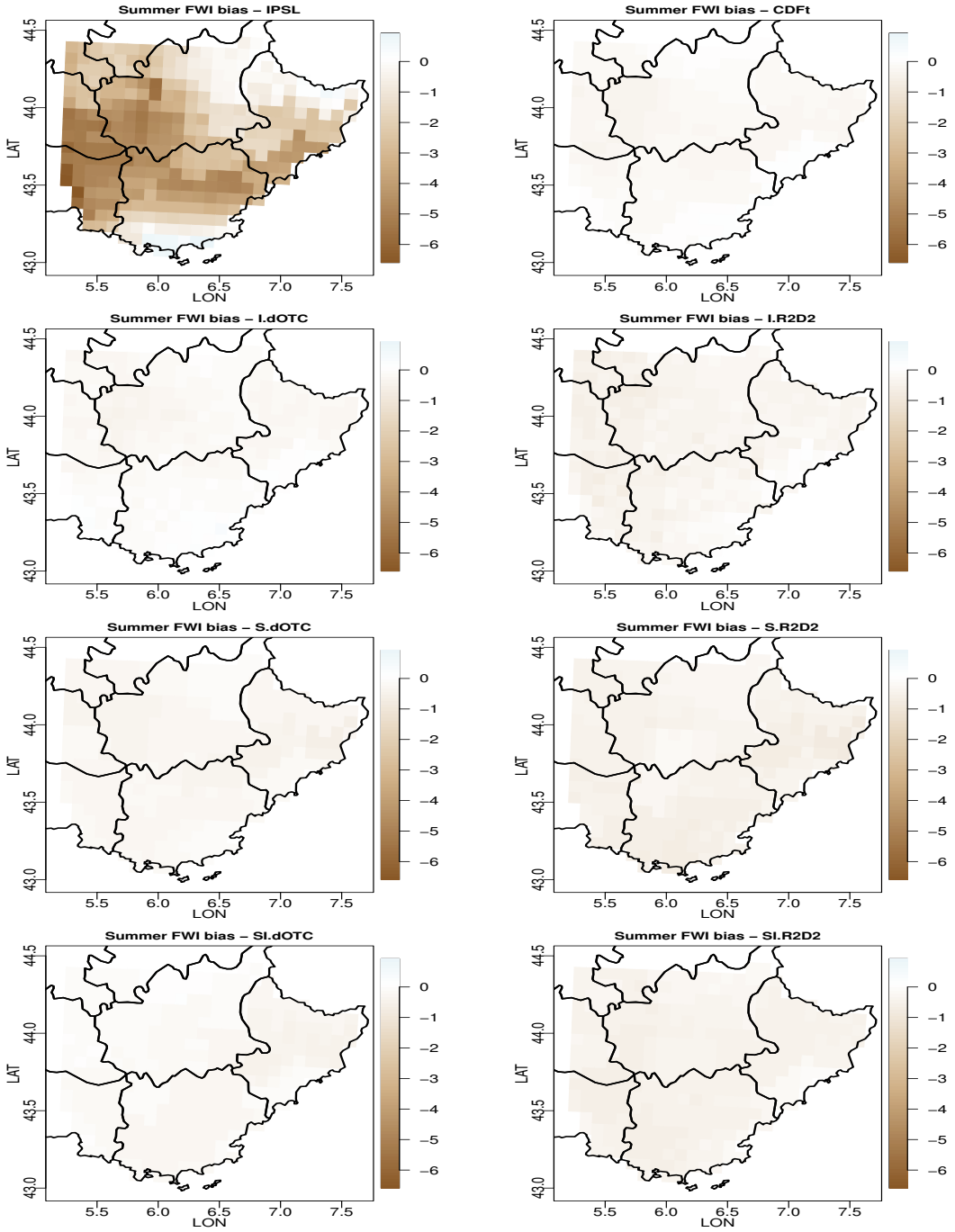

Figure 8.5: For each bias correction method: map of summer FWI bias to SAFRAN in Provence. From top to bottom and from left to right: IPSL (no correction), CDF-t, Intervar-dOTC, Intervar-R2D2, spatial-dOTC, spatial R2D2, spatial-intervar-dOTC, spatial-intervar-R2D2.

8.5 Maps for variance ratio

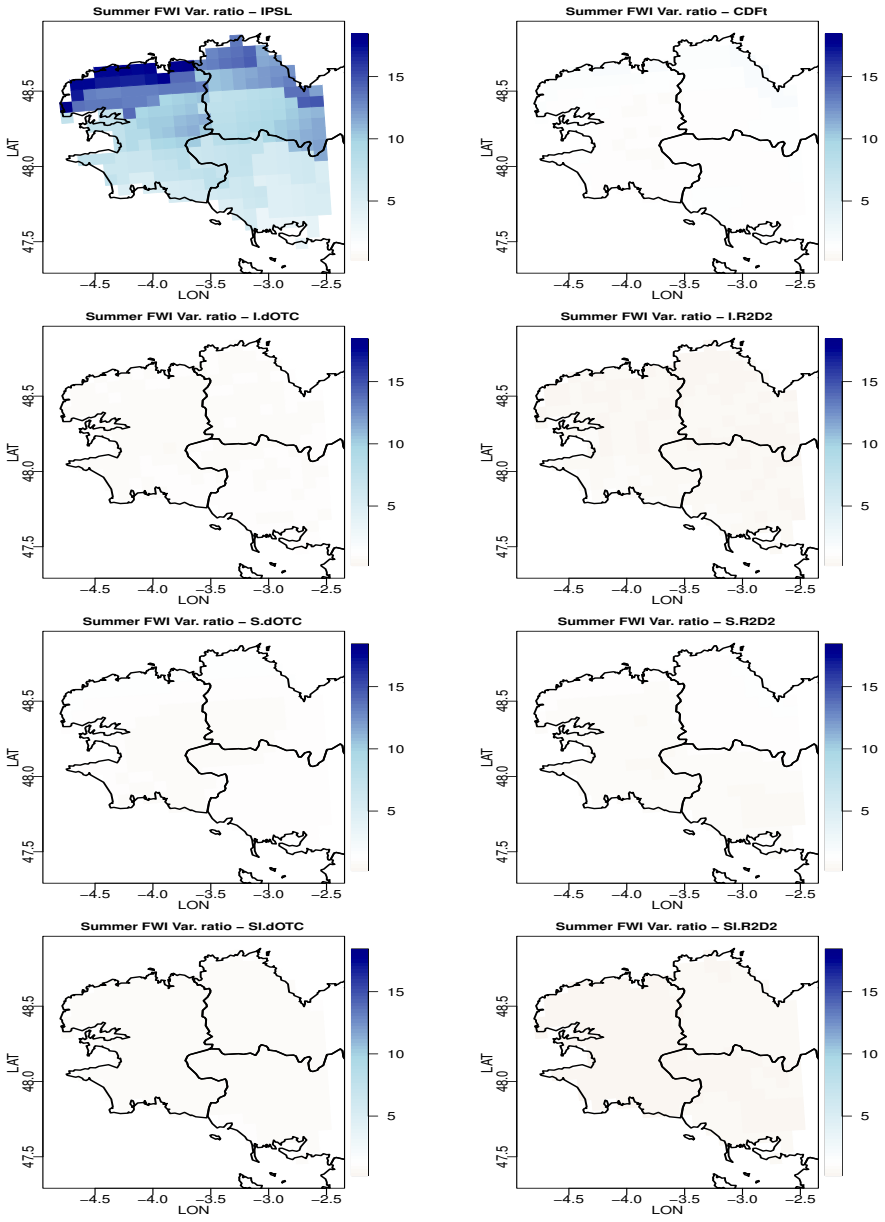

Figure 8.6: For each bias correction method: map of summer FWI variance divided by summer FWI variance for SAFRAN in Brittany. From top to bottom and from left to right: IPSL (no correction), CDF-t, Intervar-dOTC, Intervar-R2D2, spatial-dOTC, spatial R2D2, spatial-intervar-dOTC, spatial-intervar-R2D2.

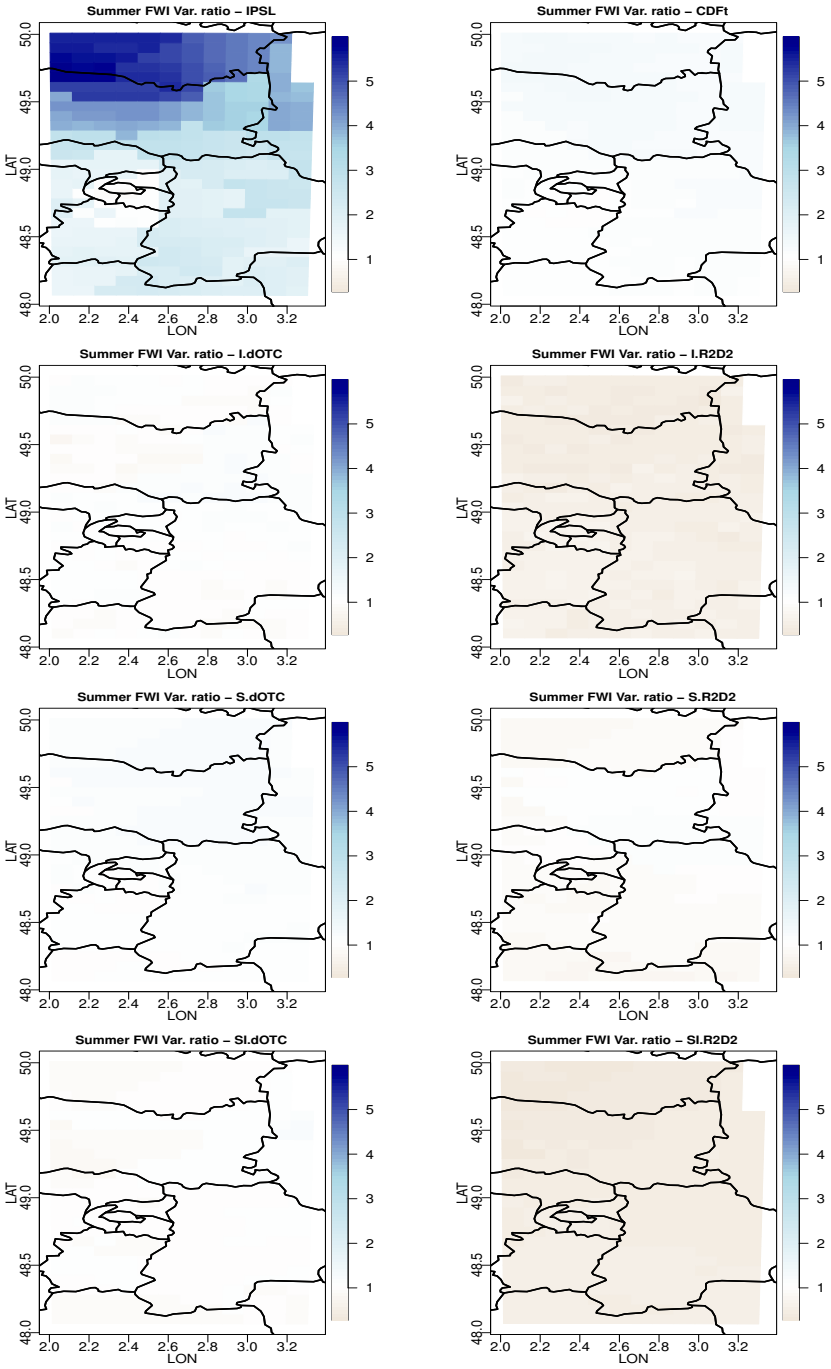

Figure 8.7: For each bias correction method: map of summer FWI variance divided by summer FWI variance for SAFRAN in Ile de France. From top to bottom and from left to right: IPSL (no correction), CDF-t, Intervar-dOTC, Intervar-R2D2, spatial-dOTC, spatial R2D2, spatial-intervar-dOTC, spatial-intervar-R2D2.

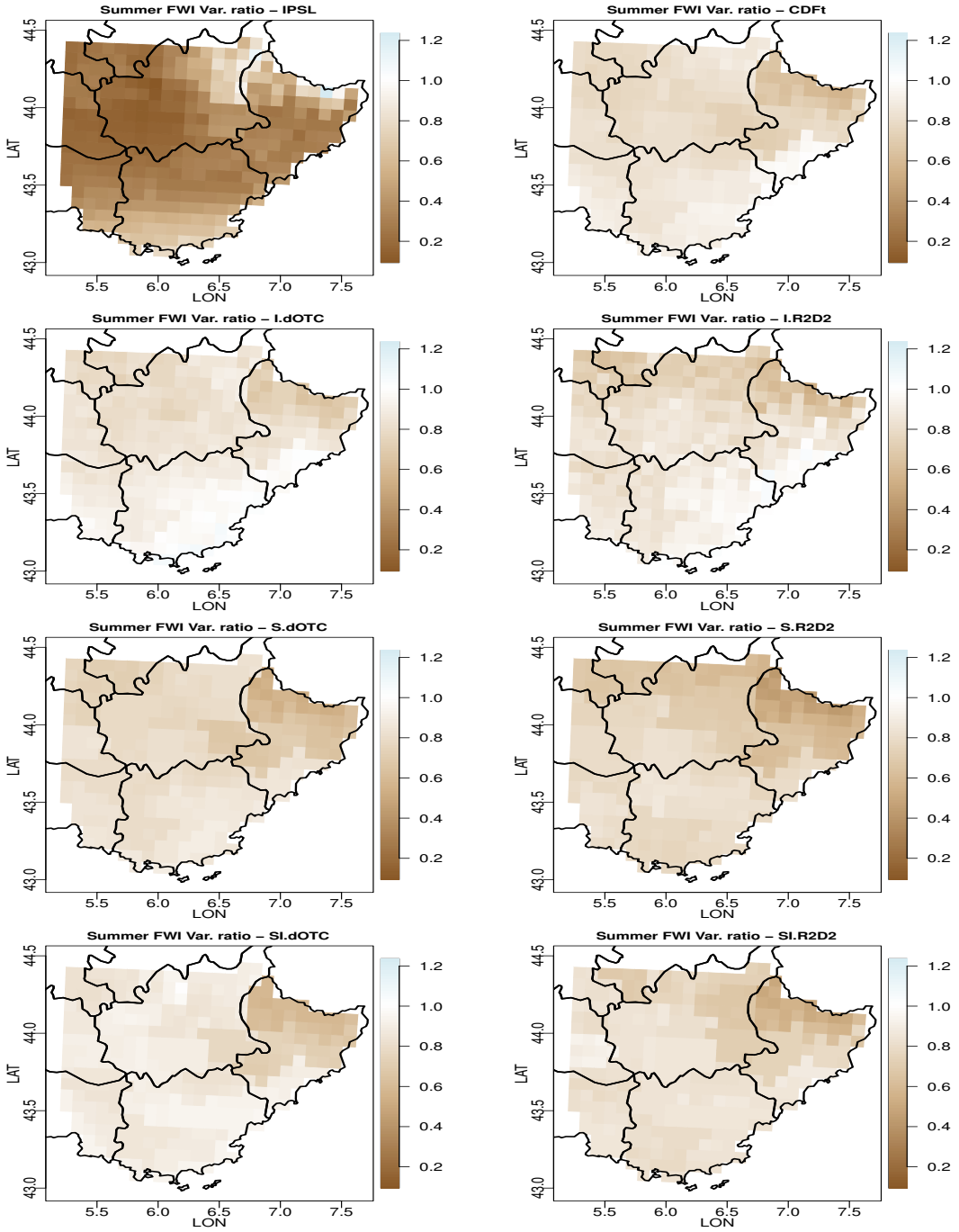

Figure 8.8: For each bias correction method: map of summer FWI variance divided by summer FWI variance for SAFRAN in Provence. From top to bottom and from left to right: IPSL (no correction), CDF-t, Intervar-dOTC, Intervar-R2D2, spatial-dOTC, spatial R2D2, spatial-intervar-dOTC, spatial-intervar-R2D2.

Chapter 9

Fire Weather Index in the future: 2036-2065

We consider the average of the Fire Weather Index computed during the meteorological summer, i.e. from June 1st to August 31st.

9.1 Boxplots

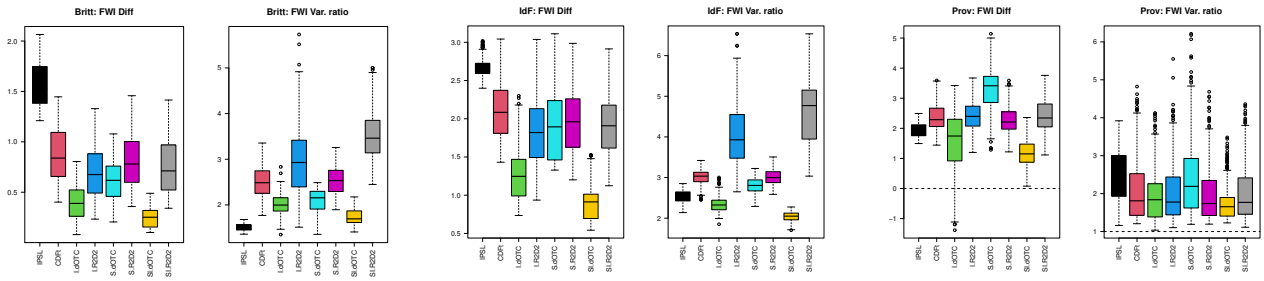

Figure 9.1: Overall summer FWI difference between future and past bias and summer FWI's variance ratio between future and past for all bias correction methods. Left column: Bretagne. Middle column: Ile de France. Right column: Provence. In each panel, from left to right: IPSL (no correction), CDF-t, Intervar-dOTC, Intervar-R2D2, spatial-dOTC, spatial R2D2, spatial-intervar-dOTC, spatial-intervar-R2D2.

9.2 Covariances

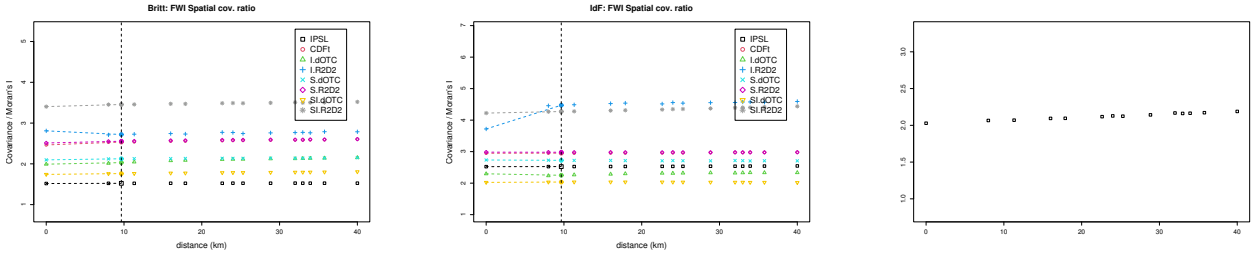

Figure 9.2: Spatial covariance and Moran's I ratio between future and past of summer FWI for all bias correction methods. Left column: Bretagne. Middle column: Ile de France. Right column: Provence.

9.3 p-values

	IPSL	CDFt	I.dOTC	I.R2D2	S.dOTC	S.R2D2	SI.dOTC	SI.R2D2
p-values for "equality-of-means" tests								
Britt.	0.000	0.000	0.000	0.000	0.000	0.000	0.000	0.000
IdF	0.000	0.000	0.000	0.000	0.000	0.000	0.000	0.000
Prov.	0.000	0.000	0.000	0.000	0.000	0.000	0.000	0.000
p-values for "equality-of-variances" tests								
Britt.	0.000	0.000	0.000	0.000	0.000	0.000	0.000	0.000
IdF	0.000	0.000	0.000	0.000	0.000	0.000	0.000	0.000
Prov.	0.000	0.000	0.000	0.000	0.000	0.000	0.000	0.000
p-values for "equality-of-Moran's I" tests								
Britt.	0.000	**0.569**	**0.172**	0.000	**0.349**	0.000	**0.202**	0.060
IdF	0.000	0.000	0.000	0.000	0.000	0.000	0.000	0.000
Prov.	0.000	0.000	0.000	0.000	0.000	0.000	0.000	0.000

Table 9.1: Statistical analysis for summer FWI in the future: p-values for the Welsh t-test of absence of differences on the average (first block); Fisher F-test of equality of variance between future and past (second block) and its adaptation to testing the equality of Moran's I (third block). Non rejection at the confidence level 0.90 is indicated in bold font.

9.4 Maps for average differences

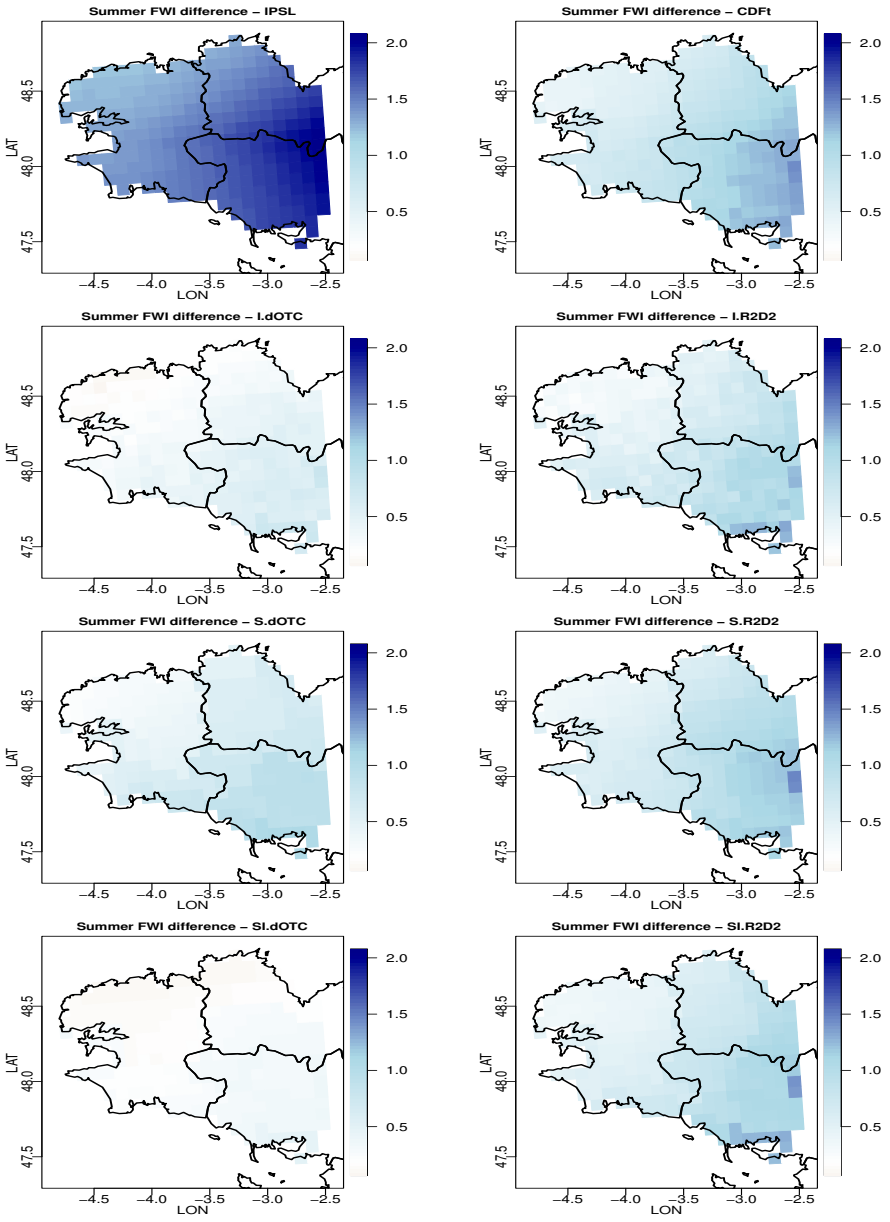

Figure 9.3: For each bias correction method: map of the summer FWI average difference between future and past in Brittany. From top to bottom and from left to right: IPSL (no correction), CDF-t, Intervar-dOTC, Intervar-R2D2, spatial-dOTC, spatial R2D2, spatial-intervar-dOTC, spatial-intervar-R2D2.

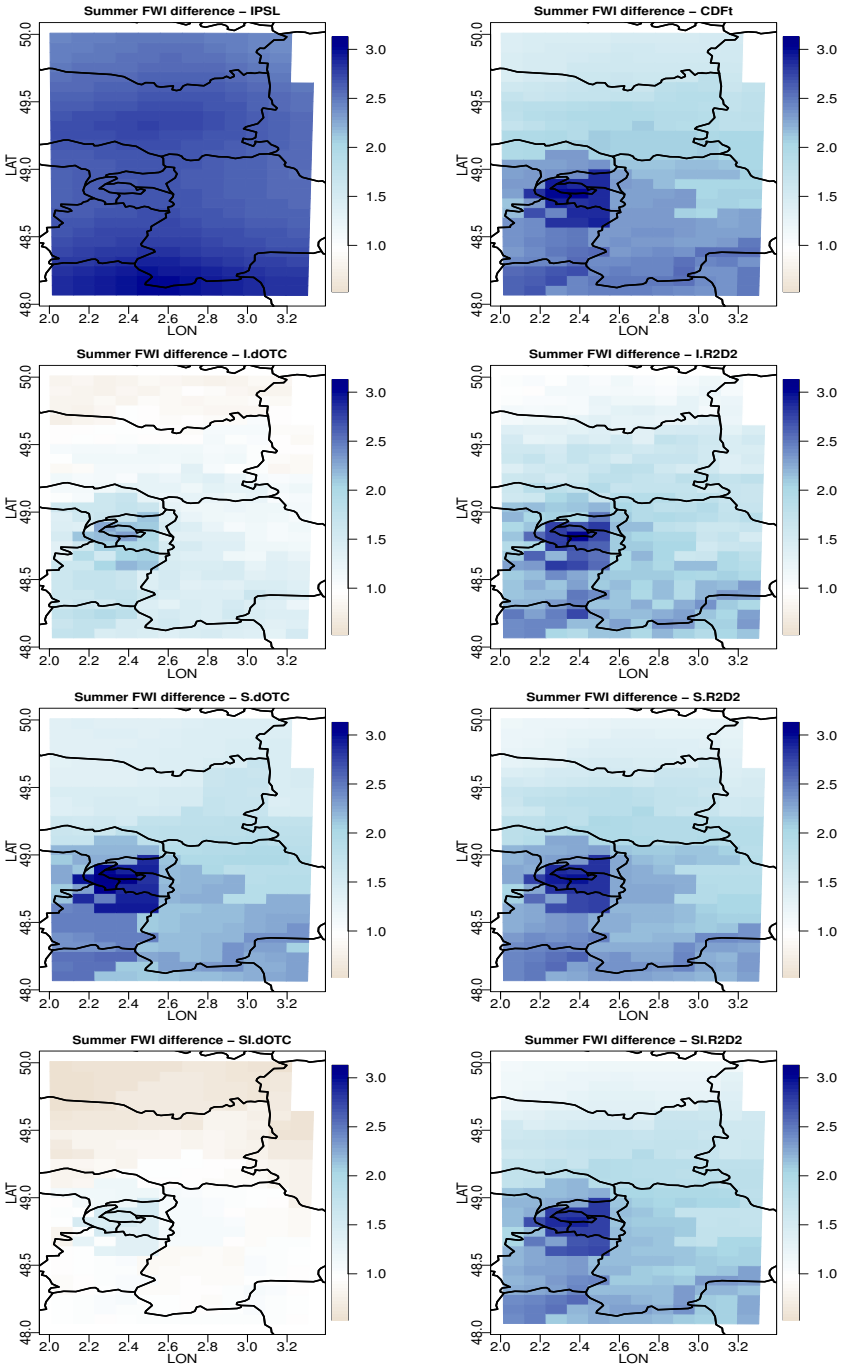

Figure 9.4: For each bias correction method: map of the summer FWI average difference between future and past in Ile de France. From top to bottom and from left to right: IPSL (no correction), CDF-t, Intervar-dOTC, Intervar-R2D2, spatial-dOTC, spatial R2D2, spatial-intervar-dOTC, spatial-intervar-R2D2.

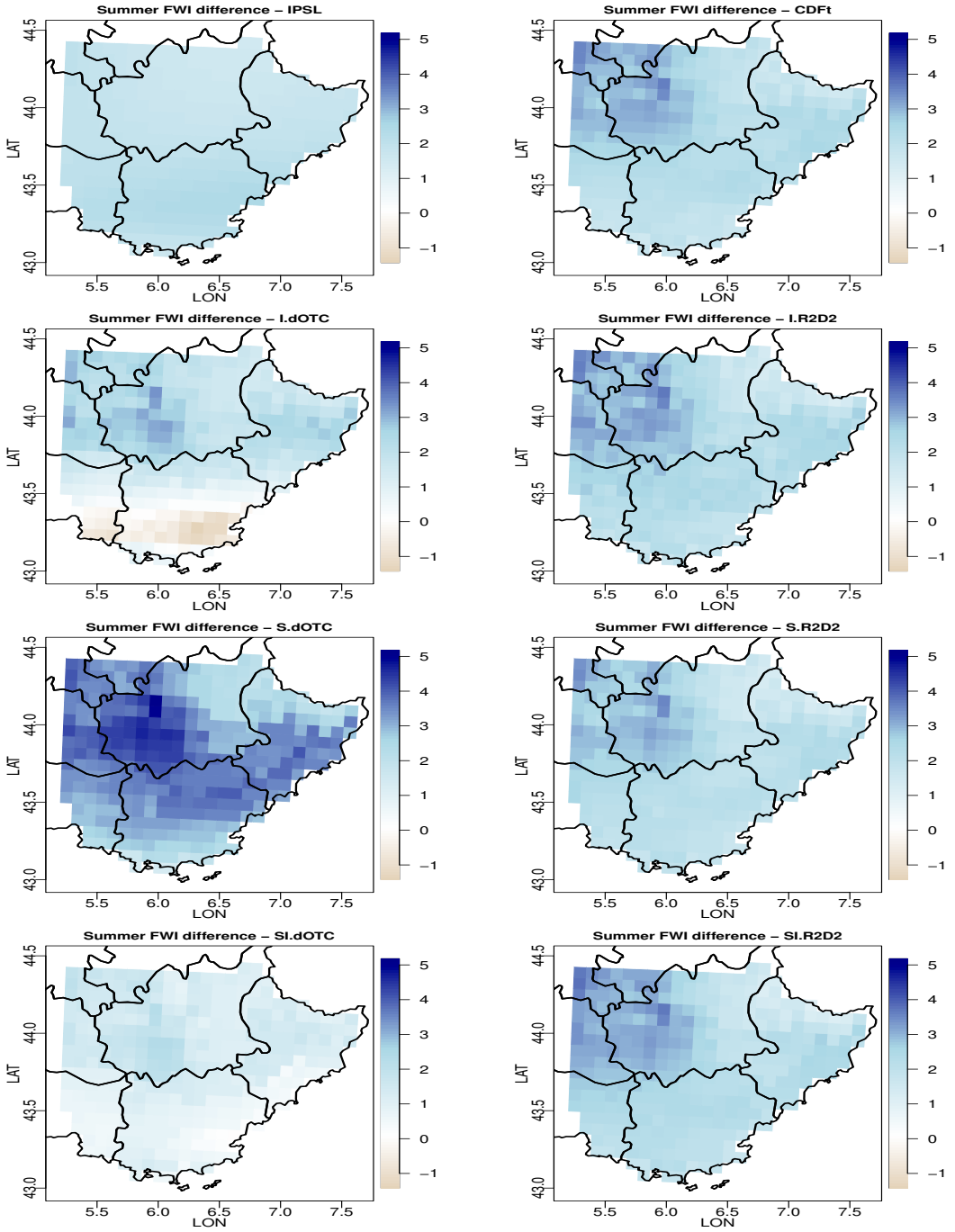

Figure 9.5: For each bias correction method: map of the summer FWI average difference between future and past in Provence. From top to bottom and from left to right: IPSL (no correction), CDF-t, Intervar-dOTC, Intervar-R2D2, spatial-dOTC, spatial R2D2, spatial-intervar-dOTC, spatial-intervar-R2D2.

9.5 Maps for variance ratio

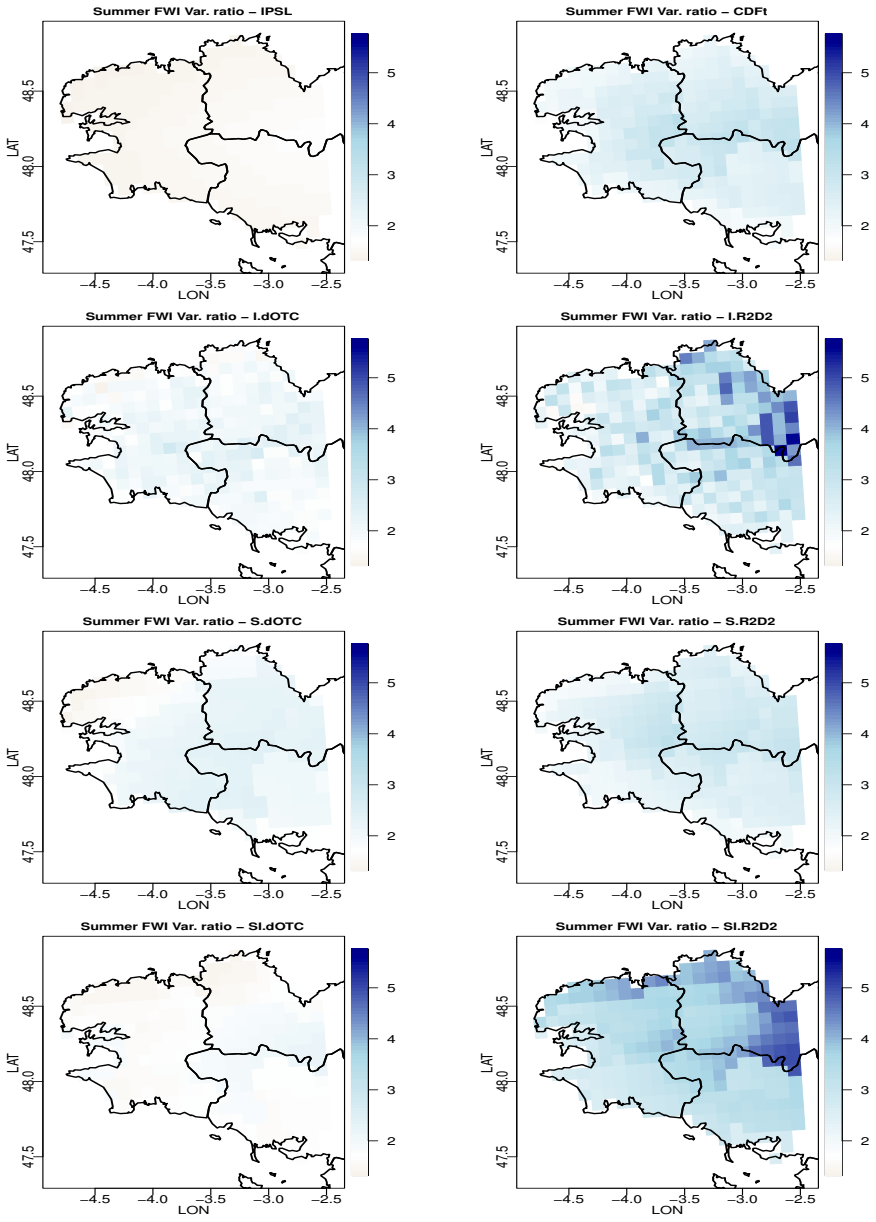

Figure 9.6: For each bias correction method: map of summer FWI variance ratio between future and past in Brittany. From top to bottom and from left to right: IPSL (no correction), CDF-t, Intervar-dOTC, Intervar-R2D2, spatial-dOTC, spatial R2D2, spatial-intervar-dOTC, spatial-intervar-R2D2.

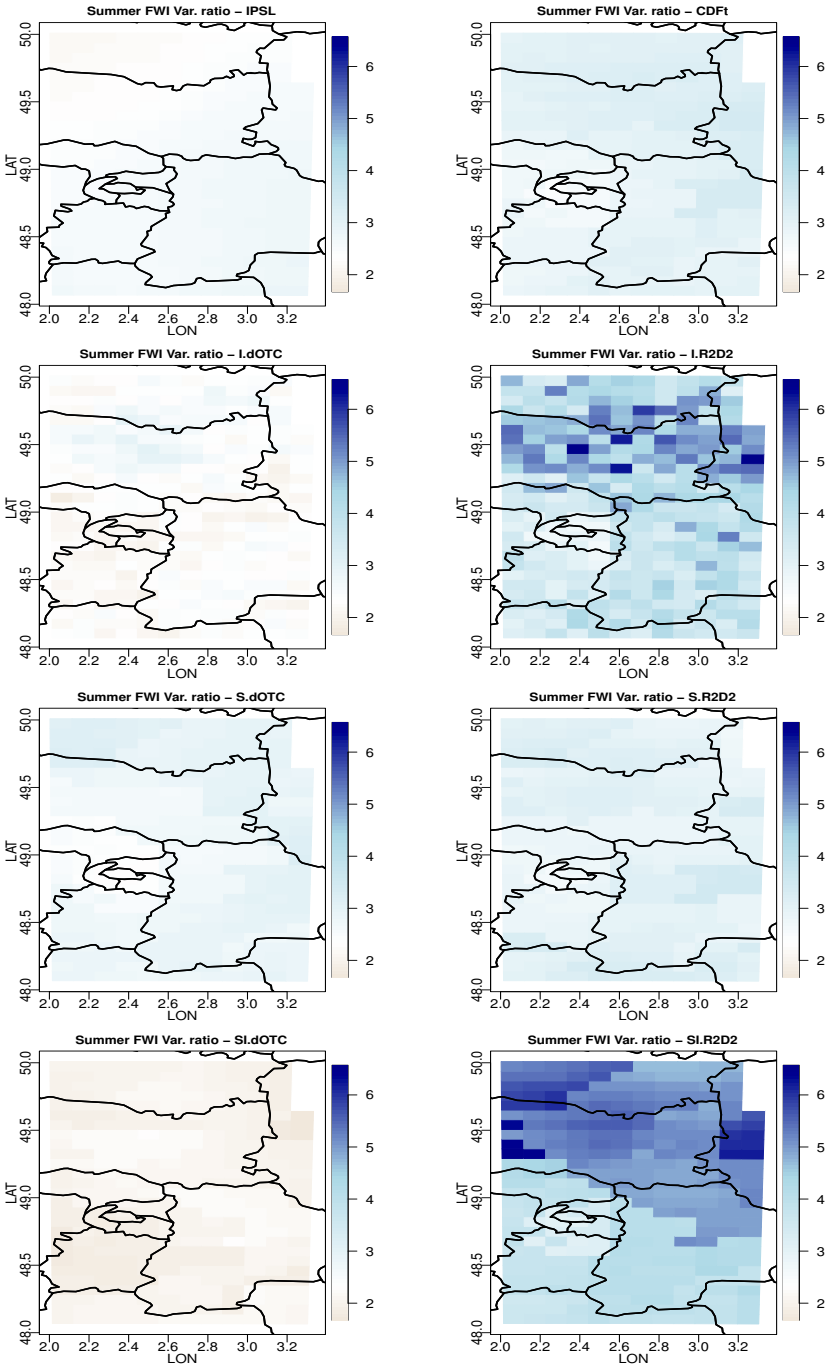

Figure 9.7: For each bias correction method: map of the summer FWI variance ratio between future and past in Ile de France. From top to bottom and from left to right: IPSL (no correction), CDF-t, Intervar-dOTC, Intervar-R2D2, spatial-dOTC, spatial R2D2, spatial-intervar-dOTC, spatial-intervar-R2D2.

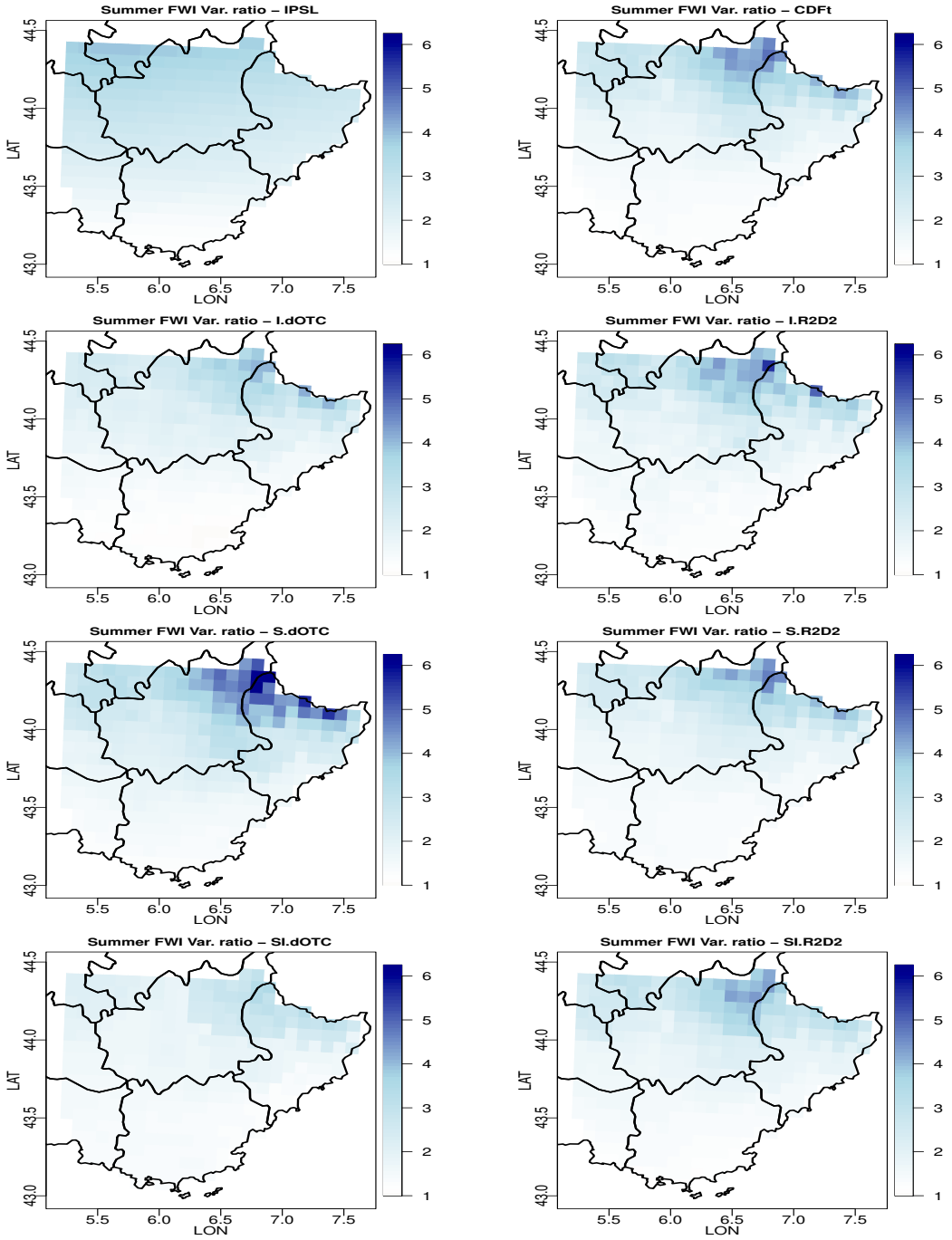

Figure 9.8: For each bias correction method: map of the summer FWI variance ratio between future and past in Provence. From top to bottom and from left to right: IPSL (no correction), CDF-t, Intervar-dOTC, Intervar-R2D2, spatial-dOTC, spatial R2D2, spatial-intervar-dOTC, spatial-intervar-R2D2.

Bibliography

Allen, R., Pereira, L., and Smith, M. (1998). *Crop evapotranspiration-Guidelines for computing crop water requirements-FAO Irrigation and drainage paper 56*, volume 56.

Boucher, O., Servonnat, J., Albright, A. L., Aumont, O., Balkanski, Y., Bastrikov, V., Bekki, S., Bonnet, R., Bony, S., Bopp, L., et al. (2020). Presentation and evaluation of the ipsl-cm6a-lr climate model. *Journal of Advances in Modeling Earth Systems*, 12(7):e2019MS002010.

Brisson, N. N. and Levrault, F. (2010). Livre vert du projet climator 2007-2010. changement climatique, agriculture et forêt en france: simulations d'impacts sur les principales espèces.

Caubel, J., García de Cortázar-Atauri, I., Launay, M., de Noblet-Ducoudré, N., Huard, F., Bertuzzi, P., and Graux, A.-I. (2015). Broadening the scope for ecoclimatic indicators to assess crop climate suitability according to ecophysiological, technical and quality criteria. *Agricultural and forest meteorology*, 207:94–106.

Chen, W., Genton, M. G., and Sun, Y. (2021). Space-time covariance structures and models. *Annual Review of Statistics and Its Application*, 8:191–215.

Chiles, J.-P. and Delfiner, P. (2012). *Geostatistics: modeling spatial uncertainty*, volume 713. John Wiley & Sons.

Chuine, I., de Cortazar-Atauri, I. G., Kramer, K., and Hänninen, H. (2013). Plant development models. *Phenology: an integrative environmental science*, pages 275–293.

Clark, M., Gangopadhyay, S., Hay, L., Rajagopalan, B., and Wilby, R. (2004). The schaake shuffle: A method for reconstructing space–time variability in forecasted precipitation and temperature fields. *Journal of Hydrometeorology*, 5(1):243–262.

Dupuy, J.-l., Fargeon, H., Martin-StPaul, N., Pimont, F., Ruffault, J., Guijarro, M., Hernando, C., Madrigal, J., and Fernandes, P. (2020). Climate change impact on future wildfire danger and activity in southern europe: a review. *Annals of Forest Science*, 77(2):1–24.

Eyring, V., Bony, S., Meehl, G. A., Senior, C. A., Stevens, B., Stouffer, R. J., and Taylor, K. E. (2016). Overview of the coupled model intercomparison project phase 6 (cmip6) experimental design and organization. *Geoscientific Model Development*, 9(5):1937–1958.

Fargeon, H., Pimont, F., Martin-StPaul, N., De Caceres, M., Ruffault, J., Barbero, R., and Dupuy, J. (2020). Projections of fire danger under climate change over france: where do the greatest uncertainties lie? *Climatic Change*, 160(3):479–493.

François, B., Vrac, M., Cannon, A. J., Robin, Y., and Allard, D. (2020). Multivariate bias corrections of climate simulations: which benefits for which losses? *Earth System Dynamics*, 11(2):537–562.

Michelangeli, P.-A., Vrac, M., and Loukos, H. (2009). Probabilistic downscaling approaches: Application to wind cumulative distribution functions. *Geophysical Research Letters*, 36(11).

Moran, P. A. P. (1950). Notes on continuous stochastic phenomena. *Biometrika*, 37(1-2):17–23.

MTES (2021). Forests: Extract from france's 2021 environmental performance review.

Robin, Y., Vrac, M., Naveau, P., and Yiou, P. (2019). Multivariate stochastic bias corrections with optimal transport. *Hydrology and Earth System Sciences*, 23(2):773–786.

Ruffault, J., Curt, T., Moron, V., Trigo, R. M., Mouillot, F., Koutsias, N., Pimont, F., Martin-StPaul, N., Barbero, R., Dupuy, J.-L., et al. (2020). Increased likelihood of heat-induced large wildfires in the mediterranean basin. *Scientific reports*, 10(1):13790.

Vallejos, R. and Osorio, F. (2014). Effective sample size of spatial process models. *Spatial statistics*, 9:66–92.

Van Wagner, C. et al. (1987). *Development and structure of the Canadian forest fire weather index system*, volume 35.

Vidal, J.-P., Martin, E., Franchistéguy, L., Baillon, M., and Soubeyroux, J.-M. (2010). A 50-year high-resolution atmospheric reanalysis over france with the safran system. *International Journal of Climatology*, 30(11):1627–1644.

Vrac, M. (2018). Multivariate bias adjustment of high-dimensional climate simulations: the rank resampling for distributions and dependences (r 2 d 2) bias correction. *Hydrology and Earth System Sciences*, 22(6):3175–3196.

Vrac, M., Noël, T., and Vautard, R. (2016). Bias correction of precipitation through singularity stochastic removal: Because occurrences matter. *Journal of Geophysical Research: Atmospheres*, 121(10):5237–5258.

Wang, X., Wotton, B. M., Cantin, A. S., Parisien, M.-A., Anderson, K., Moore, B., and Flannigan, M. D. (2017). cffdrs: an r package for the canadian forest fire danger rating system. *Ecological Processes*, 6(1):1–11.

Welch, B. L. (1947). The Generalization of ?Student's? Problem when Several Different Population Variances are Iinvolved. *Biometrika*, 34(1-2):28–35.